Formation control of nonholonomic mobile robots: the virtual structure approach

Sadowska, Anna Danuta

Formation control of nonholonomic mobile robots: the virtual structure approach

Anna Danuta Sadowska

School of Engineering and Materials Science

Queen Mary University of London

Supervisors: Dr Henri Huijberts

Dr Hasan Shaheed

A DISSERTATION SUBMITTED FOR THE DEGREE OF

DOCTOR OF PHILOSOPHY

2012

To my husband and my parents

-thank you.

Abstract

In recent years, there has been a considerable growth in applications of multi-robot systems as opposed to single-robot systems. This thesis presents our proposed solutions to a formation control problem in which mobile robots are required to create a desired formation shape and track a desired trajectory as a whole.

In the first instance, we study the formation control problem for unicycle mobile robots. We propose two control algorithms based on a cascaded approach: one based on a kinematic model of a robot and the other based on a dynamic model. We also propose a saturated controller in which actuator limitations are explicitly accounted for. To demonstrate how the control algorithms work, we present an extensive simulation and experimental study.

Thereafter we move on to formation control algorithms in which the coordination error is explicitly defined. Thus, we are able to give conditions for robots keeping their desired formation shape without necessarily tracking the desired trajectory. We also introduce a controller in which both trajectory tracking and formation shape maintenance are achieved as well as a saturated algorithm. We validate the applicability of the introduced controllers in simulations and experiments.

Lastly, we study the formation control problem for car-like robots. In this case we develop a controller using the backstepping technique. We give conditions for robots keeping their desired formation shape while failing to track their desired trajectories and present simulation results to demonstrate the applicability of the proposed controller.

Acknowledgements

I would like to take this opportunity and express my gratitude to the people who in one way or another have had some kind of involvement in the progress of my PhD studies.

In the first place, I would like to thank to my supervisor Dr Henri Huijberts, without whom this thesis would have never come into existence. I appreciate your insightful comments on my writing and guiding me through my research and putting up with my language mistakes. I would also like to thank Dr Hasan Shaheed who is my second supervisor. I appreciate your support throughout my studies. Furthermore, my gratitude goes to Dr Dragan Kostić, Dr Nathan van de Wouw and Prof. Henk Nijmeijer from the Dynamics and Control group at Eindhoven University of Technology. During the three months that I spent with the DC group, I gained a valuable knowledge which I am indebted for. I must also acknowledge Prof. Krzysztof Tchoń from Wroclaw University of Technology who introduced me into the fascinating world of Science and Robotics in particular. I very much appreciate the support that you have been giving to me thus far.

I would also like to thank to the members of my PhD examination committee: Prof. Kaspar Althoefer from King's College London and Prof. Alessandro Astolfi from Imperial College London. Thank you for your comments on my thesis which helped to improve this manuscript.

Throughout my time studying for the doctorate at Queen Mary Uni-

versity of London, I was lucky enough to have met fantastic people who have made my time at the university truly enjoyable. I would like to especially acknowledge my officemates Paula Ruiz and Mo Waked. My kind word of appreciation goes also to Stan van der Meulen and Sinan Öncü who were my officemates at Eindhoven University of Technology. Equally, I am thankful to Alejandro Alvarez-Aguirre and Sisdarmanto Adinandra for the interesting conversations we had on control of multi robot systems. Nandra - thank you for your help with the experiments!

I want to also express my deep appreciation to my loving family: my parents and sisters. Thank you for being there for me when I need you. At last, but not least, I would like to thank my husband Krzysztof. I am indeed very grateful for your endless love and support from the time we met. I look forward to our future life together.

Contents

List of Figures

Nomenclature

VC	virtual centre
$\mathbb{R}^+$	the set of positive real numbers
$\mathbb{R}_0^+$	the set of nonnegative real numbers
$\mathbb{C}^+$	the set of complex numbers with positive real part
$\mathbf{I}$	identity matrix
$\mathbf{0}$	a square matrix with all entries equal zero
q	state vector of a robot
$p = (x, y)^T$	position of a robot
θ	orientation of a robot with respect to the horizontal axis
φ	steering angle of robot's front wheel (car-like robot)

v	forward speed of a robot
ω	angular velocity of a robot (unicycle robot) or angular velocity of the steering wheel (car-like robot)
F	force
τ	torque
p_i^d	a desired position of robot i in the inertial coordinate frame
l_i^d	a desired position of robot i with respect to the virtual centre
e_i	a tracking error of robot i in the inertial coordinate frame
e_i^{xy}	a tracking error of robot i in a local coordinate frame associated with the robot
N_i	the set of neighbours of Robot i
I	formation geometry maintenance index
$\mathcal{G}$	communication graph

Men love to wonder, and that is the seed of science.

Ralph Waldo Emerson

Chapter 1

Introduction

For many years now, the occurrence of robots in numerous areas of human life, operating both in industrial and every-day applications, has been increasingly prominent. This has lead to new research being launched in robotics investigating robot control and design. Recently, the interest of researchers is being more and more shifted towards cooperative control of multi–robot systems, as opposed to single robot systems. This thesis forms another contribution in this field and concerns specifically a *formation control problem* or a *coordinated control problem* where the objective is to steer all robots in the formation in a coordinated fashion. In the realm of this thesis, this in particular means that the robots in the formation are required to create a particular geometry of the group while performing an additional control task, e.g. following a desired trajectory, see Figure 1.1.

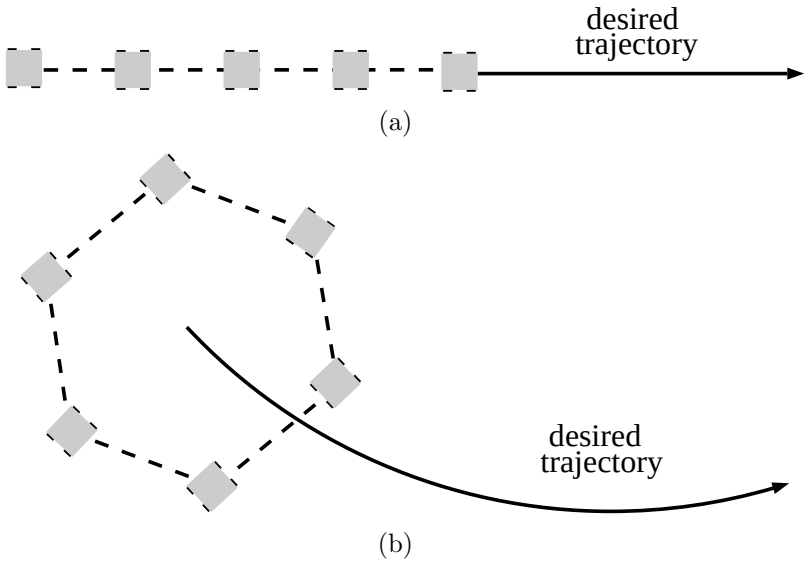

Figure 1.1: Examples of different formation shapes and trajectories (a) a platoon–shaped formation and a straight trajectory, (b) a hexagon-shaped formation and a circular trajectory.

In the remainder of this chapter we explain where applications of the formation control problem may be found and what motivates such a broad interest. We also present some existing approaches to the formation control problem.

1.1 Applications of robot formations

There are many practical situations where robot formations may be used: e.g. in moving target observation, in reconnaissance and surveillance tasks, in a warehouse, see (Jung and Sukhatme, 2002; Kolling and Carpin, 2006; Luke et al., 2005). This also includes human rescue missions as considered by Murphy (2004) who focused upon the human-robot interactions in rescue missions. Interestingly,

Figure 1.2: Robot teams during rescue mission in WTC after the September 11 attack. Photos from (CRASAR, 2012).

in practical applications of rescue robots, the robots are not assigned a task to perform it instead of the humans but with them as a part of human–robot rescue teams. To prevent further catastrophe it is therefore important that the attendance of humans in such missions is reduced. Robots in rescue missions have been successfully used to date, e.g. in the World Trade Centre, see Figure 1.2. More recently, robot teams were used to support the rescue operations during the Japan earthquake in March 2011 (Guizzo, 2011). For this particular operation, apart from wheeled robots, also snake–like mobile robots were deployed.

These are illustrated in Figure 1.3 and are built to serve as Active Scope Camera (Hatazaki et al., 2007) to enable reaching spaces unreachable to humans due to their restricted dimensions.

Within the scope of rescue robotics, Kamegawa et al. (2008, 2010, 2011) proposed to use two kinds of robots in the search operations in rescue missions. The first ones are the pioneer type robots which are human–operated and whose job includes removing any lightweight obstacles as well as opening doors to allow access to the area to the surveyor type robots. These latter robots semi–autonomously collect data from the area about the environment and possible victims trapped inside. The two types of robots communicate through a wireless network, the so–called Robohoc network, which allows robots to freely join a pre–existing group.

Also the authors of (Kantor et al., 2003) considered a similar problem in which robots are used together with humans to perform search and rescue missions. That research is concentrated on a localisation task based on the so–called Simultaneous Localisation and Mapping (Singh et al., 2002; Thrun, 2008) in an environment where possibly no infrastructure exists as well as on information flow between various agents involved. The proposed strategy is such that information collected from a variety of sensors is used to create a map of the territory. This is then transferred to the humans engaged in the mission for further investigation.

The problem of Simultaneous Localisation and Mapping was also considered in, for example, (Weiss, 2011) where mapping swarmbots were studied. The article concerned general issues of application of robots and robot teams in military actions and pointed out a number of existing problems. In particular, for a robot

Figure 1.3: A snake–like robot. Photo from (Guizzo, 2011).

team to be able to fully participate in a military mission, robots should ultimately be able to cooperate within heterogenous groups so that they can interchangeably be attached to or detached from a group. A more general concern in terms of robots taking part in military operations is the level of autonomy that the robots are granted and the need for a fault–proof mechanism of robots which would enable robots to understand a situation in which intelligent reasoning is essential.

Regarding unknown environment exploration, Hougen et al. (2000) contributed in this realm and proposed a system consisting of miniature heterogeneous robots that may be used for rescue missions, in the occurrence of hazardous substance spills and in general for reconnaissance and surveillance. In contrast, Thrun et al. (2003) concentrated on volumetric mapping of abandoned life-threatening land mines in the territory of the United States. Moreover, the research of Burgard et al. (2005) centred on general multi-robot exploration projects that resulted in

Figure 1.4: Two robots performing a cooperative furniture relocation task. Photo from (Rus et al., 1995).

the proposal of an algorithm to fulfil these tasks while minimising both the range of undiscovered areas and the associated cost.

Groups of mobile robots may also be used in everyday–life situations, for example in the circumstances considered in (Rus et al., 1995) which deals with furniture relocation without communication between robots, global knowledge or planning, see Figure 1.4. Moreover, the use of robot formations in day-to-day tasks was also studied by Endres et al. (1998) and by Jager and Nebel (2002) who regarded the issue of coordinated autonomous cleaning. It has been shown that such tasks may be successfully performed by multiple robots providing the advantages of the cleaning being performed in a distributed fashion with added robustness and speed of performing the task.

Another application, although not concerning mobile robot formations but satellite formations, is the task of observation of far-away celestial bodies, which are impossible to be directly investigated because of their vast distance from the

Earth. To this end, a group of satellites to work as interferometers may be employed. It should be noted that the interferometry, as studied by Lawton and Beard (2002), involves high precision of execution of the controller. This is due to the necessity of having each pair of the interferometer satellites kept scrupulously aligned with respect to each other for the interferometry to be realisable.

To the broad range of applications of robot formations mentioned so far, one may also add autonomous ocean mapping, see (Curtin and Bellingham, 2009; Curtin et al., 1993). The reason for ocean mapping is to provide the necessary data for three-dimensional numerical models of the ocean, thus allowing for a wider variety of hypotheses regarding the ocean to be tested as well as the oceans to be monitored more thoroughly than in the case of a two–dimensional ocean map. In contrast with the previous employments of agents like ships or satellites that could only provide data for a two-dimensional ocean image, the scenario considered in (Curtin and Bellingham, 2009; Curtin et al., 1993) engages a team of Autonomous Underwater Vehicles and therefore, more accuracy follows.

1.2 Rationale behind multiple robot systems

The omnipresence of practical applications of robot formations clearly stems from the numerous benefits of multi-robot formations over single robots, see e.g. (Arai et al., 2002; Cao et al., 1997; Chen and Wang, 2005; Parker, 2008). Arguably the major advantage is the fact that a given task may be too complicated for a single robot and hence a multiple robot formation may be necessary to fulfil it.

However, since there are several robots involved, the mathematical analysis may become complex with the transient behaviour becoming difficult to anticipate.

It was already pointed out in the previous section that an important benefit of using multiple robot groups to conduct a task instead of single robots is the fact that robots performing the task are spread out throughout the area involved. This is advantageous in many cases, e.g. reconnaissance, exploration or patrolling. In these instances, the territory that is being examined may be covered by a group of mobile robots more quickly than by a single multi-task robot. Another advantage, stemming from the distributed manner of the execution of a task, is the robustness of the approach. In a case of a single robot, failure of a robot will result in failure of the whole mission. However, in the case of a task being performed by a formation consisting of multiple robots, break down of one robot may not be fatal because the rest of the team might still be able to fulfil the task. Thus, nowadays the majority of studies on multiple robot formations gravitates towards distributed information flow in the formation in which the robustness does not depend on a particular individual in the group as there is no superior agent in the team.

Evidently, the application of robot formations is favourable in many situations. This follows from the manifold favourable qualities of the cooperative approach that were listed above. In fact, the broad range of applications of cooperative agents may be observed not only among artificial agents, like robots. It could be argued that the origin of studies in cooperative and synchronous behaviour of artificial agents have emerged from investigation of the existing occurrence of

synchronisation and cooperation phenomena among living creatures. In the next two sections we show first what are the different collective strategies between multiple mobile agents that have been identified in the literature. Then it is exemplified that in fact the principle of cooperative behaviour is ubiquitous in nature and indeed observation of this phenomenon inspired the development of the cooperative approach in control of mobile robots.

1.3 Other collective behaviour coordination strategies

In the realm of multiple agent systems, there are a number of concepts that specify mutual relations between members of a group. Apart from the formation control problem, which is of particular interest for us, one may also mention *synchronisation*, *consensus*, *rendezvous* and *flocking*. Here, all these concepts are consecutively explained and illustrated with appropriate examples.

Synchronisation is probably the most general concept among multiple agent coordination strategies mentioned in this section. According to (Blekhman, 1988; Blekhman et al., 1997, 2002), the term synchronisation is used to characterise the phenomenon of coinciding in time of a set of functionals associated with two or more processes. In particular, one may distinguish a specific subcategory within this scope, i.e. phase synchronisation which is specifically related to periodic or chaotic systems, see (Pikovsky et al., 1999, 2000; Rosenblum et al., 1996). The term phase synchronisation initially concerned periodic oscillators and referred to

the phenomenon of locking phases of the periodic motion of the oscillators while the amplitude of the vibrations remains unrestricted. Nowadays, one also regards phase synchronisation of chaotic systems which has a particular importance in private communication systems (Chen et al., 2003). In particular, by synchronising a receiving chaotic system to a transmitting chaotic system, communication can be accomplished privately over a public channel. An interesting observation noted in the mentioned papers is that the phase synchronisation of periodic systems occurs even in the presence of merely weak couplings. Another interesting feature concerning synchronisation was observed originally by Voss (2000) and later on studied in e.g. (Huijberts et al., 2007; Nijmeijer and Oguchi, 2006) which all examined the anticipating synchronisation phenomenon of chaotic oscillators. It was discovered that in a scenario involving two systems, one of which was designed to be the drive system, the second system was able to synchronise to the future drive system's state and therefore anticipate the state of the drive system.

For a robotic system, the synchronisation control problem was studied, among others, by Rodriguez-Angeles (2002) and Rodriguez-Angeles and Nijmeijer (2003) who worked on synchronisation of fully actuated robotic manipulators. They considered two major scenarios, both based on the master–slave hierarchy, one of which is called external synchronisation and the other one internal synchronisation. External synchronisation refers to the case when the non–dominant systems, or the slaves, are controlled to synchronise with the trajectories of the dominant system, also known as the master. Hence, the control of the master system is independent and such that the master tracks a given desired trajectory, while the controllers for the slave systems are designed to obtain synchronous

behaviour with the master. Conversely, in the internal or mutual synchronisation strategy, all manipulators involved equally act towards synchronisation of their trajectories towards a common desired trajectory. This is through feedback control that involves each robot manipulator obtaining information regarding other manipulators to achieve the common goal.

Similarly, in (Bouteraa et al., 2011) the problem of synchronisation of robotic manipulators was considered and resulted in a control strategy in which each manipulator was synchronised with its neighbours, as opposed with all other manipulators as proposed in (Rodriguez-Angeles, 2002; Rodriguez-Angeles and Nijmeijer, 2003). Also the authors of (Nuño et al., 2010) studied the same problem but with the possibility of the coupling time delays. They presented controllers which assure that manipulators either track a desired trajectory or reach a consensus. Moreover, the unknown network parameters like robots' inertia matrices, Coriolis matrices and the gravitational forces were estimated by robots through an adaptive control strategy. In contrast, the results in (Chung and Slotine, 2009) concern concurrent synchronisation of multiple groups of Lagrangian systems that are synchronised internally. To obtain this, a decentralised control strategy that achieves synchronisation of all robots in subgroups by ensuring coexistence of fully synchronised subgroups is presented. In the light of the terminology presented in (Rodriguez-Angeles, 2002; Rodriguez-Angeles and Nijmeijer, 2003), the three latter papers (Bouteraa et al., 2011; Chung and Slotine, 2009; Nuño et al., 2010) may be regarded to consider the internal synchronisation case.

An important collective behaviour problem that should be mentioned here is the

consensus control problem (Olfati-Saber and Murray, 2003a, 2004; Olfati-Saber et al., 2007; Ren et al., 2005; Sepulchre, 2011; Zhang et al., 2008). This consists in all agents in a group converging to a common value of the state vector that depends on the initial states of all agents in the group. If all agents have achieved the common state, one says they agree with each other or that they have reached an agreement/consensus. Contingent upon the relation between the common value of the state and the initial states of the agents, one studies the *average consensus problem* if the common value is an average, possibly weighted, of the initial states of all agents. There are also both *minimum* and *maximum consensus problems* if the common value is the minimum or the maximum amongst initial states respectively.

The basic control algorithm proposed in (Olfati-Saber and Murray, 2003a, 2004; Olfati-Saber et al., 2007; Ren et al., 2005; Sepulchre, 2011; Zhang et al., 2008) for the i^{th} agent, $i = 1, \ldots, n$, is based on an inter-agent information exchange protocol

$$u_i = \sum_{j \neq i} a_{ij}(x_j - x_i), \tag{1.1}$$

where $a_{ij} = 1$ if agents i and j are neighbours meaning they can sense each other and $a_{ij} = 0$ otherwise. This consensus algorithm was studied for a group of n mobile agents described by single integrator dynamics $\dot{x}_i = u_i$. Clearly, this dynamics are unrealistic in many cases. Yet, as shown later in this section, this approach may still be used when appropriate adjustments are made.

The behaviour of a group under (1.1) depends on the communication structure of the group. In particular, according to (Olfati-Saber et al., 2007), a group

of mobile agents reaches consensus, if the communication graph of the group is strongly connected, meaning that each agent can exchange information with each other agent possibly through other agents on the way, see (Godsil and Royle, 2001). In addition, (Olfati-Saber et al., 2007) also provides conditions for average consensus, for a network with time delays and for the discrete time case.

Given the subject of this thesis it is appealing that one can use the consensus approach to provide a framework for analysis of the formation control problem. This technique was studied by Ren (2007a) as well as by Wu et al. (2007). In (Ren, 2007a) in particular the initial formation control problem was converted to the consensus control problem by means of a state transformation and solved within the general framework as discussed above. Therefore, one may extend the usefulness of the consensus protocol (1.1) since, although it was initially studied for single integrator dynamics, it can be seen from this example that it may be applied to more complicated systems too, including mobile robots which are of a particular interest in this thesis. Moreover, the general averaging procedure of the algorithm also seems attractive to be further examined and motivated many other researches in the area of the formation control problem (Kostić et al., 2010b; Van den Broek et al., 2009), including the work contributed in this thesis.

A third major category of inter-agent coordination problems is the rendezvous problem where one requires all agents in the group to reach a common location. It was studied by Lin et al. (2003) where a so–called "stop-and-go" technique was established. In this technique, the motion of single systems is based on two main actions: one occurs in the sensing period in which no motion is performed and

only scanning is active and the other one takes place during the manoeuvring period in which agents' positions are changed.

In this field, the study by Dimarogonas and Kyriakopoulos (2007) was particularly focused on rendezvous of a group of unicycle mobile robots. In this scheme, a kind of attractive potential is to be minimised to drive robots to a common location. Once again, though, the necessary condition for coordinated behaviour is that the communication graph associated with the group is connected. It includes the case of switching graph topology as long as each configuration of the network constitutes a connected graph. This is an advantage as the set of neighbours of agents in the group may change while proceeding towards the common location. Another benefit is the information flow structure of this algorithm which is such that each robot requires information from its neighbours only.

The collective behaviour concept that is probably mostly related to and inspired by synchronous behaviours in nature is flocking, also known as swarming. Here, the control strategy normally includes dealing with a large number of agents performing a mutual task. This scheme is based on the observation of natural swarms of insects, fish or birds. One easily notices the surprising phenomenon of an ideally-distributed-communication network of natural flocks which one aims to imitate in artificial swarms. Moreover, remarkably there is no leader in a group and hence all members of the group are in general equal. Swarming phenomena were examined by Reynolds (1987) where three fundamental rules on particle behaviour in a flock were determined, namely, trying to stay close to neighbours, avoiding collisions with each other, and aiming to match velocities with regard

to each other. These rules are labelled as *cohesion*, *separation* and *alignment* respectively (Olfati-Saber, 2006) and are applied in (Olfati-Saber, 2006; Olfati-Saber and Murray, 2003b) in which the authors proposed, among others, an algorithm for flocking that substantiates the three rules of Reynold's flocks for a group of n double integrator particles.

From a different perspective, the flocking control problem was studied by Savkin (2004) where a swarm model based on local interactions between neighbours was analysed. According to the so-called Vicsek's model in its simplified version presented in (Savkin, 2004), each particle updates its position and heading depending on its previous state as well as the previous states of its neighbours. In fact, the procedure is such that the heading angle of each particle in each step is an average of its own and its neighbours' heading angles in the previous step rounded to a nearest value from a given set of discrete values between 0 and 2π. Then the new position is calculated accordingly. The advantage of this approach is that it is indeed distributed as each member requires knowledge of its neighbours only. Moreover, the set of neighbours of every agent is time–varying which embodies the fact that when the flock moves, the relative positions of particles in the flock change and therefore, neighbours change. These two features reflect the behaviour of actual flocks in nature.

Another contribution in the realm of swarming phenomena is the work by Cheah et al. (2009) and Hou et al. (2009) in which a swarming algorithm for a group of fully actuated robots is proposed. The control strategy is to fulfil two objectives: robots maintain desired minimum distances between each other while remaining

inside a prescribed moving region, e.g. a square or an ellipse. The first objective is considered a local objective of a robot while the latter is said to be a global objective since it concern a group as a whole. What is important, is the fact that the control algorithm is executed on a local level and hence robots do not need to communicate with the whole group. Instead, local interactions between neighbours suffice.

We next illustrate how all these concepts of cooperative behaviour of multiple mobile agents are realised in the natural world. This is important in that one can argue that it is the observation of synchronous phenomena in nature that lies behind the trend of utilisation of cooperative artificial agents in science and technology.

1.4 Inspiration for multi–robot systems from nature

In literature, there are numerous examples of control algorithms for groups of multiple agent which by modelling various phenomena occurring in nature try to imitate the behaviours observed amongst living creatures (Arkin et al., 2000; Howsman et al., 2002; Hsieh et al., 2008; Weitzenfeld et al., 2006). Indeed, in recent years there is a trend to emulate the behaviour of animals in artificial agents to obtain various benefits of cooperative or synchronised entities as opposed to when a single agent would be used. In terms of recording synchronous and cooperative behaviour in nature, arguably the first scientific remark on syn-

Figure 1.5: A colony of fireflies on a tree. Photo from (Welcome to Malaysia, 2010).

chronisation dates back to the year 1673 when the Dutch physicist Christiaan Huygens examined the behaviour of two coupled pendula, see (Blekhman, 1988; Klarreich, 2002). The pendula were suspended from a double beam and started with arbitrary phases but eventually synchrony was reached, in the sense that they ended up oscillating in an anti-phase manner. Although aware of the potential importance of his discovery, Huygens could not explain this "odd kind of sympathy" as named later by him. Nowadays, this phenomenon has been further studied and labelled as *self–synchronisation* (Blekhman et al., 1997, 2002; Nijmeijer, 2001), because synchronisation occurs in the absence of any external driving signal. It may be distinguished from so–called *controlled synchronisation* where a control input is introduced that ensures the existence of synchronisation between the systems.

Although it had not been discovered until the 17^{th} century, coordinated behaviour in nature may be widely observed. There are many examples where one finds

Figure 1.6: A colony of ants. Photo from (National Geographic, 2011).

cooperative or synchronous behaviour between individual systems. One may mention here, for instance, the collective flashing of fireflies, as shown in Figure 1.5. In (Buck, 1938; Buck and Buck, 1968; Stewart, 1999; Strogatz, 1997) it is described how the fireflies group in trees during the night and start to glimmer at different times. Eventually their glimmers coincide with each other and thus an observable twinkling pattern is created. This glimmering is only performed by the males with the purpose of mating. Nonetheless, it is not straightforward to explain the reason of this distinguishable synchrony which in the past was regarded to be a mere illusion (Buck, 1938; Buck and Buck, 1968). Yet, it seemed to be too much of a coincidence and therefore many scientists have studied this problem ever since. Nowadays, it is believed that by this synchronous twinkling the males are visible to the females from further distances (Stewart, 1999).

Another well-known example of insects that benefit from living in groups are ants, see Figure 1.6. It was pointed out by Miller (2007) that ant colonies have something that is called swarm intelligence which results from adding up simple actions of the individuals and gives rise to such complex actions as finding the best

path to food and defending the colony. The key to understanding their collective behaviour stems from the phenomenon of self-organisation that is the fact that there is no superior ant in the colony that would be in charge (Miller, 2007). Only by collective behaviours - the swarm intelligence - ants indeed manage to achieve the complex actions that would otherwise be infeasible for single ants.

A similar kind of behaviour may be observed in shoals of fish, see Figure 1.7. A shoal consists of a large number of fish that by forming a shoal improve their chances to survive predator attacks and increase probability of mating, see (Viscido et al., 2004). When analysing the complex behaviours of these types of animals, it is especially surprising how actions of fish in the shoal are coordinated once they are in the formation. More so, the coordination of fish is obtained just by communicating with their nearest neighbours, see (Inada, 2001).

The ubiquitous tendency of objects towards a synchronous state may not only be observed within living beings but also among astronomical objects which makes it altogether even more universal. As mentioned by Blekhman et al. (1997), one of the most prominent examples is the moon that always has the same side facing the earth. Such examples also exist in the human body, although the synchronisation phenomena in the human body are not always beneficial as in the case of epilepsy which is caused by excessive synchronous activity of the neuronal cells in the brain (Fisher et al., 2005). On the other hand, an advantageous example of synchronisation in the human body can be found in the regulation of blood pressure as controlled by the kidneys' filtering units which are called nephrons. This mechanism consists in kidneys regulating arterial blood flow by adjusting

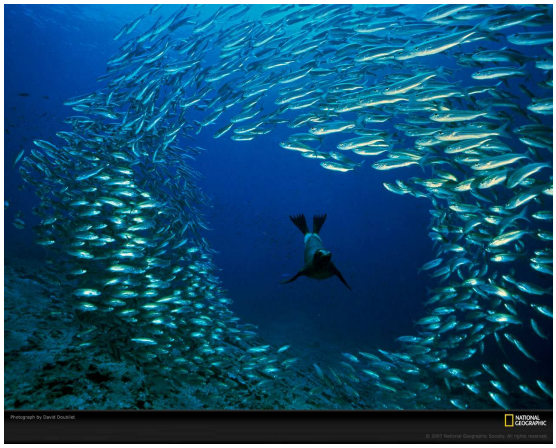

Figure 1.7: An example of a shoal of fish. Photo from (National Geographic, 2011).

the diameter of the smaller blood vessels by means of chemical substances. In particular, synchronisation occurs between neighbouring nephrons that transmit synchronous signals to each other. This is called cross-talk (Mosekilde et al., 2002).

Mindful of the numerous occurrences of synchronisation phenomena in nature, research on implementing a similar behaviour pattern for mobile robots and robotic manipulators has emerged (Ihle et al., 2006; Zou, 2008). In the next section, we demonstrate the most prominent results from our point of view in the area of formation control.

1.5 Previous developments in the area of multiple robot systems

The foregoing discussion has shown how widespread synchronous and coordinated behaviour in nature is. Indeed, observation of nature provides numerous examples of multiple mobile agents acting in cooperation to achieve a common goal. Aware of the advantages that coordinated agents can benefit from, analogous ways of functioning have been introduced for robots that take advantage of working in groups to accomplish the task. Accordingly, in this section we present an overview of the results available in the control systems and robotics literature regarding formation control of mobile robots. The formation control problem has been studied extensively and hence there are many results that introduce different formation control algorithms. In general, they may be classified into three major approaches: the behavioural approach, the leader–follower approach and the virtual structure approach. Each of these approaches are briefly described below.

The behaviour–based approach is supported by the general idea of behavioural robotics, first introduced by Brooks (1986). Within this approach, the formation control problem was examined in (Balch and Arkin, 1998; Dougherty et al., 2004) which both proposed to split up robots' complex behaviour into simple actions such as 'moving to goal' or 'keeping formation'. A clear advantage of the behavioural approach is the intuitiveness of the specific separate actions to be performed by the robots. The meaning of these manoeuvres is self-explanatory

which makes this approach easier to follow and understand. However, because there are no explicit mathematical equations of motion, it is not straightforward to analyse the behaviour of the formation in a mathematical fashion.

Another approach is the leader–follower approach, where one considers two types of robots in the formation: leaders and followers. The leaders are controlled independently, regardless of the behaviour of the followers and are only influenced by e.g. the desired trajectory they are to track. In contrast, the motion of the followers depends on the leaders associated with them. Therefore, the followers need to measure the leaders' states or communicate with them to obtain these data. An important advantage of the leader–follower control scheme is its mathematical simplicity. However, due to the existence of group leaders, the whole formation may fail to execute its task if one of the leaders fails.

Examples of the leader–follower approach are given by e.g. Desai et al. (1998, 2001) who proposed two control algorithms. In the first algorithm the aim was for the follower to maintain a desired distance ℓ and angle Ψ relative to the leader. This was called the $\ell - \Psi$ control. In contrast, in the second proposed control algorithm, the $\ell - \ell$ control, a follower followed two leaders by keeping desired distances to the two leaders. The disadvantages of these two algorithms are certain geometric restrictions of possible shapes that leaders and followers can produce. Moreover, there is no feedback information from the followers to the leaders so in effect the leaders are completely unaware of the follower's actions. This means that they are not equipped with a mechanism that would allow them to react to any malfunctions of the followers and hence the formation behaviour

may be compromised. Furthermore, only constant relative postures that the followers are able to track are considered. However, what makes these strategies interesting is the possibility to create a distributed formation control scheme for a larger number of robots governed by an appropriate segmentation of the whole formation into subgroups of two or three robots in such a way that the followers in one subgroup may be leaders in other pairs or trios of robots. Then, each of these groups may be treated individually using either one of the controllers. Therefore, there is no need for extensive communication, since all robots only transmit information to and receive from other robots in their small groups of two or three robots. However, having in mind the principles of the $\ell - \Psi$ and $\ell - \ell$ strategies, there are robots in the formation that de facto lead the whole group and so the behaviour of the whole formation depends heavily on the adequacy of these robots which may prove to be fault–prone.

The idea of the follower maintaining desired distance and angle with respect to the leader was also the subject of the work in (Li et al., 2005) and (Consolini et al., 2007). The first of these papers considered Cartesian coordinates to represent the desired position of the follower relative to the leader as opposed to polar coordinates used in the $\ell - \Psi$ strategy. By doing so, it was possible to get rid of the singularities in the control design of the original research in which the idea of relative posture tracking was concerned (Desai et al., 1998, 2001). However, due to the nature of the controller as in (Desai et al., 1998, 2001), the result in (Li et al., 2005) also inherently disregards the possibilities of the follower changing its desired distance relative to the leader. In the second paper (Consolini et al., 2007), the authors accounted for actuator limitations in that the control

law ensured saturated inputs. Moreover, contrary to the developments in (Desai et al., 1998, 2001; Li et al., 2005) where the position of the follower with respect to the leader was rigorously given, in (Consolini et al., 2007) the relative position of the follower with respect to the leader is situated in a cone centred at the leader. Hence, arguably, more flexibility of the formation follows. In turn, in (Chen et al., 2010) a leader–follower controller was developed based in principle on the $\ell - \ell$ or $\ell - \Psi$ strategies in which a receding-horizon scheme was employed. The receding-horizon scheme was presented in (Fontes, 2001; Mayne and Michalska, 1990; Mayne et al., 2000; Michalska and Mayne, 1989) and was incorporated in the leader–follower strategy in (Chen et al., 2010) to improve the convergence speed. However, relying purely on a one–way communication between the leader and the follower, as in the other papers proposing the leader–follower strategies mentioned above (Consolini et al., 2007; Desai et al., 1998, 2001; Li et al., 2005), may result in faults since the leader has no means of verifying the follower's functioning.

The authors of (Consolini et al., 2007) also used their control strategy to develop a scheme for a formation of multiple robots similar to the extension of the algorithms in (Desai et al., 1998, 2001) that we proposed earlier. The idea is such that the whole formation is divided into a number of subgroups and then leaders in one group are possibly followers in another group and so on. This is interesting because it implies that a control strategy that may be believed to work for a pair of robots only in fact works for a larger number of robots as well which consequently extends the applicability of that controller.

The leader–follower approach in the case of industrial manipulators was examined by Rodriguez-Angeles and Nijmeijer (2001a,b, 2003). It was found that in the so–called master–slave scheme, the slave system was synchronised with the master system by measuring the master system's angular position, without any knowledge of the master system's dynamics. Also Nuño et al. (2008) studied the master–slave approach for robotic manipulators with the distinction that they in particular considered the bilateral teleoperation task. Since in teleoperation the master and slave systems are normally remote from each other, time–delays are inevitable and thus communication time–delays were taken into consideration in (Nuño et al., 2008). The proposed control law is based in principle on a simple PD scheme. The bilateral teleoperation was also the subject of the work of Forouzantabar et al. (2011). These results aimed to improve transparency of teleoperation with respect to some previous work and used a PID controller. By transparency in bilateral teleoperation it is understood how precisely the human operating the master system can sense the environment through the slave system using the feedback from the slave system as compared to when the human would operate in the environment directly. Note that the results in (Forouzantabar et al., 2011; Nuño et al., 2008; Rodriguez-Angeles and Nijmeijer, 2001a,b, 2003) apply to robotic manipulators and thus cannot be directly employed for mobile robots.

The third category is the virtual structure approach in which in a certain sense the behaviour of the formation is summarised in that of a so-called virtual structure. The virtual structure is to track a given desired trajectory. Then, knowing the behaviour of the virtual structure, this behaviour is converted to that of indi-

vidual robots by imposing a certain formation shape with respect to the virtual structure. In comparison to the leader-follower approach, it may therefore be argued that the virtual structure approach allows for a greater deal of robustness as it does not depend critically on a single real (as opposed to virtual) unit. Algorithms utilising the virtual structure approach for a formation of multiple spacecraft are presented in, among others, (Ren and Beard, 2002, 2003, 2004), where the authors added a formation feedback term to the control input applied to the virtual structure to accommodate the vehicles' actual performance. Similarly in (Tan and Lewis, 1996), the control law is also constructed in such a way that should a robot in a formation be faulty, the virtual structure is to react. The disadvantage of the scheme presented in (Tan and Lewis, 1996) is that it makes allowances for constant formation geometries only. Likewise, in the scheme given in (Dong and Farrell, 2008; Dong et al., 2006) also only constant formation shapes are considered. One may argue that this feature limits the applicability of controllers and to some degree this prompted our study. The issue of time–varying formation shapes was also examined by Kostić et al. (2010b) who also studied the problem of controlling multiple mobile robots using the virtual structure approach and proposed a saturated control law where all robots in the formation communicate with all other robots to perform the formation task (all-to-all communication). Therefore, as in the aforementioned papers, the formation can react to possible perturbations. Nonetheless, it is not the virtual structure that acts in response to the perturbation but individual robots in the formation. Because of the communication between the robots, they react to possible perturbations of other robots in the formation. However, the all-to-all communication structure where all robots need to exchange information with each other in (Kostić et al.,

2010b) may not be efficient due to possibly many communication links between robots, especially in the case of a large number of robots in the formation. Also in (Do and Pan, 2007) time–varying formations were considered and a dynamic robot model and observer theory were used to estimate unmeasurable quantities. To develop the control algorithm, a backstepping technique is utilised and consequently, the resultant control algorithm is rather complex in form. Moreover, the communication structure proposed in (Do and Pan, 2007) may prove to be inefficient since it again relies on an all-to-all communication strategy. In addition to these papers, Lalish et al. (2006) studied a problem of formation control, primarily for a group of aircraft, and in the first instance introduced a completely decoupled control scheme for agents in the formation. This approach poses a question of applicability of this strategy in the sense that should any disturbances occur to any of the agents, the rest of the formation has no way to respond to it. Having said that, in the second instance, another control strategy was introduced in (Lalish et al., 2006). That algorithm employs an inter–agent collision avoidance scheme for spacecraft during manoeuvres. Yet, the control strategy requires calculating avoidance variable to localise a possible upcoming collision between all pairs of robots. As mentioned earlier, this kind of communication topology – the all-to-all communication – may be very resource–consuming and hence possibly undesirable.

The discussion about the possible flaws of the all-to-all communication structure has lead us to a different type of division of formation control algorithms. Accordingly, the formation control algorithms can be classified into those requiring a global or a local communication network, see Figures 1.8 and 1.9. In particular, in

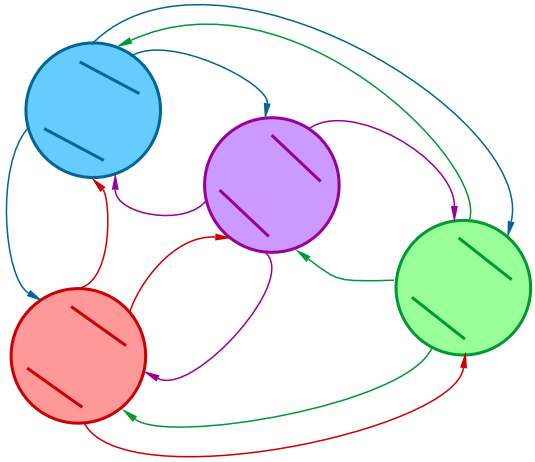

Figure 1.8: An example of a formation with a global communication network. Each agent communicates with every other robot. This is denoted by arrows representing the direction of the information flow between the robots.

algorithms employing a global communication network (all-to-all communication) all robots in the formation need to communicate with all remaining robots, see e.g. (Kostić et al., 2010b; Van den Broek et al., 2009). This type of communication structure is sometimes referred to as centralised, although this term is ambiguous in that centralised control algorithms are also those with a central governing unit. As briefly mentioned earlier, a global communication structure is burdened with high communication cost which may need to be reduced. Therefore, in formation control algorithms incorporating a local communication network, robots in the formation do not need to exchange information with all remaining robots but instead they communicate with robots in their communication neighbourhood only, see (Dong and Farrell, 2008; Jadbabaie et al., 2003; Lawton et al., 2003; Moshtagh and Jadbabaie, 2007; Ren and Sorensen, 2008; Sun et al., 2009; Wu

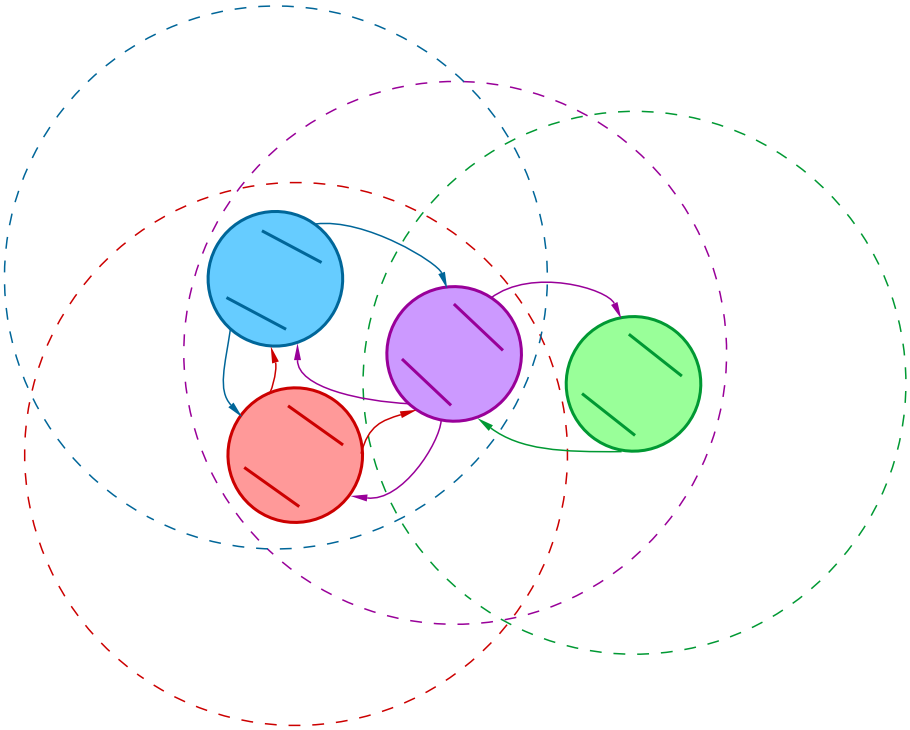

Figure 1.9: An example of a formation with a distributed communication network. Each agent is assigned with a neighbourhood marked by a circle of the same colour as the robot. The arrows denote the direction of the information flow between the robots.

et al., 2007). Such algorithms relying on local interactions between robots are called distributed or decentralised. Note that the term decentralised may also be considered more generally and refer to those control algorithms that do not have a central governing unit. Interesting results in this field are those in (Jadbabaie et al., 2003) where a coordination algorithm based on a nearest neighbour rule was proposed. Also in the more recent paper (Moshtagh and Jadbabaie, 2007), the authors contributed in the area of distributed control and studied a problem of flocking for which a distributed geodesic control law was given. This scheme

relates to coordination and velocity alignment of nonholonomic mobile agents to obtain flocking by means of minimising a so–called misalignment energy. Clearly, in comparison to the work communicated in this thesis, both (Jadbabaie et al., 2003) and (Moshtagh and Jadbabaie, 2007) consider the flocking control problem as opposed to the formation control problem.

Also in (Lafferriere et al., 2005) a decentralised formation control algorithm was proposed. The authors developed a condition for agents converging to their desired positions within the formation based on connectivity of the communication graph of the formation. Moreover, if one of the agents in the formation is steered independently, a kind of a leader–follower scheme follows in which all other robots follow the independently steered robot due to local interactions. However, this controller only works for agents with linear dynamics. Hence, its applicability is questionable. This is not an issue in (Dong, 2011) in which a decentralised formation control algorithm is given for nonholonomic robots for which both kinematic and dynamic models are considered. More specifically, this paper concerns a stabilisation task in which robots are to converge to a given desired formation shape and equate their orientations on the plane. To this end, a backstepping based controller is developed for which robustness to communication time–delay is analysed. In relation to the work in this thesis, the results in (Dong, 2011) concern a stabilisation task to a desired formation shape as opposed to a trajectory tracking task.

The above control algorithms apply either to a general nonholonomic system in chained form eg. (Dong and Farrell, 2008; Dong et al., 2006), spacecraft (Ren

and Beard, 2002, 2003, 2004) or unicycle mobile robot eg. (Kostić et al., 2010b; Van den Broek et al., 2009). On the other hand, to our knowledge, only little work regarding specifically formations of car–like nonholonomic mobile robots has been performed. This includes (Ramaswamy and Balakrishnan, 2008) which proposed a control scheme based on the leader–follower strategy. In particular, again the idea of the follower maintaining desired distance and angle between itself and the leader was studied on the level of the robots' dynamics, as opposed to solely kinematics of the robots. However, inherent to the principles of the leader–follower scheme, this strategy is also burdened with a disposition to failure since it is highly dependent on a single unit. Also (Hsu and Liu, 2005) exploited the leader–follower scheme but in addition it also included some results in the realm of the behavioural approach to formation control. The strategy, as per principles of behavioural robotics, is such that individual behaviours like goal seeking or obstacle avoidance are combined to create the overall formation control. However, clearly both approaches bear the normal disadvantages of the leader–follower and behavioural approach, as mentioned earlier. Nonetheless, the article goes deeper into the problem of formation control and also considered the cooperative control of multiple robot teams (see also (Chung and Slotine, 2009)). Consequently, the robots use a set of behaviours to not only individually join a pre-existing formation or to remove itself from the formation but also to merge or split two existing formations.

This summarises the main current results in the area of cooperative behaviour of mobile robots. We are now able to present contributions of this thesis that are aimed to tackle some of the existing problems in the area of formation control of

mobile robots.

1.6 Main contributions and outline

In this section, we identify the contributions of this thesis. Further to the earlier discussions, the aim of our research is to design a formation control law in which robots in the formation follow a given desired trajectory as a whole and form a desired formation geometry. To this end, we consider the dynamic equation of motion of mobile robots and based on this we develop control algorithms to solve the formation control problem. The main contributions of the thesis are placed in Chapters 3, 4 and 5. We briefly review them in Table 1.1.

The outline of the thesis and a more detailed description of the main contributions of the thesis listed in Table 1.1 are as follows.

Chapter 2 In this chapter we derive mathematical models of motion of a mobile robot. Since our research concerns unicycle mobile robots and car–like mobile robots, dynamic models for both types of robots are presented. Afterwards, we formally formulate the formation control problem that is considered in this thesis. To this end we translate the verbal description of the formation control problem studied in this thesis into desired mathematical behaviours of individual robots in the formation. Then, we show the equivalence of the formation control problem with convergence to zero of appropriately defined error variables of each robot in the formation. This

Chapter number	Main contributions
Chapter 3	• a formation controller based on the kinematic model of a unicycle robot • a dynamic formation controller for a dynamic model of a robot • a saturated formation controller to account for actuators limitations • analysis of the influence of the communication between the robots
Chapter 4	• explicit definition of the coordination error between a pair of robots in a formation • a formation controller ensuring explicitly both trajectory tracking and coordination • a formation controller in which only coordination between the robots in achieved • a saturated controller ensuring directly trajectory tracking and coordination
Chapter 5	• a formation controller for car-like mobile robots • extension of the formation controller to ensure coordination of robots only

Table 1.1: A list of major contributions of the thesis.

lays foundations for the introduction of our developments – the formation control algorithms – in the subsequent chapters.

Chapter 3 After the general formulation of the formation control problem, we are now able to present our main results. In this chapter, we propose a controller for formation control of unicycle mobile robots using the cascaded approach. In principle, this approach allows to redefine the stability analysis of a complicated nonlinear system into stability analysis of two simpler systems when additional conditions on the interconnecting term hold. Using this method, we are able to design a formation control algorithm in which a standard tracking controller is supplemented with mutual coupling terms

to account for robots interactions. The importance of the mutual coupling terms can be specifically viewed when some of the robots are subject to a perturbation. In such circumstances, through inter–robot communication, robots are aware of possible problems occurring to other robots and hence can try to counteract the perturbations. In a similar way, the formation control problem was tackled in (Van den Broek et al., 2009). However, our work advances this paper in several ways. First of all, the control algorithm in (Van den Broek et al., 2009) was only studied for two robots in the formation while our contribution covers the case of an arbitrary number of robots in the formation. Moreover, the results in (Van den Broek et al., 2009) provide only a local convergence proof as opposed to a global convergence which is warranted in our contribution.

This nominal controller is then extended into a novel dynamic formation control algorithm in which both a dynamic and kinematic model as opposed to solely a kinematic model is considered. Moreover, we also propose an extension of the nominal controller in which actuator limitations are explicitly taken into account. This extension is particularly important in practice as clearly for actual robots input magnitudes are limited due to technical restrictions. Arguably, this aspect was also missing in (Van den Broek et al., 2009). After the introduction of the formation control algorithms and the stability analysis of the closed–loop error dynamics, we validate the applicability of the algorithms in simulations for all three controllers and in experiments for the nominal controller.

It is worth noting that the formation control algorithms presented in this

chapter are distributed which means that robots in the formation are only able and required to communicate to their neighbours as opposed to all other robots. This, from our point of view, is a considerable contribution with respect to other results available in the literature (Kostić et al., 2010b; Lalish et al., 2006; Van den Broek et al., 2009) as it reduces the communication costs. Furthermore, contrary to the results presented in (Dong and Farrell, 2008; Dong et al., 2006) where only constant formation shapes were taken care of, we allow for time–varying formation shapes. Hence this is a more useful and applicable approach.

The results presented in Chapter 3 are partially done in collaboration with colleagues at Eindhoven University of Technology, the Netherlands who acted as advisors on the topics included in this chapter and helped with performing the experiments. These results are in part published in (Sadowska et al., 2011a,b).

Chapter 4 In this chapter we propose another solution to the formation control problem for unicycle mobile robots using control algorithms derived by explicitly defining the coordination error between a pair of robots. Note that in the developments in Chapter 3, coordination was obtained implicitly via tracking control of all robots with additional terms representing inter-robot communication. Here, the coordination of robots is explicitly acted upon. To this end, we express all tracking errors as well as the coordination errors in the world frame, whereas in the literature, the tracking error is normally expressed in the local coordinate frame of each robot. This concerns the literature in the field of the tracking control of a unicycle robot. Similarly,

tracking errors in local coordinate frames are also normally used in the literature regarding the formation control in which trajectory tracking is one of the objectives of the robots in the formation (Kostić et al., 2010b; Van den Broek et al., 2009) including our own work presented in the previous chapter. However, in the scenario discussed in this chapter, using the tracking error variables expressed in the world frame proves to lend itself to be more useful in the stability analysis. Moreover, it lays the foundations to show that for robots to be coordinated with each other, tracking errors should be in consensus (Olfati-Saber and Murray, 2003a, 2004) with each other. By coordination of robots we understand robots forming the desired formation shape regardless of the trajectory tracking of the formation. In this sense, the work presented in this chapter advances the previous results derived using the cascaded approach in that here robots explicitly act towards coordination of robots in the formation.

We propose four control algorithms in this setting. The first, most basic algorithm assures that robots track a desired trajectory as an entity and create a desired formation shape. In the second algorithm, the formation is only guaranteed to achieve its desired geometry without necessarily tracking the desired trajectory. To our best knowledge, studying this *Pure Coordination*, as we named it, is novel in the robotics literature. The third algorithm solves the formation control problem in which one of the robots is chosen to be superior to the others and acts as a leader. The followers follow the leader through local communication. The fourth algorithm is an extension of the first algorithm in which actuator constraints are taken into account. We perform simulation and experimental studies to show how the proposed

strategies work in practice.

The results in Chapter 4 also benefit from their distributed character which makes them arguably superior to the results in (Kostić et al., 2010b; Lalish et al., 2006; Van den Broek et al., 2009). Moreover, as in the results in Chapter 3 time–varying formation geometries are allowed.

Our work presented in Chapter 4 is partially included in the publication (Sadowska et al., 2012). Similarly to the results given in Chapter 3, these results have been obtained as a collaborative effort with colleagues from Eindhoven University of Technology who partially supervised this work as well as helped with collecting the experimental data.

Chapter 5 Subsequent to the formation control algorithms for unicycle mobile robots we present a formation control algorithm for car–like mobile robots. This was inspired by scrutinising the existing literature in the realm of formation control. It was shown in Section 1.5 that available results for formation control of car–like mobile robots are rather limited. Arriving at this conclusion has instigated our research in this field.

The approach presented here is based on the virtual structure approach and as such it may be considered preferable to other existing algorithms for car–like robots (Hsu and Liu, 2005; Ramaswamy and Balakrishnan, 2008) that are mostly based on the leader–follower approach. The benefit is that in the virtual structure strategies, there are no leaders and in general all robots are considered as equal. Therefore, failure of any single robots will in principle not result in failure of the whole formation. Contrariwise, in the leader–follower strategies, the performance of a single robot – the leader

– is vital for the formation.

The derivation of the formation control algorithm is similar to the one in Chapter 4 in that the coordination error for a robot is expressed in a coordinate frame in which also the tracking error for this robot is expressed. In Chapter 4 this was the world frame and hence the coordinate frame was ultimately identical for all robots. However, while in Chapter 4 it proved useful to express all errors in the global coordinate frame, in Chapter 5 we express the coordination errors as well as tracking errors of each individual robot in a local coordinate frame associated with this robot. By doing so, the analysis is more straightforward mathematically in the settings given in Chapter 5 as opposed to a common global coordinate frame for all robots as used in Chapter 4. Having said that, in the proofs we still end up with expressions in terms of the tracking errors given in the world frame and so we again arrive at the conclusion that the formation shape maintenance is equivalent to the consensus of the tracking error variables given in the world frame. Note that while in Chapters 4 and 5 slightly modified definitions of tracking and coordination errors are used, the results for either definition of the tracking and coordination errors are equivalent. The choice of the particular coordinate frame in each of the chapters follows from the convenience of the mathematical analysis in the particular settings.

The formation control algorithm introduced in Chapter 5 is designed using the backstepping technique. To confirm the applicability of the formation control algorithm, we include simulation results.

Chapter 6 In this chapter, we perform simulations study for all major forma-

tion control algorithms introduced in the thesis in Chapters 3, 4 and 5. This is to compare the performance yielded by each of the algorithms to distinguish strengths and possible weaknesses of each of the algorithms in various circumstances.

Chapter 7 In the last chapter of the thesis we present our concluding remarks on the subject of the formation control problem. We also propose further work that could be done in the realm of the formation control problem.

Appendix A In this appendix we present some mathematical results regarding the material that is being used throughout the thesis.

Appendix B In this appendix we concentrate on the stability analysis of dynamical systems. In particular we first introduce the Lyapunov direct method, then we discuss stability of invariant sets. Afterwards, we elaborate on stability analysis of an equilibrium of a cascaded system and at the end we present the backstepping technique.

Appendix C This appendix presents some basic definitions and facts regarding graph theory.

Appendix D This appendix gives a brief description of the E-Puck mobile robot that is used in experiments in this thesis.

Chapter 2

Modeling and problem statement

In this chapter we first derive kinematic and dynamic models of nonholonomic mobile robots in Section 2.1. Then, in Section 2.2, we formulate the formation control problem.

2.1 Mathematical model of a nonholonomic mobile robot

In this section we derive mathematical models of nonholonomic mobile robots: in Subsection 2.1.1 a model of a unicycle mobile robot, in Subsection 2.1.2 a model of a car–like mobile robot and in Subsection 2.1.3 we describe a chained–form representation of a kinematic model of a generic nonholonomic mobile robot.

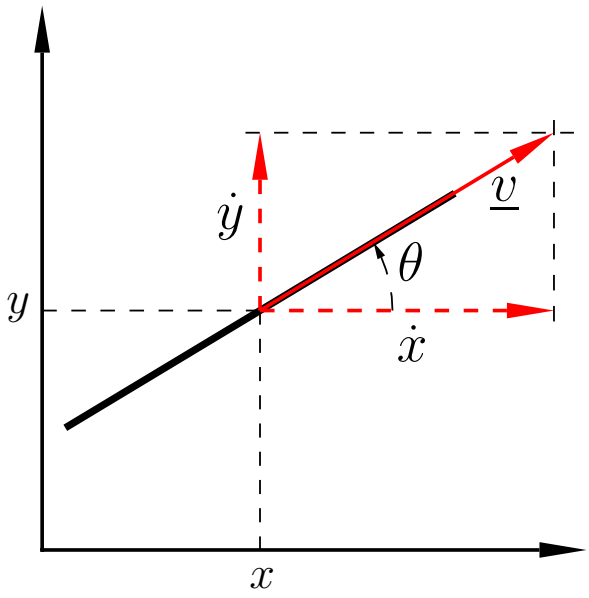

Figure 2.1: Orthogonal projection of a robot wheel (view from the top of the wheel).

The kinematic model of a mobile robot is normally obtained from nonholonomic constraints on the mobility of the robot. In general, we consider two types of constraints: the lateral slip constraint and the longitudinal slip constraint (Campion et al., 1991; De Wit et al., 1996). The lateral slip constraint stems from the inability of robot wheels to move sideways. Wheel velocity may be decomposed into two components as shown in Figure 2.1

$$\begin{aligned} \dot{x} &= v\cos\theta, \\ \dot{y} &= v\sin\theta, \end{aligned} \tag{2.1}$$

in which v is the forward speed of the robot.

By multiplying the first equation by $\sin\theta$ and the second one by $\cos\theta$ and adding

both equations, one obtains

$$\dot{x}\sin\theta - \dot{y}\cos\theta = 0, \tag{2.2}$$

which is the lateral slip constraint. In contrast, the longitudinal slip constraints result from the assumption that there is no longitudinal slip of the robot's wheels, which implies that

$$v = R\dot{\varphi}, \tag{2.3}$$

where φ is the angular velocity of the wheel and R is the radius of the wheel, see Figure 2.2. Noting that from (2.1) it follows that $v = \dot{x}\cos\theta + \dot{y}\sin\theta$, we thus obtain

$$\dot{x}\cos\theta + \dot{y}\sin\theta - R\dot{\varphi} = 0. \tag{2.4}$$

It can be shown that the kinematic constraints given by (2.2) and (2.4) cannot be integrated, i.e. there does not exist a function $f(x, y, \theta, \varphi)$ such that the constraints are equivalent to $\dfrac{d}{dt}f(x, y, \theta, \varphi) = 0$. This kind of constraints is called *nonholonomic*. Conversely, if constraints can be integrated, they are named *holonomic* constraints. As an example of holonomic constraints, consider the following dynamic system (Lefeber, 2000)

$$\begin{aligned} \dot{x} &= \ \omega y, \\ \dot{y} &= -\omega x, \end{aligned} \tag{2.5}$$

which implies the velocity constraint

$$x\dot{x} + y\dot{y} = 0. \tag{2.6}$$

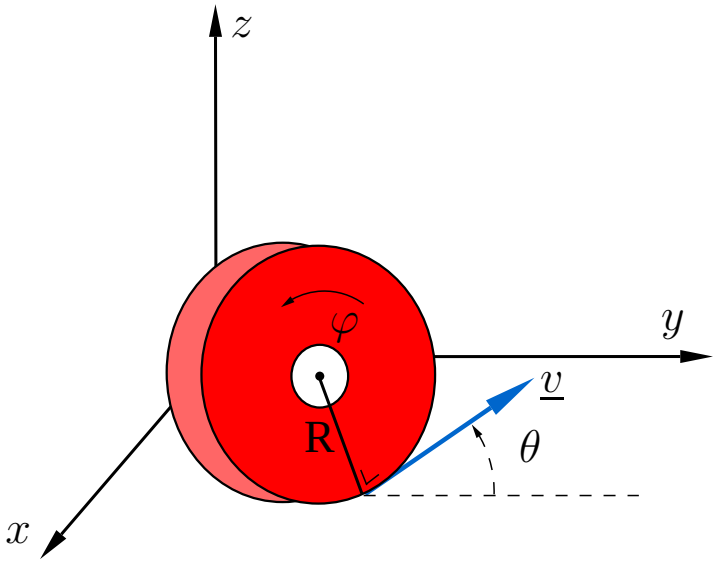

Figure 2.2: Mobile robot's wheel.

Equation (2.6) may be integrated to yield

$$\frac{1}{2}x^2 + \frac{1}{2}y^2 = c, \tag{2.7}$$

where $c \in \mathbb{R}^+$. Hence (2.6) is a holonomic constraint.

All nonholonomic constraints that apply to a particular robot may be grouped and presented in the matrix form $A(q)\dot{q} = 0$, where $A(q)$ is the so–called Pfaffian matrix associated with the nonholonomic constraints and q is the vector of generalised positions. For example, given that mobile robot's constraints are (2.2) and (2.4), the Pfaffian matrix is

$$A = \begin{bmatrix} \sin\theta & -\cos\theta & 0 & 0 \\ \cos\theta & \sin\theta & 0 & -R \end{bmatrix}. \tag{2.8}$$

The kinematic model of the robot is then

$$\dot{q} = G(q)\eta, \tag{2.9}$$

where the matrix $G(q)$ contains linearly independent column vectors $g_i(q)$ such that $g_i(q) \in \ker A^T(q)$ and η is a vector of auxiliary velocities. For the Pfaffian matrix in (2.8), the resultant matrix $G(q)$ is calculated as

$$G = \begin{bmatrix} \cos\theta & 0 \\ \sin\theta & 0 \\ 0 & 1 \\ \frac{1}{R} & 0 \end{bmatrix}. \tag{2.10}$$

At this point, it is worth to mention that one can use the well-known Frobenius theorem (Bloch, 2003; Sastry, 1999) to determine whether a dynamic system (2.9) is nonholonomic or holonomic. This is particularly interesting since it may be very difficult to verify the integrability of the constraints *per se*. From the Frobenius theorem it can be deduced that a system (2.9) is holonomic if the distribution $\Delta = \text{span}\{g_1(q), \ldots, g_r(q)$, in which r is the dimension of the null space of $A^T(q)$, is involutive, i.e. we have that $g_i(q), g_j(q) \in \Delta$ implies that $[g_i(q), g_j(q)] \in \Delta$. Here, $[g_i(q), g_j(q)]$ denotes the Lie bracket (Sastry, 1999) defined as

$$[g_i(q), g_j(q)] = \frac{\partial g_j}{\partial q} g_i - \frac{\partial g_i}{\partial q} g_j. \tag{2.11}$$

Using this result, we can show that for the system in (2.5), we have that

$$g_1(q) = \begin{bmatrix} 0 \\ -\omega y \end{bmatrix}, \quad g_2(q) = \begin{bmatrix} \omega x \\ 0 \end{bmatrix} \quad \text{and} \quad [g_i(q), g_j(q)] = \begin{bmatrix} 0 \\ 0 \end{bmatrix}, \tag{2.12}$$

which confirms the holonomic nature of the constraint in (2.6) as shown earlier.

For the sake of simplicity, we only consider the lateral slip constraint in the sequel.

2.1.1 Unicycle mobile robot

Consider a unicycle mobile robot as depicted in Figure 2.3. The state vector $q = \text{col}(x, y, \theta)$ denotes position (x, y) of the centre of mass of the robot and orientation θ with respect to the horizontal axis, respectively. The control inputs are the forward velocity v and the angular velocity ω.

It is assumed that the robot moves without side slip which is equivalent to the nonholonomic constraint in (2.2). Hence, the matrix $G(q)$ is given by

$$G(q) = \begin{bmatrix} \cos\theta & 0 \\ \sin\theta & 0 \\ 0 & 1 \end{bmatrix}, \tag{2.13}$$

and the kinematic model immediately follows (Campion and Chung, 2008; De Wit

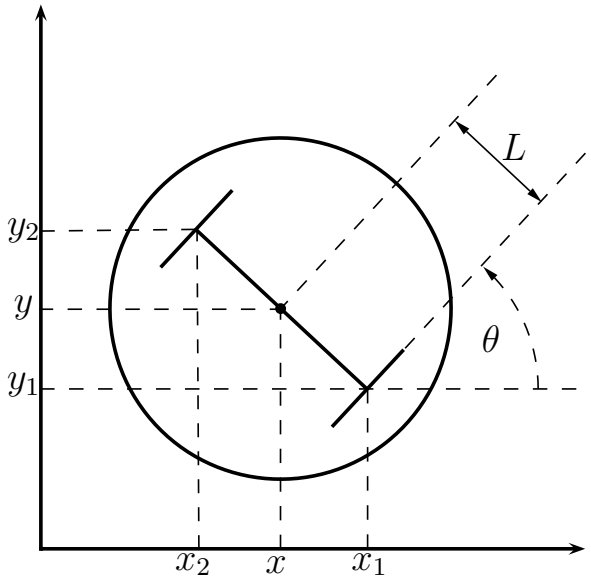

Figure 2.3: A unicycle-type mobile robot. (x, y) denote the position of the barycentre of the robot, (x_1, y_1) and (x_2, y_2) denote the centres of the two wheels of the robot and θ stands for the orientation with respect to the inertial horizontal axis.

et al., 1996; Siciliano et al., 2009):

$$\begin{aligned} \dot{x} &= v\cos\theta, \\ \dot{y} &= v\sin\theta, \\ \dot{\theta} &= \omega. \end{aligned} \tag{2.14}$$

In addition to the kinematic model of a unicycle robot, we can also obtain the dynamic model. Normally, it may be obtained using either the Newton's Second Law of Motion or the Euler–Lagrange formalism. We use the first approach and

arrive at (cf. (Jiang and Nijmeijer, 1997; Panteley et al., 1998)):

$$\begin{aligned} \dot{v} &= \frac{F}{m}, \\ \dot{\omega} &= \frac{\tau}{J}, \end{aligned} \tag{2.15}$$

in which m denotes the mass of the robot, J is its moment of inertia around the vertical axis passing through its centre of mass and the control inputs F and τ denote force and torque respectively. The full dynamic model of a unicycle mobile robot is then given by

$$\begin{aligned} \dot{x} &= v\cos\theta, \\ \dot{y} &= v\sin\theta, \\ \dot{\theta} &= \omega, \\ \dot{v} &= \frac{F}{m}, \\ \dot{\omega} &= \frac{\tau}{J}. \end{aligned} \tag{2.16}$$

2.1.2 Car–like mobile robot

A simple schematic of a car–like mobile robot is given in Figure 2.4. Here, the state vector is $q = \mathrm{col}(x, y, \theta, \varphi)$ denoting the robot's Cartesian position (x, y) of the mid–point of the robot's rear axle, orientation of the robot's body θ and front wheel steering angle φ.

We consider two constraints for rolling–without–slipping, one for the mid–point of the rear axle

$$\dot{x}\sin\theta - \dot{y}\cos\theta = 0, \tag{2.17}$$

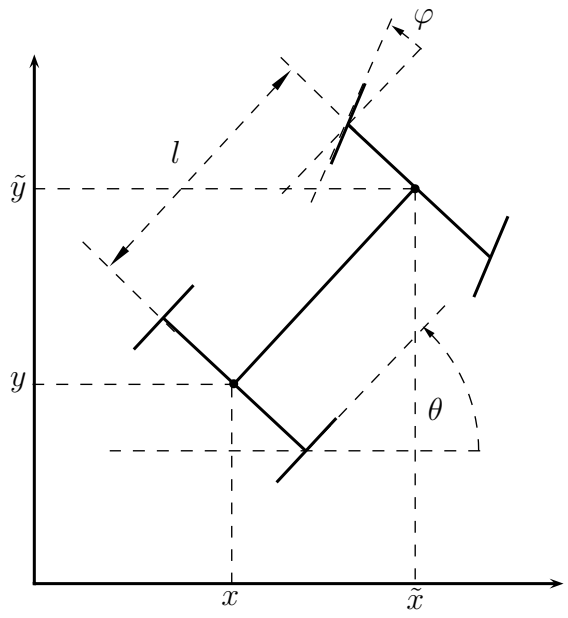

Figure 2.4: A car–like mobile robot. (x, y) denotes the position of the centre of the rear axle of the robot, $(\tilde{x}, \tilde{y})$ denotes the centre of the front axle of the robot, θ stands for the orientation with respect to the inertial horizontal axis and φ is the wheel steering angle.

and one for the front axle

$$\dot{\tilde{x}} \sin(\theta + \varphi) - \dot{\tilde{y}} \cos(\theta + \varphi) = 0. \tag{2.18}$$

Keeping in mind the dependence of $(\tilde{x}, \tilde{y})$ on (x, y):

$$\begin{aligned} \tilde{x} &= x + l \cos\theta, \\ \tilde{y} &= y + l \sin\theta, \end{aligned} \tag{2.19}$$

we obtain the counterpart of (2.18) in terms of (x, y)

$$\dot{x}\sin(\theta+\varphi) - \dot{y}\cos(\theta+\varphi) - \dot{\theta}l\cos\varphi = 0. \tag{2.20}$$

Then, the associated Pffafian matrix is given by

$$A = \begin{bmatrix} \sin\theta & -\cos\theta & 0 & 0 \\ \sin(\theta+\varphi) & \cos(\theta+\varphi) & -l\cos\varphi & 0 \end{bmatrix}, \tag{2.21}$$

and consequently the kinematics of a car–like robot follows forthwith (De Luca et al., 1998; De Wit et al., 1996; Morin and Samson, 2006; Murray et al., 1994; Siciliano et al., 2009; Spong et al., 2006):

$$\begin{aligned} \dot{x} &= v\cos\theta, \\ \dot{y} &= v\sin\theta, \\ \dot{\theta} &= \frac{v}{l}\tan\varphi, \\ \dot{\varphi} &= \omega, \end{aligned} \tag{2.22}$$

in which v is the robot's forward velocity and ω is the front wheel's angular velocity. Model (2.22), with such a choice of the kernel of the Pfaffian matrix A (2.21), becomes singular when $\varphi = \pm\frac{\pi}{2}$ which is equivalent to the front wheels being perpendicular to the car body. Understandably, a car–like robot (5.1) is not controllable in this situation which can also be verified by checking the Lie Algebra rank condition (De Luca et al., 1998; Isidori, 2000). However, as pointed out in (De Luca et al., 1998) this is not a problem in most cases because of a restricted range of φ in practice and the ability to directly control φ. Moreover,

one might choose an alternative kernel of matrix A, for example such that matrix G is given by

$$G(q) = \begin{bmatrix} \cos\theta\cos\varphi & 0 \\ \sin\theta\cos\varphi & 0 \\ \dfrac{\sin\varphi}{l} & 0 \\ 0 & 1 \end{bmatrix}. \tag{2.23}$$

The disadvantage of it, though, is the fact that while in (2.22) the control inputs v and ω have practical meaning, in (2.23) the meaning of the control inputs is less obvious.

2.1.3 Chained form representation of kinematics of a nonholonomic mobile robot

The chained form is a special representation in which kinematic equation of motion of nonholonomic systems can be presented:

$$\begin{aligned} \dot{x}_1 &= u_1, \\ \dot{x}_2 &= u_2, \\ \dot{x}_3 &= x_2 u_1, \\ &\vdots \\ \dot{x}_n &= x_{n-1} u_1. \end{aligned} \tag{2.24}$$

It is a well–known fact that a chained form can be obtained for numerous nonholonomic systems by means of a local or global coordinate transformation (De Wit

et al., 1996; Leroquais and d'Andrea Novel, 1995; Murray and Sastry, 1993). This includes the unicycle mobile robot (2.14), when the following state transformation

$$\begin{aligned} x_1 &= \theta, \\ x_2 &= x\cos\theta + y\sin\theta, \\ x_3 &= x\sin\theta - y\cos\theta, \end{aligned} \tag{2.25}$$

and input change

$$\begin{aligned} u_1 &= v\cos\theta, \\ u_2 &= \frac{1}{\cos^2\theta}\omega. \end{aligned} \tag{2.26}$$

are applied. This change of coordinates is only local as it is singular for $\theta = \pm\frac{\pi}{2}$ (De Wit et al., 1996; Morin and Samson, 2008). A global transformation (De Luca et al., 1998) of the unicycle robot model (2.14) into the chained form can be obtained if we redefine u_1 and u_2 as

$$\begin{aligned} u_1 &= \omega, \\ u_2 &= v - x_3\omega. \end{aligned} \tag{2.27}$$

Similarly, the kinematics of a car–like robot (2.22) can be transformed into the chained form. To this end, one uses the well-known coordinate change (De Luca et al., 1998; De Wit et al., 1996; Morin and Samson, 2006; Murray et al., 1994;

Siciliano et al., 2009; Spong et al., 2006)

$$\begin{aligned} x_1 &= x, \\ x_2 &= \frac{\tan\varphi}{l\cos^3\theta}, \\ x_3 &= \tan\theta, \\ x_4 &= y, \end{aligned} \tag{2.28}$$

and the input transformation

$$\begin{aligned} u_1 &= v\cos\theta, \\ u_2 &= \frac{l\omega\cos^2\theta + 3v\sin\theta\sin^2\varphi\cos\theta}{l^2\cos^3\theta\cos^4\varphi}. \end{aligned} \tag{2.29}$$

From (2.28) and (2.29) it is visible that the chained form for (2.22) is defined excluding $\theta = \pm\frac{\pi}{2}$ and for $\varphi \neq \pm\frac{\pi}{2}$, see (De Luca et al., 1998) for details.

2.2 General formulation of the formation control problem

In this section we give a formal problem statement of the formation control problem studied in this thesis.

Consider a formation consisting of N nonholonomic mobile robots with identical dynamics

$$\dot{q}_i = f_i(t, q_i, u_i), \qquad (i = 1, \ldots, N) \tag{2.30}$$

where $f_i(t, q_i, u_i)\colon \mathbb{R} \times \mathbb{R}^n \times \mathbb{R}^m \to \mathbb{R}^n$, $q_i \in \mathbb{R}^n$ and $u_i \in \mathbb{R}^m$ is the robot's control input. Let $\mathcal{I} = \{1, \ldots, N\}$ denote the set of indices of robots in the formation. Without loss of generality, let the state vector q_i be such that $q_i = \mathrm{col}(p_i, r_i)$, where $p_i = \mathrm{col}(x_i, y_i)$ denotes the Cartesian position of a representative point of the robot i and r_i is the remaining part of the state vector. In the case of a unicycle robot $r_i = \theta_i$ and for a car–like mobile robot $r_i = \mathrm{col}(\theta_i, \varphi_i)$.

The formation control problem studied in this thesis requires robots to converge to a desired formation shape and for such a formation as a whole to track a given desired trajectory denoted as $q_{vc}^d(t)$. To solve a problem defined like this, we use the so-called *virtual structure approach* (Do and Pan, 2007; Lewis and Tan, 1997; Ren and Sorensen, 2008; Van den Broek et al., 2009). Following (Lewis and Tan, 1997), the virtual structure is a rigid body whose vertices are formed by the robots in the formation. The virtual structure is then supposed to track the given desired trajectory for the formation control problem to be solved. Consequently, let $q_{vc}(t) = \mathrm{col}(p_{vc}(t), r_{vc}(t))$ represent the state vector of the so-called *virtual centre* (see eg. Ren and Sorensen, 2008; Van den Broek et al., 2009) of the formation which is a moving coordinate frame attached to a certain point in the virtual structure, the orientation of which follows from the desired trajectory of the formation $q_{vc}^d(t)$. Note that the virtual centre does not need to be placed in an actual geometric centroid of the virtual structure but may be in any point considered as central for a particular application. The virtual structure follows a given desired trajectory if the virtual centre tracks this trajectory. Then, one may define the positions of the vertices of the virtual structure or in other words a desired formation shape with respect to the virtual centre with the aid

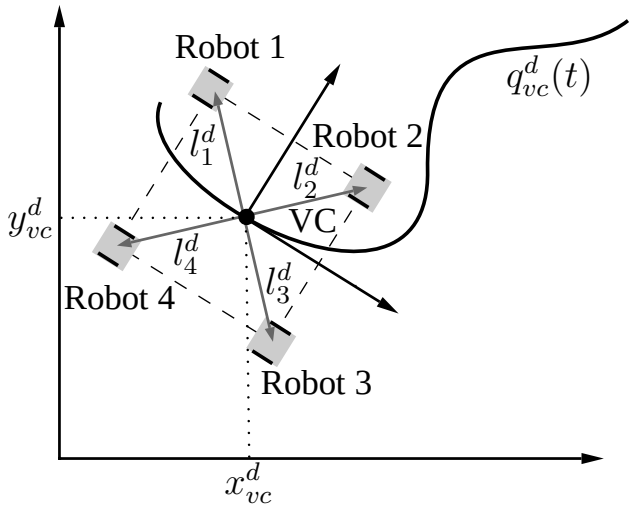

Figure 2.5: Desired positions of robots in the formation with respect to the virtual centre's position and a given formation shape. In the local virtual-centre-fixed frame desired positions are l^d_1, l^d_2, l^d_3, l^d_4 and in the global coordinate system these positions become (x^d_i, y^d_i) for Robot $i \in \{1, \ldots, 4\}$.

of vectors $l^d_i = \text{col}\left(l^d_{ix}, l^d_{iy}\right)$, $\forall i \in \mathcal{I}$. In practice, the vectors l^d_i express the position coordinates of robot i with respect to the local coordinate system of the virtual centre whose orientation coincides with the given desired trajectory $q^d_{vc}(t)$.

In this thesis, we use an extended concept of the virtual structure since we allow for the desired formation shape to be time–varying and determined by time–varying vectors $l^d_i(t)$, $i \in \mathcal{I}$. Hence the original characterisation of the virtual structure being a rigid body in (Lewis and Tan, 1997) should rather be redefined to a more general geometric structure to accommodate for the possibility of the virtual structure changing its shape.

To execute the formation control problem, based on the desired trajectory of the formation and the desired formation geometry, one can define desired trajectories

for individual robots in the formation $p_i^d(t) = (x_i^d(t), y_i^d(t))^T$ as the trajectories of the vertices of the virtual structure whose virtual centre tracks $q_{vc}^d(t)$. This gives

$$p_i^d(t) = p_{vc}^d(t) + R(\theta_{vc}^d(t))l_i^d(t), \tag{2.31}$$

where

$$R(\theta) = \begin{bmatrix} \cos\theta & -\sin\theta \\ \sin\theta & \cos\theta \end{bmatrix} \tag{2.32}$$

is a rotation matrix, and θ_{vc}^d is the desired orientation of the virtual centre. Note that having position coordinates $p_i(t)$, $p_i^d(t)$ and $p_{vc}^d(t)$, the remaining part of the state vectors q_{vc}^d, q_i and q_i^d are uniquely defined due to nonholonomic constraints, see further chapters for details. With the aid of (2.31) we define desired states for all individual robots by $q_i^d(t) = ((p_i^d)^T(t), (r_i^d(t))^T)^T$. Note that vectors p_i, p_i^d, p_{vc} and p_{vc}^d are given relative to the world frame while, as mentioned earlier, l_i^d is expressed with respect to the moving virtual-centre-fixed coordinate system.

Now, for the formation problem to be solved, we require the following set of equalities to hold asymptotically

$$p_i(t) - p_i^d(t) = \begin{pmatrix} 0 \\ 0 \end{pmatrix}, \qquad i \in \mathcal{I}, \tag{2.33}$$

and consequently, the error variable

$$e_i(t) = p_i(t) - p_i^d(t) \tag{2.34}$$

should converge to zero. Differentiating (2.34) along dynamics (2.30) and dynamics of $q_i^d(t)$, we obtain

$$\dot{e}_i(t) = f_{pi}(t, q_i, u_i) - f_{pi}^d(t), \tag{2.35}$$

where f_{pi} and f_{pi}^d are such that $f_i = \text{col}(f_{pi}, f_{ri})$ and $f_i^d = \text{col}(f_{pi}^d, f_{ri}^d)$ in which $\dot{q}_i^d = f_i^d(t)$ defines dynamics of $q_i^d(t)$.

Then, the formation control problem can be stated as follows.

Problem Statement. Consider N mobile robots, each given by kinematic equations (2.30), a desired trajectory of the virtual center of the formation $q_{vc}^d(t)$ and desired formation shape $l_i^d(t)$, $i \in \mathcal{I}$. The formation control problem consists in finding closed–loop controls u_i ($i \in \mathcal{I}$) such that the origin of the error dynamics (2.35) is globally asymptotically stable.

It is important to remark that although we consider the virtual centre of the formation and define the desired trajectory of the virtual centre, we do not explicitly look at its dynamics or calculate its trajectory. In fact, we merely use the concept of the virtual centre to define the desired trajectories of individual robots in the formation given the desired trajectory of the virtual centre and the desired formation shape. Indeed, when the formation control problem as defined above is solved, one may say that the virtual centre's trajectory coincides with its desired trajectory. Consequently, when the formation control problem is solved, the vertices of the virtual structure follow the same trajectories as the robots in the formation. However, we do not consider the trajectory of the virtual centre as such otherwise. On the contrary, we only consider the trajectories and behaviour of individual robots in the formation and then by examining the convergence of

individual robots to their desired trajectories we state that the virtual centre also converges to its desired trajectory by the formulation of the formation control problem.

Chapter 3

Cascaded approach to the formation control of unicycle mobile robots

3.1 Introduction

In this chapter we present a formation control algorithm based on a cascaded approach. These results have been previously published in part in (Sadowska et al., 2011a,b).

Further to the general problem formulation, we consider a formation consisting of N identical unicycle mobile robots with a nonholonomic no-side-slip constraint $\dot{x}\sin\theta - \dot{y}\cos\theta = 0$, where the state vector $q = (x,\, y,\, \theta)$ represents position $(x,\, y)$

and orientation θ. Hence, the motion of each robot in the group is given by (see Section 2.1.1 and (Campion and Chung, 2008; de Wit et al., 1996; Siciliano et al., 2009))

$$\begin{aligned} \dot{x}_i &= v_i \cos\theta_i, \\ \dot{y}_i &= v_i \sin\theta_i, \\ \dot{\theta}_i &= \omega_i, \end{aligned} \tag{3.1}$$

where $u_i = (v_i, \omega_i)^T$ is the control input of the i^{th} robot with v_i the forward velocity and ω_i the angular velocity, (x_i, y_i) are the Cartesian coordinates of the robot and θ_i is its orientation, $i \in \mathcal{I} = \{1, \ldots, N\}$. Given the robot's trajectory $q_i(t)$, $v_i(t)$ and $\omega_i(t)$ can then be obtained from

$$\begin{aligned} v_i &= \sqrt{(\dot{x}_i)^2 + (\dot{y}_i)^2}, \\ \omega_i &= \frac{\ddot{y}_i \dot{x}_i - \ddot{x}_i \dot{y}_i}{(\dot{x}_i)^2 + (\dot{y}_i)^2}. \end{aligned} \tag{3.2}$$

The existence of these expressions is well-known in the robotics literature (Laumond, 1998; Morin and Samson, 2008) and is a consequence of the differential flatness of (3.1) (Fliess et al., 1995).

Following the virtual structure approach, an additional virtual robot with identical kinematics (3.1) as for all robots in the group is introduced and placed in the so–called virtual centre of the formation. Based upon the position and orientation of the virtual centre, desired positions of robots in the formation are given with the aid of possibly time–varying bounded vectors $l_i^d(t) = \left(l_{xi}^d(t), l_{yi}^d(t)\right)^T$ given with respect to the local coordinate system associated with the virtual robot that is in accordance to its orientation. We also assume that $\frac{d}{dt}(l_i^d(t))$ is bounded.

For the formation control problem to be solved, we require first that the virtual centre follows a predefined trajectory $(x_{vc}^d(t), y_{vc}^d(t), \theta_{vc}^d(t))$, where $(x_{vc}^d(t), y_{vc}^d(t))$ denotes desired Cartesian positions and $\theta_{vc}^d(t)$ denotes a desired orientation of the virtual centre satisfying the no–side–slip constraint $\dot{x}\sin\theta - \dot{y}\cos\theta = 0$. Simultaneously, all robots in the formation should maintain a given spatial pattern with respect to the virtual centre defined by the desired formation shape $l_i^d(t)$, $i \in \mathcal{I}$. In terms of the behaviours of individual robots, this requirement is tantamount to the condition that robots should converge to their desired trajectories calculated according to

$$\begin{aligned} x_i^d &= x_{vc}^d + l_{xi}^d \cos\theta_{vc}^d - l_{yi}^d \sin\theta_{vc}^d, \\ y_i^d &= y_{vc}^d + l_{xi}^d \sin\theta_{vc}^d + l_{yi}^d \cos\theta_{vc}^d, \end{aligned} \tag{3.3}$$

These functions are determined to the specification of a particular desired trajectory of the virtual centre and a particular desired formation shape. Moreover, as for θ_{vc}^d, the remaining state variable, θ_i^d, also follows from the nonholonomic, no-side-slip constraint and (3.3).

Let v_{vc}^d and ω_{vc}^d be the desired forward and angular velocities respectively that are associated with the given desired trajectory $(x_{vc}^d(t), y_{vc}^d(t))$ of the virtual structure and can be calculated similarly to (3.2). Assume that v_{vc}^d and ω_{vc}^d are bounded. Using expressions in (3.2), we may obtain the counterparts v_i^d and ω_i^d of v_{vc}^d and ω_{vc}^d. We present them here for the sake of completeness:

$$\begin{aligned} v_i^d(t) &= \sqrt{(\dot{x}_i^d(t))^2 + (\dot{y}_i^d(t))^2}, \\ \omega_i^d(t) &= \frac{\ddot{y}_i^d(t)\dot{x}_i^d(t) - \ddot{x}_i^d(t)\dot{y}_i^d(t)}{(\dot{x}_i^d(t))^2 + (\dot{y}_i^d(t))^2}. \end{aligned} \tag{3.4}$$

The boundedness of v_{vc}^d, ω_{vc}^d, l_i^d and $\dot{l}_i^d$ as assumed implies the boundedness of v_i^d

and ω_i^d.

Following (Kanayama et al., 1990), to simplify the analysis of the behaviour of the robots in the settings of this chapter, the error variables of robot i are defined by

$$\begin{pmatrix} x_i^e \\ y_i^e \\ \theta_i^e \end{pmatrix} = \begin{bmatrix} \cos\theta_i & \sin\theta_i & 0 \\ -\sin\theta_i & \cos\theta_i & 0 \\ 0 & 0 & 1 \end{bmatrix} \begin{pmatrix} x_i^d - x_i \\ y_i^d - y_i \\ \theta_i^d - \theta_i \end{pmatrix}, \tag{3.5}$$

and correspond to the error coordinates in the local robot-associated frame. This choice of error variables is used to simplify the stability analysis in the settings as considered in this chapter. It is shown in (Kanayama et al., 1990) that the error dynamics are given by

$$\begin{aligned} \dot{x}_i^e &= \omega_i y_i^e - v_i + v_i^d \cos\theta_i^e, \\ \dot{y}_i^e &= -\omega_i x_i^e + v_i^d \sin\theta_i^e, \qquad\qquad i \in \mathcal{I} \\ \dot{\theta}_i^e &= \omega_i^d - \omega_i. \end{aligned} \tag{3.6}$$

Therefore, the formation control problem may be stated as follows: design control inputs v_i and ω_i that render the origin of the error dynamics (3.6) globally asymptotically stable.

Bearing in mind Section 1.5, the main contribution of this chapter may be considered as a distributed formation control algorithm, i.e. such that each robot i can only communicate with robots $j \in N_i$, where N_i is a set of neighbours of robot i defined in Definition C.2. The algorithm is based upon the virtual structure approach and motivated by (Van den Broek et al., 2009). Note that the control

algorithm presented in (Van den Broek et al., 2009) is centralised, i.e. robots need to communicate with all other robots in the formation. Moreover, the algorithm (Van den Broek et al., 2009) is nonlinear in terms of some of the error variables and only provides local convergence. In addition, in (Van den Broek et al., 2009) the analysis of the formation control algorithm is only given for two robots in the formation, which obviously is a considerable limitation. In comparison with (Van den Broek et al., 2009), the feedback terms introduced for the formation control are linear functions of the robot states. Moreover, our results hold globally and the case of an arbitrary number of robots in the formation is studied. Therefore, the applicability of our results is broader. In addition, we extend our main result to a simplified dynamic control algorithm that takes into consideration mobile robots' dynamic properties like mass or moment of inertia. Also the case of robot actuator limitations is taken care of. Further, it is important to remark that our contribution also includes a numerical and experimental investigation of the impact of connected and disconnected communication structures on robots' behaviour in a formation.

The control algorithms that we establish to solve the formation control problem are based on the well-known cascade approach, see (Panteley and Loria, 1998; Panteley et al., 1998). By using this control scheme, we are able to enjoy the major advantage of the cascade approach, i.e. the ability to decompose a task of stabilising the origin of a complex nonlinear system into stabilising two simpler systems when an additional condition regarding the interconnection term is satisfied.

The outline of this chapter is as follows. We give our main results in Section 3.2. In particular, in Subsection 3.2.1 we introduce the kinematic control law and in Subsection 3.2.2 we propose the simplified dynamic control law. After that, we present a practical extension of our results accounting for the actual actuator limitations in Subsection 3.2.3 where a saturated version of the control algorithm is given. In Section 3.3 we present simulation results and in Section 3.4 we present experimental results that validate the controllers. Section 3.5 contains a discussion of the results obtained.

3.2 Control design

3.2.1 Kinematic formation control algorithm

In this section, we introduce a formation control algorithm based on the virtual structure approach to solve the formation control problem. The formation control algorithm should ensure that the formation follows a given desired trajectory as a whole. For this to be possible, the virtual centre of the formation ought to follow the given desired trajectory while the robots in the formation maintain a given formation shape given with the aid of time-varying coordinates $(l_{xi}^d(t), l_{yi}^d(t))$, $i \in \mathcal{I}$ with respect to the virtual centre. To allow the robots to react to any perturbation occurring to any of the robots in the formation, the formation controller should be designed to balance between the robots tracking their desired trajectories and keeping the desired formation shape. To meet this objective, we employ a modified version of the control algorithm proposed originally for a single non-

holonomic system by Panteley et al. (1998) and revisited afterwards by Jakubiak et al. (2002). The augmentation that is crucial for a formation control algorithm involves the inclusion of a mutual coupling between the robots. Therefore, for the i^{th} robot we introduce additional mutual coupling terms $x_i^e - x_j^e$, $y_i^e - y_j^e$ and $\theta_i^e - \theta_j^e$ for each robot $j \in N_i$. Note that in (Rodriguez-Angeles and Nijmeijer, 2003, 2004) the concept of mutual coupling was employed in the synchronisation of industrial robots. However, in that work the mutual coupling terms were introduced at the level of the desired trajectories. In our work, the mutual coupling terms are introduced in the control input of each individual robot which results in the following controller:

$$\begin{aligned} v_i &= v_i^d + c_i^x x_i^e - c_i^y \omega_i^d y_i^e + \sum_{j \in N_i} \widetilde{c}_{ij}^x (x_i^e - x_j^e) - \sum_{j \in N_i} \widetilde{c}_{ij}^y \omega_i^d (y_i^e - y_j^e), \\ \omega_i &= \omega_i^d + c_i^\theta \theta_i^e + \sum_{j \in N_i} \widetilde{c}_{ij}^\theta (\theta_i^e - \theta_j^e), \qquad\qquad i \in \mathcal{I}, \end{aligned} \tag{3.7}$$

where c_i^x, c_i^y, c_i^θ for $i \in \mathcal{I}$ represent tracking control gains and $\widetilde{c}_{ij}^x$, $\widetilde{c}_{ij}^y$, $\widetilde{c}_{ij}^\theta$ for $i \in \mathcal{I}$, $j \in N_i$ represent mutual coupling gains. Note that the original tracking algorithm for a single mobile robot proposed by Panteley et al. (1998) can be retrieved by setting all coupling gains to zero, i.e. $\widetilde{c}_{ij}^x = 0$, $\widetilde{c}_{ij}^y = 0$, $\widetilde{c}_{ij}^\theta = 0$. In the case of formation control, these mutual coupling gains are crucial for robots in the formation to be aware of their neighbours' states. The importance of the mutual coupling terms can be particularly viewed if some of the robots in the formation are subject to a perturbation.

In the following theorem, we examine when the formation control problem as defined in this chapter is solved using the control law given in (3.7).

Theorem 3.2.1. *Consider a group of N nonholonomic mobile robots* (3.1)*, a desired trajectory of the virtual centre of the formation $(x_{vc}^d(t), y_{vc}^d(t))$ giving bounded desired forward $v_{vc}^d(t)$ and angular $\omega_{vc}^d(t)$ velocities of the virtual centre, a desired formation shape given by coordinates $l_i^d(t)$ that are bounded and such that $\dot{l}_i^d(t)$ are also bounded, and associated desired trajectories of robots in the formation* (3.3) *together with desired forward and angular velocities* (3.4)*. Let the control law be defined in* (3.7) *in which c_i^x, c_i^y, c_i^θ, $\widetilde{c}_{ij}^x$,$\widetilde{c}_{ij}^y$, $\widetilde{c}_{ij}^\theta$ are positive parameters such that $\widetilde{c}_{ij}^x = \widetilde{c}_{ji}^x$ and $\widetilde{c}_{ij}^y = \widetilde{c}_{ji}^y$ and $\widetilde{c}_{ij}^\nu \neq 0$ iff $j \in N_i$ for all $\nu \in \{x, y, \theta\}$. Assume that for $i \in \mathcal{I}$, $\omega_i^d(t)$ are such that $\bar{\Omega}^d(t) = \mathrm{col}(\omega_1^d(t), \ldots, \omega_N^d(t))$ satisfies the persistence of excitation condition in Definition A.2, and $v_i^d(t)$ is nonzero, for all t. Then the origin is a globally $\mathcal{K}$–exponentially stable equilibrium point of the closed–loop error dynamics (3.6, 3.7) and hence the control law* (3.7) *solves the formation control problem.*

Proof. Application of the control law (3.7) yields the following closed–loop error dynamics of the overall formation

$$\underbrace{\begin{pmatrix} \dot{X}^e \\ \dot{Y}^e \end{pmatrix} = \begin{bmatrix} -\mathbf{C}^x & \mathbf{\Omega}^d\Big(\mathbf{C}^y + \mathbf{I}\Big) \\ -\mathbf{\Omega}^d & \mathbf{0} \end{bmatrix} \begin{pmatrix} X^e \\ Y^e \end{pmatrix}}_{\dot{z}_1 = f_1(t, z_1)} + \underbrace{\begin{bmatrix} \bar{\mathbf{Y}}^e \mathbf{C}^\theta + \mathbf{V}^d \mathbf{\Theta}_{\cos} \\ -\bar{\mathbf{X}}^e \mathbf{C}^\theta + \mathbf{V}^d \mathbf{\Theta}_{\sin} \end{bmatrix}}_{g(t, z_1, z_2)} \Theta^e,$$

$$\underbrace{\dot{\Theta}^e = -\mathbf{C}^\theta \Theta^e}_{\dot{z}_2 = f_2(z_2)}, \tag{3.8}$$

where $X^e = \mathrm{col}(x_1^e, \ldots, x_N^e)$, $Y^e = \mathrm{col}(y_1^e, \ldots, y_N^e)$, $\Theta^e = \mathrm{col}(\theta_1^e, \ldots, \theta_N^e)$, $\bar{\mathbf{X}}^e = \mathrm{diag}(x_1^e, \ldots, x_N^e)$, $\bar{\mathbf{Y}}^e = \mathrm{diag}(y_1^e, \ldots, y_N^e)$, $\mathbf{I}$ is the identity matrix of appropriate dimensions, $\mathbf{0}$ is a matrix with all entries equal zero of appropriate dimensions, $\mathbf{\Omega}^d =$

$\mathrm{diag}(\omega_1^d, \ldots, \omega_N^d)$, $\mathbf{V}^d = \mathrm{diag}(v_1^d, \ldots, v_N^d)$, $\mathbf{\Theta}_{\cos} = \mathrm{diag}\left(\frac{\cos\theta_1^e - 1}{\theta_1^e}, \ldots, \frac{\cos\theta_N^e - 1}{\theta_N^e}\right)$ and $\mathbf{\Theta}_{\sin} = \mathrm{diag}\left(\frac{\sin\theta_1^e}{\theta_1^e}, \ldots, \frac{\sin\theta_N^e}{\theta_N^e}\right)$. Note that the functions $\frac{\sin\theta_i^e}{\theta_i^e}$ and $\frac{\cos\theta_i^e - 1}{\theta_i^e}$ are smooth if their definition is extended to $\theta_i^e = 0$ in the standard way and as such they are used in the sequel of the thesis without further commentary.

The remaining matrices $\mathbf{C}^x$, $\mathbf{C}^y$ and $\mathbf{C}^\theta$ in (3.8) are given by:

$$\mathbf{C}^x = \begin{bmatrix} c_1^x + \sum_{j\in N_1} \widetilde{c}_{1j}^x & -\widetilde{c}_{12}^x & \cdots & -\widetilde{c}_{1N}^x \\ \vdots & \ddots & \ddots & \vdots \\ -\widetilde{c}_{N-11}^x & \ddots & c_{N-1}^x + \sum_{j\in N_{N-1}} \widetilde{c}_{N-1j}^x & -\widetilde{c}_{N-1N}^x \\ -\widetilde{c}_{N1}^x & -\widetilde{c}_{N2}^x & \cdots & c_N^x + \sum_{j\in N_N} \widetilde{c}_{Nj}^x \end{bmatrix}, \tag{3.9}$$

$$\mathbf{C}^y = \begin{bmatrix} c_1^y + \sum_{j\in N_1} \widetilde{c}_{1j}^y & -\widetilde{c}_{12}^y & \cdots & -\widetilde{c}_{1N}^y \\ \vdots & \ddots & \ddots & \vdots \\ -\widetilde{c}_{N-11}^y & \ddots & c_{N-1}^y + \sum_{j\in N_{N-1}} \widetilde{c}_{N-1j}^y & -\widetilde{c}_{N-1N}^y \\ -\widetilde{c}_{N1}^y & -\widetilde{c}_{N2}^y & \cdots & c_N^y + \sum_{j\in N_N} \widetilde{c}_{Nj}^y \end{bmatrix}, \tag{3.10}$$

$$\mathbf{C}^\theta = \begin{bmatrix} c_1^\theta + \sum_{j\in N_1} \widetilde{c}_{1j}^\theta & -\widetilde{c}_{12}^\theta & \cdots & -\widetilde{c}_{1N}^\theta \\ \vdots & \ddots & \ddots & \vdots \\ -\widetilde{c}_{N-11}^\theta & \ddots & c_{N-1}^\theta + \sum_{j\in N_{N-1}} \widetilde{c}_{N-1j}^\theta & -\widetilde{c}_{N-1N}^\theta \\ -\widetilde{c}_{N1}^\theta & -\widetilde{c}_{N2}^\theta & \cdots & c_N^\theta + \sum_{j\in N_N} \widetilde{c}_{Nj}^\theta \end{bmatrix}, \tag{3.11}$$

where for $i \neq j$, we have $\mathbf{C}_{ij}^x \neq 0$, $\mathbf{C}_{ij}^y \neq 0$ and $\mathbf{C}_{ij}^\theta \neq 0$ iff $j \in N_i$. For matrix $\mathbf{C}^x$,

we may define deleted absolute row sums (Horn and Johnson, 1990) as

$$R_i(\mathbf{C}^x) = \sum_{\substack{j\in\mathcal{I}\\ j\neq i}} |\mathbf{C}^x_{ij}| = \sum_{j\in N_i} \widetilde{c}^x_{ij}, \tag{3.12}$$

where $i = 1, \ldots, N$. Then, by the Geršgorin disc theorem (Horn and Johnson, 1990), all eigenvalues of $\mathbf{C}^x$ lie in the region defined by

$$\begin{aligned} G(\mathbf{C}^x) &= \bigcup_{i=1}^{N} \Big\{ z \in \mathbb{C} \;\Big|\; |z - \mathbf{C}^x_{ii}| \leq R_i(\mathbf{C}^x) \Big\} \\ &= \bigcup_{i=1}^{N} \Big\{ z \in \mathbb{C} \;\Big|\; |z - (c^x_i + \sum_{j\in N_i} \widetilde{c}^x_{ij})| \leq \sum_{j\in N_i} \widetilde{c}^x_{ij} \Big\} \subset \mathbb{C}^+, \end{aligned} \tag{3.13}$$

where $\mathbb{C}^+$ denotes the open right-half plane of the complex plane. In addition, since $\mathbf{C}^x$ is symmetric, it is positive definite. Similarly, it may be shown that also $\mathbf{C}^y$ is positive definite.

The formation error dynamics (3.8) has the cascade form (B.25). Thus, if the assumptions in Corollary B.18 hold, the origin of (3.8) is globally $\mathcal{K}$-exponentially stable.

To show this, let us first consider the first stage of the cascade, i.e. $\dot{z}_1 = f_1(z_1)$:

$$\begin{aligned} \dot{z}_{11} &= -\mathbf{C}^x z_{11} + \mathbf{\Omega}^d(\mathbf{I} + \mathbf{C}^y) z_{12}, \\ \dot{z}_{12} &= -\mathbf{\Omega}^d z_{11}, \end{aligned} \tag{3.14}$$

in which $z_1 = \mathrm{col}(z_{11}, z_{12}) := \mathrm{col}(X^e, Y^e)$. Consider a Lyapunov function candi-

date for (3.14) of the form

$$V(z_{11}, z_{12}) = \frac{1}{2}(z_{11}^T z_{11} + z_{12}^T(\mathbf{I} + \mathbf{C}^y)z_{12}). \tag{3.15}$$

Then, the time derivative of (3.15) along trajectories of (3.14) yields

$$\dot{V}(z_{11}, z_{12}) = -z_{11}^T \mathbf{C}^x z_{11} + z_{11}^T \mathbf{\Omega}^d(\mathbf{I} + \mathbf{C}^y)z_{12} - z_{12}^T(\mathbf{I} + \mathbf{C}^y)\mathbf{\Omega}^d z_{11} = -z_{11}^T \mathbf{C}^x z_{11} \leq 0, \tag{3.16}$$

where the second equality holds because $\mathbf{C}^y$ is symmetric and the inequality follows from the fact that $\mathbf{C}^x$ is positive definite. Additionally, from Theorem B.12 we know that $z_1 = 0$ is a globally exponentially stable equilibrium point of (3.14) if, besides (3.16), the observability Gramian of the pair $(A(t), C)$ satisfies (B.21) where

$$A(t) = \begin{bmatrix} -\mathbf{C}^x & \mathbf{\Omega}^d\Big(\mathbf{C}^y + \mathbf{I}\Big) \\ -\mathbf{\Omega}^d & \mathbf{0} \end{bmatrix} \qquad C = \begin{bmatrix} \sqrt{\mathbf{C}^x} & \mathbf{0} \end{bmatrix}. \tag{3.17}$$

Following the developments in (Alvarez Aguirre, 2011; Khalil, 1996) it can indeed be shown that given the fact that $\bar{\Omega}^d(t)$ is persistently exciting according to Definition A.2, the pair $(A(t), C)$ is completely uniformly observable and hence Condition (B.21) is satisfied. Thus, Theorem B.12 can be used to show that $z_1 = 0$ is a globally exponentially stable equilibrium of (3.14) which proves the validity of Assumption 1 in Corollary B.18.

The second assumption from Corollary B.18 can be proven to be true immediately

since $\dot{z}_2 = f_2(z_2)$ is the following linear time-invariant system:

$$\dot{\Theta}^e = -\mathbf{C}^\theta \Theta^e. \tag{3.18}$$

Once again using the Geršgorin disc theorem (Horn and Johnson, 1990), it may be shown that all eigenvalues of $\mathbf{C}^\theta$ lie in $\mathbb{C}^+$. Hence, $\Theta^e = 0$ is a globally exponentially stable equilibrium point of (3.18). This proves Assumption 2 in Corollary B.18.

Next, we show that $g(t, z_1, z_2)$ from (3.8) satisfies Assumption 3 from Corollary B.18. After some manipulations, we obtain

$$\|g(t, z_1, z_2)\|_F \leq 2Nv^* + \|\mathbf{C}^\theta\|\|z_1\|, \tag{3.19}$$

where

$$\begin{aligned} v_i^* &= \sup\{|v_i^d(t)| \mid t \geq 0\}, \\ v^* &= \max\{v_i^* \mid i = 1, \ldots, N\}, \end{aligned} \tag{3.20}$$

and $\|\cdot\|_F$ denotes the Frobenius norm, see (Khalil, 1996). By assumption v_i^d for $i \in \mathcal{I}$ are bounded and hence, Assumption 3 in Corollary B.18 is satisfied with $k_1(\cdot) = 2Nv^*$ and $k_2(\cdot) = \|\mathbf{C}^\theta\|$. Therefore it follows from Corollary B.18, that the origin $(z_1, z_2) = (0, 0)$ of the cascade system (3.8) is globally $\mathcal{K}$–exponentially stable. Therefore, the control law (3.7) solves the formation control problem studied in this chapter. □

Remark 3.2.2. Theorem 3.2.1 only poses rather weak constraints on the control

parameters. Therefore, there is a considerable freedom to design the control parameters in a way which is desirable for a specific application. In particular, to focus on tracking of the individual robot trajectories, the tracking gains c_i^x, c_i^y, c_i^θ should dominate the mutual coupling gains $\widetilde{c}_{ij}^x$, $\widetilde{c}_{ij}^y$, $\widetilde{c}_{ij}^\theta$. Conversely, when keeping formation is the major objective, the mutual coupling gains $\widetilde{c}_{ij}^x$, $\widetilde{c}_{ij}^y$ and $\widetilde{c}_{ij}^\theta$ ought to dominate the tracking gains c_i^x, c_i^y, c_i^θ.

Remark 3.2.3. The condition $c_i^y > 0$ may be weakened to $c_i^y > -1$. This is because we only require the matrix $(\mathbf{I} + \mathbf{C}^y)$ in (3.15) to be a positive definite matrix, as opposed to the matrix $\mathbf{C}^y$ being positive definite. However, it was noted in (Van den Broek et al., 2009) that the choice of a negative control parameter c_i^y may cause some undesirable transient behaviour of robots in the formation.

Remark 3.2.4. In the literature, control algorithms have been proposed that implement obstacle avoidance strategies on the level of desired trajectories, see e.g. (Kostić et al., 2010a; Sadowska et al., 2012). Such algorithms for obstacle avoidance can also be integrated with the formation control strategy proposed in this chapter by feeding such adapted reference trajectories to the formation controller. Having said that, in this work we refrain from such a technical extension and concentrate on the formation control design as such.

Remark 3.2.5. The distributed character of the control law in Theorem 3.2.1 can be further enhanced when only some selected members of the group are able to communicate with the virtual centre. These selected robots will receive information directly from the virtual centre about, for example, the desired trajectory of the formation. Then, if the communication graph of the formation is connected, all other robots would obtain all necessary information about the virtual centre

too through local interaction with their neighbours. Note that this modification does not alter the control law in Theorem 3.2.1. It is merely a proposition how in practice communication cost can be further dimished.

Remark 3.2.6. The persistence of excitation condition that is required in Theorem 3.2.1 can be relaxed in the manner proposed in (Loria et al., 1999). This technical extension would allow robots to track trajectories such that $\omega_i^d(t) = 0$, i.e. straight lines.

3.2.2 Dynamic formation control algorithm

In this section we consider a distributed dynamic formation control algorithm based on a simple dynamic model of a mobile robot introduced in Section 2.1.2 (Jiang and Nijmeijer, 1997; Panteley et al., 1998):

$$\begin{aligned} \dot{x}_i &= v_i \cos\theta_i, \\ \dot{y}_i &= v_i \sin\theta_i, \\ \dot{\theta}_i &= \omega_i, \\ \dot{v}_i &= \frac{F_i}{m_i}, \\ \dot{\omega}_i &= \frac{\tau_i}{J_i}. \end{aligned} \tag{3.21}$$

The notation is as follows: m_i denotes the mass of robot $i \in \mathcal{I}$, J_i is its moment of inertia about an axis through the robot's barycentre which is perpendicular to the ground, F_i is force and τ_i is torque. The control inputs are the force F_i and the torque τ_i.

The dynamic formation control algorithm is an extension of the kinematic control law presented in the previous subsection and is motivated by the developments in (Panteley et al., 1998). Based on the control law defined in Theorem 3.2.1, we define nominal forward and angular velocities as

$$\begin{aligned}\bar{v}_i &= v_i^d + c_i^x x_i^e - c_i^y \omega_i^d y_i^e + \sum_{j\in N_i} \widetilde{c}_{ij}^x (x_i^e - x_j^e) - \sum_{j\in N_i} \widetilde{c}_{ij}^y \omega_i^d (y_i^e - y_j^e),\\ \bar{\omega}_i &= \omega_i^d + c_i^\theta \theta_i^e + \sum_{j\in N_i} \widetilde{c}_{ij}^\theta (\theta_i^e - \theta_j^e).\end{aligned} \tag{3.22}$$

Also, we define additional velocity error variables by

$$\begin{aligned}v_i^e &= v_i - \bar{v}_i,\\ \omega_i^e &= \omega_i - \bar{\omega}_i.\end{aligned} \tag{3.23}$$

Differentiating (3.23), we obtain time derivatives of the new error variables defined along solutions of (3.21) for each robot $i \in \mathcal{I}$ in the formation:

$$\begin{aligned}\dot{v}_i^e &= \frac{F_i}{m_i} - \dot{\bar{v}}_i,\\ \dot{\omega}_i^e &= \frac{\tau_i}{J_i} - \dot{\bar{\omega}}_i.\end{aligned} \tag{3.24}$$

Combining (3.6) and (3.24) yields the following error dynamics:

$$\begin{aligned}\dot{x}_i^e &= \bar{\omega}_i y_i^e - \bar{v}_i + v_i^d \cos\theta_i^e + \omega_i^e y_i^e - v_i^e,\\ \dot{y}_i^e &= -\bar{\omega}_i x_i^e + v_i^d \sin\theta_i^e - \omega_i^e x_i^e,\\ \dot{\theta}_i^e &= \omega_i^d - \bar{\omega}_i - \omega_i^e,\\ \dot{v}_i^e &= \frac{F_i}{m_i} - \dot{\bar{v}}_i,\\ \dot{\omega}_i^e &= \frac{\tau_i}{J_i} - \dot{\bar{\omega}}_i,\end{aligned} \tag{3.25}$$

for which we should design control laws for F_i and τ_i, such that it possesses a globally asymptotically stable equilibrium point at the origin. Using the expressions of $\bar{v}_i$ and $\bar{\omega}_i$ in (3.22), we obtain the following error dynamics for the overall formation

$$\begin{aligned}
\begin{pmatrix} \dot{X}^e \\ \dot{Y}^e \\ \dot{V}^e \end{pmatrix} &= \begin{bmatrix} -\mathbf{C}^x & \mathbf{\Omega}^d\Big(\mathbf{C}^y + \mathbf{I}\Big) & -\mathbf{I} \\ -\mathbf{\Omega}^d & \mathbf{0} & \mathbf{0} \\ \mathbf{0} & \mathbf{0} & \mathbf{0} \end{bmatrix} \begin{pmatrix} X^e \\ Y^e \\ V^e \end{pmatrix} + \begin{pmatrix} \mathbf{0} \\ \mathbf{0} \\ \mathbf{I} \end{pmatrix} \Big(\mathbf{M}^{-1}F - \dot{\bar{V}}\Big) \\
&\quad + \begin{bmatrix} \bar{\mathbf{Y}}^e\mathbf{C}^\theta + \mathbf{V}^d\theta_{\cos} & \bar{\mathbf{Y}}^e \\ -\bar{\mathbf{X}}^e\mathbf{C}^\theta + \mathbf{V}^d\theta_{\sin} & -\bar{\mathbf{X}}^e \\ \mathbf{0} & \mathbf{0} \end{bmatrix} \begin{pmatrix} \Theta^e \\ \Omega^e \end{pmatrix}, \qquad (3.26) \\
\begin{pmatrix} \dot{\theta}^e \\ \dot{\Omega}^e \end{pmatrix} &= \begin{bmatrix} -\mathbf{C}^\theta & -\mathbf{I} \\ \mathbf{0} & \mathbf{0} \end{bmatrix} \begin{pmatrix} \theta^e \\ \Omega^e \end{pmatrix} + \begin{pmatrix} \mathbf{0} \\ \mathbf{I} \end{pmatrix} \Big(\mathbf{J}^{-1}T - \dot{\bar{\Omega}}\Big),
\end{aligned}$$

where $V^e = \mathrm{col}(v_1^e, \ldots, v_N^e)$, $\Omega^e = \mathrm{col}(\omega_1^e, \ldots, \omega_N^e)$, $\mathbf{M} = \mathrm{diag}(m_1, \ldots, m_N)$, $\mathbf{J} = \mathrm{diag}(J_1, \ldots, J_N)$, $F = \mathrm{col}(F_1, \ldots, F_N)$, $T = \mathrm{col}(\tau_1, \ldots, \tau_N)$, $\dot{\bar{V}} = \mathrm{col}(\dot{\bar{v}}_1, \ldots, \dot{\bar{v}}_N)$ and $\dot{\bar{\Omega}} = \mathrm{col}(\dot{\bar{\omega}}_1, \ldots, \dot{\bar{\omega}}_N)$. Moreover, the constant matrices $\mathbf{C}^x$, $\mathbf{C}^y$ and $\mathbf{C}^\theta$ are defined in (3.9)–(3.11). The control design, as motivated by (Panteley et al., 1998), now relies on defining the control inputs F and T for the whole formation in such a way that the resultant closed–loop error dynamics have a cascade structure as in (B.25) and are globally $\mathcal{K}$–exponentially stable.

To this end, we propose the following control law

$$\begin{aligned}
F &= \mathbf{M}\Big(\dot{\bar{V}} + \mathbf{C}^{vx}X^e - \mathbf{C}^{vv}V^e\Big), \\
T &= \mathbf{J}\Big(\dot{\bar{\Omega}} - \mathbf{C}^{\omega}\Omega^e\Big),
\end{aligned} \qquad (3.27)$$

where $\mathbf{C}^{vx} = \text{diag}(c_1^{vx}, \ldots, c_n^{vx})$, $\mathbf{C}^{vv} = \text{diag}(c_1^{vv}, \ldots, c_n^{vv})$ and $\mathbf{C}^{\omega} = \text{diag}(c_1^{\omega}, \ldots, c_n^{\omega})$ are positive definite matrices. Equivalently, (3.27) may be written as

$$\begin{aligned} F_i &= m_i(\dot{\bar{v}}_i + c_i^{vx} x_i^e - c_i^{vv} v_i^e), \\ \tau_i &= J_i(\dot{\bar{\omega}}_i - c_i^{\omega} \omega_i^e). \end{aligned} \tag{3.28}$$

It is shown in the following theorem that indeed application of the control law (3.27) to the formation of mobile robots with the open–loop error dynamics (3.26) globally exponentially stabilises the zero equilibrium of the formation error dynamics (3.26).

Theorem 3.2.7. *Consider N unicycle mobile robots satisfying* (3.21)*, a desired trajectory of the virtual centre of the formation (x_{vc}^d, y_{vc}^d) such that resulting desired forward $v_{vc}^d(t)$ and angular $\omega_{vc}^d(t)$ velocities are bounded, and a desired formation shape $l_i^d(t)$, $i \in \mathcal{I}$, such that both $l_i^d(t)$ and $\dot{l}_i(t)$ are bounded. Consider the control law defined in* (3.28)*, where c_i^{vx}, c_i^{vv}, c_i^{ω} are positive parameters, both $\bar{v}_i$ and $\bar{\omega}_i$ are defined in* (3.22) *and additional kinematic control parameters in* (3.22) *satisfy the conditions given in Theorem 3.2.1. Assume that for all $i \in \mathcal{I}$, $\omega_i^d(t)$ in* (3.4) *is such that $\bar{\Omega}^d(t) = \text{col}(\omega_1^d(t), \ldots, \omega_N^d(t))$ satisfies the persistence of excitation condition in Definition A.2, and $v_i^d(t)$ in* (3.4) *is nonzero. Then, the origin of the closed–loop error dynamics (3.21, 3.28) is globally $\mathcal{K}$–exponentially stable and hence, the formation control problem is solved.*

Proof. The error dynamics of the whole formation controlled by (3.27) are

$$\begin{aligned}
\underbrace{\begin{pmatrix} \dot{X}^e \\ \dot{Y}^e \\ \dot{V}^e \end{pmatrix} = \begin{bmatrix} -\mathbf{C}^x & \mathbf{\Omega}^d\Big(\mathbf{C}^y + \mathbf{I}\Big) & -\mathbf{I} \\ -\mathbf{\Omega}^d & \mathbf{0} & \mathbf{0} \\ \mathbf{C}^{vx} & \mathbf{0} & -\mathbf{C}^{vv} \end{bmatrix} \begin{pmatrix} X^e \\ Y^e \\ V^e \end{pmatrix}}_{\dot{z}_1 = f_1(t, z_1)} \\
+ \underbrace{\begin{bmatrix} \bar{\mathbf{Y}}^e\mathbf{C}^\theta + \mathbf{V}^d\mathbf{\Theta}_{\cos} & \bar{\mathbf{Y}}^e \\ -\bar{\mathbf{X}}^e\mathbf{C}^\theta + \mathbf{V}^d\mathbf{\Theta}_{\sin} & -\bar{\mathbf{X}}^e \\ \mathbf{0} & \mathbf{0} \end{bmatrix}}_{g(z_1, z_2)} \begin{pmatrix} \Theta^e \\ \Omega^e \end{pmatrix}, \\
\underbrace{\begin{pmatrix} \dot{\Theta}^e \\ \dot{\Omega}^e \end{pmatrix} = - \begin{bmatrix} \mathbf{C}^\theta & \mathbf{I} \\ \mathbf{0} & \mathbf{C}^\omega \end{bmatrix} \begin{pmatrix} \Theta^e \\ \Omega^e \end{pmatrix}}_{\dot{z}_2 = f_2(z_2)},
\end{aligned} \tag{3.29}$$

which has the cascade structure as in (B.25). Thus, if the three assumptions of Corollary B.18 are satisfied, then the origin of (3.29) is a globally $\mathcal{K}$–exponentially stable equilibrium. To prove that this is indeed the case, consider the first stage of the cascade system, $\dot{z}_1 = f_1(t, z_1)$, which is a linear time-varying system of the form

$$\begin{aligned}
\dot{z}_{11} &= -\mathbf{C}^x z_{11} + \mathbf{\Omega}^d(\mathbf{I} + \mathbf{C}^y) z_{12} - z_{13}, \\
\dot{z}_{12} &= -\mathbf{\Omega}^d z_{11}, \\
\dot{z}_{13} &= \mathbf{C}^{vx} z_{11} - \mathbf{C}^{vv} z_{13},
\end{aligned} \tag{3.30}$$

where $z_1 = \mathrm{col}(z_{11}, z_{12}, z_{13}) := \mathrm{col}(X^e, Y^e, V^e)$. We define a positive definite

Lyapunov function candidate for this system by

$$V(z_1) = \frac{1}{2}\Big(z_{11}^T z_{11} + z_{12}^T\big(\mathbf{C}^y + \mathbf{I}\big)z_{12} + z_{13}^T(\mathbf{C}^{vx})^{-1}z_{13}\Big). \tag{3.31}$$

By differentiating (3.31) with respect to time along trajectories of (3.30), one arrives at

$$\begin{aligned}\dot{V}(z_{11}, z_{12}, z_{13}) &= -z_{11}^T\mathbf{C}^x z_{11} + z_{11}^T\mathbf{\Omega}^d(\mathbf{I}+\mathbf{C}^y)z_{12} - z_{11}^T z_{13} \\ &\quad - z_{11}^T\mathbf{\Omega}^d(\mathbf{I}+\mathbf{C}^y)z_{12} + z_{13}^T(\mathbf{C}^{vx})^{-1}\mathbf{C}^{vx}z_{11} - z_{13}^T(\mathbf{C}^{vx})^{-1}\mathbf{C}^{vv}z_{13} \\ &= -z_{11}^T\mathbf{C}^x z_{11} - z_{13}^T(\mathbf{C}^{vx})^{-1}\mathbf{C}^{vv}z_{13} \leq 0. \end{aligned} \tag{3.32}$$

Consequently, using similar arguments as in the proof of Theorem 3.2.1, we can prove by Theorem B.12 that the origin $z_1 = 0$ is a globally exponentially stable equilibrium. Thus, Assumption 1 of Corollary B.18 holds.

As for Assumption 2 in Corollary B.18, let us rewrite subsystem $\dot{z}_2 = f_2(z_2)$ as

$$\dot{z}_2 = -\begin{bmatrix}\mathbf{C}^\theta & \mathbf{I} \\ \mathbf{0} & \mathbf{C}^\omega\end{bmatrix} z_2 =: -\mathbf{H}z_2, \tag{3.33}$$

which is a time-invariant linear system. Because $\mathbf{H}$ is an upper block triangular matrix, the set of its eigenvalues is created by merging the sets of eigenvalues of $\mathbf{C}^\theta$ and $\mathbf{C}^\omega$. As shown before, all eigenvalues of $\mathbf{C}^\theta$ have positive real parts. Moreover, $\mathbf{C}^\omega$ is a positive definite diagonal matrix. Therefore, all eigenvalues of both $\mathbf{C}^\theta$ and $\mathbf{C}^\omega$ lie in the open right half of the complex plane and so do all eigenvalues of $\mathbf{H}$. Thus, (3.33) is globally exponentially stable which proves

Assumption 2 of Corollary B.18.

As for Assumption 3 in Corollary B.18, it may be easily shown that

$$\|g(t, z_1, z_2)\|_F \leq 2Nv^* + \|\mathbf{C}^\theta + \mathbf{I}\|\|z_1\|, \tag{3.34}$$

in which v^* is defined in (3.20) and $\|\cdot\|_F$ denotes the Frobenius norm (Khalil, 1996). Hence Assumption 3 in Corollary B.18 is satisfied with $k_1(\cdot) = 2Nv^*$ and $k_2(\cdot) = \|\mathbf{C}^\theta + \mathbf{I}\|$. Therefore, by Corollary B.18, the origin of the cascaded system (3.29) is globally $\mathcal{K}$–exponentially stable. Hence, the dynamic formation control problem studied is solved. □

Remark 3.2.8. As in the kinematic control algorithm, also in the dynamic formation control algorithm, there is a trade-off between two control objectives: tracking of individual robot trajectories and keeping formation. Regarding pure trajectory tracking, this objective may be influenced by setting appropriate kinematic tracking gains c_i^x, c_i^y, c_i^θ or dynamic tracking parameters c_i^{vx}, c_i^{vv}, c_i^ω. In turn, the formation geometry maintenance can be affected by mutual coupling terms $\widetilde{c}_{ij}^x$, $\widetilde{c}_{ij}^y$ and $\widetilde{c}_{ij}^\theta$.

3.2.3 Saturated control

In this section we propose an extension of the *kinematic* formation control algorithm given in Section 3.2.1 which accounts for robot actuator limitations. A saturated version of the controller is given in which control inputs of each robot

satisfy

$$|v_i| \leq \bar{v}_i \qquad |\omega_i| \leq \bar{\omega}_i \qquad \forall\, i \in \mathcal{I}. \tag{3.35}$$

This extension is significant because the nominal control law could be a very large signal if the initial state is unfavourable. However, in real robots such large inputs cannot be realised due to hardware limitations. Therefore, it is important to extend the results given earlier in this chapter to take into account this practical issue. Thus, to accommodate for actuator limitations, the formation control problem may be re–stated as follows: find control inputs v_i and ω_i for each robot in the formation such that the origin of the error dynamics (3.6) is globally asymptotically stable and the control inputs satisfy the upper bound condition (3.35).

Mindful of the bounds that the control inputs are to satisfy, we define so–called saturation function as follows.

Definition 3.2.9 (**Saturation function**)**.** A scalar function $\nu\colon \mathbb{R} \to \mathbb{R}$ is called a saturation function if it is nondecreasing, $\nu(s)s > 0$ for $s \neq 0$, $|\nu(s)| \leq c|s|$ for $c > 0$, and there exists $\bar{\nu} < +\infty$ such that $\nu(\cdot) \leq \bar{\nu}$.

Simple examples of saturation functions are $f(s) = \bar{f}\frac{2}{\pi}\arctan(s)$, $f(s) = \bar{f}\tanh(s)$ or

$$f(s) = \begin{cases} s & \text{for } |s| \leq \bar{f}, \\ \operatorname{sign}(s)\bar{f} & \text{for } |s| > \bar{f}. \end{cases} \tag{3.36}$$

The saturated formation controller is based on the nominal formation controller given in Section 3.2.1 in which, for the sake of simplicity, we disregard the y_i^e

terms. By doing so, we are able to concentrate on presenting the method of extending the controller to achieve a saturated version. Extending further the controller to obtain the full saturated version of the controller proposed in Section 3.2.1 incorporating the y_i^e terms remains an open problem requiring more in-depth technical investigation.

Recall the nominal controller from (3.7) without the y_i^e terms:

$$\begin{aligned} v_i &= v_i^d + c_i^x x_i^e + \sum_{j\in N_i} \widetilde{c}_{ij}^x (x_i^e - x_j^e), \\ \omega_i &= \omega_i^d + c_i^\theta \theta_i^e + \sum_{j\in N_i} \widetilde{c}_{ij}^\theta (\theta_i^e - \theta_j^e). \end{aligned} \qquad (i \in \mathcal{I}) \tag{3.37}$$

The right hand side of these equalities could in some situations be larger than the actuator limits of the actual robots. In this case, the formation control law, for each robot $i \in \mathcal{I}$, is modified and given by

$$\begin{aligned} v_i &= v_i^d + c_i^x \alpha(x_i^e) + \sum_{j\in N_i} \widetilde{c}_{ij}^x (\alpha(x_i^e) - \alpha(x_j^e)), \\ \omega_i &= \omega_i^d + c_i^\theta \gamma(\theta_i^e) + \sum_{j\in N_i} \widetilde{c}_{ij}^\theta (\gamma(\theta_i^e) - \gamma(\theta_j^e)), \end{aligned} \tag{3.38}$$

where c_i^x, c_i^θ, $\widetilde{c}_{ij}^x$ and $\widetilde{c}_{ij}^\theta$ are control parameters and $\alpha(\cdot)$ and $\gamma(\cdot)$, for $i \in \mathcal{I}$ are saturation function as defined above.

For the *saturated* formation control problem to be solvable, the formation control task needs to be feasible. Accordingly, the desired trajectory of the formation and the desired formation shape should be such that the desired feedforward terms v_i

and ω_i associated with the desired trajectories of individual robots satisfy

$$v_i^* < v_i^{\max} < \bar{v}_i, \tag{3.39}$$

$$\omega_i^* < \omega_i^{\max} < \bar{\omega}_i, \tag{3.40}$$

where

$$v_i^* = \sup\{|v_i^d(t)| \mid t \geq 0\}, \tag{3.41}$$

$$\omega_i^* = \sup\{|\omega_i^d(t)| \mid t \geq 0\}. \tag{3.42}$$

We now state the theorem in which we give conditions under which the formation control law given in (3.38) solves the formation control problem as mentioned in this section.

Theorem 3.2.10. *Consider a group of N nonholonomic robots* (3.1) *and a desired trajectory of the virtual centre of the formation $(x_{vc}^d(t), y_{vc}^d(t))$ with associated bounded desired forward $v_{vc}^d(t)$ and angular $\omega_{vc}^d(t)$ velocities. Consider also a desired formation geometry given by time–varying coordinates $l_i^d(t)$ such that both $l_i^d(t)$ and $\dot{l}_i^d(t)$ are bounded, and the resultant desired trajectories of robots in the formation* (3.3) *and the desired forward and angular velocities* (3.4)*. Let the control law be defined in* (3.38)*, in which c_i^x, c_i^θ, $\widetilde{c}_{ij}^x$ and $\widetilde{c}_{ij}^\theta$ are positive control parameters such that $\widetilde{c}_{ij}^\nu = \widetilde{c}_{ji}^\nu$ and $\widetilde{c}_{ij}^\nu \neq 0$ iff $j \in N_i$ for $\nu \in \{x, \theta\}$. Moreover, $\alpha(\cdot)$ and $\gamma(\cdot)$ are saturation functions subject to $|\alpha(\cdot)| \leq \bar{\alpha}$ and $|\gamma(\cdot)| \leq \bar{\gamma}$, and for $i \in \mathcal{I}$, $\omega_i^d(t)$ is such that $\bar{\Omega}^d(t) = \mathrm{col}(\omega_1^d(t), \ldots, \omega_N^d(t))$ satisfies the persistence of excitation condition, see Definition A.2, and $v_i^d(t)$ is nonzero for all t and*

Conditions (3.39, 3.40) are satisfied. The control parameters c_i^x, c_i^θ, $\widetilde{c}_{ij}^x$ *and* $\widetilde{c}_{ij}^\theta$ *and the saturation functions upper bounds* $\bar{\alpha}$ *and* $\bar{\gamma}$ *are chosen to satisfy*

$$\bar{v}_i \geq v_i^* + \bar{\alpha}\left(c_i^x + 2\sum_{j\in N_i}\widetilde{c}_{ij}^x\right), \tag{3.43}$$

$$\bar{\omega}_i \geq \omega_i^* + \bar{\gamma}\left(c_i^\theta + 2\sum_{j\in N_i}\widetilde{c}_{ij}^\theta\right), \tag{3.44}$$

for given $\bar{v}_i$ *and* $\bar{\omega}_i$, $i \in \mathcal{I}$. *Then, the origin of the closed–loop error dynamics (3.6, 3.38) is rendered globally uniformly asymptotically stable, and* v_i *and* ω_i *satisfy* (3.35).

Proof. The closed–loop error dynamics (3.6, 3.38) are

$$\begin{aligned}
\dot{x}_i^e &= \Big(\omega_i^d + c_i^\theta\gamma(\theta_i^e) + \sum_{j\in N_i}\widetilde{c}_{ij}^\theta(\gamma(\theta_i^e)-\gamma(\theta_j^e))\Big)y_i^e + v_i^d\cos\theta_i^e - v_i^d \\
&\quad - c_i^x\alpha(x_i^e) - \sum_{j\in N_i}\widetilde{c}_{ij}^x(\alpha(x_i^e)-\alpha(x_j^e)), \\
\dot{y}_i^e &= -\Big(\omega_i^d + c_i^\theta\gamma(\theta_i^e) + \sum_{j\in N_i}\widetilde{c}_{ij}^\theta(\gamma(\theta_i^e)-\gamma(\theta_j^e))\Big)x_i^e + v_i^d\sin\theta_i^e, \\
\dot{\theta}_i^e &= -c_i^\theta\gamma(\theta_i^e) - \sum_{j\in N_i}\widetilde{c}_{ij}^\theta(\gamma(\theta_i^e)-\gamma(\theta_j^e)), \qquad (i\in\mathcal{I})
\end{aligned} \tag{3.45}$$

or, equivalently, in the matrix form for the whole formation

$$\underbrace{\begin{pmatrix}\dot{X}^e\\ \dot{Y}^e\end{pmatrix} = \begin{bmatrix}-\mathbf{C}^x A\\ \mathbf{0}\end{bmatrix} + \mathbf{S}\otimes\mathbf{\Omega^d}\begin{pmatrix}X^e\\ Y^e\end{pmatrix}}_{\dot{z}_1 = f_1(t,z_1)} + \underbrace{\begin{bmatrix}\bar{\mathbf{Y}}^e\mathbf{C}^\theta\\ -\bar{\mathbf{X}}^e\mathbf{C}^\theta\end{bmatrix}\Gamma + \begin{bmatrix}\mathbf{V}^d\mathbf{\Theta}_{\cos}\\ \mathbf{V}^d\mathbf{\Theta}_{\sin}\end{bmatrix}\Theta^e}_{g(t,z_1,z_2)z_2},$$

$$\underbrace{\dot{\Theta}^e = -\mathbf{C}^\theta\Gamma}_{\dot{z}_2 = f_2(z_2)}, \tag{3.46}$$

in which the notation is explained in earlier sections of this chapter and in addition $A = \mathrm{col}(\alpha(x_1^e), \ldots, \alpha(x_n^e))$, $\Gamma = \mathrm{col}(\gamma(\theta_1^e), \ldots, \gamma(\theta_n^e))$ and

$$S = \begin{bmatrix} 0 & 1 \\ -1 & 0 \end{bmatrix}. \tag{3.47}$$

Clearly, system (3.46) has the cascade form (B.25). Thus, if the assumptions of Theorem B.17 hold, the origin of the overall system is globally $\mathcal{K}$-exponentially stable. Hereafter, we elaborate on each of the assumptions.

1. Subsystem $\dot{z}_2 = f_2(z_2)$ is globally uniformly asymptotically stable which can be verified using the Lyapunov function candidate $V(\Theta^e) = \frac{1}{2}(\Theta^e)^T\Theta^e$. Its time derivative along system trajectories is

$$\begin{aligned}
\dot{V} &= -(\Theta^e)^T \mathbf{C}^\theta \Gamma = -\sum_{i=1}^{N} \left(\gamma(\theta_i^e)\theta_i^e (c_i^\theta + \sum_{j\in N_i} \widetilde{c}_{ij}^\theta) - \gamma(\theta_i^e) \sum_{j\in N_i} \widetilde{c}_{ij}^\theta \theta_j^e \right) \\
&= -\left(\sum_{i=1}^{N} c_i^\theta \gamma(\theta_i^e)\theta_i^e + \sum_{(i,j)\in\mathcal{E}} \widetilde{c}_{ij}^\theta \left(\gamma(\theta_i^e)\theta_i^e + \gamma(\theta_j^e)\theta_j^e - \gamma(\theta_i^e)\theta_j^e - \gamma(\theta_j^e)\theta_i^e \right) \right) \\
&= -\left(\sum_{i=1}^{N} c_i^\theta \gamma(\theta_i^e)\theta_i^e + \sum_{(i,j)\in\mathcal{E}} \widetilde{c}_{ij}^\theta \left(\theta_i^e - \theta_j^e \right) \left(\gamma(\theta_i^e) - \gamma(\theta_j^e) \right) \right) \leq 0,
\end{aligned} \tag{3.48}$$

   where $\mathcal{E}$ denotes a set of all pairs of neighbours. So $\Theta^e = 0$ is a globally uniformly asymptotically stable equilibrium point.

2. The origin of subsystem $\dot{z}_1 = f_1(t, z_1)$ is uniformly globally stable, since using a quadratic Lyapunov function $V(X^e, Y^e) = \frac{1}{2}\left((X^e)^T X^e + (Y^e)^T Y^e\right)$, we obtain $\dot{V} \leq -(X^e)^T \mathbf{C}^x A \leq 0$. Moreover, we can be rewrite the system

dynamic equation as

$$\underbrace{\begin{pmatrix}\dot{X}^e\\ \dot{Y}^e\end{pmatrix} = \begin{bmatrix}-\mathbf{I} & \mathbf{\Omega}^d\\ -\mathbf{\Omega}^d & \mathbf{0}\end{bmatrix}\begin{pmatrix}X^e\\ Y^e\end{pmatrix}}_{\dot{w}=F_0(t,w)} + \underbrace{\begin{bmatrix}X^e - \mathbf{C}^x A\\ \mathbf{0}\end{bmatrix}}_{K(t,w)}, \tag{3.49}$$

where $w := \mathrm{col}(X^e, Y^e)$. Global uniform asymptotic stability of the origin $w = 0$ can be proven using Proposition B.18.1 with $F_0(t,w)$ and $K(t,w)$ defined as in (3.49). We can immediately say that the origin of the system $\dot{w} = F_0(t,w)$ is globally exponentially stable using the Lyapunov function candidate $V(X^e, Y^e) = \frac{1}{2}\left((X^e)^T X^e + (Y^e)^T Y^e\right)$ and the same rationale as in the proof of Theorem 3.2.1. Thus, the origin of $\dot{w} = F_0(t,w)$ is globally uniformly asymptotically stable. Furthermore, $\|K(t,w)\| \leq (1 + c\|\mathbf{C}^x\|_F)\,\|X^e\|$ for some positive constant c and letting $h(t,w) = X^e$ we have $\|h(t,w)\| \leq \|X^e\| \leq \|w\|$. Moreover, using again $V(X^e, Y^e) = \frac{1}{2}\left((X^e)^T X^e + (Y^e)^T Y^e\right)$ yields $\dot{V} \leq -(X^e)^T \mathbf{C}^x A \leq -\mu(\|X^e\|)$, where $\mu \in \mathcal{K}_\infty$. By integrating $\dot{V}$ we obtain $V(t) - V(0) \leq -\int_0^t \mu(\|h(\tau)\|)\mathrm{d}\tau$ which for $t \to \infty$ gives $\|\mu(\|h(t,x)\|)\|_1 \leq V(0) - V(t) \leq V(0) \leq \frac{1}{2}\|w(0)\|^2$. Hence all conditions of Proposition B.18.1 hold and thus in light of this proposition the origin of the whole system is globally uniformly asymptotically stable.

3. The final condition of Corollary B.18 can be proven if $g(t, z_1, z_2)z_2$ is rearranged as

$$g(t, z_1, z_2)z_2 = \begin{bmatrix}\bar{\mathbf{Y}}^e \mathbf{C}^\theta\\ -\bar{\mathbf{X}}^e \mathbf{C}^\theta\end{bmatrix}\Gamma + \begin{bmatrix}\mathbf{V}^d \mathbf{\Theta}_{\cos}\\ \mathbf{V}^d \mathbf{\Theta}_{\sin}\end{bmatrix}\Theta^e$$

$$= \left(\begin{bmatrix} \bar{\mathbf{Y}}^e \mathbf{C}^\theta \\ -\bar{\mathbf{X}}^e \mathbf{C}^\theta \end{bmatrix} \bar{\Gamma} + \begin{bmatrix} \mathbf{V}^d \mathbf{\Theta}_{\cos} \\ \mathbf{V}^d \mathbf{\Theta}_{\sin} \end{bmatrix} \right) \Theta^e, \tag{3.50}$$

where $\bar{\Gamma} = \operatorname{diag}\left(\frac{\gamma(\theta_1^e)}{\theta_1^e}, \ldots, \frac{\gamma(\theta_n^e)}{\theta_n^e} \right)$. Consequently, it can be deduced that

$$\|g(t, z_1, z_2)\|_F \leq 2Ndv^* + \|\mathbf{C}^\theta\| \|z_1\|, \tag{3.51}$$

in which v^* is defined in (3.20) and $d > 0$, see Definition 3.2.9. Thus, the final assumptions of Corollary B.18 holds with $k_1(z_2) = 2Ndv^*$ and $k_2(z_2) = \|\mathbf{C}^\theta\|$.

Therefore by Corollary B.18 the origin of the error dynamics of (3.46) is globally uniformly asymptotically stable. Accordingly, the formation control problem is solved.

It remains to prove that the control inputs v_i and ω_i satisfy (3.35). Straightforward calculations using the triangular inequality lead us to

$$|v_i| \leq v_i^* + \bar{\alpha} \left(c_i^x + 2 \sum_{j \in N_i} \widetilde{c}_{ij}^x \right) \leq \bar{v}_i, \tag{3.52}$$

$$|\omega_i| \leq \omega_i^* + \bar{\gamma} \left(c_i^\theta + 2 \sum_{j \in N_i} \widetilde{c}_{ij}^\theta \right) \leq \bar{\omega}_i, \tag{3.53}$$

which indeed establishes (3.35). □

Remark 3.2.11. Since the control algorithm presented in Theorem 3.2.10 is based on the same reasoning as the control algorithm given in Theorem 3.2.1, we can again choose control parameters c_i^x, c_i^θ, $\widetilde{c}_{ij}^x$ and $\widetilde{c}_{ij}^\theta$, in a way that would best

suit the particular application of the control algorithm. Accordingly, to focus on tracking of robots' individual trajectories, the tracking control gains c_i^x and c_i^θ should prevail over the mutual coupling gains $\widetilde{c}_{ij}^x$ and $\widetilde{c}_{ij}^\theta$. Alternatively, if keeping formation is the priority, then $\widetilde{c}_{ij}^x$ and $\widetilde{c}_{ij}^\theta$ should be dominant with respect to c_i^x and c_i^θ.

Remark 3.2.12. In the proof above we show global uniform asymptotic stability of the equilibrium points of subsystems $\dot{z}_1 = f_1(t, z_1)$ and $\dot{z}_2 = f_2(z_2)$. In fact also local uniform exponential stability can be established which together with the claim of the global uniform asymptotic stability yields global $\mathcal{K}$-exponential stability of the origins of subsystems $\dot{z}_1 = f_1(t, z_1)$ and $\dot{z}_2 = f_2(z_2)$ (Burger, 2011). However, the result to obtain global $\mathcal{K}$-exponential stability of the origin of a cascaded system in which the origin of the disconnected subsystems are only globally $\mathcal{K}$-exponentially stable as opposed to globally exponentially stable is more involving and requires some more conditions to be met (Aneke, 2003). In this thesis we do not analyse such a technical extension of our result.

Remark 3.2.13. For large tracking errors x_i^e and θ_i^e and such that $\text{sign}(x_i^e) = \text{sign}(x_j^e)$ and $\text{sign}(\theta_i^e) = \text{sign}(\theta_j^e)$, the control law (3.38) becomes decoupled since both $\alpha(x_i^e) - \alpha(x_j^e)$ and $\gamma(\theta_i^e) - \gamma(\theta_j^e)$ are approximately zero.

In the next section, we show simulation results of the *nominal* formation controller given in Section 3.2.1 as well as its extensions: the dynamic formation control algorithm given in Section 3.2.2 and the saturated formation control algorithm proposed in this section.

(a) (b)

Figure 3.1: Communication graph structures used in simulations: (a) disconnected graph (b) connected graph.

3.3 Simulation study

In this section we illustrate the behaviour of robots in a formation when the three control algorithms proposed in Section 3.2 are applied. We consider the case of three robots with two different communication structures: a disconnected one, as illustrated in Figure 3.1(a) and a connected one, as illustrated in Figure 3.1(b).

For both disconnected and connected communication networks, we allow for perturbations to occur. In particular, we consider the perturbation of Robot 1 due to a displacement of this robot at time $t = 200$ from its current position along $(\delta x, \delta y) = (15, -26)$ in the inertial coordinate frame. This perturbation, although unrealistic in practice, serves well to present the behaviour of robots in the formation in the presence of perturbations.

To show advantages of the formation control algorithms proposed in this chapter we consider a formation geometry maintenance index defined as follows. Let $p_i(t) = \text{col}(x_i(t), y_i(t))$ denote a robot's actual position with respect to the inertial coordinate frame and $l_i^d(t)$ a robot's desired position in the formation relative to the virtual centre. Then the formation geometry maintenance index is defined

according to

$$I(t) = \sum_{i=1}^{3} \sum_{\substack{j=1 \\ j \neq i}}^{3} \left(\|p_i(t) - p_j(t)\| - \|l_i^d(t) - l_j^d(t)\| \right)^2, \tag{3.54}$$

which shows discrepancy between the actual formation shape and the desired one. In particular, it measures the difference between actual and desired distances between all pairs of robots in the formation. Note that $I(t) = 0$ occurs if and only if the formation shape is maintained, modulo a rotation or a reflection (a mirror image), see Figure 3.2. We still consider a formation shape to be maintained despite a possible rotation or a reflection because we are purely interested here in verifying the geometric shape of the formation. Appropriate location of a formation in the plane as well as appropriate orientation of robots in the formation count among desired trajectory tracking component which we do not measure via index I (3.54).

We choose the desired trajectory of the formation as

$$\begin{aligned} \dot{x}_{vc}^d &= 5 \cos \theta_{vc}^d, \\ \dot{y}_{vc}^d &= 5 \sin \theta_{vc}^d, \\ \dot{\theta}_{vc}^d &= 0.2 \sin t, \end{aligned} \tag{3.55}$$

in which $x_{vc}^d(0) = 0$, $y_{vc}^d(0) = 0$ and $\theta_{vc}^d(0) = 0$. Moreover, initial conditions of robots in the formation are given by $(x_1(0), y_1(0), \theta_1(0)) = \left(-23.56, 4.01, -\frac{\pi}{3}\right)$, $(x_2(0), y_2(0), \theta_2(0)) = (5, 1.23, -\pi)$ and $(x_3(0), y_3(0), \theta_3(0)) = \left(12, 15.55, \frac{\pi}{2}\right)$. Furthermore, the desired formation shape is defined via $l_1^d = \left(-10, -\frac{10\sqrt{3}}{3}\right)^T$, $l_2^d =$

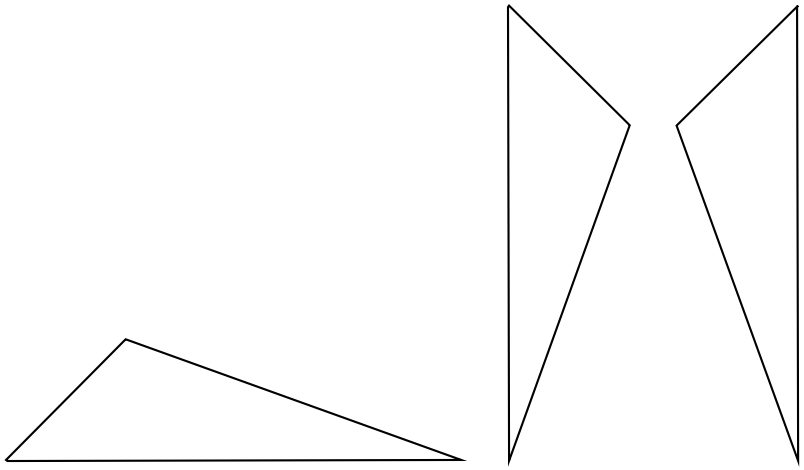

Figure 3.2: Examples of congruent triangular formations that are considered identical according to the index (3.54) (a) an original formation shape, (b) a rotated formation shape, (c) a reflected formation shape.

$\left(10, -\frac{10\sqrt{3}}{3}\right)^T$ and $l_3^d = \left(0, \frac{20\sqrt{3}}{3}\right)^T$ and forms an equilateral triangle as illustrated in Figure 3.3 in which the length of the sides equals 20. All simulations in this section are performed for the period of $t \in [0, 300]$, where t denotes simulation time.

Remark 3.3.1. The purpose of the simulations in this chapter is to give a proof-of-concept that with mutual coupling gains dominating the tracking gains, more priority is given to the cooperative behaviour of the robots towards the desired formation shape. Therefore, no optimisation of controller parameters has taken place, but rather a set of controller parameters highlighting this phenomenon has been chosen.

We give the particular values of the control parameters used in simulations in each of the proceeding subsections of this section.

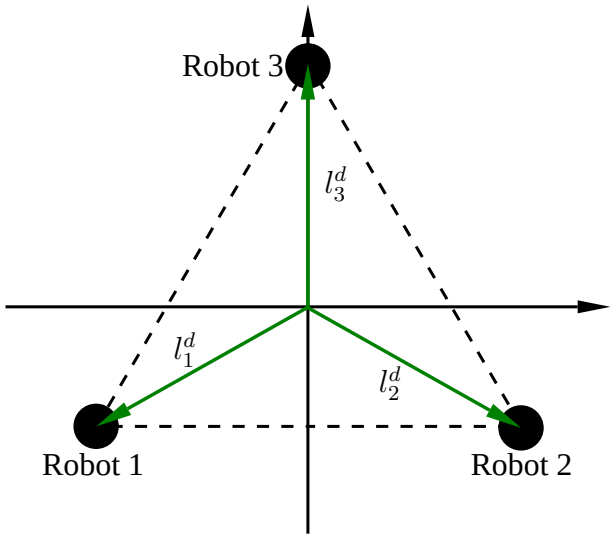

Figure 3.3: Desired formation geometry used in the simulations and experiments.

3.3.1 Kinematic formation control algorithm

In this section we present simulation results regarding the kinematic formation control law given in Section 3.2.1. Besides the simulation settings introduced in the introduction of this section, the additional control parameters are summarised in Table 3.1.

With such a choice of simulation settings, all conditions in Theorem 3.2.1 are now met and hence global exponential stability of the formation error dynamics is guaranteed. First, the simulations presented next illustrate that the robots (asymptotically) form the desired formation. Secondly, they illustrate the benefit of mutual coupling between the robots in terms of the robustness of the formation keeping properties in the face of perturbations and the convergence speed with which the robots form the desired formation. The simulation results are shown

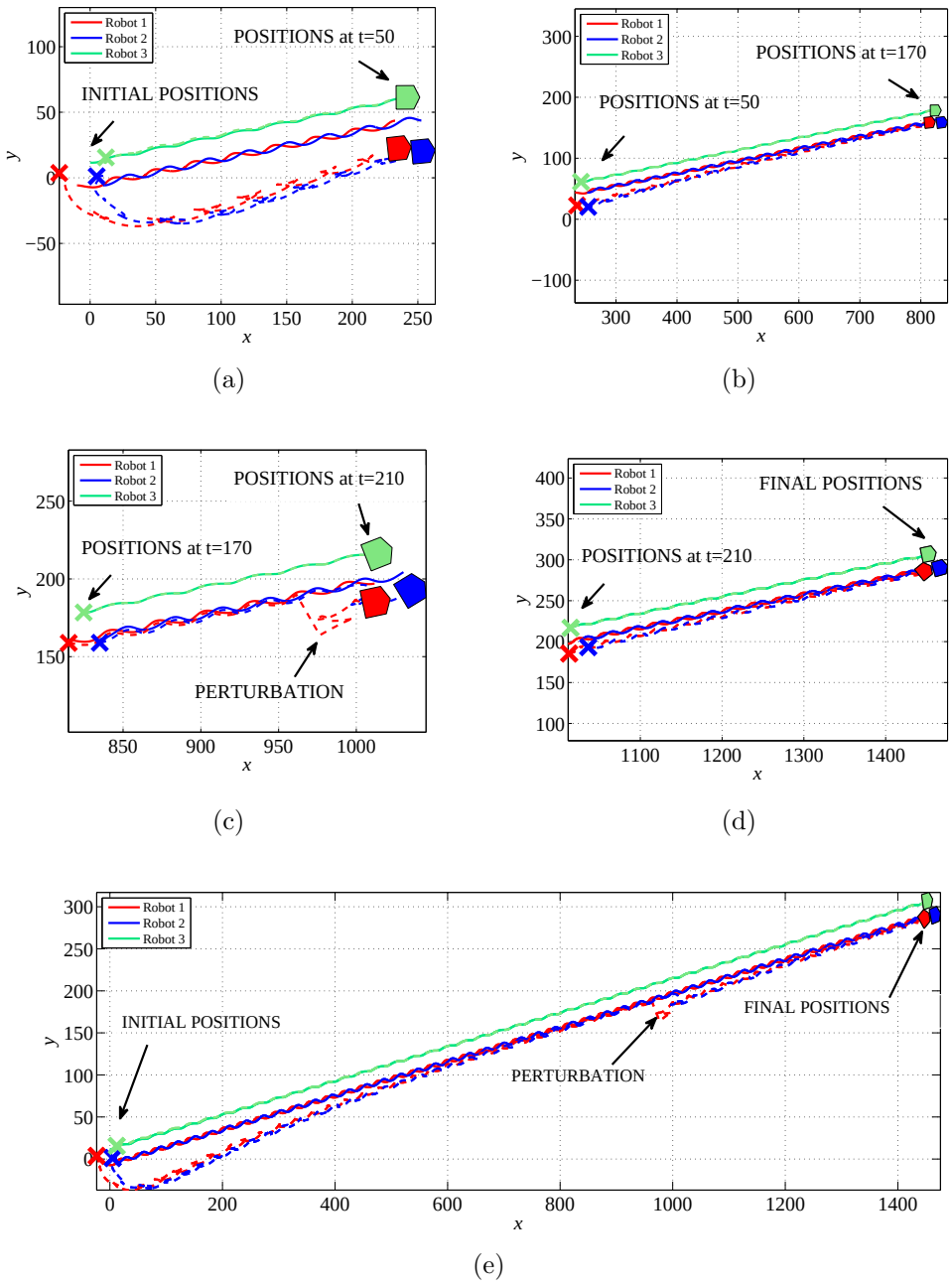

Figure 3.4: Desired robot paths (solid line) and actual robots paths (dashed line) in the plane in the case of a disconnected communication graph using the kinematic control algorithm (3.7). (a) paths between $t = 0$ and $t = 50$ (b) paths between $t = 50$ and $t = 170$ (c) paths between $t = 170$ and $t = 210$ (d) paths between $t = 210$ and $t = 300$ (e) whole paths.

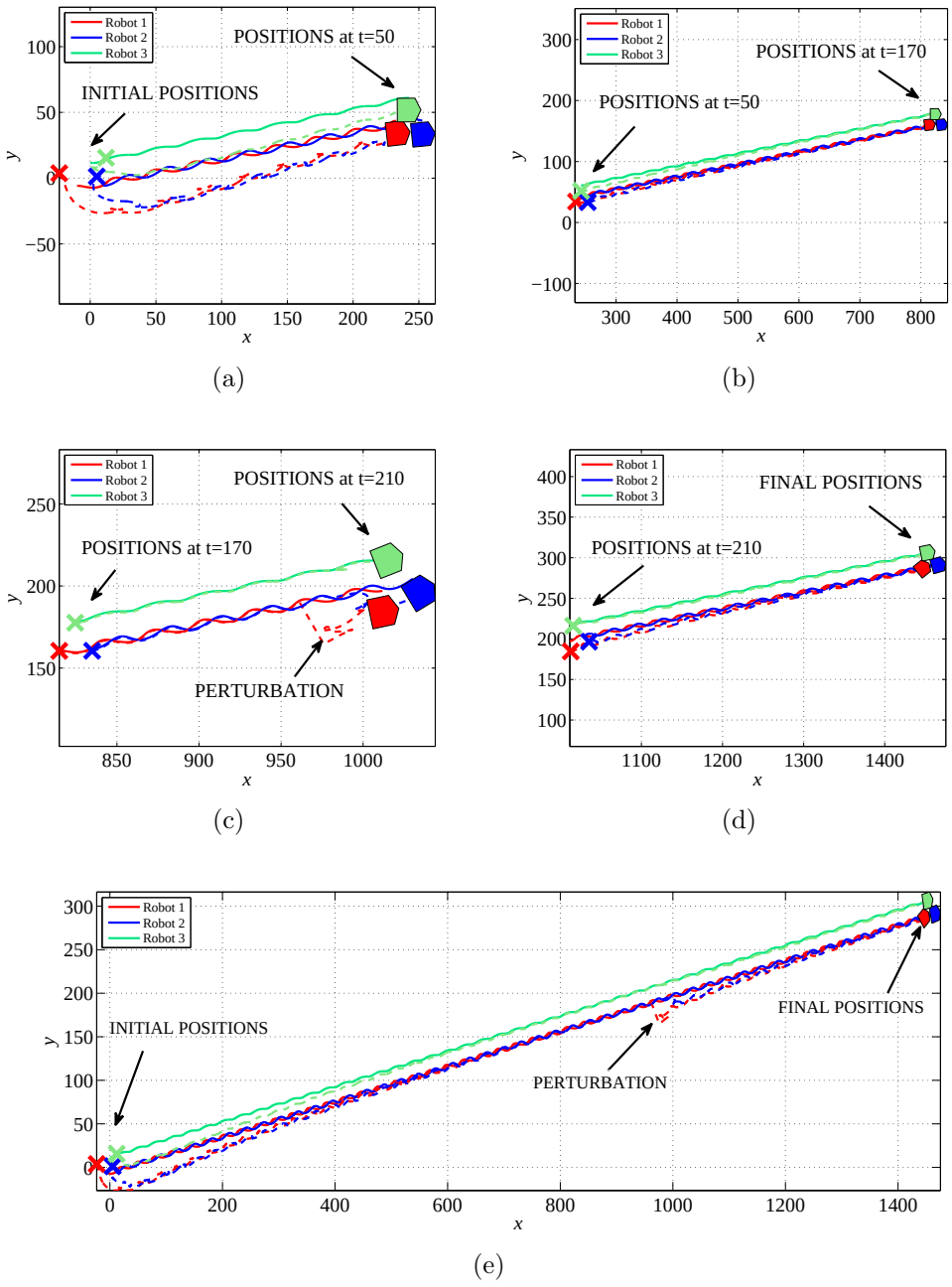

Figure 3.5: Desired robot paths (solid line) and actual robots paths (dashed line) in the plane in the case of a connected communication graph using the kinematic control algorithm (3.7): (a) paths between $t = 0$ and $t = 50$ (b) paths between $t = 50$ and $t = 170$ (c) paths between $t = 170$ and $t = 210$ (d) paths between $t = 210$ and $t = 300$ (e) whole paths.

Robot number	**Control gains**		
Robot 1	$c_1^x = 6$ $\widetilde{c}_{12}^x = 19$ $\widetilde{c}_{13}^x = 0$	$c_1^y = 4$ $\widetilde{c}_{12}^y = 15$ $\widetilde{c}_{13}^y = 0$	$c_1^\theta = 0.1$ $\widetilde{c}_{12}^\theta = 3$ $\widetilde{c}_{13}^\theta = 0$
Robot 2	$c_2^x = 6$ $\widetilde{c}_{21}^x = 19$ $\widetilde{c}_{23}^x = 27$	$c_2^y = 1.5$ $\widetilde{c}_{21}^y = 15$ $\widetilde{c}_{23}^y = 15$	$c_2^\theta = 0.3$ $\widetilde{c}_{21}^\theta = 3$ $\widetilde{c}_{23}^\theta = 3$
Robot 3	$c_3^x = 2$ $\widetilde{c}_{31}^x = 0$ $\widetilde{c}_{32}^x = 27$	$c_3^y = 3$ $\widetilde{c}_{31}^y = 0$ $\widetilde{c}_{32}^y = 15$	$c_3^\theta = 0.5$ $\widetilde{c}_{31}^\theta = 0$ $\widetilde{c}_{32}^\theta = 3$

Table 3.1: List of control parameters used in simulations in Section 3.3.1. Note that in the case of a disconnected communication graph, coupling gains $\widetilde{c}_{23}^\nu$ and $\widetilde{c}_{32}^\nu$ for $\nu \in \{x, y, \theta\}$ are set to 0.

in Figures 3.4–3.6. In Figure 3.4, we depict the robots' paths in the case of the disconnected communication graph of the formation in Figure 3.1(a). It can be seen that the robots in the formation converge to the desired formation geometry which is the equilateral triangle. This is owing to the individual tracking control of each robot. Then, when Robot 1 is perturbed, only Robot 1 and Robot 2 try to counteract its effect and keep the formation shape while Robot 3 is unaware of the perturbation and thus it does not divert from its desired trajectory in order for the formation shape to be maintained. Also at the beginning of the simulations, the disconnected Robot 3 swiftly converges to its desired trajectory regardless of the ill-positioned Robots 1 and 2, see Figure 3.4(a).

The results are different when the communication graph is connected, see Figure 3.5. The formation shape is restored faster when the communication graph is connected, see Figures 3.4(a) and 3.5(a). When the perturbation takes place, both unperturbed robots diverge temporarily from their desired trajectories in favour

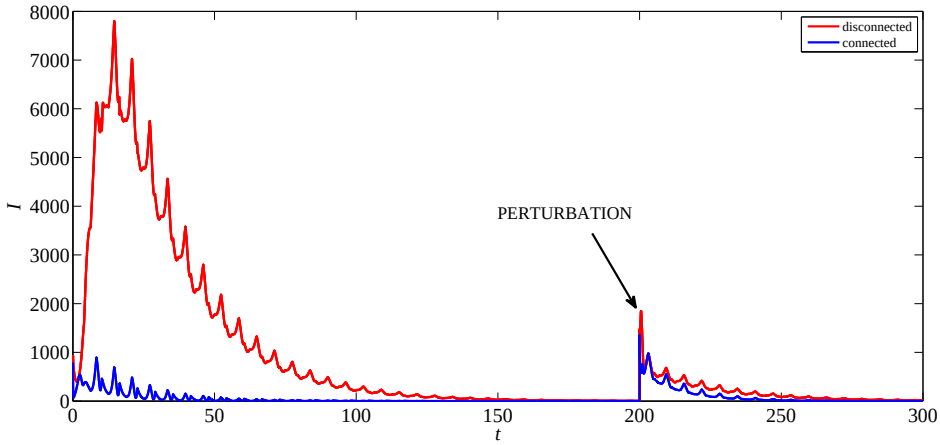

Figure 3.6: Comparison between formation geometry maintenance index I using the kinematic control algorithm for a connected and a disconnected communication graph.

of keeping the formation geometry. This is due to the fact that the communication graph is connected and the particular choice of mutual coupling terms $\widetilde{c}_{ij}^{x}$, $\widetilde{c}_{ij}^{y}$, $\widetilde{c}_{ij}^{\theta}$ which dominate chosen tracking control gains c_i^x, c_i^y and c_i^θ. This affects the value of the formation geometry maintenance index, see Figure 3.6. Recall that the index I is a measure of the discrepancy between the actual formation shape and the desired one. After the perturbation, the formation geometry maintenance index is larger in the case of the disconnected communication graph than in the case of the connected communication graph. Something similar may also be observed at the beginning of the simulations. As a result of non-zero initial conditions, the formation geometry maintenance index is also nonzero and converges to zero faster when the connectivity condition of the communication graph holds.

We summarise our findings in the following. Formation behaviour under the for-

mation control law in (3.7) can be improved if the communication graph $\mathcal{G}$ of the formation is connected. This requirement stems from the fact that each robot needs to be able to exchange information with the rest of the group so that every member of the formation is aware of the actual performance of the whole group. Only if the communication graph is connected, we can be sure that the actual performance is known to each robot through their neighbours. This guarantees that the two objectives of trajectory tracking and formation keeping are carried on independently. Note that, an all-to-all communication is not required but it suffices if the communication network is distributed with the communication graph being connected in the sense that there is a connection from each robot to all other robots, possibly through other robots on the way, see Definition C.4. On the contrary, when the communication graph of the formation is disconnected, i.e. there are robots in the formation completely decoupled from the rest of the formation, one obtains pure trajectory tracking by some of the robots. By implication this also solves the formation control problem, but as illustrated by the simulation results, a better performance in terms of the robustness of the formation with respect to perturbations may be obtained when the communication graph is indeed connected.

3.3.2 Dynamic formation control algorithm

In this section we present the simulation results for the dynamic formation control law given in Section 3.2.2. We provide all control parameters used in the simulations appearing in this section in Tables 3.1 and 3.2.

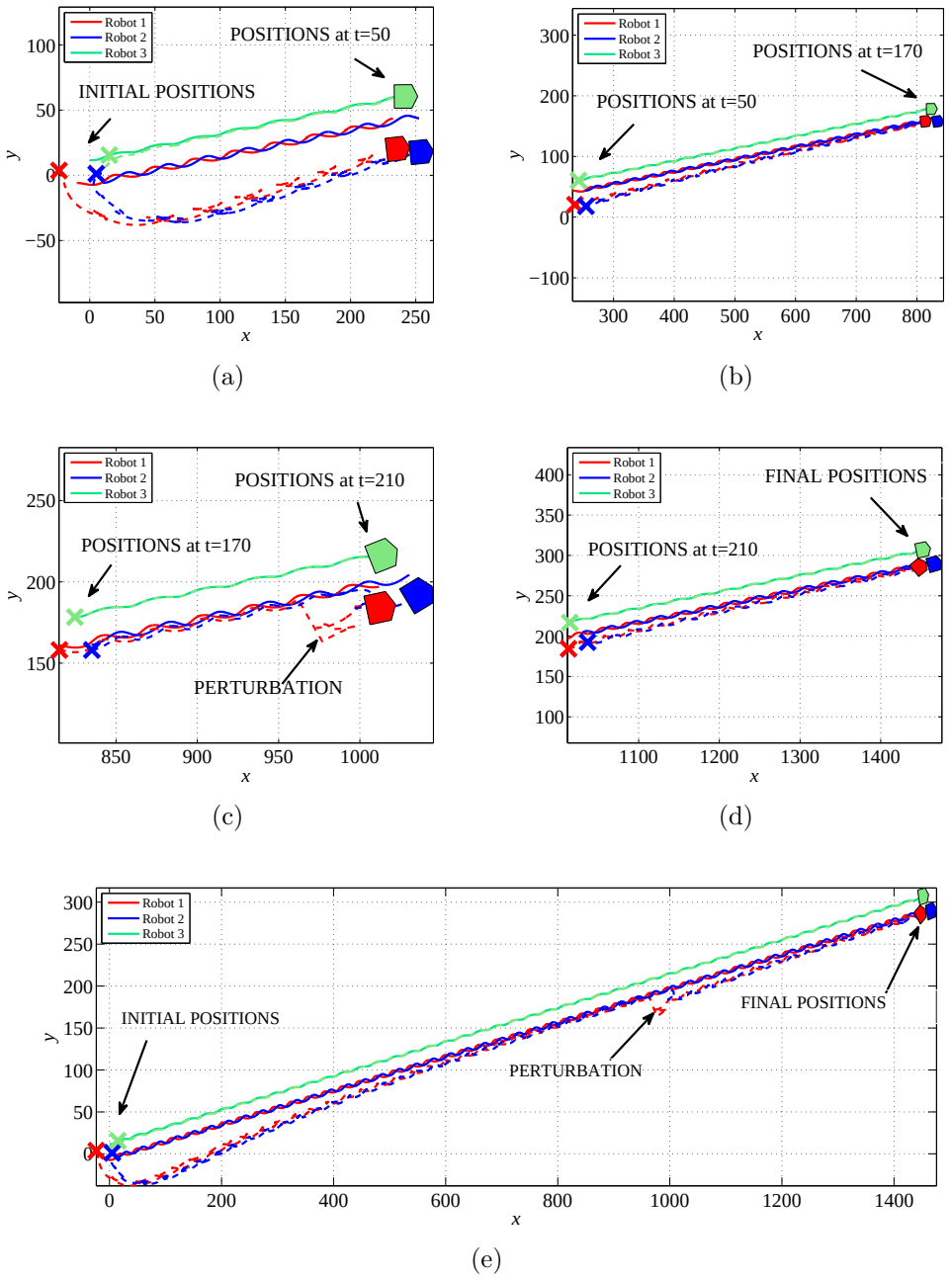

Figure 3.7: Desired robot paths (solid line) and actual robots paths (dashed line) in the plane in the case of a disconnected communication graph using the dynamic control algorithm (3.28). (a) paths between $t = 0$ and $t = 50$ (b) paths between $t = 50$ and $t = 170$ (c) paths between $t = 170$ and $t = 210$ (d) paths between $t = 210$ and $t = 300$ (e) whole paths.

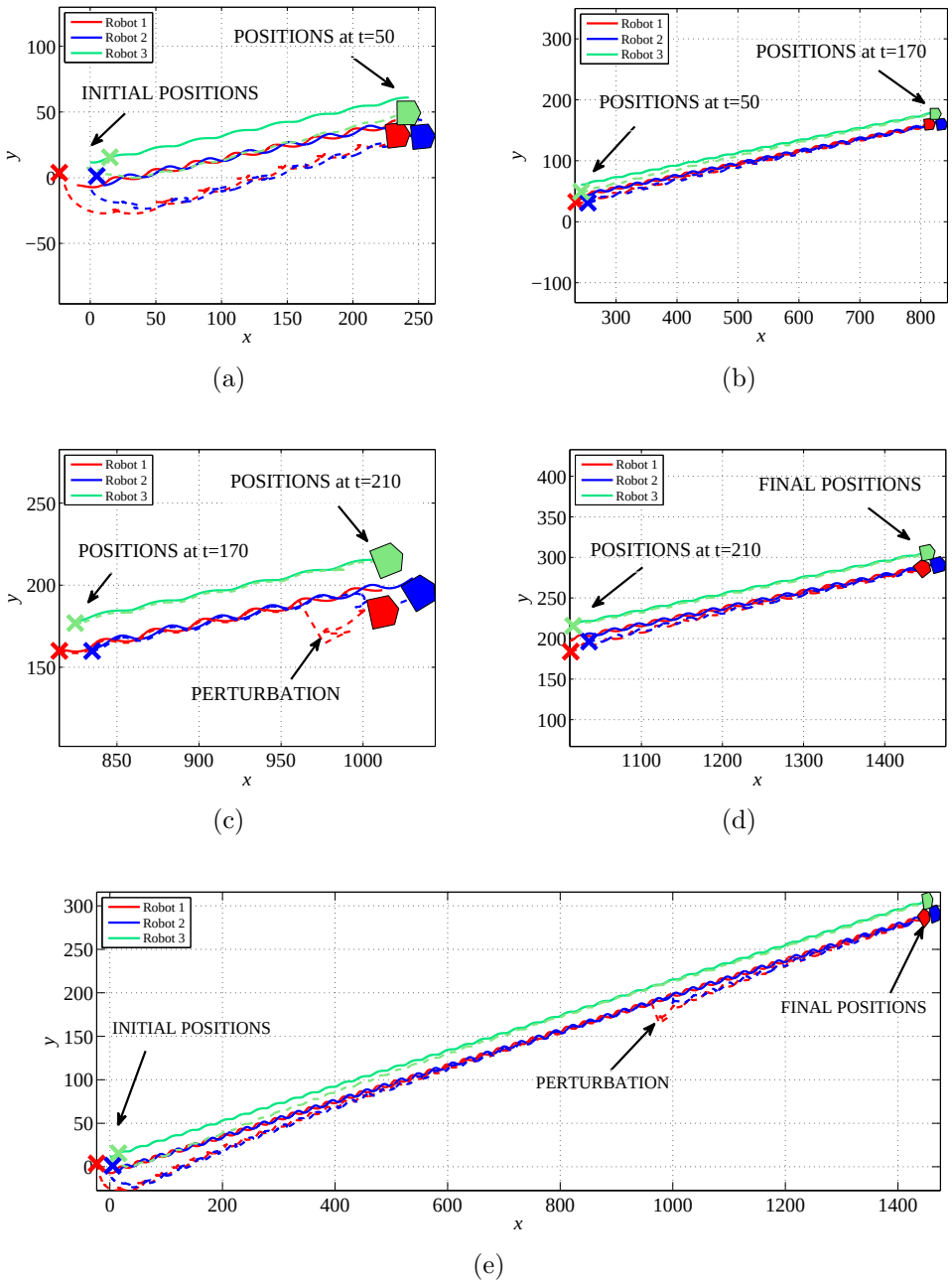

Figure 3.8: Desired robot paths (solid line) and actual robots paths (dashed line) in the plane in the case of a connected communication graph using the dynamic control algorithm (3.28). (a) paths between $t = 0$ and $t = 50$ (b) paths between $t = 50$ and $t = 170$ (c) paths between $t = 170$ and $t = 210$ (d) paths between $t = 210$ and $t = 300$ (e) whole paths.

Robot number	**Control gains**		
Robot 1	$c_1^{vv} = 15$	$c_1^{vx} = 15$	$c_2^{\omega} = 15$
Robot 2	$c_2^{vv} = 15$	$c_2^{vx} = 15$	$c_2^{\omega} = 15$
Robot 3	$c_3^{vv} = 9$	$c_3^{vx} = 9$	$c_3^{\omega} = 15$

Table 3.2: List of control parameters used in simulations in Section 3.3.2.

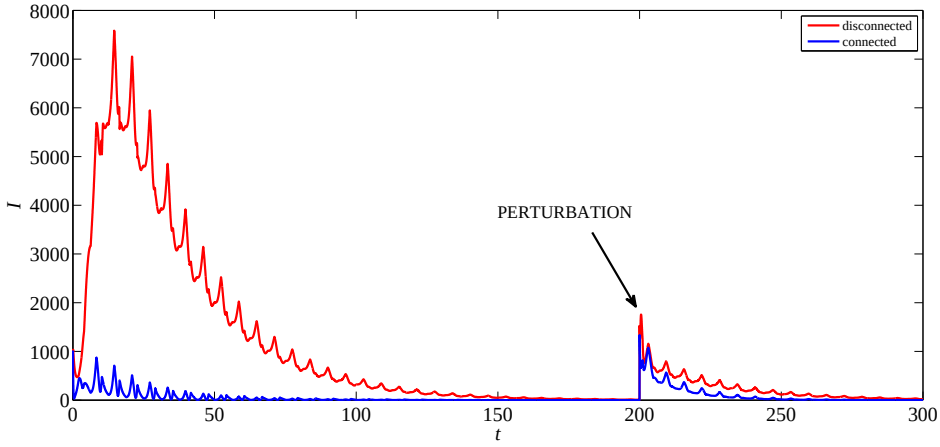

Figure 3.9: Comparison between formation geometry maintenance index I using the dynamic control algorithm for a connected and a disconnected communication graph.

In Figure 3.7, robot paths in the case of a disconnected communication graph are shown. It can be concluded that initially all robots converge to their desired positions in the formation and form the shape of the equilateral triangle. This situation changes entirely when a perturbation is applied to Robot 1. Since Robot 3 is disconnected from the other robots in the group, it does not react when the perturbation occurs, as illustrated in Figure 3.7. On the other hand, in the case of a connected communication graph, even though only Robot 1 is perturbed, both remaining robots after the perturbation also adjust their positions to keep the desired geometry. This comes about on account of the mutual coupling terms

that cause the robots to again face a trade–off between trajectory tracking and formation shape preservation, as in the case of the kinematic control law in the previous subsection. It may be seen in Figure 3.8 that when Robot 1 is perturbed, both Robot 2 and Robot 3 react to this perturbation so that the perturbation is counteracted and the formation shape remains close to the desired formation geometry in the transient after the perturbation.

As in the previous set of simulations, we can even more clearly observe the advantage of having a connected communication graph by presenting the formation geometry maintenance index, see Figure 3.9. In particular, we can observe two positive aspects of such a communication structure. First of all, the index has a larger magnitude in the case of the communication graph being disconnected both at the beginning of the simulations and when the perturbation occurs. Moreover, it approaches zero at a faster rate when the communication graph is connected.

3.3.3 Saturated formation control algorithm

In this section we present simulation results of the saturated formation control algorithm given in Section 3.2.3. It is assumed that the maximum actuator inputs that robots can produce are $\bar{v}_i = 10$ and $\bar{\omega}_i = 2$ for all robots in the formation. Therefore, the control parameters are selected as shown in Table 3.3. Moreover, using (3.43, 3.44) and the aforementioned control parameters we choose $\alpha(s) = 0.9\tanh(s)$ and $\gamma(s) = 0.5\tanh(s)$. With such a choice of control parameters, the control inputs v_i and ω_i obtained in the saturated control algorithm (3.38) are guaranteed to satisfy the limits $\bar{v}_i = 10$ and $\bar{\omega}_i = 2$

Robot number	**Control gains**	
Robot 1	$c_1^x = 0.4$ $\widetilde{c}_{12}^x = 1.5$ $\widetilde{c}_{13}^x = 0$	$c_1^\theta = 0.7$ $\widetilde{c}_{12}^\theta = 0.9$ $\widetilde{c}_{13}^\theta = 0$
Robot 2	$c_2^x = 0.15$ $\widetilde{c}_{21}^x = 1.5$ $\widetilde{c}_{23}^x = 1.5$	$c_2^\theta = 0.7$ $\widetilde{c}_{21}^\theta = 0.9$ $\widetilde{c}_{23}^\theta = 0.9$
Robot 3	$c_3^x = 0.3$ $\widetilde{c}_{31}^x = 0$ $\widetilde{c}_{32}^x = 1.5$	$c_3^\theta = 0.7$ $\widetilde{c}_{31}^\theta = 0$ $\widetilde{c}_{32}^\theta = 0.9$

Table 3.3: List of control parameters used in simulations in Section 3.3.3. In the case of a disconnected communication graph, coupling gains $\widetilde{c}_{23}^\nu$ and $\widetilde{c}_{32}^\nu$ are set to 0 for $\nu \in \{x, \theta\}$.

The simulation results of the formation control algorithm with saturated inputs are given in Figures 3.10 – 3.12. In particular, in Figures 3.10 and 3.11 we present the robot paths in the plane in the case of the disconnected communication graph and the connected communication graph, respectively. Based on these results, it is concluded that in the case of a disconnected communication graph, robots in the formation do not create the desired formation shape which is an equilateral triangle nor do they follow the prescribed trajectory as a whole. It can be particularly seen in Figures 3.10(a) and 3.10(b) that when the communication graph is disconnected, the tracking is not achieved for Robot 3 which is disconnected from the rest of the formation as its actual trajectory does not coincide with its desired trajectory. It appears that due to lack of interactions with the rest of the group, this robot needs some more time to converge to its desired trajectory and thus its desired location within the formation. On contrary, the formation control task is fulfilled in the case of the connected communication graph as both trajectory tracking and formation shape are attained by all robots in the formation.

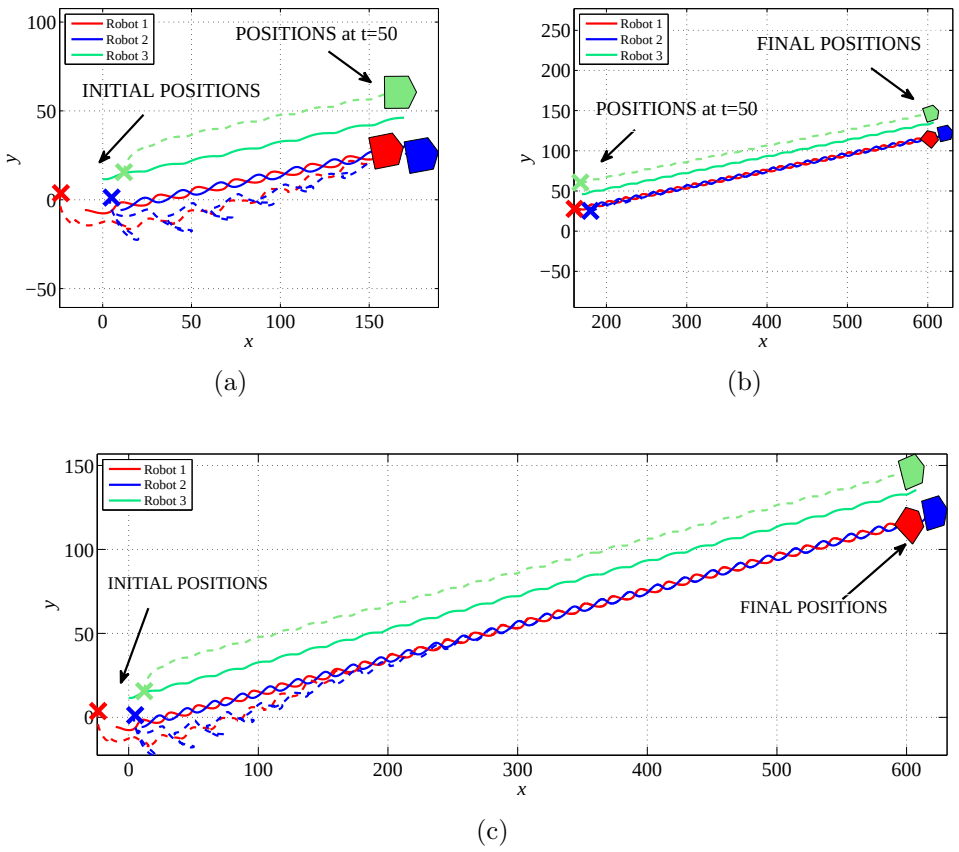

Figure 3.10: Desired robot paths (solid line) and actual robots paths (dashed line) in the plane in the case of a disconnected communication graph using the saturated control algorithm (3.38). (a) paths between $t = 0$ and $t = 50$ (b) paths between $t = 50$ and $t = 300$ (c) whole paths.

In addition to these results, we again depict the formation geometry maintenance index, see Figure 3.12. This is to show that also in the case of the saturated formation controller robots benefit from being able to exchange information with their neighbours. The comparison between the value of the index in the case of a disconnected and a connected communication topology of the formation reveals that the robots in the formation are more oriented towards formation shape maintenance when coupling between robots is allowed. There is a large disparity

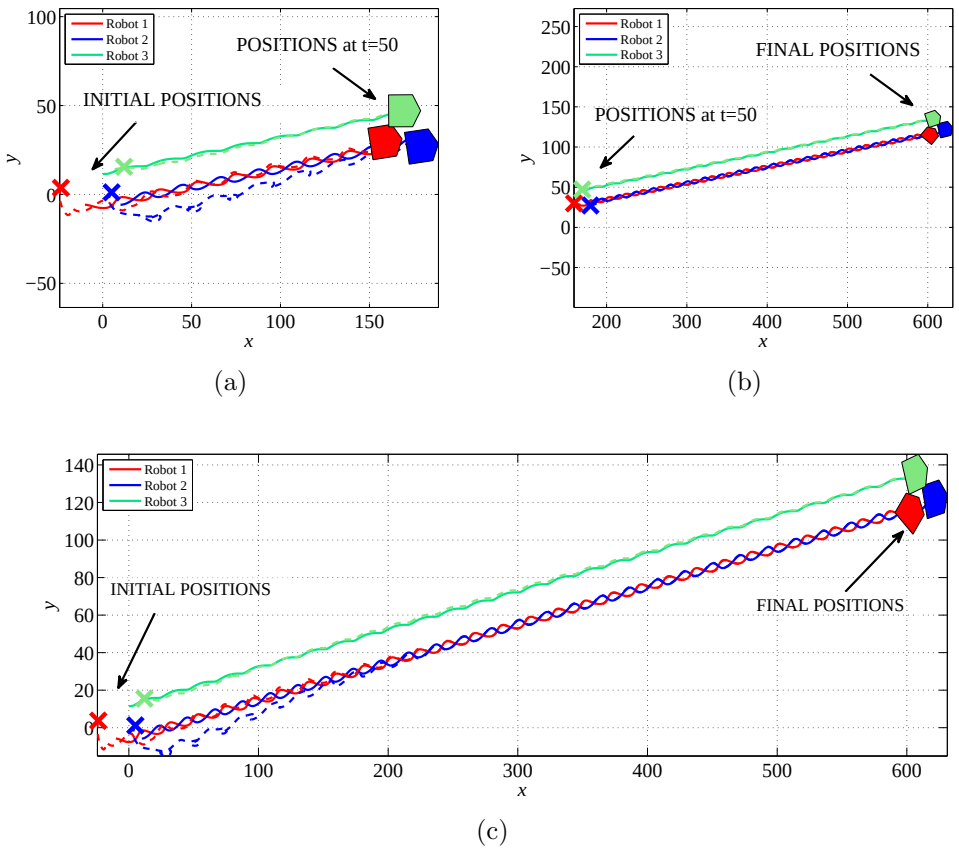

Figure 3.11: Desired robot paths (solid line) and actual robots paths (dashed line) in the plane in the case of a connected communication graph using the saturated control algorithm (3.38). (a) paths between $t = 0$ and $t = 50$ (b) paths between $t = 50$ and $t = 300$ (c) whole paths.

between the values of the index in both cases in favour of the connected communication graph. In fact, in the case of a disconnected communication graph, it is confirmed that the robots did not manage to create the desired formation shape although they are converging to this state and need more time to accomplish this task. Once again therefore it is seen that the robots converge to their desired formation shape faster and with smaller transient error in terms of the formation geometry maintaining when information exchange between the robots

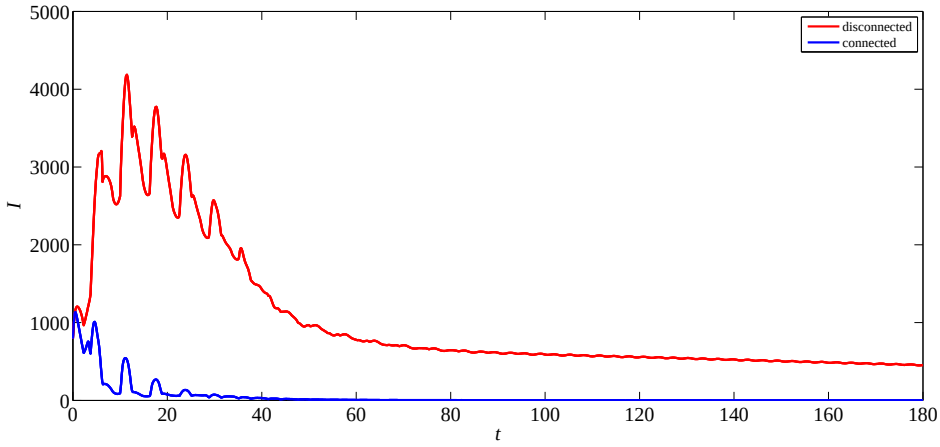

Figure 3.12: Comparison between formation geometry maintenance index I using the saturated control algorithm for a connected and a disconnected communication graph.

in the formation is in operation.

Note that in the simulations regarding the saturated formation control algorithm we do not apply the perturbation to any of the robots. This is because in this subsection we want to merely emphasise that formation control problem can be solved using the saturated formation control algorithm as opposed to expounding on all aspects of robots behaviour in the formation.

3.4 Experiments

In this section we illustrate the behaviour of a mobile robot formation under the influence of the kinematic control law given in Theorem 3.2.1 based on experiments. The experimental setup is described in Subsection 3.4.1. Then, the results

obtained in experiments are given in Subsection 3.4.2.

3.4.1 Experimental setup

The experimental setup is shown in Figure 3.13. The experiments were performed at Eindhoven University of Technology in Eindhoven, the Netherlands, with three E-Puck mobile robots (Mondada and Bonani, 2007; Mondada et al., 2009). The E-Puck robot is a differentially driven unicycle robot with two individually driven wheels actuated by stepper motors (for a more detailed description of E-Puck robots, refer to Appendix D). In the experimental setup, a camera is used to localise the robots in the arena. To that end, on top of each robot a unique marker is attached so that each robot can be distinguished from the others on camera images (Adinandra, 2012; Caarls et al., 2009). These images are sent to the PC for processing and subsequently robots' positions and orientations are determined. The PC is also used to generate the desired trajectories for the robots according to the desired trajectory of the overall formation and the desired formation shape. Moreover, because of the restricted processing power of the microcontroller available on the E-Pucks, the PC also calculates the control algorithms for all robots and consequently evaluates the resulting velocities of the robots' wheels. The obtained velocities of the robots' right and left wheels are sent via a BlueTooth communication protocol to the robots to execute the control algorithm.

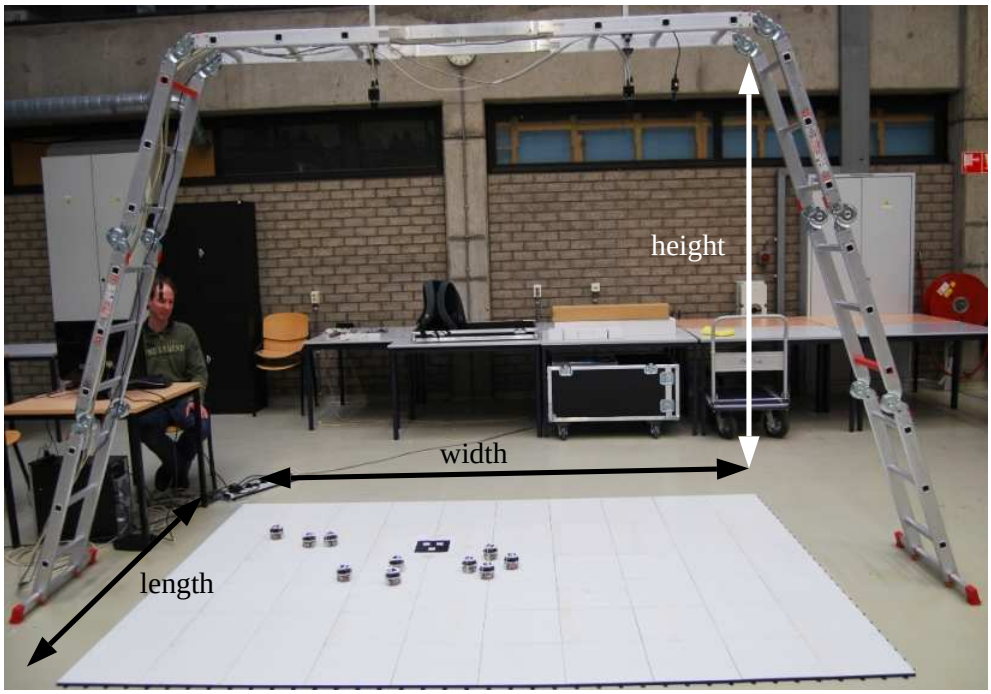

The arena: length $= 2.2$ [m], width $= 3.2$ [m], height $= 2.3$ [m].

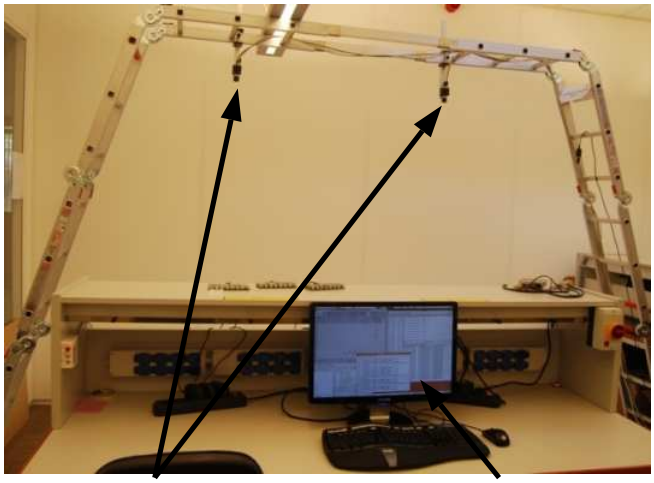

Figure 3.13: The experimental setup.

Control gains		
$c_i^x = 1\ \frac{1}{\text{s}}$	$c_i^y = 30$	$c_i^\theta = 0.5\ \frac{1}{\text{s}}$
$\widetilde{c}_{ij}^x = 2.5\ \frac{1}{\text{s}}$	$\widetilde{c}_{ij}^y = 30$	$\widetilde{c}_{ij}^\theta = 0.1\ \frac{1}{\text{s}}$

Table 3.4: List of control parameters used in experiments in Section 3.4.

3.4.2 Experimental results

In this section we present experimental validation of the control law given in Theorem 3.2.1. The control parameters employed in the experiments are summarised in Table 3.4, where we use the fact that from (3.7) it can be deduced that while the units of c_i^x, $\widetilde{c}_{ij}^x$, c_i^θ and c_{ij}^θ are $\frac{1}{s}$, both c_i^y and $\widetilde{c}_{ij}^y$ are unitless. Similarly to the simulation results in Section 3.3, the control parameters for experiments were chosen to show the influence of the mutual coupling gains, see Remark 3.3.1.

The desired virtual structure's trajectory is given by

$$x_{vc}^d(t) = 0.05t - 1.2, \tag{3.56}$$

$$y_{vc}^d(t) = 0.1\cos(0.3t) + 0.025t - 0.7, \tag{3.57}$$

where x_{vc}^d and y_{vc}^d are in meters and t is in seconds.

As in the simulations, the desired formation shape is an equilateral triangle as shown in Figure 3.3 where $l_1^d = \left(-0.15\text{ m}, -\frac{0.15}{\sqrt{3}}\text{ m}\right)^T$, $l_2^d = \left(0.15\text{ m}, -\frac{0.15}{\sqrt{3}}\text{ m}\right)^T$ and $l_3^d = \left(0\text{ m}, \frac{0.3}{\sqrt{3}}\text{ m}\right)^T$. Thus the sides of the triangle have a length of 0.3 m. The perturbation is a manual displacement of one of the robots in the formation executed after around 30 s.

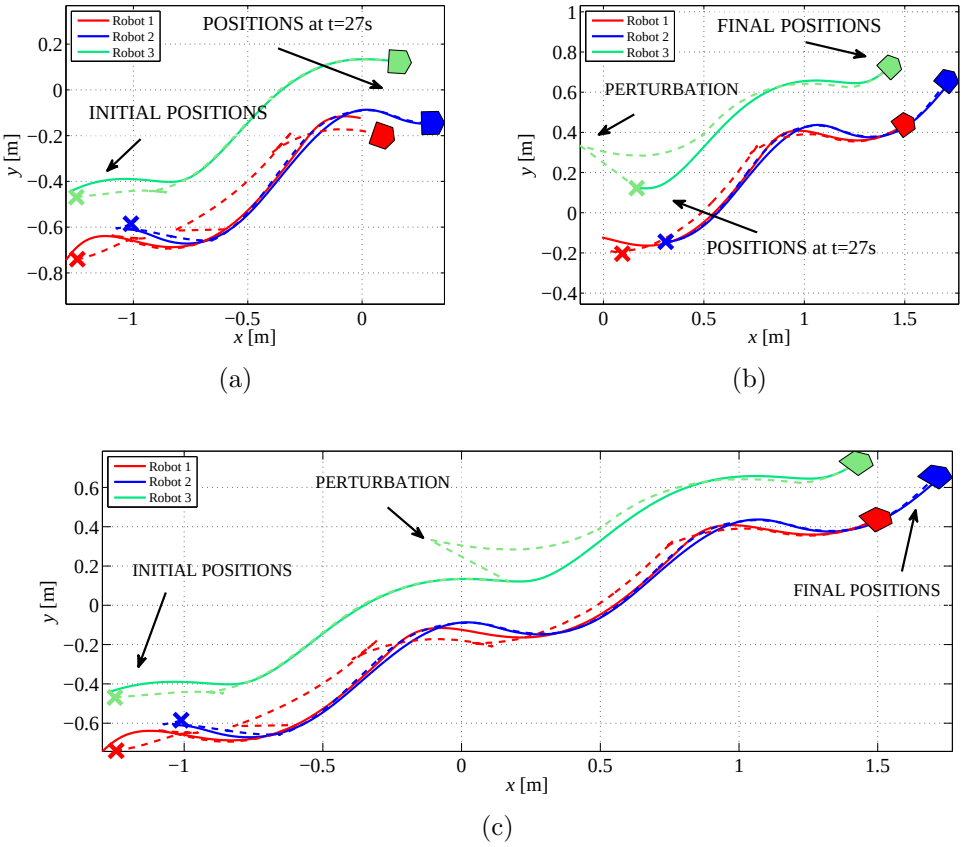

Figure 3.14: Desired robot paths (solid line) and actual robots paths (dashed line) in the plane obtained in experiments in the case of a disconnected communication graph. (a) paths between $t = 0$ s and $t = 27$ s (b) paths after $t = 27$ s (c) whole paths.

The experimental results are presented in Figures 3.14-3.16. In particular, in Figure 3.14 we present the robots' paths in the case of completely uncoupled robots, where $\widetilde{c}_{ij}^{x} = 0$, $\widetilde{c}_{ij}^{y} = 0$ and $\widetilde{c}_{ij}^{\theta} = 0$. This is equivalent to a completely disconnected communication graph of the formation. In turn, in Figure 3.15, the robots' paths in the plane are presented when the communication graph is connected according to the communication network shown in Figure 3.1(b). It can be seen in the plots, that in both cases robots in the formation converge

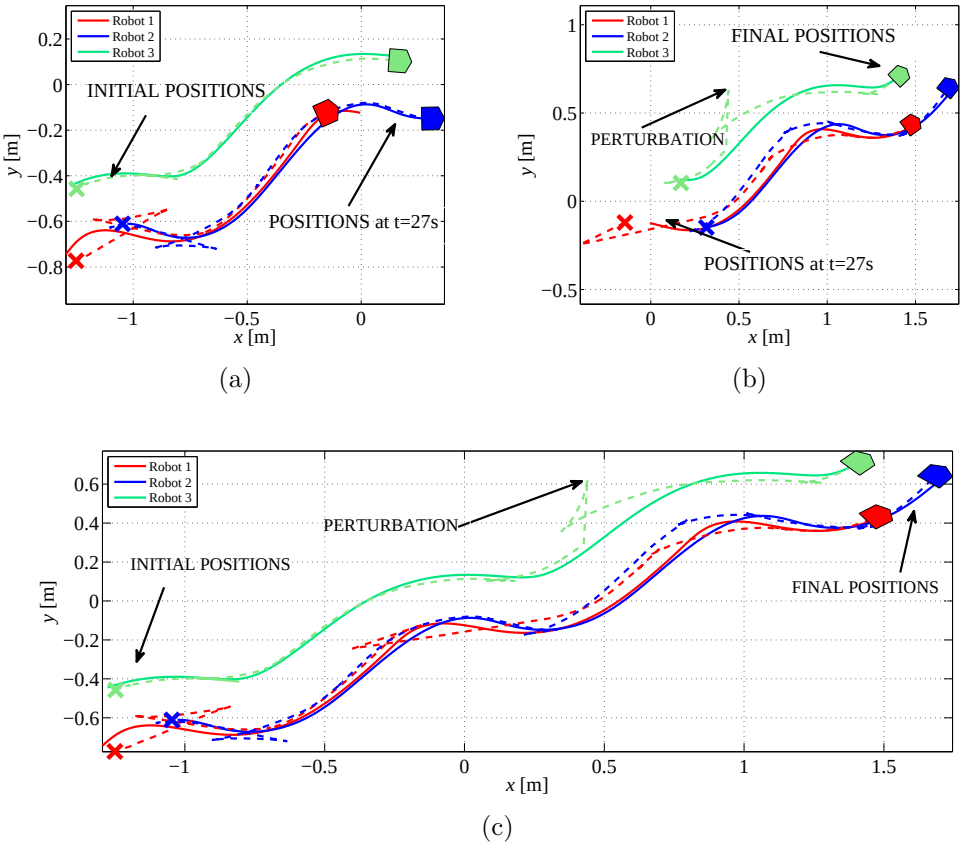

Figure 3.15: Desired robot paths (solid line) and actual robots paths (dashed line) in the plane obtained in experiments in the case of a connected communication graph. (a) paths between $t = 0$ s and $t = 27$ s (b) paths after $t = 27$ s (c) whole paths.

to the desired formation shape. Moreover, after the perturbation has occurred, the neighbours of the perturbed robot in Figure 3.15 diverge from their desired trajectories to recover the formation shape. This formation keeping behaviour is induced by the coupling terms added to the formation control algorithm and is absent in Figure 3.14 for a disconnected communication graph. We can therefore again confirm that these additional coupling terms in (3.7) enhance actual formation behaviour of robots in the formation.

The beneficial influence of allowing robots in the formation to exchange information with each other is also confirmed by examining Figure 3.16 which compares the formation geometry maintenance index (3.54) for a connected and a disconnected communication graph. Clearly, when the communication graph is connected, the index is smaller except for the perturbation peak. This is purely due to the fact that in experiments the displacement is done manually and therefore is not equal in the case of a connected and a disconnected communication graph. In fact, it is larger in the experiment with the connected communication graph which may be seen explicitly by comparing Figure 3.14 and Figure 3.15. Apart from the very moment of the perturbation, the formation geometry maintenance index is smaller for the case of a connected communication graph. Moreover, despite the larger perturbation magnitude, the formation geometry maintenance index decreases faster in the case of a connected communication graph.

In Section 6.2 we present a simulation study based on the settings of the experiments given in this section. This gives us a chance to compare the performance of the formation control algorithm (3.7) under similar conditions in the experiments and in the simulations.

3.5 Discussion

In this chapter, a formation control algorithm for unicycle mobile robots based on the virtual structure approach was proposed. We have designed two controllers depending on the kind of the unicycle robot: one based on a kinematic model

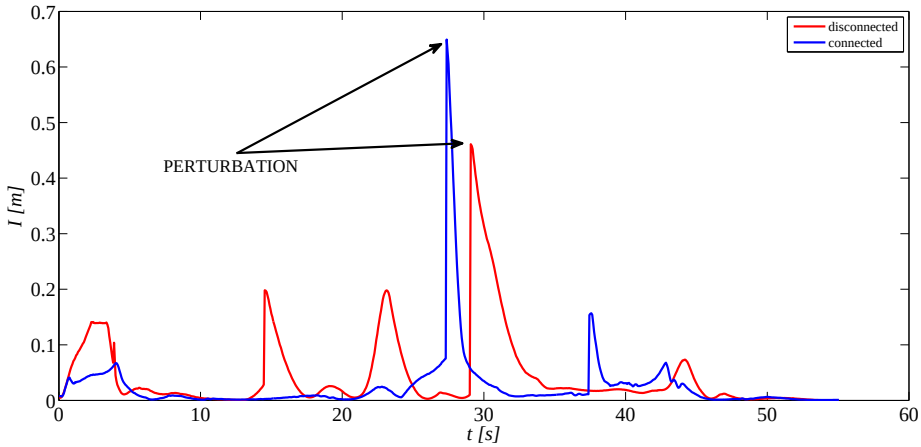

Figure 3.16: Comparison between formation geometry maintenance index I for a connected and a disconnected communication graph in experiments.

of a mobile robot and one based on a dynamic model of a mobile robot. They both comprise terms in the control law associated with communication between robots in the formation – the mutual coupling terms. These are a causative factor for increased robustness should some robots in the formation be confronted with perturbations. This is because the mutual coupling terms relate to information exchange between robots as opposed to schemes where information flow is unidirectional only, e.g. leader-follower or master-slave approaches. Moreover, we give a stability proof of the proposed approach for a formation of an arbitrary number of robots. In doing so, we are able to claim an exponential convergence rate of the formation error variables to zero, which is associated with a certain amount of robustness. In addition to that, we also study the effect of robot actuator limitations which resulted in a saturated control algorithm for formation control. To corroborate the proposed formation control algorithms in practice, simulations and experiments were performed for a three-robot system. The results obtained

support the claim of the significance of the inclusion of the mutual coupling terms in the formation control law. In particular, we have observed that if the communication graph of the formation is connected and mutual coupling is employed, the performance of the formation is enhanced. More specifically, sensitivity to perturbations is reduced in the sense that when a perturbation occurs, robots try to maintain a desired formation shape thus counteracting the perturbation. Furthermore, the simulation and experimental results also illustrate that the relation between the mutual coupling gains and the tracking gains may serve to balance between tracking individual trajectories and keeping the desired formation shape. If the emphasis is put on individual trajectory tracking, the tracking gains should prevail over the mutual coupling gains. On the other hand, if the formation shape maintenance is the leading objective, the mutual coupling gains ought to prevail over the tracking gains.

The strength of the algorithms presented follows among others from their simplicity in that the kinematic control law is linear in terms of the tracking errors of robots in the formation and the dynamic control law in addition depends linearly on the first derivative of the kinematic control inputs. Furthermore, the weak condition of the persistence of excitation of the angular velocity of a desired trajectory to be tracked, allows for a broad range of practical applications.

Chapter 4

Coordination–based control design for formations of unicycle mobile robots

4.1 Introduction

In this chapter, we study a formation control problem in which the objective is again for a group of unicycle robots to maintain a given time–varying formation geometry while following a desired trajectory. These results are partially published in (Sadowska et al., 2012).

In the developments in the previous chapter the coordination of robots in the formation was achieved implicitly via tracking control of all robots in the formation

with additional terms in the control law related to the robots' interactions. Conversely, in this chapter we take advantage of the method introduced in (Kostić et al., 2010b) which to a certain extent serves as a basis for the development of the control algorithm in this chapter. It was already mentioned in the Introduction that Kostić et al. (2010b) proposed a saturated formation control algorithm for time–varying formation shapes utilising a global communication network. Moreover, besides considering tracking errors of all robots, also a coordination error between a pair of robots in the formation control law is exploited in (Kostić et al., 2010b). This type of additional variables, likewise studied in (Sun et al., 2009), is also explicitly taken into account in the control law proposed in this chapter. In this sense, our results may be considered as an extension of (Kostić et al., 2010b) with the following additional contributions. First, we solve the formation control problem for the case of a distributed communication structure in lieu of a global one. This means that robots in the formation are only required to have access to information regarding the states of robots in their communication neighbourhood, instead of all other robots in the formation. Having a distributed communication network is undoubtedly advantageous, as it reduces the communication cost. This partially motivated our research. Secondly, we allow for non-identical or even in some cases non-symmetric coupling between robots. Thirdly, we also propose a saturated formation control law that takes into consideration actuator limitations and is distributed as opposed to the saturated control algorithm in (Kostić et al., 2010b) in which communication structure was global. Lastly, we include a simulation and experimental study to observe the difference between different communication structures of the formation. Therefore, the results given in this chapter possess the advantages of a distributed communication network

which is highly relevant in practice, and are more general than those in (Kostić et al., 2010b).

Although the main focus of this chapter is on coordination of a group of unicycle mobile robots, we show that this subject is closely related to the consensus control problem as defined in (Bliman and Ferrari-Trecate, 2008; DeLellis et al., 2010; Hui and Haddad, 2008; Olfati-Saber and Murray, 2003a, 2004; Olfati-Saber et al., 2007; Ren et al., 2005; Zhang et al., 2008). In particular we show that physical coordination of robots in the formation is equivalent to the consensus of tracking error variables given in a common coordinate system. To this end, we express all tracking error variables in the world frame to show that when the tracking error variables are in consensus, the robots form a desired formation shape. This is also what distinguishes the work presented in this chapter from the previous chapter, where all tracking error variables were given in local moving frames associated with individual robots. In such a case, when coupling terms are included, robots de facto act on consensus of tracking error variables given in local frames. However, in general consensus of the local error variables does not imply physical coordination of robots in the formation. Therefore, in Chapter 3 the robots in the formation may not create the desired formation shape despite the consensus of the considered tracking error variables. Moreover, in principle coordination is obtained only when tracking error variables are all zero.

We consider a formation consisting of N identical unicycle–type mobile robots. Let again $\mathcal{I} = \{1, \ldots, N\}$ denote the set of indices of robots in the formation. For the sake of completeness, let us recall that the kinematic equations of motion of

the i^{th} robot, $i \in \mathcal{I}$ as follows (Campion and Chung, 2008; De Wit et al., 1996; Siciliano et al., 2009):

$$\begin{aligned} \dot{x}_i &= v_i \cos\theta_i, \\ \dot{y}_i &= v_i \sin\theta_i, \\ \dot{\theta}_i &= \omega_i, \end{aligned} \tag{4.1}$$

in which $p_i(t) = (x_i(t), y_i(t))^T$ denotes the position of robot i and θ_i is the heading angle of this robot both with respect to the world frame. Moreover, v_i is the forward speed and ω_i is the angular velocity of the robot. Let $q_i(t) = \text{col}(p_i(t), \theta_i(t))$ denote the state of robot i at time t and let $q^d_{vc}(t) = \text{col}(p^d_{vc}(t), \theta^d_{vc}(t)) = \text{col}(x^d_{vc}(t), y^d_{vc}(t), \theta^d_{vc}(t))$ denote the given desired trajectory of the *virtual centre* of the formation. Then, a desired formation shape is defined using $l^d_i(t) = \text{col}\left(l^d_{ix}(t), l^d_{iy}(t)\right)$, which are bounded and subject to $\frac{d}{dt}(l^d_i(t))$ being bounded, $\forall i \in \mathcal{I}$, where $l^d_i(t)$ expresses the desired position coordinates of robot i relative to the local coordinate system of the virtual centre. Note that, in the case of a unicycle robot, the orientation variable is always uniquely determined using the no–side–slip constraint (2.2) and a robot's trajectory.

Following the Problem Statement in Chapter 2, the objective of the formation control problem is such that the formation as a whole should track a given desired trajectory $q^d_{vc}(t)$ and the desired formation shape $l^d_i(t)$, $i \in \mathcal{I}$, should be maintained by all robots in the formation. Assume that the velocities v^d_{vc} and ω^d_{vc} associated with the desired trajectory of the virtual centre are bounded. As per the Problem Statement in Chapter 2, it is clear that the formation control objective is met if all robots in the formation track their individual trajectories $p^d_i(t) = (x^d_i(t), y^d_i(t))^T$ defined using the information about the desired trajectory

of the virtual centre and the desired formation shape. In particular, the desired trajectory of each robot $i \in \mathcal{I}$ is given by

$$p_i^d = p_{vc}^d + R(\theta_{vc}^d) l_i^d, \tag{4.2}$$

where the rotation matrix $R(\theta)$ is given in (2.32). Then, the full desired state is $q_i^d(t) = ((p_i^d)^T(t), \theta_i^d(t))^T$ for each robot in the formation.

Now, let the position tracking error in the inertial coordinate frame e_i be defined as

$$e_i(t) = p_i^d(t) - p_i(t), \qquad (i \in \mathcal{I}). \tag{4.3}$$

According to (Kanayama et al., 1990), error e_i relates to the error e_i^{xy} defined in (3.5) given in the local robot-associated coordinate frame as follows:

$$e_i = R(\theta_i) e_i^{xy}. \tag{4.4}$$

We also define the angular error coordinate θ_i^e by $\theta_i^e = \theta_i^d - \theta_i$.

The usual well–known approach to solve the trajectory tracking problem is to analyse the convergence of the local error coordinates e_i^{xy}, see (Fierro and Lewis, 1997; Jiang and Nijmeijer, 1997; Kanayama et al., 1990; Morin and Samson, 2008). This approach is also followed in the previous chapter. However, as mentioned earlier in this section we now propose to use the global error variables e_i instead of the local variables e_i^{xy}. As is illustrated in the subsequent part of this chapter, this choice plays a role in stability analysis of the control algorithm.

Bearing in mind (4.1), (4.3) and (4.4), and using $\dot{R}(\theta_i) = \omega_i(t)SR(\theta_i)$ where

$$S = \begin{bmatrix} 0 & -1 \\ 1 & 0 \end{bmatrix}, \tag{4.5}$$

the error dynamics in global coordinates are given by

$$\begin{aligned} \dot{e}_i &= R(\theta_i)S\omega_i(t)e_i^{xy} + R(\theta_i)\left(-S\omega_i(t)e_i^{xy} + \begin{pmatrix} v_i^d\cos\theta_i^e - v_i \\ v_i^d\sin\theta_i^e \end{pmatrix}\right) \\ &= R(\theta_i^d - \theta_i^e)\begin{pmatrix} v_i^d\cos\theta_i^e - v_i \\ v_i^d\sin\theta_i^e \end{pmatrix}, \end{aligned} \tag{4.6}$$

and

$$\dot{\theta}_i^e = \omega_i^d - \omega_i. \tag{4.7}$$

The desired velocities v_i^d, ω_i^d of a robot in the formation are derived from the desired velocities of the virtual centre and the desired position of a robot in the formation according to (3.4). As in the previous chapter, by the assumptions on v_{vc}^d, ω_{vc}^d and l_i^d we have that v_i^d, $i \in \mathcal{I}$, are bounded.

It was said before that the objective of the control law proposed in this chapter is twofold. First, robots need to create a given formation geometry and secondly, the formation as a whole needs to follow a prescribed trajectory. If the error variables (4.3) are zero, both objectives are satisfied because of the definition of the desired trajectories of the individual robots (4.2). However, note that the first objective can be independently verified. In particular, it follows from an earlier discussion that the first objective is satisfied if there exist a time–varying vector

$p_{vc}(t)$ and a function θ_{vc} such that for all robots $i \in \mathcal{I}$ and all t the following is fulfilled

$$p_i(t) - p_{vc}(t) = R(\theta_{vc}(t))l_i^d(t). \tag{4.8}$$

This is tantamount to all robots in the formation maintaining their desired formation shape irrespective of the trajectory tracking of the virtual centre. Therefore, when Condition (4.8) holds for all robots in the formation, the desired formation shape has been attained. However the actual position of the formation in the plane at a specific time instance may differ from the desired position determined by the desired trajectory of the virtual centre. If in addition, we consider a more strict requirement that the actual orientation of the formation needs to coincide with the desired value, i.e. $\theta_{vc} = \theta_{vc}^d$, we obtain the following condition

$$p_i(t) - p_{vc}(t) = R(\theta_{vc}^d)l_i^d(t) = p_i^d(t) - p_{vc}^d(t), \tag{4.9}$$

where we used (4.2). Condition (4.9) is equivalent to $e_i = e_j$. As a consequence of this reasoning and following the developments in (Kostić et al., 2010b), we declare a pair of robots i and j in the formation being coordinated with respect to one another when $e_i = e_j$, irrespective of whether or not trajectory tracking is ensured for these robots. Therefore, we define the coordination error between a pair of robots i and j as

$$\sigma_{ij} = e_i - e_j. \tag{4.10}$$

Then, we say that a desired formation geometry is obtained when all robots are coordinated with respect to each other. In other words, the coordination error

needs to be zero for all pairs of robots $i, j \in \mathcal{I}$:

$$\sigma_{ij} = 0, \quad \forall i, j \in \mathcal{I}. \tag{4.11}$$

Condition (4.11) is referred to as coordination of a group of robots. From (4.10), it is clear that if both $e_i = 0$ and $e_j = 0$ then also $\sigma_{ij} = 0$. Nonetheless, we later show that coordination may be achieved with nonzero position tracking errors of robots in the formation.

It needs to be remarked that in contrast to the results presented in (Kostić et al., 2010b), we do not rotate the vector σ_{ij} to obtain $\bar{\sigma}_{ij} = R^T(\theta_i + \theta_j)\sigma_{ij}$ in the local frame, common for robot i and robot j. Conversely, similarly to the tracking error of individual robots, the coordination error σ_{ij} is expressed in the common coordinate frame for all robots in the formation, i.e. the world frame. The rationale behind this choice is to get rid of some conservatism brought by this selection of the coordination error $\bar{\sigma}_{ij}$ in (Kostić et al., 2010b), where the coordination of robots is not possible without zero tracking errors. We explain this issue in more detail in Section 4.2

From the definition of the coordination errors σ_{ij}, it is apparent that coordination of a group of mobile robots is equivalent to consensus (Olfati-Saber and Murray, 2003a, 2004; Olfati-Saber et al., 2007) of the tracking error variables in the world frame. Therefore, we connect in our work the notion of consensus with coordination of a group of mobile robots in the sense of convergence to the desired formation geometry.

Note that the coordination error σ_{ij} defined in (4.11) satisfies

$$\dot{\sigma}_{ij} = R(\theta_i) \begin{pmatrix} v_i^d \cos\theta_i^e - v_i \\ v_i^d \sin\theta_i^e \end{pmatrix} - R(\theta_j) \begin{pmatrix} v_j^d \cos\theta_j^e - v_j \\ v_j^d \sin\theta_j^e \end{pmatrix}, \tag{4.12}$$

where we used (4.6).

In consideration of the new error variables e_i, θ_i^e and σ_{ij} introduced above, the objective of the formation control problem discussed in this chapter is to render the origin of (4.6, 4.7) globally asymptotically stable. Obviously, in this case we have that $\sigma_{ij} \to 0$ as $t \to \infty$. However, we also show that it is possible to obtain coordination of robots in the formation despite nonzero position tracking errors. In this case, we require that $\{(\theta_i^e, \sigma_{ij}) = (0,0), \forall i, j \in \mathcal{I}\}$ is a globally asymptotically stable set, see Definition B.14, for (4.6, 4.7). To solve these problems, we propose adequate formation control algorithms in the next section.

In light of the above, the main contributions of this chapter may be summarised as follows. We introduce a distributed formation control algorithm for unicycle mobile robots that explicitly ensures both trajectory tracking and coordination of cooperative robots. The control algorithm solves the formation control problem for time-varying formation geometries. In the control law design, we analyse the tracking error variables expressed in the world frame which paves the way to the determination of the analogy between the notion of consensus and coordination in the case of cooperative nonholonomic mobile robots. We also extend the formation control law by introducing a distributed saturated control that explicitly accommodates for actuator constraints. Moreover, we study the influence

of a connected and disconnected communication graph of the formation on the formation behaviour and perform simulation and experimental validation of the applicability of the control algorithms proposed.

The outline of this chapter is as follows. In Section 4.2 we present the control design. This includes the case when robots in the formation create a given formation shape and the virtual centre tracks a desired trajectory in Subsection 4.2.1 as well as the case when the trajectory tracking of the virtual centre is not obtained and only coordination of robots in the formation is achieved, see Subsection 4.2.2. To expand the applicability of our results, we also examine the case of saturated control law in Subsection 4.2.4. To illustrate the behaviour of robots when the proposed control law is applied, we include a simulation study in Section 4.3 and experimental study in Section 4.4. Concluding remarks are given in Section 4.5.

4.2 Control design

In this section, we introduce a number of formation control laws. In particular, in Subsection 4.2.1 we give our main result that describes formation control law in which the closed–loop error dynamics of the tracking error variables are globally asymptotically stable. This ensures that the desired formation shape is achieved and the formation as a whole tracks its desired trajectory. In Subsection 4.2.2 we relax some of the requirements of the main results and provide conditions for Pure Coordination, where robots do create their desired formation shape but do not necessarily track their desired trajectories. At the end of this section, we also give

an extension of our main result in a kind of leader–follower–like scheme where one robot is assigned as leader and others are followers, see Subsection 4.2.3. Further, in Subsection 4.2.4 we present the results regarding a saturated controller and we discuss the properties and benefits of the controllers in Subsection 4.2.5.

4.2.1 Tracking and coordination

In this subsection, we propose a formation control law that achieves the control objective to drive the tracking errors e_i and θ_i^e to zero for all $i \in \mathcal{I}$ while the error dynamics are stable. In other words, we aim to globally asymptotically stabilise the tracking error dynamics (4.6, 4.7) (therefore also $\sigma_{ij} \to 0$ as $t \to \infty$). To this end, we propose the following control law:

$$v_i(t) = v_i^d(t) + \begin{pmatrix} 1 & 0 \end{pmatrix} R^T(\theta_i) \left(\mathbf{C}_i^e e_i + \sum_{j \in N_i} \mathbf{C}_{ij}^\sigma \sigma_{ij} \right), \tag{4.13}$$

$$\omega_i(t) = \omega_i^d(t) + c_i^\theta \theta_i^e + v_i^d(t) \left(e_i^T \mathbf{C}_i^e + \sum_{j \in N_i} \sigma_{ij}^T \mathbf{C}_{ij}^\sigma \right) R(\theta_i) \begin{pmatrix} \dfrac{\cos\theta_i^e - 1}{\theta_i^e} \\ \dfrac{\sin\theta_i^e}{\theta_i^e} \end{pmatrix}, \tag{4.14}$$

where $\mathbf{C}_i^e$, $\mathbf{C}_{ij}^\sigma$ and c_i^θ, $i, j \in \mathcal{I}$, are control parameters to be defined. Note that (4.13, 4.14) constitutes a smooth control law.

We now give our main result in the following theorem that states the conditions under which controller (4.13, 4.14) globally asymptotically stabilises both the tracking and coordination error dynamics. Further, in the sequel of this section, we explain some consequences of our main result and provide some extensions of

the result.

Theorem 4.2.1. *Consider N unicycle mobile robots with kinematics described by (4.1). Consider a desired trajectory of the virtual centre of the formation $q_{vc}^d(t) = \left(x_{vc}^d(t), y_{vc}^d(t), \theta_{vc}^d(t)\right)^T$ such that the corresponding velocities v_{vc}^d and ω_{vc}^d are bounded, for each $i \in \mathcal{I}$ a desired formation shape given by a bounded vector $l_i^d(t)$ subject to $\dot{l}_i^d(t)$ being bounded. Consider also the corresponding desired trajectory $q_i^d(t) = \left(x_i^d(t), y_i^d(t), \theta_i^d(t)\right)^T$ given by (4.2), together with matching feedforward control inputs $v_i^d(t)$ and $\omega_i^d(t)$ given in (3.4), with $v_i^d(t)$ bounded away from zero and $\omega_i^d(t)$ bounded. Assume that $c_i^\theta > 0$, $\mathbf{C}_i^e = \mathrm{diag}(c_i^{xe}, c_i^{ye})$, $\mathbf{C}_{ij}^\sigma = \mathrm{diag}(c_{ij}^{x\sigma}, c_{ij}^{y\sigma})$, where $c_i^{xe} > 0$, $c_i^{ye} > 0$, $c_{ij}^{x\sigma} > 0$ and $c_{ij}^{y\sigma} > 0$ subject to $\mathbf{C}_{ij}^\sigma = \mathbf{C}_{ji}^\sigma$ for $i \in \mathcal{I}$, $j \in N_i$. Then, the origin of the closed–loop error dynamics (4.6, 4.7, 4.13, 4.14) is a globally asymptotically stable equilibrium.*

Proof. Consider a radially unbounded Lyapunov function candidate

$$V = \frac{1}{2}\sum_{i=1}^{N}\left((\theta_i^e)^2 + e_i^T\mathbf{C}_i^e e_i + \frac{1}{2}\sum_{j\in N_i}\sigma_{ij}^T\mathbf{C}_{ij}^\sigma\sigma_{ij}\right). \tag{4.15}$$

The time derivative of V in (4.15) along trajectories of (4.6, 4.7) is

$$\dot{V} = \sum_{i=1}^{N}\left(\theta_i^e(\omega_i^d(t) - \omega_i) + e_i^T\mathbf{C}_i^e R(\theta_i)\begin{pmatrix} v_i^d(t)\cos\theta_i^e - v_i \\ v_i^d(t)\sin\theta_i^e \end{pmatrix}\right.$$
$$\left. + \frac{1}{2}\sum_{j\in N_i}\sigma_{ij}^T\mathbf{C}_{ij}^\sigma\left(R(\theta_i)\begin{pmatrix} v_i^d(t)\cos\theta_i^e - v_i \\ v_i^d(t)\sin\theta_i^e \end{pmatrix} - R(\theta_j)\begin{pmatrix} v_j^d(t)\cos\theta_i^e - v_j \\ v_j^d(t)\sin\theta_j^e \end{pmatrix}\right)\right)$$

$$= \sum_{i=1}^{N} \left(\theta_i^e \left(\omega_i^d(t) - \omega_i + v_i^d(t) \left(e_i^T \mathbf{C}_i^e + \sum_{j \in N_i} \sigma_{ij}^T \mathbf{C}_{ij}^\sigma \right) R(\theta_i) \begin{pmatrix} \frac{\cos\theta_i^e - 1}{\theta_i^e} \\ \frac{\sin\theta_i^e}{\theta_i^e} \end{pmatrix} \right) \right.$$

$$\left. + \left(e_i^T \mathbf{C}_i^e + \sum_{j \in N_i} \sigma_{ij}^T \mathbf{C}_{ij}^\sigma \right) R(\theta_i) \begin{pmatrix} 1 \\ 0 \end{pmatrix} \left(v_i^d(t) - v_i \right) \right), \tag{4.16}$$

where the second equality holds because of the symmetry of the coupling terms $\mathbf{C}_{ij}^\sigma = \mathbf{C}_{ji}^\sigma$. Furthermore, when the control law for v_i and ω_i given by (4.13, 4.14) is applied, $\dot{V}$ becomes

$$\dot{V} = -\sum_{i=1}^{N} \left(c_i^\theta (\theta_i^e)^2 + \left\| \begin{pmatrix} 1 & 0 \end{pmatrix} R^T(\theta_i) \left(\mathbf{C}_i^e e_i + \sum_{j \in N_i} \mathbf{C}_{ij}^\sigma \sigma_{ij} \right) \right\|^2 \right) \leq 0, \tag{4.17}$$

where $\| \cdot \|$ denotes the Euclidean norm of a vector. Therefore, the equilibrium $(e_i, \theta_i^e) = (0, 0)$, for all $i \in \mathcal{I}$, is stable. Moreover, by Theorem B.11, we can show that $\lim_{t\to\infty} \dot{V} = 0$, and hence the system trajectories converge to the manifold defined by

$$\theta_i^e = 0, \tag{4.18}$$

$$\begin{pmatrix} 1 & 0 \end{pmatrix} R^T(\theta_i) \left(\mathbf{C}_i^e e_i + \sum_{j \in N_i} \mathbf{C}_{ij}^\sigma \sigma_{ij} \right) = 0. \tag{4.19}$$

Furthermore, consider the closed-loop error dynamics of θ_i^e given by

$$\dot{\theta}_i^e = -c_i^\theta \theta_i^e - v_i^d(t) \left(e_i^T \mathbf{C}_i^e + \sum_{j \in N_i} \sigma_{ij}^T \mathbf{C}_{ij}^\sigma \right) R(\theta_i) \begin{pmatrix} \frac{\cos\theta_i^e - 1}{\theta_i^e} \\ \frac{\sin\theta_i^e}{\theta_i^e} \end{pmatrix}. \tag{4.20}$$

Note that from (4.18) it is evident that $\theta_i^e \to 0$ as $t \to \infty$. Therefore, applying

Lemma A.6, one concludes that also

$$\begin{pmatrix} 0 & 1 \end{pmatrix} R^T(\theta_i) \left(\mathbf{C}_i^e e_i + \sum_{j \in N_i} \mathbf{C}_{ij}^\sigma \sigma_{ij} \right) \to 0 \quad \text{as} \quad t \to \infty, \tag{4.21}$$

where the fact that $c_i^\theta > 0$ and $v_i^d(t) \neq 0 \ \forall i \in \mathcal{I}$, $\forall t$ was used. (4.19) together with (4.21) yields

$$R^T(\theta_i) \left(\mathbf{C}_i^e e_i + \sum_{j \in N_i} \mathbf{C}_{ij}^\sigma \sigma_{ij} \right) \to 0 \quad \text{as} \quad t \to \infty, \tag{4.22}$$

which is equivalent to

$$\mathbf{C}_i^e e_i + \sum_{j \in N_i} \mathbf{C}_{ij}^\sigma \sigma_{ij} \to 0 \quad \text{as} \quad t \to \infty, \tag{4.23}$$

due to the regularity of the rotation matrix $R(\theta_i)$. The property in (4.23) may be written in a compact matrix form in terms of tracking errors e_i for all $i \in \mathcal{I}$ as follows

$$\begin{bmatrix} c_1^{xe} + \sum_{j \in N_1} c_{1j}^{x\sigma} & -c_{12}^{x\sigma} & \cdots & -c_{1N}^{x\sigma} \\ \vdots & \ddots & \ddots & \vdots \\ -c_{N-1,1}^{x\sigma} & \ddots & c_{N-1}^{xe} + \sum_{j \in N_{N-1}} c_{N-1,j}^{x\sigma} & -c_{N-1,N}^{x\sigma} \\ -c_{N1}^{x\sigma} & -c_{N2}^{x\sigma} & \cdots & c_N^{xe} + \sum_{j \in N_N} c_{Nj}^{x\sigma} \end{bmatrix} e^x \to 0, \tag{4.24}$$

$$\begin{bmatrix} c_1^{ye} + \sum_{j\in N_1} c_{1j}^{y\sigma} & -c_{12}^{y\sigma} & \cdots & -c_{1N}^{y\sigma} \\ \vdots & \ddots & \ddots & \vdots \\ -c_{N-1,1}^{y\sigma} & \ddots & c_{N-1}^{ye} + \sum_{j\in N_{N-1}} c_{N-1,j}^{y\sigma} & -c_{N-1,N}^{y\sigma} \\ -c_{N1}^{y\sigma} & -c_{N2}^{y\sigma} & \cdots & c_N^{ye} + \sum_{j\in N_N} c_{Nj}^{y\sigma} \end{bmatrix} e^y \to 0, \quad (4.25)$$

as $t \to \infty$, where $e^x = \text{col}(e_1^x, \ldots, e_N^x)$, $e^y = \text{col}(e_1^y, \ldots, e_N^y)$ and $e_i = \text{col}(e_i^x, e_i^y)$.

The matrices in (4.24) and (4.25) have the same structure as matrix A in (A.3). Thus, based on Lemma A.5, we conclude that the matrices in (4.24) and (4.25) are non-singular which in turn implies that both e^x and e^y converge to 0 as $t \to \infty$. Thus, the origin of the (e_i, θ_i^e)–dynamics is globally asymptotically stable. □

Remark 4.2.2. Under the conditions of Theorem 4.2.1 we have that for all $i, j \in \mathcal{I}$, $\sigma_{ij}(t) \to 0$ as $t \to \infty$, so coordination is asymptotically achieved.

The following corollary is an extension to Theorem 4.2.1 in which, apart from considering synchronisation of position errors as earlier, a coordination of angular errors is added. This is done in the spirit of results in Theorem 3.2.1 in which also synchronisation of angular errors is employed. The additional term $\theta_i^e - \theta_j^e$ for all neighbours of robot i relates to synchronisation of velocity ratios, since from the kinematics of a nonholonomic mobile robot we have that

$$\tan\theta_i = \frac{\dot{y}_i}{\dot{x}_i}. \quad (4.26)$$

Therefore, adding synchronisation in terms of angular errors to the formation

control law may be viewed as adding a velocity matching factor similarly to e.g. (Moshtagh and Jadbabaie, 2007; Olfati-Saber, 2006; Yu et al., 2008). This allows for further adjustments of the control law to a particularly required application. More specifically, the synchronisation of angular errors can be useful to promote averaging of robot heading angles as in flocking (cf. (Savkin, 2004)). We discuss further benefits of this mechanism in Chapter 6.

Corollary 4.2.3. *Consider N unicycle-type mobile robots with kinematics* (4.1) *and a formation control algorithm given in Theorem 4.2.1 and (4.13, 4.14) with a supplementary synchronisation factor in terms of $\theta_i^e - \theta_j^e$ as shown below:*

$$\omega_i(t) = \omega_i^d(t) + c_i^\theta \theta_i^e + \sum_{j \in N_i} c_{ij}^\theta (\theta_i^e - \theta_j^e) \tag{4.27}$$
$$+ v_i^d(t) \left(e_i^T \mathbf{C}_i^e + \sum_{j \in N_i} \sigma_{ij}^T \mathbf{C}_{ij}^\sigma \right) R(\theta_i) \begin{pmatrix} \dfrac{\cos\theta_i^e - 1}{\theta_i^e} \\ \dfrac{\sin\theta_i^e}{\theta_i^e} \end{pmatrix}.$$

Besides the conditions on the control parameters defined in Theorem 4.2.1, let

- *$\forall i \in \mathcal{I}$ and $\forall j \in N_i$, $c_{ij}^\theta > 0$;*
- *if $c_{ij}^\theta \neq c_{ji}^\theta$, then $\forall i \in \mathcal{I}$, $\forall j \in N_i$ $c_i^\theta > \frac{1}{2} \sum_{j \in N_i} \left(c_{ji}^\theta + c_{ij}^\theta \right)$.*

Then, the origin of (4.6, 4.7, 4.13, 4.27) is globally asymptotically stable and $\sigma_{ij} \to 0$ as $t \to \infty$.

Proof. (Sketch) Consider again the Lyapunov function candidate (4.15). The

time derivative of this function is given by

$$\dot{V} = -(\Theta_e)^T \mathbf{C}^\theta \Theta_e - \sum_{i=1}^{N} \left\| \begin{pmatrix} 1 & 0 \end{pmatrix} R^T(\theta_i) \left(\mathbf{C}_i^e e_i + \sum_{j \in N_i} \mathbf{C}_{ij}^\sigma \sigma_{ij} \right) \right\|^2, \qquad (4.28)$$

where $\Theta_e = \text{col}(\theta_1^e, \ldots, \theta_N^e)$ and $\mathbf{C}^\theta$ has the structure of the matrices in (4.24) and (4.25). Thus, if $c_{ij}^\theta = c_{ji}^\theta$, $\mathbf{C}^\theta$ is a positive definite matrix by Lemma A.5 and if $c_{ij}^\theta \neq c_{ji}^\theta$ and $c_i^\theta > \frac{1}{2} \sum_{j \in N_i} \left(c_{ji}^\theta + c_{ij}^\theta \right)$, then the symmetric part of matrix $\mathbf{C}^\theta$ is positive definite. Hence, (4.28) yields that $\dot{V} \leq 0$.

Further stability analysis of the origin of the closed–loop tracking and coordination error dynamics is similar to the one presented above for Theorem 4.2.1. Therefore, one concludes that $(e_i, \theta_i^e) = (0, 0)$ for $i, j \in \mathcal{I}$ is a globally asymptotically stable equilibrium of (4.6, 4.7, 4.13, 4.27). Therefore, the formation control problem is solved. □

4.2.2 Pure Coordination

Although it is not necessary in Theorem 4.2.1 for the communication graph to be connected, if the connectivity condition is satisfied, the formation behaviour is enhanced. This may be observed in particular when we assume that for all $i \in \mathcal{I}$ the position tracking control gains are set to be zero, i.e. $c_i^{xe} = 0$ and $c_i^{ye} = 0$, for all $i \in \mathcal{I}$, which is the case studied in the following theorem. Before we can state the theorem though, we need to formally introduce the following technicalities. Let $e = \text{col}(e_1, \ldots, e_N)$ and $\Theta_e = \text{col}(\theta_1^e, \ldots, \theta_N^e)$. Assume first

that the communication graph of the formation is disconnected and that the graph has $k > 1$ connected components, i.e. $\mathcal{I} = \mathcal{I}_1 \cup \ldots \cup \mathcal{I}_k$, where $\mathcal{I}_\ell$ is the largest set of vertices in the ℓ-th connected component. Then define $\mathcal{E}$ as

$$\mathcal{E} = \bigcap_{\ell=1}^{k} \{e \,|\, e_i = e_j,\, i,j \in \mathcal{I}_\ell\}, \tag{4.29}$$

and Ω as

$$\Omega = \{(\theta_i^e, e_i) \,|\, \Theta_e = 0, e \in \mathcal{E}\}. \tag{4.30}$$

When the communication graph is connected, the set $\mathcal{E}$ is equal to

$$\bar{\mathcal{E}} = \{e \,|\, e_i = e_j,\, i,j \in \mathcal{I}\}, \tag{4.31}$$

and Ω to

$$\bar{\Omega} = \{(\theta_i^e, e_i) \,|\, \Theta_e = 0, e \in \bar{\mathcal{E}}\}. \tag{4.32}$$

We can now present the theorem.

Theorem 4.2.4 (Pure Coordination)**.** *Consider a formation consisting of N unicycle mobile robots* (4.1)*, a given desired trajectory of the virtual centre of the formation $q_{vc}^d(t) = \left(x_{vc}^d(t), y_{vc}^d(t), \theta_{vc}^d(t)\right)^T$ with bounded feedforward inputs v_{vc}^d and ω_{vc}^d, and a desired formation geometry given by bounded vectors $l_i^d(t)$ such that $\dot{l}_i^d(t)$ is bounded, $i \in \mathcal{I}$, that together define desired trajectories of individual robots in the formation $q_i^d(t) = \left(x_i^d(t), y_i^d(t), \theta_i^d(t)\right)^T$ according to* (4.2) *and their desired forward and angular velocities $v_i^d(t)$ and $\omega_i^d(t)$. Assume further that for $i \in \mathcal{I}$, $v_i^d(t)$ is bounded away from zero and $\omega_i^d(t)$ is bounded. Let the formation control law be given in (4.13, 4.14) in which for all $i \in \mathcal{I}$, $c_i^{xe} = 0$ and $c_i^{ye} = 0$,*

i.e.

$$v_i(t) = v_i^d(t) + \begin{pmatrix} 1 & 0 \end{pmatrix} R^T(\theta_i) \sum_{j \in N_i} \mathbf{C}_{ij}^{\sigma} \sigma_{ij}, \tag{4.33}$$

$$\omega_i(t) = \omega_i^d(t) + c_i^{\theta} \theta_i^e + v_i^d(t) \sum_{j \in N_i} \sigma_{ij}^T \mathbf{C}_{ij}^{\sigma} R(\theta_i) \begin{pmatrix} \dfrac{\cos\theta_i^e - 1}{\theta_i^e} \\ \dfrac{\sin\theta_i^e}{\theta_i^e} \end{pmatrix}, \tag{4.34}$$

and, moreover, $c_i^{\theta} > 0$, $\forall i \in \mathcal{I}$, $\mathbf{C}_{ij}^{\sigma} = \mathrm{diag}(c_{ij}^{x\sigma}, c_{ij}^{y\sigma})$, *where* $c_{ij}^{x\sigma} > 0$ *and* $c_{ij}^{y\sigma} > 0$ *satisfy* $\mathbf{C}_{ij}^{\sigma} = \mathbf{C}_{ji}^{\sigma}$, $\forall i, j \in \mathcal{I}$. *Then*

1. *if the communication graph of the formation is disconnected and robots create* k *connected components, the set* Ω *given in* (4.30) *is a globally asymptotically stable set of (4.6, 4.7);*

2. *if the communication graph of the formation is connected, the set* $\bar{\Omega}$ *in* (4.32) *is globally asymptotically stable; hence the desired formation shape is attained for all robots in the formation.*

Proof. Consider the Lyapunov function candidate

$$V = \frac{1}{2} \sum_{i=1}^{N} \left((\theta_i^e)^2 + \frac{1}{2} \sum_{j \in N_i} \sigma_{ij}^T \mathbf{C}_{ij}^{\sigma} \sigma_{ij} \right). \tag{4.35}$$

The time derivative of this function along solutions of the closed–loop system

(4.6, 4.7) with controller (4.33, 4.34) yields

$$\dot{V} = -\sum_{i=1}^{N} \left(c_i^{\theta} (\theta_i^e)^2 + \sum_{j \in N_i} \sigma_{ij}^T \mathbf{C}_{ij}^{\sigma} R(\theta_i) \begin{pmatrix} 1 \\ 0 \end{pmatrix} \begin{pmatrix} 1 & 0 \end{pmatrix} R^T(\theta_i) \sum_{j \in N_i} \mathbf{C}_{ij}^{\sigma} \sigma_{ij} \right) \leq 0. \tag{4.36}$$

Therefore, following Lemma B.16 the set $\{\theta_i^e = 0, \sigma_{ij} = 0\}$ is stable for all $(i,j) \in \{i \in \mathcal{I}, j \in N_i\}$. Moreover, based on the rationale presented in the proof of Theorem 4.2.1, we can show that as $t \to \infty$

$$\theta_i^e \to 0, \qquad (i \in \mathcal{I}), \tag{4.37}$$

and

$$\sum_{j \in N_i} \mathbf{C}_{ij}^{\sigma} \sigma_{ij} \to 0, \qquad (i \in \mathcal{I},\, j \in N_i), \tag{4.38}$$

which in terms of the components e_i^x and e_i^y of the tracking error e_i gives

$$\underbrace{\begin{bmatrix} \sum_{j \in N_1} c_{1j}^{x\sigma} & -c_{12}^{x\sigma} & \cdots & -c_{1N}^{x\sigma} \\ \vdots & \ddots & \ddots & \vdots \\ -c_{N-1,1}^{x\sigma} & \ddots & \sum_{j \in N_{N-1}} c_{N-1,j}^{x\sigma} & -c_{N-1,N}^{x\sigma} \\ -c_{N1}^{x\sigma} & -c_{N2}^{x\sigma} & \cdots & \sum_{j \in N_N} c_{Nj}^{x\sigma} \end{bmatrix}}_{L_x} e^x \to 0 \quad \text{as} \quad t \to \infty, \tag{4.39}$$

$$\underbrace{\begin{bmatrix} \sum\limits_{j\in N_1} c_{1j}^{y\sigma} & -c_{12}^{y\sigma} & \cdots & -c_{1N}^{y\sigma} \\ \vdots & \ddots & \ddots & \vdots \\ -c_{N-1,1}^{y\sigma} & \ddots & \sum\limits_{j\in N_{N-1}} c_{N-1,j}^{y\sigma} & -c_{N-1,N}^{y\sigma} \\ -c_{N1}^{y\sigma} & -c_{N2}^{y\sigma} & \cdots & \sum\limits_{j\in N_N} c_{Nj}^{y\sigma} \end{bmatrix}}_{L_y} e^y \to 0 \quad \text{as} \quad t \to \infty. \tag{4.40}$$

By comparing matrices L_x and L_y in (4.39) and (4.40), respectively, with a general Laplacian matrix given in Definition C.3, we conclude that both L_x and L_y are in fact Laplacian matrices associated with the weighted communication graph of the formation. For $k > 1$ connected components in $\mathcal{I}$, the eigenspace associated with the zero eigenvalue of L_x and L_y is created by $\mathrm{Im}(E^1, \ldots, E^k)$, where vectors $E^\ell \in \mathbb{R}^N$, $\ell \in \{1, \ldots, k\}$, consist of elements E_j^ℓ such that $E_j^\ell = 1$ if $j \in \mathcal{I}_\ell$ and $E_j^\ell = 0$ otherwise. Thus, the form of this eigenspace implies that for all pairs of neighbours $i, j \in \mathcal{I}_\ell$, $\ell \in \{1, \ldots, k\}$ we have $e_i(t) \to e_j(t)$ as $t \to \infty$. Therefore, we can conclude that the set Ω is a globally asymptotically stable set. Thus, Part 1 of Theorem 4.2.4 holds.

Now, if the comminication graph is connected, we have $k = 1$. Following (Olfati-Saber and Murray, 2004; Olfati-Saber et al., 2007), a Laplacian matrix of a connected communication graph has a single zero eigenvalue with associated eigenspace $\mathrm{span}\{\mathbf{1}_N\}$, where $\mathbf{1}_N \in \mathbb{R}^{N\times 1}$ is a vector with all entries equal to 1. Hence $e^x \to k^x \mathbf{1}_N$ and $e^y \to k^y \mathbf{1}_N$ as $t \to \infty$, where $k^x, k^y \in \mathbb{R}$. Therefore, for all pairs of robots i, j we have $e_i(t) \to e_j(t)$ as $t \to \infty$. Hence for all $i, j \in \mathcal{I}$, $\sigma_{ij} \to 0$. Furthermore, in view of Part 1 of the theorem and the connectedness of

the communication graph of the formation, we conclude that the set $\bar{\Omega}$ is globally asymptotically stable and thus, all robots in the formation create the desired formation shape. This proves Part 2 of the theorem. □

Remark 4.2.5. In Theorem 4.2.4 we do not prove that $e_i(t) \to 0$ as $t \to \infty$, hence trajectory tracking is not necessarily obtained. Instead, the group of robots reaches the prescribed formation geometry and, due to the effect of the feedforward terms $v_i^d(t)$ and $\omega_i^d(t)$, follows a trajectory that is translated with respect to the desired one. Therefore, the control scheme proposed in Theorem 4.2.4 may be referred to as pure coordination. Note that, in contrast to the tracking error $e_i(t)$, for pure coordination the angular error θ_i^e does need to converge to zero.

Remark 4.2.6. A representative example of an application of the pure coordination control scheme introduced in Theorem 4.2.4 is that of distributed sensor networks, see (Gungor and Hancke, 2009; Jiang et al., 2008; Kumar et al., 2008; Li et al., 2008). In such an application, the focus of attention is for robots to create a given formation geometry and to cover a certain area, not the accurate absolute positioning of robots in the plane or trajectory tracking. Similarly, in multiple aircraft manoeuvres the exact position of the formation in the sky is not of major importance (within reason). Instead, the coordinated motion of the formation is the key objective. Clearly, this second example does not concern unicycle robots but aircraft formations and hence the control law in Theorem 4.2.4 cannot be directly applied.

Based on Theorem 4.2.4, we can see that by ensuring that the communication graph is connected, one obtains consensus of the tracking error variables e_i if the

tracking gains $\mathbf{C}_i^e$ are zero. Therefore, if the communication graph is connected and both tracking control gains $\mathbf{C}_i^e$ and coordination gains $\mathbf{C}_{ij}^\sigma$ are nonzero, we may act simultaneously upon the two control objectives - coordination and trajectory tracking. This is in spite of the fact that in Theorem 4.2.1, the connectivity of the communication graph is not required. The prevalent behaviour – trajectory tracking or coordination – for a particular application can be determined by choosing appropriate values of the tracking gains $\mathbf{C}_i^e$ and coordination gains $\mathbf{C}_{ij}^\sigma$. To illustrate results of this work, we show the existing trade-off between tracking and coordination in simulations in Section 4.3; a quantitative distinction between dominance of one of these two behaviours is recommended for future research.

4.2.3 Leader–follower–like strategy

The result in this subsection is an extension of Theorem 4.2.1 and is motivated by the results in (Ren, 2007b) which concerns a formation of single integrator vehicles. Our result considers a group of mobile robots where only one robot $i_l \in \mathcal{I}$ is aware of its position tracking error. The remaining robots only act towards coordination of the group. Therefore, this control algorithm may be interpreted as a leader-follower-like scheme. Accordingly, robot i_l is the leader of the formation and all other robots $i_f \in \mathcal{I} \setminus \{i_l\}$ are the followers with the augmentation of the leader adjusting its position with respect to its followers due to the effect of the coupling gains $\mathbf{C}_{i_l j}^\sigma$.

Theorem 4.2.7 (Leader-Follower)**.** *Let $i_l \in \mathcal{I}$ and consider a formation of N unicycle-type mobile robots with kinematics* (4.1) *and the formation control algo-*

rithm given in (4.13, 4.14) and Theorem 4.2.1 with the following conditions on the control parameters:

- $\forall i \in \mathcal{I}$*:* $c_i^\theta > 0$ *and* $\forall j \in N_i$*:* $\mathbf{C}_{ij}^\sigma = \mathrm{diag}(c_{ij}^{x\sigma}, c_{ij}^{y\sigma})$*,* $c_{ij}^{x\sigma} > 0$ *and* $c_{ij}^{y\sigma} > 0$*;*
- $\forall i \in \mathcal{I}$*:* $\mathbf{C}_i^e = \mathrm{diag}(c_i^{xe}, c_i^{ye})$*, subject to* $c_{i_l}^{xe} > 0$*,* $c_{i_l}^{ye} > 0$ *and* $\forall i_f \in \mathcal{I} \setminus \{i_l\}$*:* $c_{i_f}^{xe} = 0$*,* $c_{i_f}^{ye} = 0$*.*

Then the origin of (4.6, 4.7, 4.13, 4.14) is globally asymptotically stable if the communication graph of the formation is connected. Hence $\sigma_{ij} \to 0$ *as* $t \to \infty$*, and thus coordination is achieved.*

Proof. (Sketch) Proceeding as in the proof of Theorem 4.2.1 and assuming that the communication graph is connected, we use the Lyapunov function candidate (4.15). Its time derivative along system trajectories is negative semi-definite. Thus, stability of the origin of (4.6, 4.7, 4.13, 4.14) follows. Furthermore, one can conclude that $\theta_i^e \to 0$ as $t \to \infty$ and one obtains matrices similar to (4.24) and (4.25) with $c_{i_l}^{xe} > 0$, $c_{i_l}^{ye} > 0$ and $c_{i_f}^{xe} = 0$, $c_{i_f}^{ye} = 0$. Hence, these matrices are non-singular as, by assumption, the communication graph is connected. Thus, $e_i(t) \to 0$ as $t \to \infty$. Therefore, the origin of the (e_i, θ_i^e)–dynamics is globally asymptotically stable. This implies that also $\sigma_{ij} \to 0$ as $t \to \infty$ which implies coordination of robots in the formation. □

4.2.4 Saturated control

In this section we propose an extension of the aforementioned control algorithms in which actuator constraints are taken into consideration. Therefore, the resultant control law should satisfy a condition like (3.35), i.e. $|v_i(t)| \leq \bar{v_i}$ and $|\omega_i(t)| \leq \bar{\omega_i}$ for all t, $i \in \mathcal{I}$. To this end, we define

$$\begin{bmatrix} \xi_i \\ \chi_i \end{bmatrix} = R^T(\theta_i) \left(\frac{\mathbf{C}_i^e e_i}{1 + e_i^T \mathbf{C}_i^e e_i} + \frac{\sum\limits_{j \in N_i} \mathbf{C}_{ij}^\sigma \sigma_{ij}}{1 + \sum\limits_{j \in N_i} \sigma_{ij}^T \mathbf{C}_{ij}^\sigma \sigma_{ij}} \right), \tag{4.41}$$

and propose the following control law

$$v_i(t) = v_i^d(t) + \alpha_i(\xi_i), \tag{4.42}$$

$$\omega_i(t) = \omega_i^d(t) + \beta_i(\theta_i^e) + v_i^d(t) \begin{bmatrix} \xi_i & \chi_i \end{bmatrix} \begin{pmatrix} \frac{\cos\theta_i^e - 1}{\theta_i^e} \\ \frac{\sin\theta_i^e}{\theta_i^e} \end{pmatrix}, \tag{4.43}$$

in which $\alpha_i(\cdot)$ and $\beta_i(\cdot)$ are saturation functions, see Definition 3.2.9 and the remaining control parameters are defined earlier in this chapter. It was already discussed in Section 3.2.3 that the saturated formation control problem can only be solved if the desired trajectories (4.2) are such that the actuator constraints (3.35) are respected. As discussed in Section 3.2.3, this implies that the following conditions need to be fulfilled

$$v_i^* < v_i^{\max} < \bar{v}_i, \tag{4.44}$$

$$\omega_i^* < \omega_i^{\max} < \bar{\omega}_i, \tag{4.45}$$

in which v^* and ω^* denote the upper bounds of the desired feedforward inputs

$$v_i^* = \sup\{|v_i^d(t)| \mid t \geq 0\}, \tag{4.46}$$

$$\omega_i^* = \sup\{|\omega_i^d(t)| \mid t \geq 0\}. \tag{4.47}$$

In the following theorem we present the stability analysis of the origin of the error dynamics (4.6, 4.7) when robots are controlled by (4.42, 4.43).

Theorem 4.2.8. *Consider N unicycle robots with kinematics* (4.1)*, a desired trajectory of the virtual centre of the formation $q_{vc}^d(t) = \left(x_{vc}^d(t), y_{vc}^d(t), \theta_{vc}^d(t)\right)^T$ for which the corresponding forward v_{vc}^d and angular velocities ω_{vc}^d are bounded. Let for each robot $i \in \mathcal{I}$ the desired formation geometry be defined with the aid of a bounded vector $l_i^d(t)$ subject to $\dot{l}_i^d(t)$ being bounded, and an associated desired trajectory $q_i^d(t) = \left(x_i^d(t), y_i^d(t), \theta_i^d(t)\right)^T$ such that the associated feedforward control inputs $v_i^d(t)$ and $\omega_i^d(t)$ given in* (3.4) *are such that Conditions* (4.44) *and* (4.45) *are met and $v_i^d(t)$ be bounded away from zero and $\omega_i^d(t)$ be bounded. Let $\alpha_i(\cdot)$ and $\beta_i(\cdot)$, $i \in \mathcal{I}$, be saturation functions such that $|\alpha_i(\cdot)| \leq \bar{\alpha}_i$ and $|\beta_i(\cdot)| \leq \bar{\beta}_i$. Moreover, assume that $c_i^\theta > 0$, $\mathbf{C}_i^e = \text{diag}(c_i^{xe}, c_i^{ye})$, $\mathbf{C}_{ij}^\sigma = \text{diag}(c_{ij}^{x\sigma}, c_{ij}^{y\sigma})$, where $c_i^{xe} > 0$, $c_i^{ye} > 0$, $c_{ij}^{x\sigma} > 0$ and $c_{ij}^{y\sigma} > 0$ subject to $\mathbf{C}_{ij}^\sigma = \mathbf{C}_{ji}^\sigma$ for $i \in \mathcal{I}$, $j \in N_i$ and all control parameters are such that*

$$\bar{v}_i \geq v_i^* + \bar{\alpha}_i, \tag{4.48}$$

$$\bar{\omega}_i \geq \omega_i^* + \bar{\beta}_i + 2v_i^* \left(\sqrt{c_i^{xe}} + \sqrt{c_i^{ye}} + \sum_{j \in N_i} \left(\sqrt{c_{ij}^{x\sigma}} + \sqrt{c_{ij}^{y\sigma}} \right) \right). \tag{4.49}$$

Then, the formation control law (4.42, 4.43) renders the origin of the error dy-

namics (4.6, 4.7) globally asymptotically stable while the resultant control inputs v_i *and* ω_i *satisfy* (3.35).

Proof. Consider the Lyapunov function candidate

$$V = \frac{1}{2}\sum_{i=1}^{N}\left(\ln\left(1+e_i^T\mathbf{C}_i^e e_i\right)+\frac{1}{2}\ln\left(1+\sum_{j\in N_i}\sigma_{ij}^T\mathbf{C}_{ij}^\sigma\sigma_{ij}\right)+(\theta_i^e)^2\right). \tag{4.50}$$

The time–derivative of V along system dynamics (4.6, 4.7) yields

$$\begin{aligned}
\dot{V} &= \sum_{i=1}^{N}\left(\frac{e_i^T\mathbf{C}_i^e}{1+e_i^T\mathbf{C}_i^e e_i}R(\theta_i)\begin{pmatrix}v_i^d(t)\cos\theta_i^e - v_i\\ v_i^d(t)\sin\theta_i^e\end{pmatrix}+\theta_i^e(\omega_i^d(t)-\omega_i)\right.\\
&\quad\left.+\frac{1}{2}\frac{\sum_{j\in N_i}\sigma_{ij}^T\mathbf{C}_{ij}^\sigma}{1+\sum_{j\in N_i}\sigma_{ij}^T\mathbf{C}_{ij}^\sigma\sigma_{ij}}\left(R(\theta_i)\begin{pmatrix}v_i^d(t)\cos\theta_i^e - v_i\\ v_i^d(t)\sin\theta_i^e\end{pmatrix}-R(\theta_j)\begin{pmatrix}v_j^d(t)\cos\theta_i^e - v_j\\ v_j^d(t)\sin\theta_j^e\end{pmatrix}\right)\right)\\
&= \sum_{i=1}^{N}\left(\left(\frac{e_i^T\mathbf{C}_i^e}{1+e_i^T\mathbf{C}_i^e e_i}+\frac{\sum_{j\in N_i}\sigma_{ij}^T\mathbf{C}_{ij}^\sigma}{1+\sum_{j\in N_i}\sigma_{ij}^T\mathbf{C}_{ij}^\sigma\sigma_{ij}}\right)R(\theta_i)\begin{pmatrix}v_i^d(t)\cos\theta_i^e - v_i\\ v_i^d(t)\sin\theta_i^e\end{pmatrix}\right.\\
&\quad\left.+\theta_i^e(\omega_i^d(t)-\omega_i)\right)\\
&= \sum_{i=1}^{N}\left(\begin{bmatrix}\xi_i & \chi_i\end{bmatrix}\begin{pmatrix}v_i^d(t)-v_i\\ 0\end{pmatrix}+\theta_i^e\left(\omega_i^d(t)-\omega_i+v_i^d(t)\begin{bmatrix}\xi_i & \chi_i\end{bmatrix}\begin{pmatrix}\frac{\cos\theta_i^e-1}{\theta_i^e}\\ \frac{\sin\theta_i^e}{\theta_i^e}\end{pmatrix}\right)\right),
\end{aligned} \tag{4.51}$$

where we used $\sigma_{ij} = -\sigma_{ji}$. Then, using the control law (4.42, 4.43), we obtain

$$\dot{V} = -\sum_{i=1}^{N}\left(\xi_i\alpha(\xi_i)+\theta_i^e\beta_i(\theta_i^e)\right)\leq 0. \tag{4.52}$$

Therefore, the origin of (4.6, 4.7) is stable. Furthermore, using Theorem B.11 we conclude that $\lim_{t\to\infty}\dot{V}=0$ and so for all $i\in\mathcal{I}$ we have

$$\xi_i\to 0 \qquad \text{and} \qquad \theta_i^e\to 0. \tag{4.53}$$

Consequently, by Lemma A.7 we can demonstrate that $\chi_i\to 0$ as $t\to\infty$, $i\in\mathcal{I}$, using the dynamic closed–loop equation of θ_i^e

$$\dot{\theta}_i^e=-\beta_i(\theta_i^e)-v_i^d(t)\begin{bmatrix}\xi_i & \chi_i\end{bmatrix}\begin{pmatrix}\dfrac{\cos\theta_i^e-1}{\theta_i^e}\\ \dfrac{\sin\theta_i^e}{\theta_i^e}\end{pmatrix}, \tag{4.54}$$

and the fact that

$$\lim_{s\to 0}\frac{\cos s-1}{s}=0 \qquad \text{and} \qquad \lim_{s\to 0}\frac{\sin s}{s}=1. \tag{4.55}$$

This shows that

$$\frac{\mathbf{C}_i^e e_i}{1+e_i^T\mathbf{C}_i^e e_i}+\frac{\displaystyle\sum_{j\in N_i}\mathbf{C}_{ij}^{\sigma}\sigma_{ij}}{1+\displaystyle\sum_{j\in N_i}\sigma_{ij}^T\mathbf{C}_{ij}^{\sigma}\sigma_{ij}}\to 0 \quad \text{as} \quad t\to\infty, \tag{4.56}$$

which can then be presented in the matrix form for the horizontal and vertical components of vector $e_i=\mathrm{col}(e_i^x,e_i^y)$ for all robots in the formation, i.e. $e^x=(e_1^x,\ldots,e_N^x)^T$ and $e^y=(e_1^y,\ldots,e_N^y)^T$ as

$$A^{\nu}e^{\nu}\to 0. \tag{4.57}$$

Here $\nu \in \{x, y\}$ and A^ν is a matrix of the form of (A.3) in which the diagonal elements are

$$a_{ii}^\nu = \frac{c_i^\nu}{1 + e_i^T \mathbf{C}_i^e e_i} + \frac{\sum\limits_{j \in N_i} c_{ij}^{\sigma\nu}}{1 + \sum\limits_{j \in N_i} \sigma_{ij}^T \mathbf{C}_{ij}^\sigma \sigma_{ij}}, \tag{4.58}$$

and the off-diagonal elements are

$$a_{ij}^\nu = -\frac{c_{ij}^{\sigma\nu}}{1 + \sum\limits_{j \in N_i} \sigma_{ij}^T \mathbf{C}_{ij}^\sigma \sigma_{ij}}, \quad i \neq j. \tag{4.59}$$

Thus, by Lemma A.5, matrix A^ν is positive definite, since $a_{ij}^\nu = a_{ji}^\nu$. Therefore $e_i \to 0$ as $t \to \infty$ for all $i \in \mathcal{I}$. As a result, the origin of the error dynamics (4.42, 4.43, 4.6, 4.7) is globally asymptotically stable.

To show that v_i and ω_i satisfy (3.35), simple manipulations using the triangular inequality suffice. This shows that

$$|v_i| \leq v_i^* + \bar{\alpha}_i \leq \bar{v}_i, \tag{4.60}$$

$$|\omega_i| \leq \omega_i^* + \bar{\beta}_i + 2v_i^* \left(\sqrt{c_i^{xe}} + \sqrt{c_i^{ye}} + \sum_{j \in N_i} \left(\sqrt{c_{ij}^{x\sigma}} + \sqrt{c_{ij}^{y\sigma}} \right) \right) \leq \bar{\omega}_i, \tag{4.61}$$

which consequently proves our claim. □

In Theorem 4.2.8 we obtain both convergence to the desired formation shape and trajectory tracking of the formation, as in Theorem 4.2.8 except in this section we also account for actuator limitations. Similarly to the results in Theorem 4.2.4 we can also consider the case when robots form a desired formation shape but

do not track their desired trajectories. For this purpose, we redefine ξ_i and χ_i in (4.41) as

$$\begin{bmatrix} \xi_i \\ \chi_i \end{bmatrix} = R^T(\theta_i) \frac{\sum_{j \in N_i} \mathbf{C}_{ij}^{\sigma} \sigma_{ij}}{1 + \sum_{j \in N_i} \sigma_{ij}^T \mathbf{C}_{ij}^{\sigma} \sigma_{ij}}. \tag{4.62}$$

We study the pure coordination control problem with the saturation of the control inputs of robots in the formation in the following corollary.

Corollary 4.2.9. *Consider N unicycle mobile robots* (4.1) *and the control law given in Theorem 4.2.8 and control inputs in (4.42, 4.43) in which ξ_i and χ_i, $i \in \mathcal{I}$ are given in* (4.62) *and the control parameters satisfy*

$$\bar{v}_i \geq v_i^* + \bar{\alpha}_i, \tag{4.63}$$

$$\bar{\omega}_i \geq \omega_i^* + \bar{\beta}_i + 2v_i^* \sum_{j \in N_i} \left(\sqrt{c_{ij}^{x\sigma}} + \sqrt{c_{ij}^{y\sigma}} \right). \tag{4.64}$$

Define $\bar{\mathcal{E}}$ as in (4.31) *and $\Theta_e = \mathrm{col}(\theta_1^e, \ldots, \theta_N^e)$. If the communication graph of the formation is connected, then the set $\bar{\Omega}$* (4.32) *is globally asymptotically stable and hence coordination of all robots in the formation is achieved while the control inputs v_i and ω_i meet Condition* (3.35).

Proof. The proof follows the same lines as the proof of Theorems 4.2.4 and 4.2.8 with the following Lyapunov function candidate

$$V = \frac{1}{2} \sum_{i=1}^{N} \left(\frac{1}{2} \ln \left(1 + \sum_{j \in N_i} \sigma_{ij}^T \mathbf{C}_{ij}^{\sigma} \sigma_{ij} \right) + (\theta_i^e)^2 \right). \tag{4.65}$$

For this reason, we omit the proof here. □

4.2.5 Discussion

In Theorem 4.2.1 as well as in the succeeding Theorems 4.2.4, 4.2.7 and 4.2.8, and Corollaries 4.2.3 and 4.2.9, there is a great deal of freedom regarding the choice of control parameters. Not only the coupling parameters do not need to be identical but also there is no need for symmetric coupling parameters regarding the angular errors. Also, the tracking control gains in general are only required to satisfy the mild condition of being positive. Therefore, one may adapt the control algorithm according to the actual required performance of the mobile robot formation and therewith obtain a desired behaviour. In particular, one may choose larger tracking gains to prioritise trajectory tracking in comparison to maintaining the formation shape. On the other hand, if it is desired to keep the desired formation geometry rather than to track individual robot trajectories, this may be achieved by using larger coordination gains and smaller tracking gains. In the extreme case when coordination gains are the only non-zero parameters, we obtain pure coordination, see Theorem 4.2.4. Note that this only refers to the tracking gains of the position errors. As far as gains c_i^θ related to the angular error θ_i^e are concerned, these always need to be non-zero since in both trajectory tracking with coordination and in pure coordination, one requires that the orientation tracking error θ_i^e converges to zero.

This almost unconstrained freedom of choice of control parameters is with the exception of the saturation formation controller in which some slightly stricter conditions are required, i.e. the parameters need to be selected in such a way that the resultant control inputs do not disregard the bounds for v_i and ω_i.

However, the choice of the control parameters should also be dictated by the kind of prevailing behaviour – tracking or formation maintenance – that is required in an application.

Since our results are based on the same rationale as (Kostić et al., 2010b), it also inherently possesses the interesting property of allowing $\omega_i^d(t)$ to be discontinuous as long as it is bounded. This allows for a great range of desired trajectories to be tracked. For example, a rectangular trajectory with rounded corners is possible to be tracked.

In the following section, we demonstrate the influence of the control parameters on the behaviour of multiple mobile robots to illustrate the aforementioned advantages of the control algorithms proposed in Theorem 4.2.1 and Theorem 4.2.4 as well as the saturated version in Theorem 4.2.8.

4.3 Simulation results

In this section we present a validation of the control algorithms given in Section 4.2 by means of simulations of formations of three robots. In particular, in Subsection 4.3.1 we give simulation results regarding the control algorithm given in Theorem 4.2.1, and in Subsection 4.3.2 regarding the pure coordination control algorithm given in Theorem 4.2.4. Afterwards, in Subsection 4.3.3 we present simulation results of the controller given in Theorem 4.2.8.

To investigate the influence of communication graph topologies on formation be-

(a) (b)

Figure 4.1: Communication graph structures used in simulations: (a) disconnected graph (b) connected graph.

haviour, we first consider a disconnected communication graph and later a connected communication graph of the formation. The two communication structures considered are presented in Figure 4.1. The disconnected communication graph presented in Figure 4.1(a) refers to completely uncoupled robots, i.e. the case when robots cannot communicate with each other or sense each other by measurements.

In the simulations throughout this section, various control parameters were tuned to present the advantages of incorporating the coordination terms in the formation control law, see Remark 3.3.1.

4.3.1 Tracking and Coordination

In this subsection, we illustrate the behaviour of robots controlled by the control algorithm given in Theorem 4.2.1. In all simulations in this subsection, we use the following desired trajectory for the virtual centre

$$\begin{aligned} x_{vc}^d(t) &= 3\sin\theta_{vc}^d(t) + 3.5, \\ y_{vc}^d(t) &= 3\cos\theta_{vc}^d(t) + 0.5, \\ \theta_{vc}^d(t) &= 0.13t - \frac{\pi}{2}, \end{aligned} \tag{4.66}$$

Robot number	**Control gains**		
Robot 1	$c_1^{xe} = 5$ $c_{12}^{x\sigma} = 50$ $c_{13}^{x\sigma} = 0$	$c_1^{ye} = 30$ $c_{12}^{y\sigma} = 120$ $c_{13}^{y\sigma} = 0$	$c_1^{\theta} = 0.5$
Robot 2	$c_2^{xe} = 3$ $c_{21}^{x\sigma} = 50$ $c_{23}^{x\sigma} = 45$	$c_2^{ye} = 30$ $c_{21}^{y\sigma} = 120$ $c_{23}^{y\sigma} = 110$	$c_2^{\theta} = 0.5$
Robot 3	$c_3^{xe} = 4$ $c_{31}^{x\sigma} = 0$ $c_{32}^{x\sigma} = 45$	$c_3^{ye} = 29$ $c_{31}^{y\sigma} = 0$ $c_{32}^{y\sigma} = 110$	$c_3^{\theta} = 0.5$

Table 4.1: List of control parameters used in simulations in Subsections 4.3.1 and 4.3.2.

which is a circle with radius $R_{vc}^d = 3$, $v_{vc}^d = 0.39$ and $\omega_{vc}^d = 0.13$. Moreover, the desired formation shape is time–invariant and forms an equilateral triangle, such that the mobile robots maintain the Cartesian positions $l_1^d = \left(-0.3, -\frac{0.3}{\sqrt{3}}\right)^T$, $l_2^d = \left(0.3, -\frac{0.3}{\sqrt{3}}\right)^T$ and $l_3^d = \left(0, \frac{0.6}{\sqrt{3}}\right)^T$ relative to the local coordinate frame associated with the virtual centre of the formation.

Control parameters used in the simulations are given in Table 4.1. Note that for the disconnected communication graph, we set all coupling gains $c_{ij}^{x\sigma}$ and $c_{ij}^{y\sigma}$ to zero. In addition to the aforementioned simulation settings, the initial conditions of robots are $q_1(0) = (4.65, -1.28, 0.43)^T$, $q_2(0) = (-2.24, -3.73, 0.62)^T$, $q_3(0) = (-2.43, 0.97, 0.52)^T$. Moreover, in both simulations we apply a perturbation at $t = 25$, where t denotes simulation time, to observe robot behaviour after the perturbation. This perturbation is equivalent to displacing the position of Robot 1 along vector $(\delta x, \delta y) = (1, -0.5)$ to observe the robots' behaviour after the perturbation.

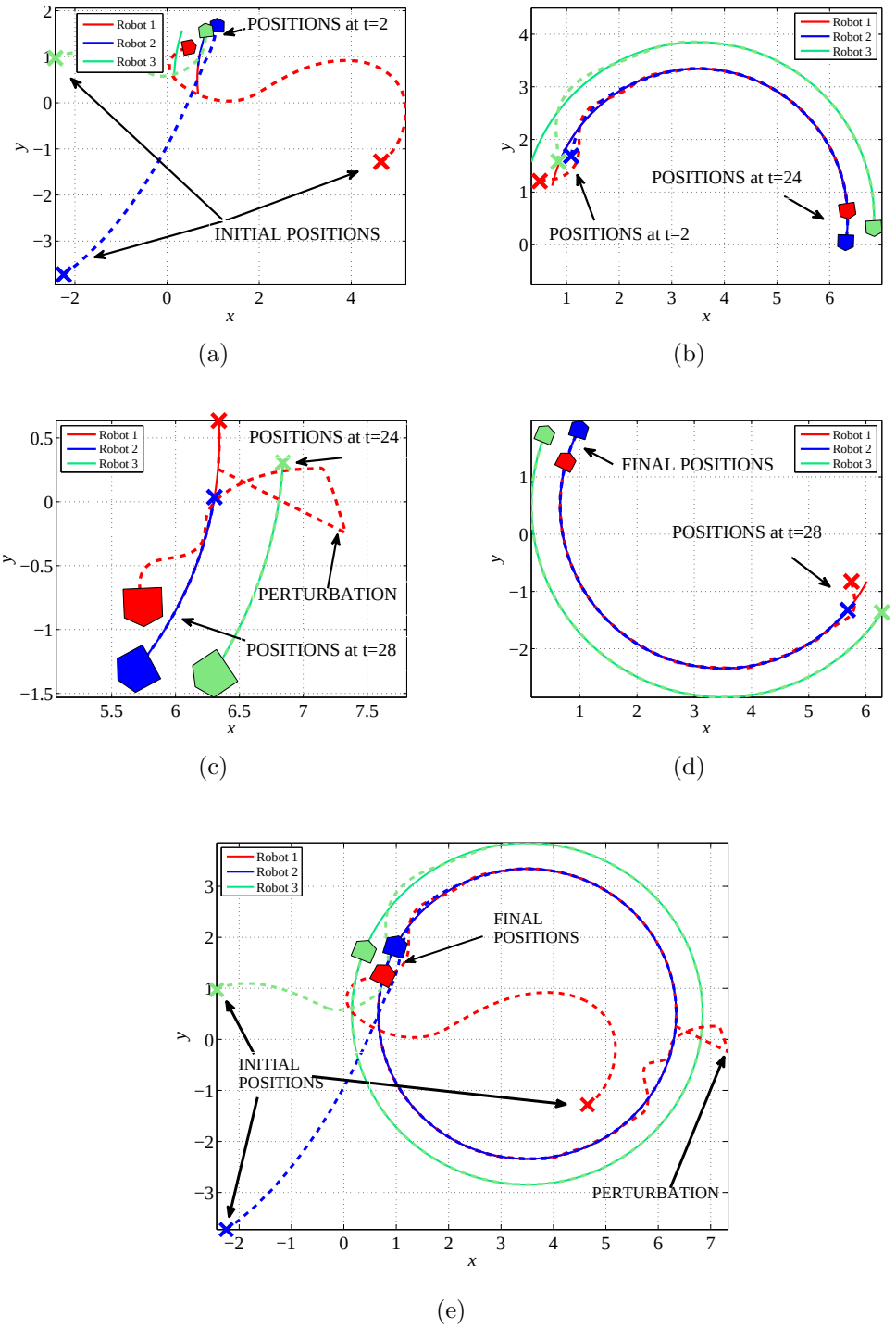

Figure 4.2: Desired robot paths (solid line) and actual robots paths (dashed line) in the plane in the case of a disconnected communication graph using the control algorithm (4.13, 4.14). (a) paths between $t = 0$ and $t = 2$ (b) paths between $t = 2$ and $t = 24$ (c) paths between $t = 24$ and $t = 28$ (d) paths between $t = 28$ and $t = 50$ (e) whole paths.

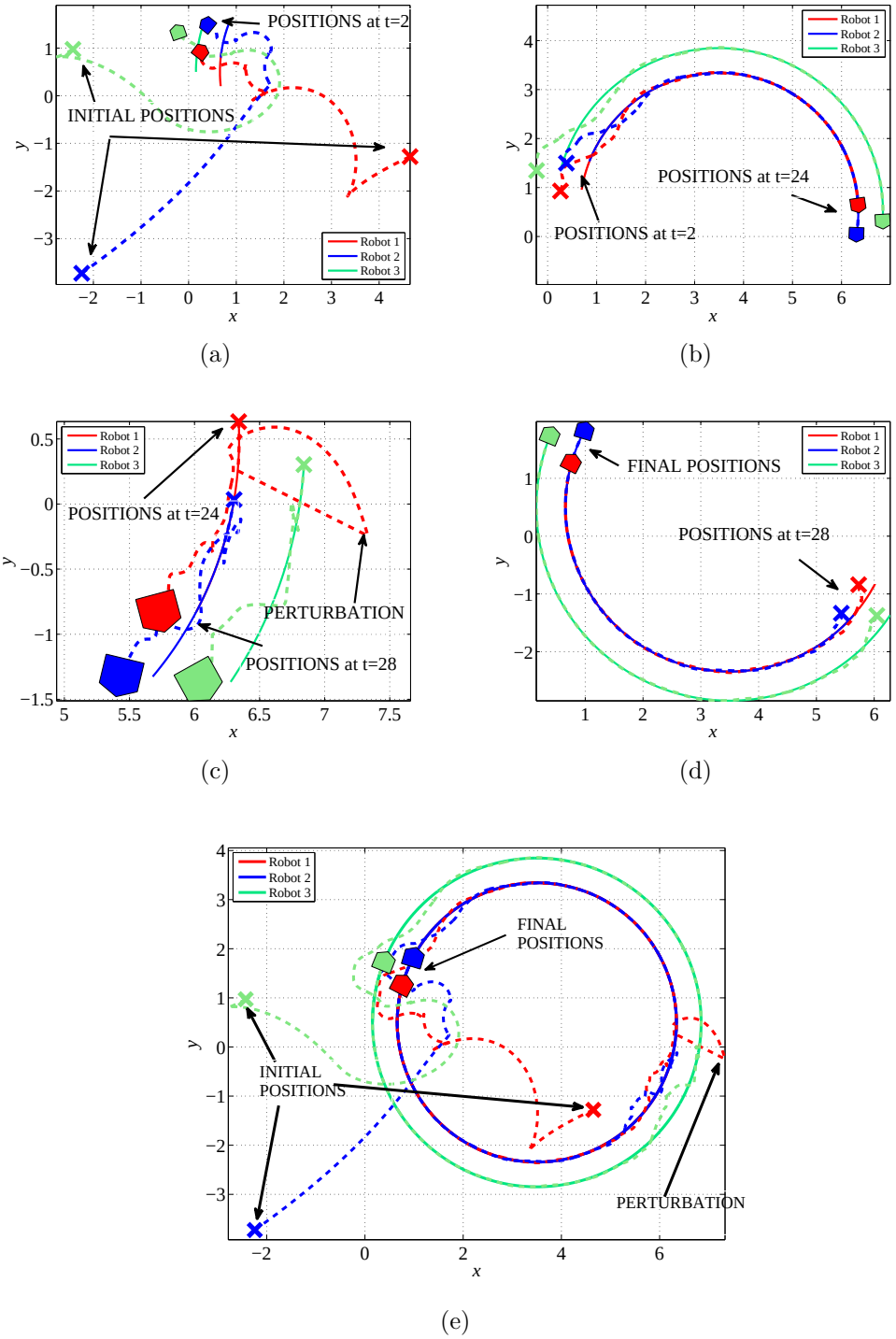

Figure 4.3: Desired robot paths (solid line) and actual robots paths (dashed line) in the plane in the case of a connected communication graph using the control algorithm (4.13, 4.14). (a) paths between $t = 0$ and $t = 2$ (b) paths between $t = 2$ and $t = 24$ (c) paths between $t = 24$ and $t = 28$ (d) paths between $t = 28$ and $t = 50$ (e) whole paths.

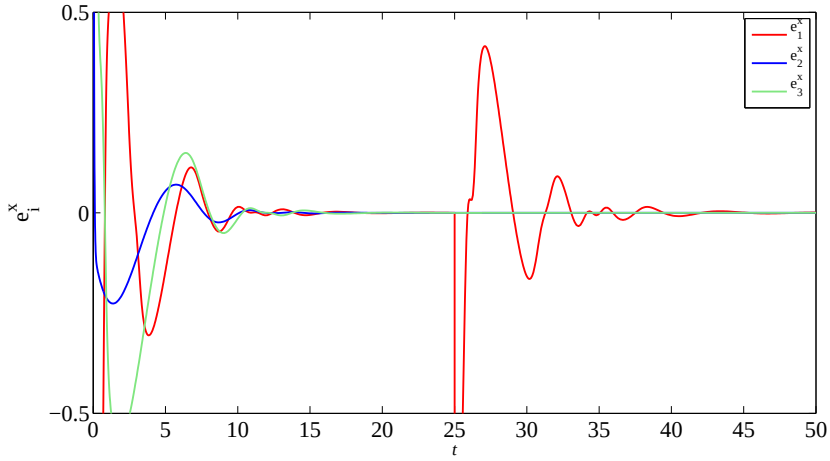

(a)

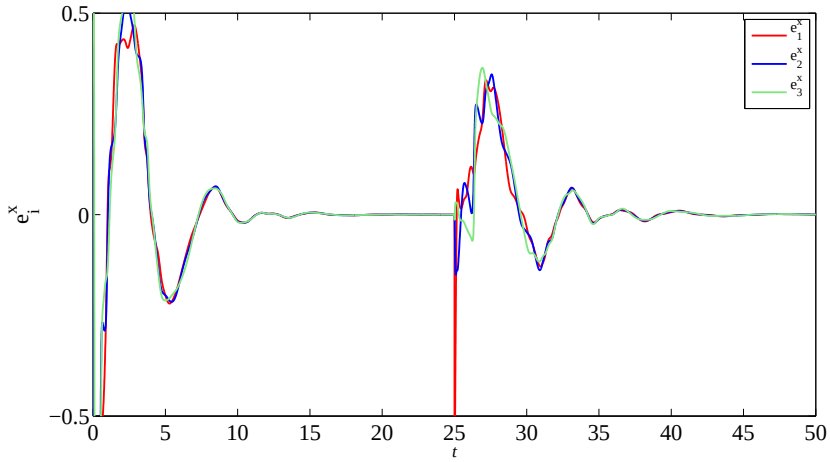

(b)

Figure 4.4: Tracking errors (x – coordinate): (a) disconnected communication graph (b) connected communication graph.

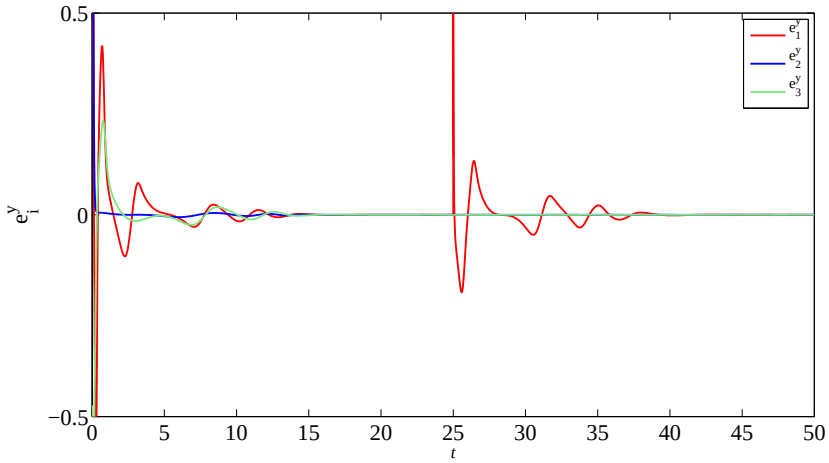

(a)

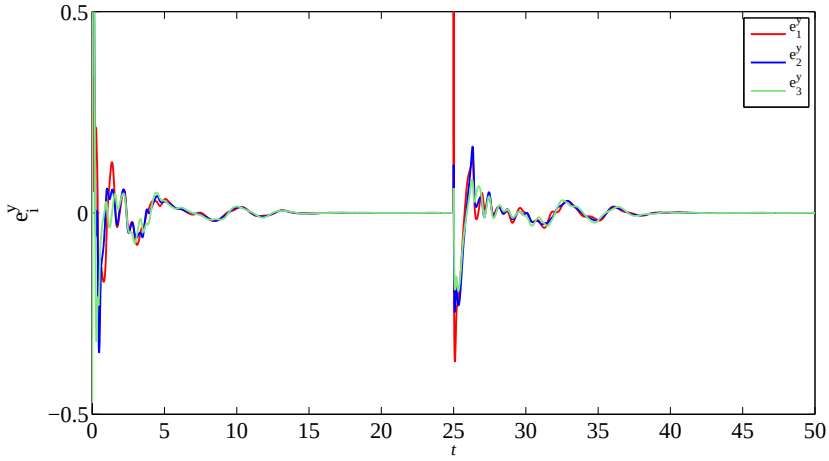

(b)

Figure 4.5: Tracking errors (y – coordinate): (a) disconnected communication graph (b) connected communication graph.

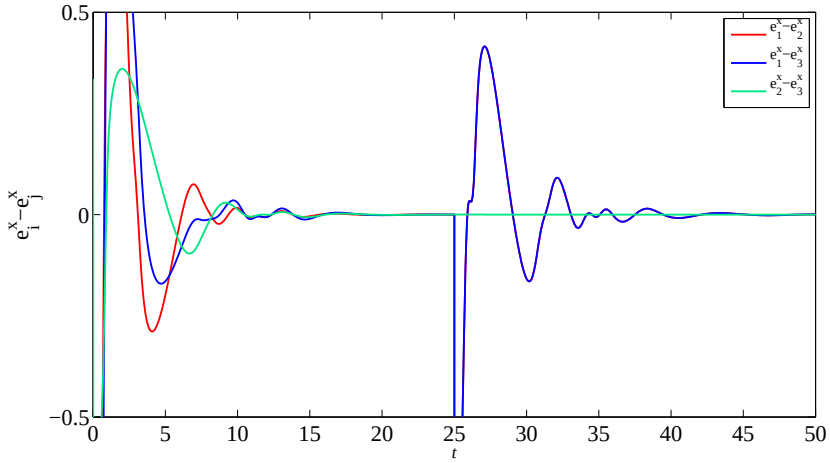

(a)

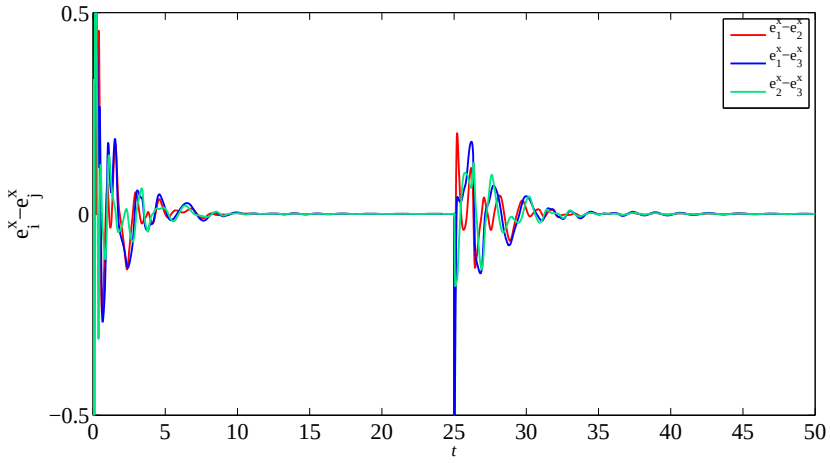

(b)

Figure 4.6: Coordination errors (x – coordinate): (a) disconnected communication graph (b) connected communication graph.

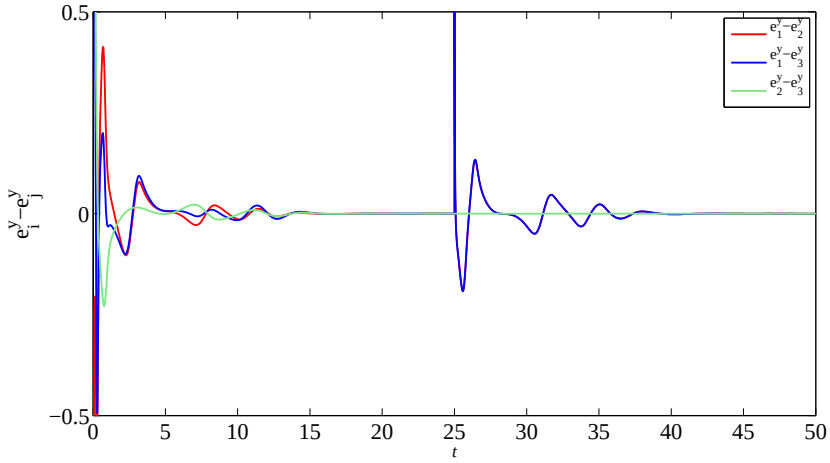

(a)

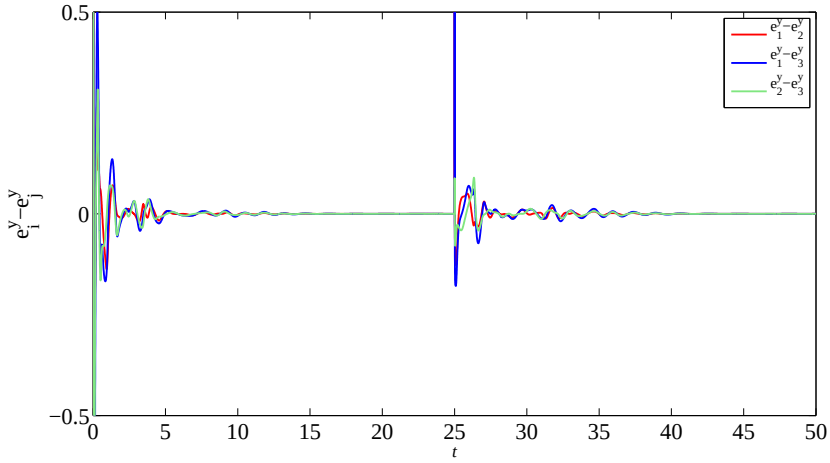

(b)

Figure 4.7: Coordination errors (y – coordinate): (a) disconnected communication graph (b) connected communication graph.

The simulation results are shown in Figures 4.2–4.7. In particular, in Figures 4.2 and 4.3 we present robot paths in the plane in the case of a disconnected and a connected communication graph respectively. As shown in these figures, it can be observed that robots converge to the desired formation geometry which is an equilateral triangle. Moreover, when Robot 1 is perturbed and the communication graph is disconnected, see Figure 4.2, none of the unperturbed robots in the formation reacts to the perturbation to maintain the formation shape. In contrast, when the communication graph is connected, see Figure 4.3, the two unperturbed robots also diverge from their desired trajectories in favour of formation keeping. Therefore, the formation shape is restored faster.

We can also observe the advantageous influence of the communication graph being connected in Figures 4.4–4.7 that show tracking and coordination errors in x – and y – direction, respectively. It can be seen that the errors are not only smaller when the communication graph is connected but it is also apparent that in that case the robots aim to achieve coordination as well as tracking their desired trajectories simultaneously. By comparing Figure 4.4 with Figure 4.6 and Figure 4.5 with Figure 4.7, we notice that for the connected communication graph, the coordination errors in fact converge to zero faster than the tracking errors. In other words, the tracking errors are in consensus with each other before they jointly vanish. This may be compared to the phenomena observed by Rodriguez-Angeles and Nijmeijer (2003, 2004) for fully actuated robotic manipulators. They noticed that by coupling the robotic manipulators, the manipulators tend to act in synchrony. We may observe a similar behaviour in our simulations. Due to the connectivity of the communication graph, the robots restore their desired forma-

tion geometry despite the lack of tracking of individual desired robot trajectories. In Figures 4.4(b) and 4.5(b), we clearly see that tracking errors coincide with each other before they converge to zero. According to the definition of the coordination in (4.11), coincidence of tracking errors denotes coordination of robots in the formation. In other words, we see that because of strong coupling gains $c_{ij}^{x\sigma}$ and $c_{ij}^{y\sigma}$ as compared to the tracking gains c_i^{xe} and c_i^{ye}, see Table 4.1, the robots aim to first restore the formation geometry before they return back to their desired individual trajectories. Indeed, in Figures 4.3(a) and 4.3(c) it is seen that robots converge to the desired formation shape before they converge together to the desired trajectories.

4.3.2 Pure Coordination

In this section we present simulation results for a group of mobile robots under the pure coordination control algorithm (4.33, 4.34). The control parameters are again given in Table 4.1 where in the case of a disconnected communication graph all communication links are disabled, i.e. for all $i, j \in \mathcal{I}$, $c_{ij}^{x\sigma} = 0$ and $c_{ij}^{y\sigma} = 0$. Moreover, all Cartesian tracking gains are zero, i.e. $c_i^{xe} = 0$ and $c_i^{ye} = 0$, for all $i \in \mathcal{I}$, as per the requirements of the pure coordination algorithm.

As an illustration of the pure coordination control algorithm, the desired trajectory of the virtual centre of the formation is taken to be a straight line given by

$$x_{vc}^d(t) = 0.5 + 0.4t,$$

$$y_{vc}^d(t) = 0.5, \tag{4.67}$$
$$\theta_{vc}^d(t) = 0,$$

where $v_{vc}^d(t) = 0.4$. To exhibit further advantages of the control algorithms proposed in this chapter, the desired formation geometry is now time-varying, and is created by coordinates $l_1^d = (0, -0.5 - 0.2\sin(0.25t))^T$, $l_2^d = (0, 0)^T$ and $l_3^d = (0, 0.5 + 0.2\sin(0.25t))^T$. Moreover, the initial states of robots in the formation are $q_1(0) = (-4.5, -1, \pi)^T$, $q_2(0) = (2.62, -4.45, -\frac{\pi}{4})^T$, $q_3(0) = (2.47, 0.98, \frac{\pi}{3})^T$.

The results of the simulations regarding the pure coordination control algorithm are given in Figures 4.8–4.13. It can be seen that if the communication graph of the formation is disconnected, robots neither track their individual trajectories, nor are coordinated with each other, see Figure 4.8. However, due to the feedback part concerning the angular error in the control algorithm, the robots' heading angles converge to their desired values. In contrast, when the communication graph is connected, robots create a given desired formation shape, see Figure 4.9. As seen in this figure, the robots do not track their desired trajectories since their paths do not coincide with the desired paths. This might have been expected as we are dealing with coordination only. Nonetheless, we can see that the robots indeed form the desired formation shape, which is the objective of the pure coordination control algorithm.

Similar conclusions can be drawn with the aid of Figures 4.10–4.13 that present horizontal and vertical components of the tracking and coordination errors. We can see that when the communication graph of the formation is disconnected

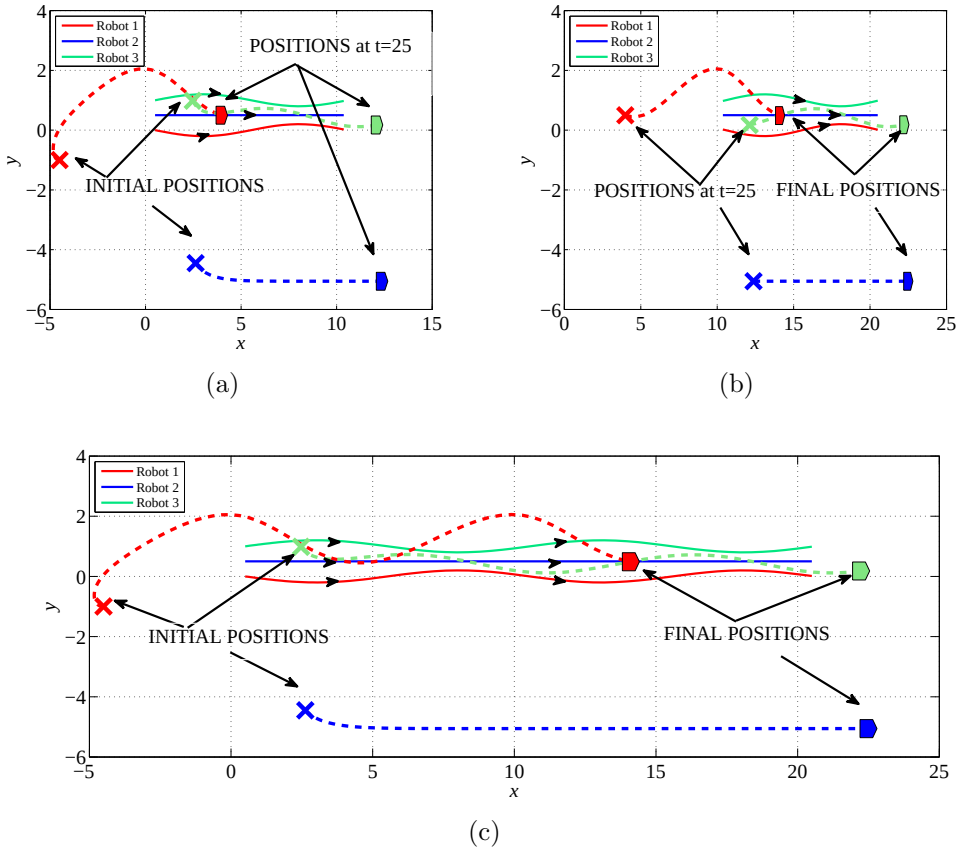

Figure 4.8: Desired robot paths (solid line) and actual robots paths (dashed line) in the plane in the case of a disconnected communication graph using the control algorithm (4.33, 4.34). (a) paths between $t = 0$ and $t = 25$ (b) paths between $t = 25$ and $t = 30$ (c) whole paths.

and hence the robots cannot communicate with each other, the tracking errors are nonzero and different from each other, as illustrated in Figures 4.10(a) and 4.11(a). Thus the coordination errors are also nonzero, see Figures 4.12(a) and 4.13(a). Conversely, when the communication graph is connected, the coordination errors go to zero, see Figures 4.12(b) and 4.13(b). Moreover, although robots do not track their individual trajectories and hence the position errors do not converge to zero, see Figures 4.10(b) and 4.11(b), we can distinctly see in

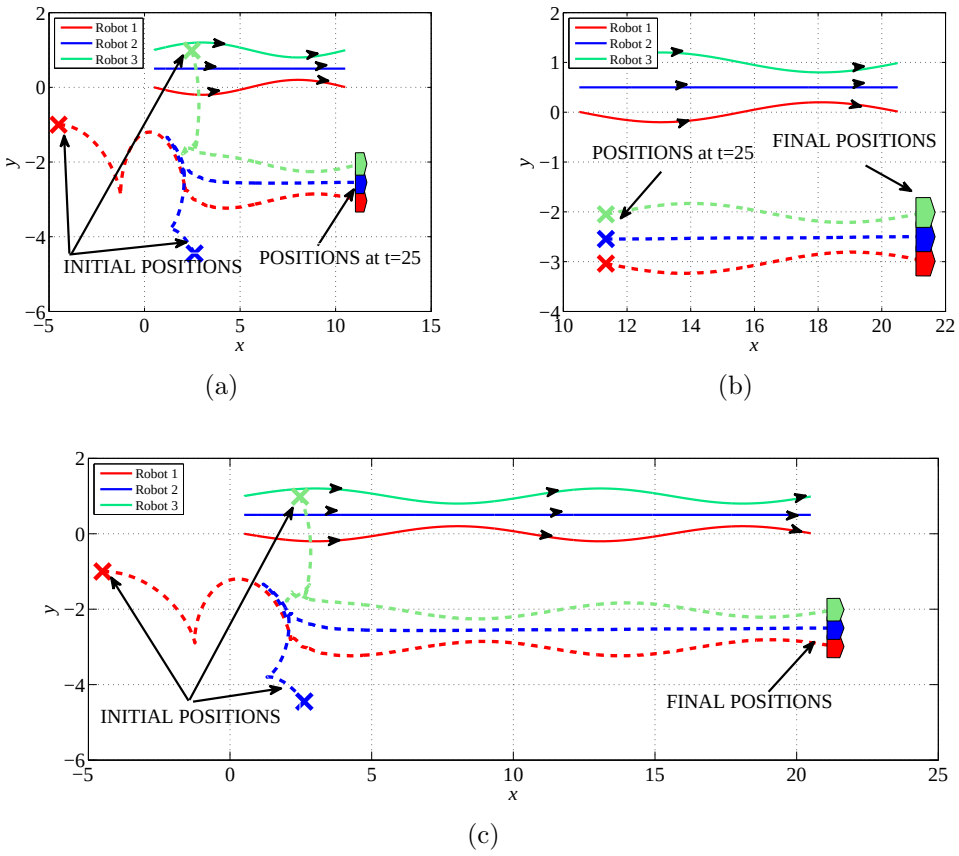

Figure 4.9: Desired robot paths (solid line) and actual robots paths (dashed line) in the plane in the case of a connected communication graph using the control algorithm (4.33, 4.34). (a) paths between $t = 0$ and $t = 25$ (b) paths between $t = 25$ and $t = 30$ (c) whole paths.

these figures that the position errors reach consensus. This illustrates that in order to achieve consensus of the tracking error variables robots need to be able to sufficiently exchange information with each other.

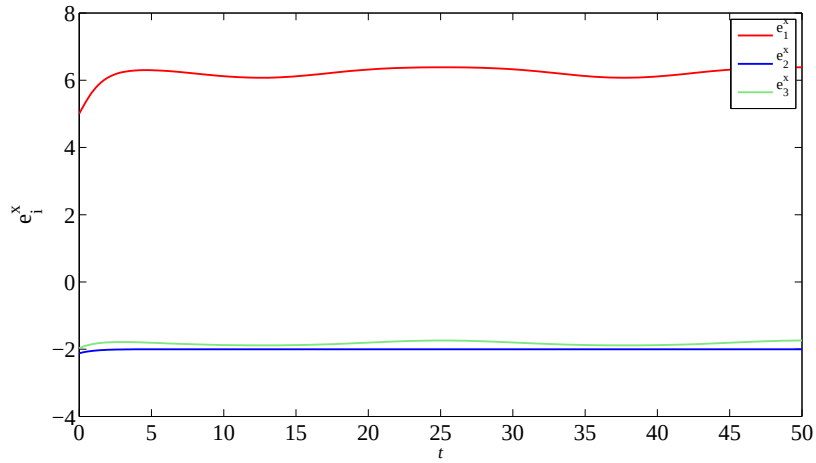

(a)

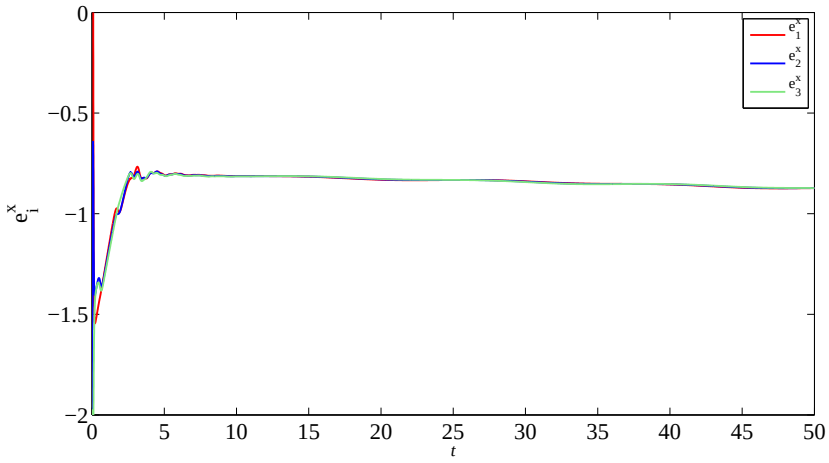

(b)

Figure 4.10: Tracking errors (x – coordinate): (a) disconnected communication graph (b) connected communication graph.

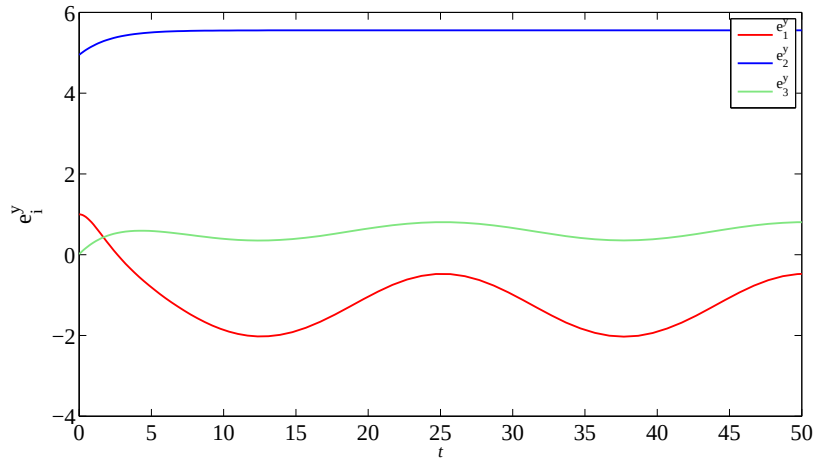

(a)

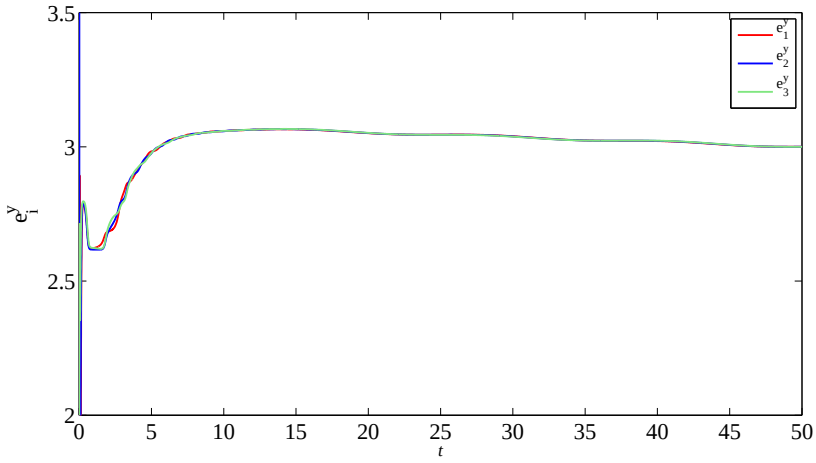

(b)

Figure 4.11: Tracking errors (y – coordinate): (a) disconnected communication graph (b) connected communication graph.

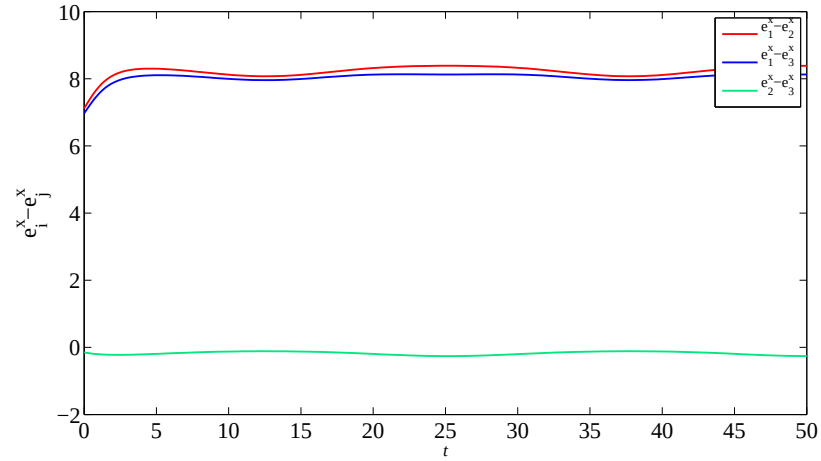

(a)

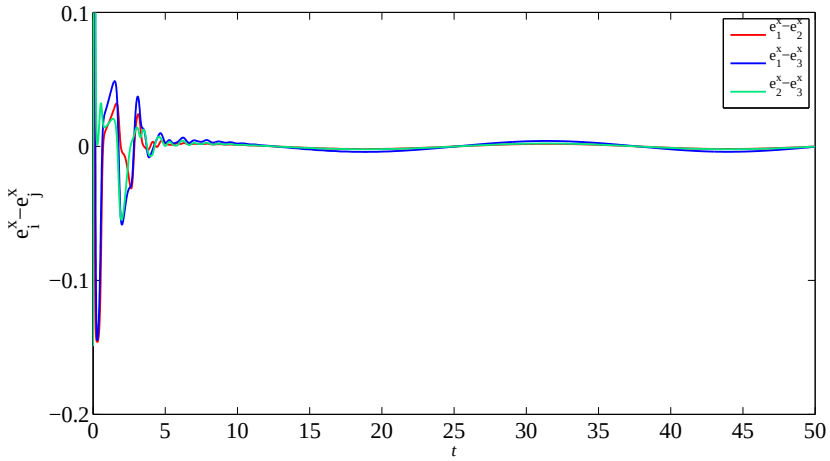

(b)

Figure 4.12: Coordination errors (x – coordinate): (a) disconnected communication graph (b) connected communication graph.

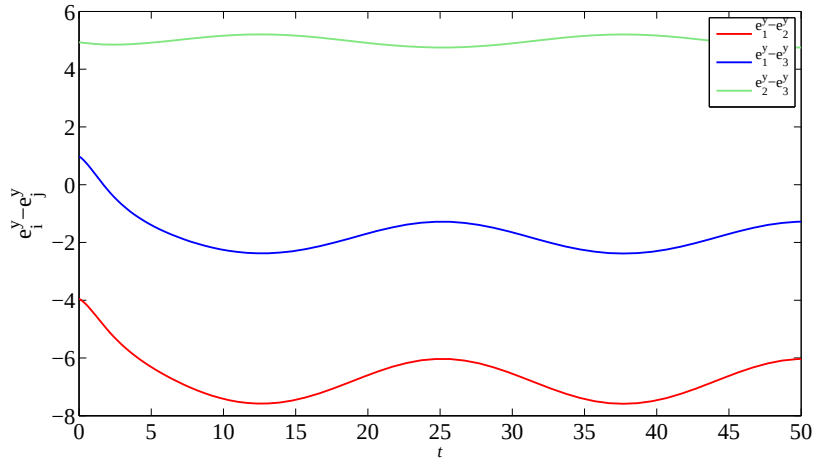

(a)

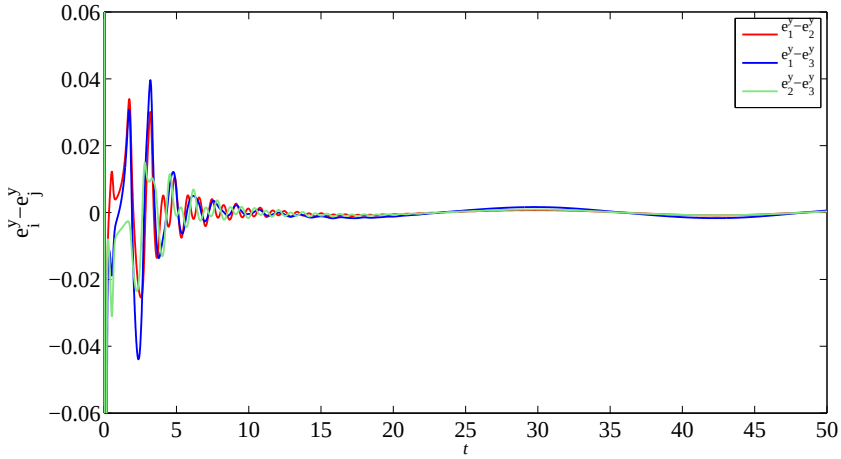

(b)

Figure 4.13: Coordination errors (y – coordinate): (a) disconnected communication graph (b) connected communication graph.

Robot number	**Control gains**		
Robot 1	$c_1^{xe} = 5$ $c_{12}^{x\sigma} = 30$ $c_{13}^{x\sigma} = 0$	$c_1^{ye} = 30$ $c_{12}^{y\sigma} = 160$ $c_{13}^{y\sigma} = 0$	$c_1^{\theta} = 0.5$
Robot 2	$c_2^{xe} = 3$ $c_{21}^{x\sigma} = 40$ $c_{23}^{x\sigma} = 35$	$c_2^{ye} = 30$ $c_{21}^{y\sigma} = 160$ $c_{23}^{y\sigma} = 150$	$c_2^{\theta} = 0.5$
Robot 3	$c_3^{xe} = 4$ $c_{31}^{x\sigma} = 0$ $c_{32}^{x\sigma} = 35$	$c_3^{ye} = 29$ $c_{31}^{y\sigma} = 0$ $c_{32}^{y\sigma} = 150$	$c_3^{\theta} = 0.5$

Table 4.2: List of control parameters used in simulations in Subsection 4.3.3.

4.3.3 Saturated control

In this section we present simulation results of a group of three robots controlled by the control law given in Theorem 4.2.8. In comparison to the simulations presented in previous subsections of this section, we only give results for the connected communication case as opposed to both connected and disconnected cases. This is because the principles of operation of both the saturated controller and the nominal controllers are the same so the influence of the connectivity of communication graphs is the same. Having said that, the aim of this section is to demonstrate the applicability of the formation control algorithm when actuators are constrained. Therefore, in this section we also do not apply any perturbation to any of the robots.

The control parameters are given in Table 4.2. Moreover, the robots' initial states are as follows: $q_1(0) = \mathrm{col}(-0.65, 0.69, 0.43)$, $q_2(0) = \mathrm{col}(-2.24, -3.73, 0.62)$, $q_3(0) = \mathrm{col}(-2.43, 0.97, 0.52)$. It is assumed that $\bar{v}_i = 2$ and $\bar{\omega}_i = 2$. To this end, in consideration of selected control parameters, we take $\alpha_i(s) = 1.5\tanh(s)$ and

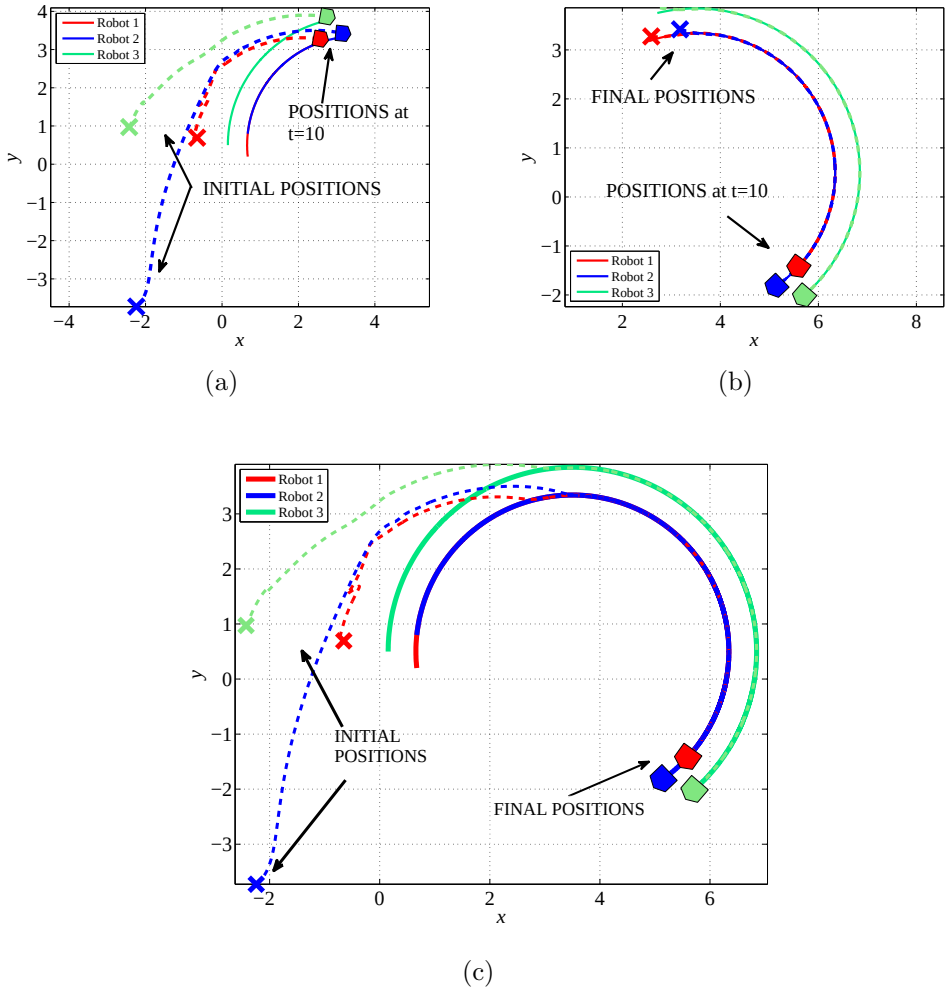

Figure 4.14: Desired robot paths (solid line) and actual robots paths (dashed line) in the plane in the case of a connected communication graph using the saturated control algorithm (4.42, 4.43). (a) paths between $t = 0$ and $t = 10$ (b) paths between $t = 10$ and $t = 30$ (c) whole paths.

$\beta_i(s) = 2.5\tanh(s)$ to ensure that the resulting control inputs v_i and ω_i in (4.48) and (4.49) are guaranteed not to exceed $\bar{v}_i$ and $\bar{\omega}_i$, respectively.

The simulation results for the saturated controller in Theorem 4.2.8 are shown in Figures 4.14–4.16. In particular, in Figure 4.14 we present robots paths in the plane. As expected, robots create the desired formation shape – the equilateral triangle and follow the desired circular trajectory. What is more interesting though is what we can observe in Figures 4.15–4.16 which shows horizontal and vertical components respectively of tracking and coordination errors. It can again be seen that the coordination errors, see Figures 4.15(b) and 4.16(b), vanish faster than the tracking errors, see Figures 4.15(a) and 4.16(a). This is on account of the mutual coupling gains that prevail over the tracking gains and hence robots prioritise coordination over tracking of individual trajectories. Indeed, in terms of the tracking errors, we can observe consensus of the tracking errors as it happened in the simulations for the nominal (non–saturated) controller.

4.4 Experimental results

In this section we present experimental results for the saturated formation control algorithm introduced in Section 4.2.4. The experiments were performed in Eindhoven University of Technology and the experimental setup is presented in Section 3.4.2.

In the experiments, we consider a formation consisting of four robots and two

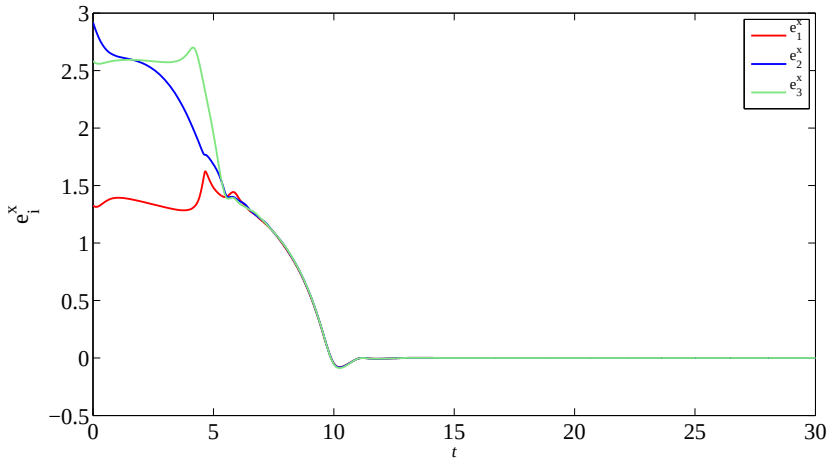

(a)

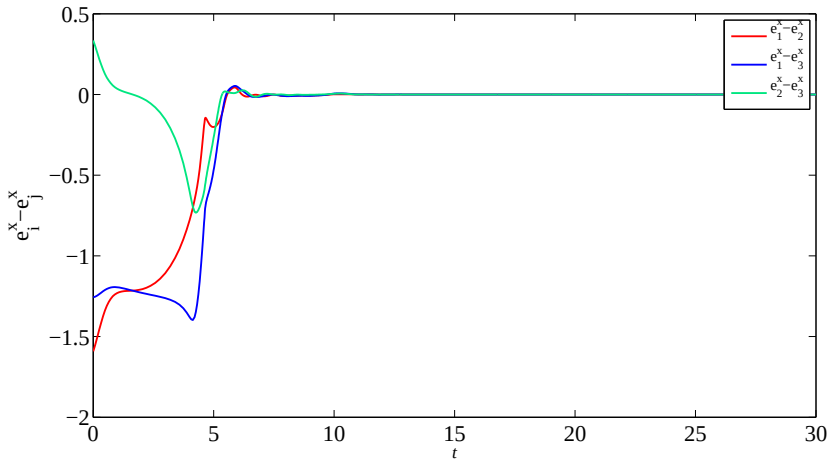

(b)

Figure 4.15: Horizontal components of (a) tracking errors and (b) coordination error in the case of the saturated formation control algorithm (4.42, 4.43).

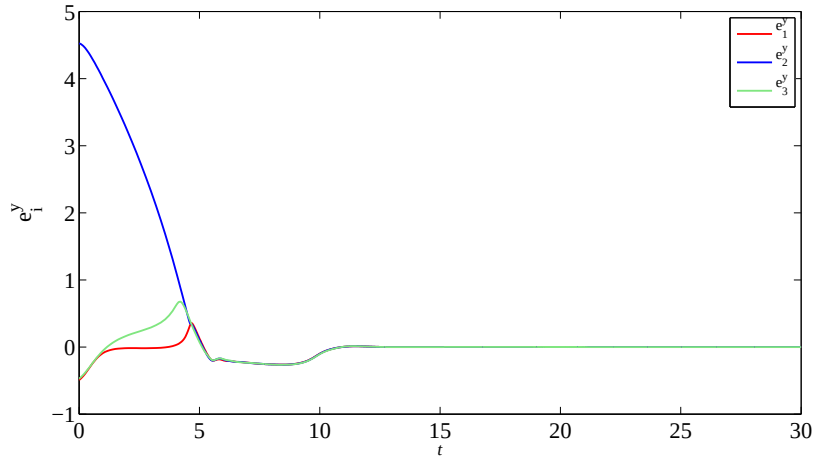

(a)

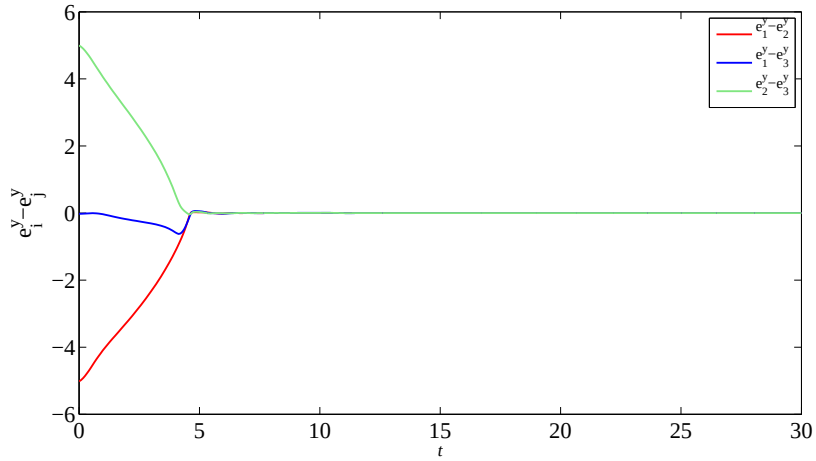

(b)

Figure 4.16: Vertical components of (a) tracking errors and (b) coordination error in the case of the saturated formation control algorithm (4.42, 4.43).

communication structures. The first communication structure is when robots cannot communicate with any other robots. This case relates to a pure trajectory tracking algorithm with no coupling between robots. The second case refers to full coupling, i.e. all robots communicate with all other robots.

The actuator bounds for the robots are $\bar{v}_i = \bar{v} = 0.13\ \frac{\text{m}}{\text{s}}$ and $\bar{\omega}_i = \bar{\omega} = 1.7\ \frac{\text{rad}}{\text{s}}$, as per the specification of the E-Puck robots, see Appendix D. For the resulting control inputs v_i and ω_i to not exceed the bounds $\bar{v}_i$ and $\bar{\omega}_i$ respectively, the control parameters are as follows: $c_i^{xe} = 5$, $c_i^{ye} = 100$, $c_{ij}^{x\sigma} = 30$ and $c_{ij}^{x\sigma} = 80$ and the saturation functions are chosen to be $\alpha_i(s) = \alpha(s) = 0.05\tanh(s)$ and $\beta_i(s) = \beta(s) = 0.1\tanh(s)$. The control parameters c_i^{xe}, c_i^{ye}, $c_{ij}^{x\sigma}$ and $c_{ij}^{x\sigma}$ were chosen on the basis of presenting various features of the control algorithm, see Remark 3.3.1 and using formulae (4.42, 4.43) so that the resulting control inputs do not surpass $\bar{v}_i$ and $\bar{\omega}_i$. Moreover, the desired trajectory of the virtual centre is a circle given by

$$\begin{aligned} x_{vc}^d(t) &= 0.9 - 0.1\sin\theta_{vc}^d, \\ y_{vc}^d(t) &= 0.1\cos\theta_{vc}^d, \\ \theta_{vc}^d(t) &= -0.1t - \frac{\pi}{2}, \end{aligned} \tag{4.68}$$

where x_{vc}^d and y_{vc}^d are in meters and θ_{vc}^d is in radians. Thus, the desired forward speed of the virtual centre is $v_{vc}^d = 0.01\ \frac{\text{m}}{\text{s}}$ and the desired angular velocity is $\omega_{vc}^d = -0.1\ \frac{\text{rad}}{\text{s}}$. Furthermore, the desired formation shape, shown in Figure 4.17, is such that the desired position of Robot 1 coincides with that of the virtual centre. Subsequent robots are collinear with each other and are 0.2 m apart from

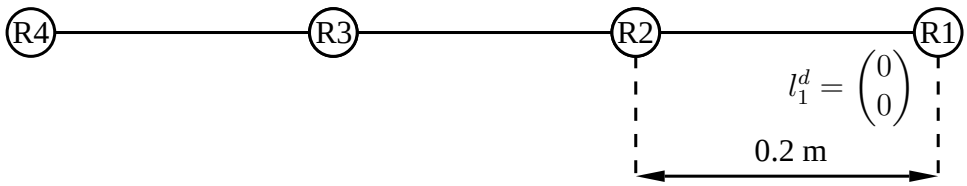

Figure 4.17: Desired formation geometry used in the experiments.

each other.

With a choice of the control parameters as mentioned above, the formation control problem is solved and the control inputs v_i and ω_i respect the required bounds $\bar{v}_i$ and $\bar{\omega}_i$, $i \in \mathcal{I}$. We present the experimental results in Figures 4.18–4.21. It should be noted here that due to the limitations of the experimental setup, the behaviour of robots is only observed approximately. This is due to the occurrence of, for example, noise. In Figure 4.18 we depict the robot paths in the plane when robots are decoupled and in Figure 4.19 we show a corresponding graph for a connected communication graph. In both cases robots eventually converge to the desired formation shape and the formation as a whole tracks the desired trajectory. Moreover, it is evidenced that when robots are not allowed to communicate with each other and if any of the robots is perturbed, the unperturbed robots do not react to the perturbation, see Figure 4.18. This is on account of robots not being informed about any perturbation due to the lack of communication links. On the contrary, when the communication graph is connected, the robots try to keep the desired formation shape and thus temporarily leave their desired individual trajectories after the perturbation. It is clearly visible in Figure 4.19 that indeed after the displacement of Robot 2, the remaining robots abandon their desired individual trajectories to preserve the formation shape.

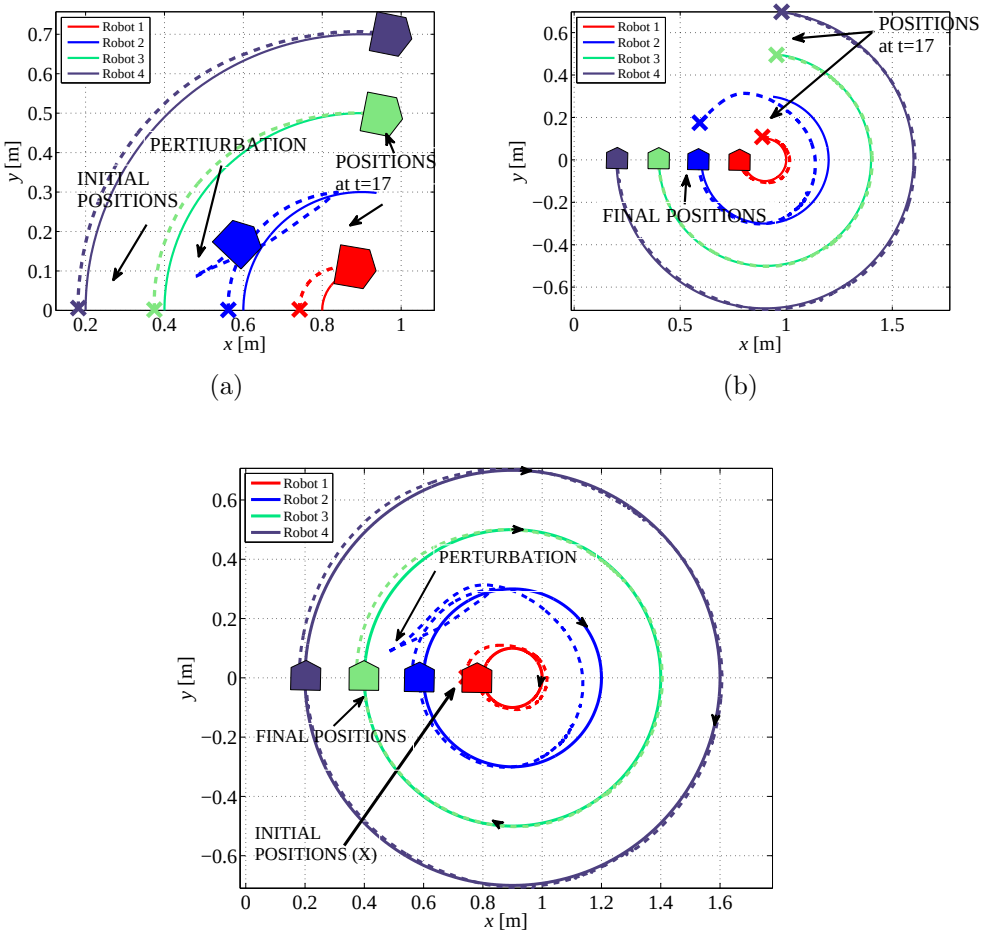

Figure 4.18: Desired robot paths (solid line) and actual robots paths (dashed line) in the plane obtained in experiments in the case of a disconnected communication graph using the saturated control algorithm (4.42, 4.43). (a) paths between $t = 0$ s and $t = 17$ s (b) paths after $t = 17$ s (c) whole paths.

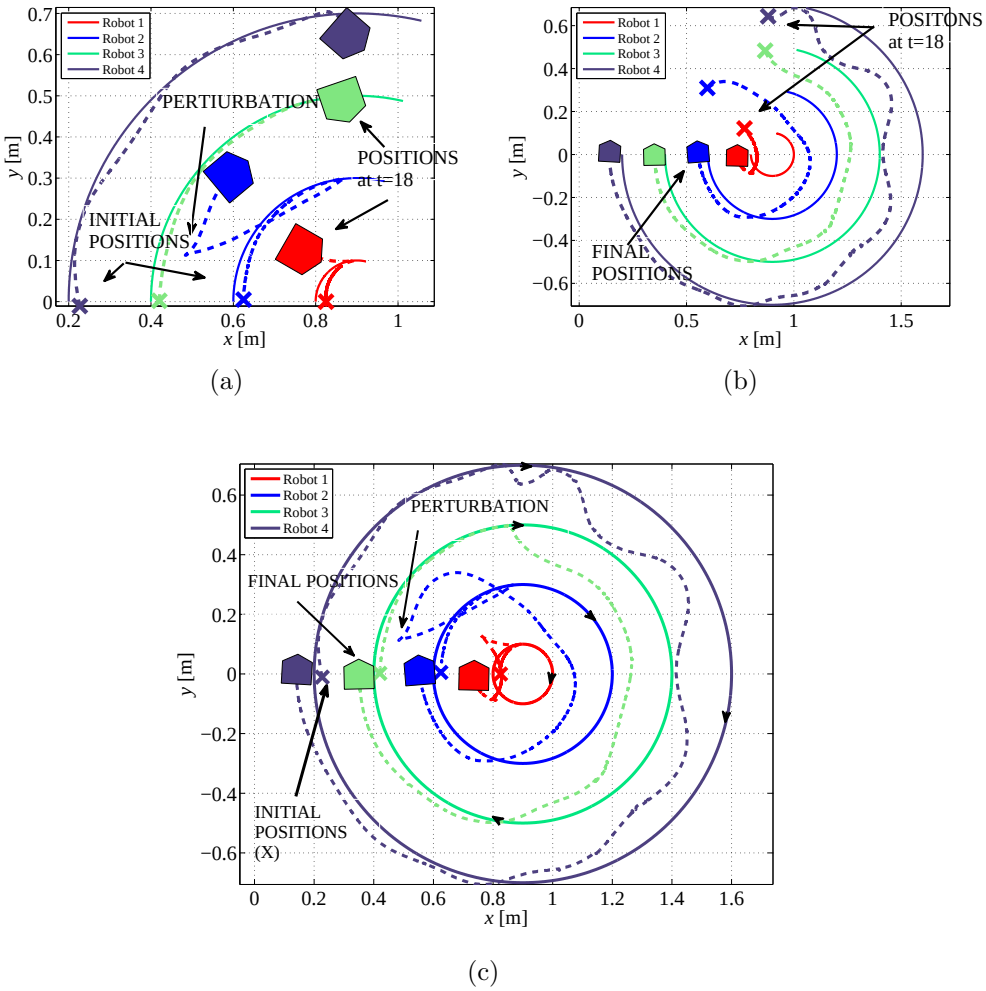

Figure 4.19: Desired robot paths (solid line) and actual robots paths (dashed line) in the plane obtained in experiments in the case of a connected communication graph using the saturated control algorithm (4.42, 4.43). (a) paths between $t = 0$ s and $t = 18$ s (b) paths after $t = 18$ s (c) whole paths.

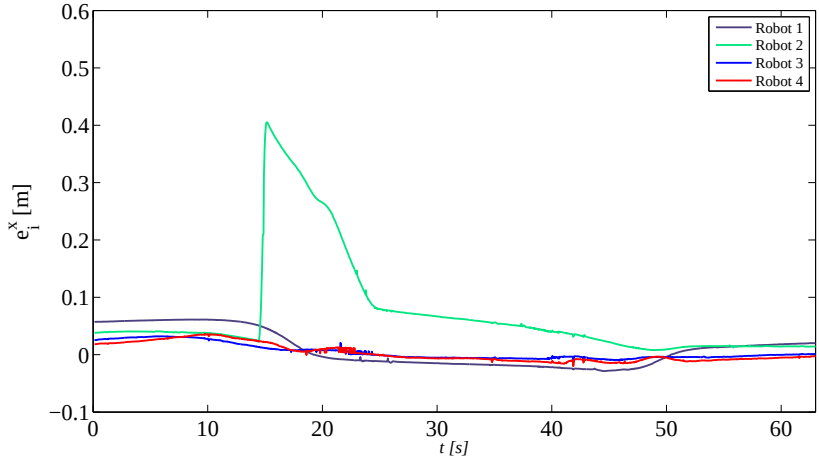

(a)

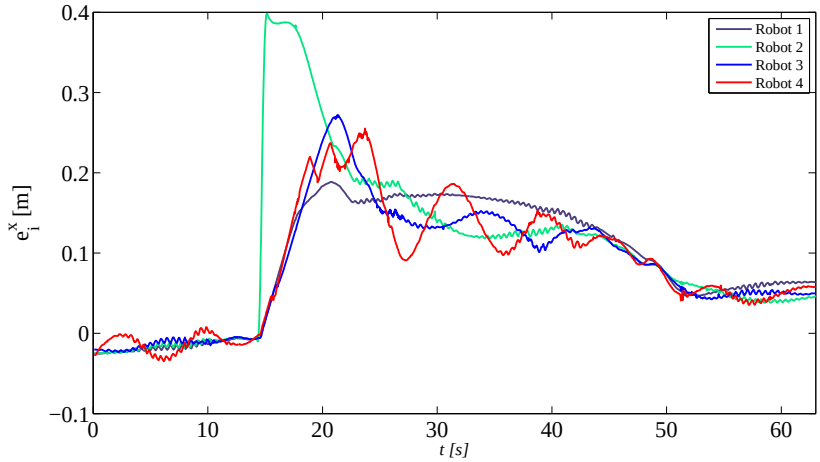

(b)

Figure 4.20: Horizontal components of tracking errors for (a) decoupled robots and (b) coupled robots in the case of the saturated formation control algorithm (4.42, 4.43) obtained in experiments.

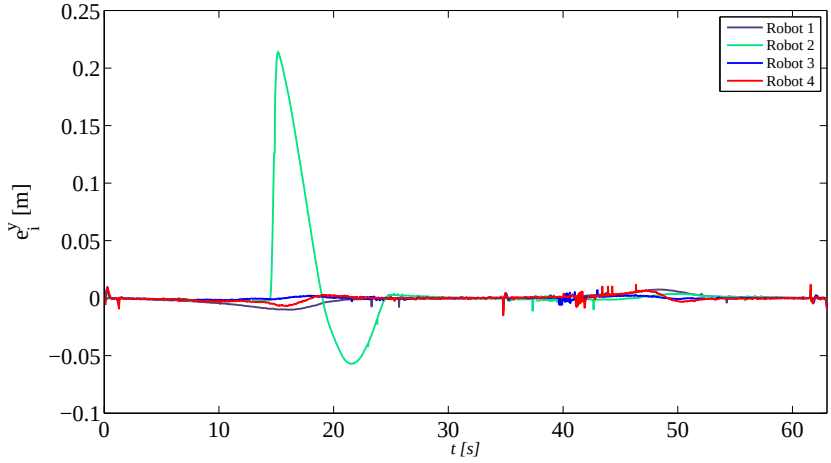

(a)

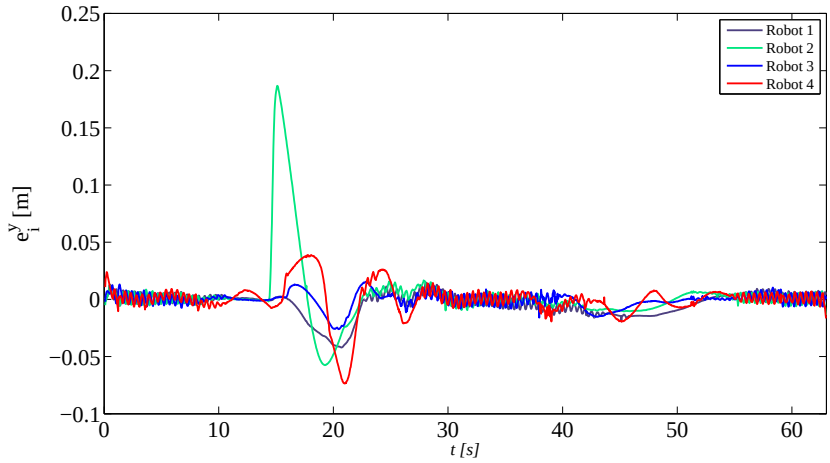

(b)

Figure 4.21: Vertical components of tracking errors for (a) decoupled robots and (b) coupled robots in the case of the saturated formation control algorithm (4.42, 4.43) obtained in experiments.

As far as the formation geometry maintenance is concerned, we can also consider Figures 4.20 and 4.21. These figures present the horizontal and vertical components, respectively, of the tracking error variables in the case of a disconnected and connected communication graph. It was pointed out earlier in this chapter that the formation shape is kept if the tracking error variables given in the world frame are in consensus with each other. In both cases of the disconnected and connected communication graph, we manually displaced Robot 2 at around $t = 15$ s. This displacement is to serve as a perturbation to demonstrate the response from robots should a perturbation occur. When the communication graph is disconnected, the unperturbed robots do not diverge from their desired trajectories which is shown in Figures 4.20(a) and 4.21(a). Notice that the errors of the unperturbed robots remain close to zero despite the perturbation occurring to Robot 2. This is because of the lack of information exchange between the robots which makes it impossible for other robots to sense the perturbation. In the opposite case when the communication graph is connected, we can see clearly that after the perturbation the tracking error variables coincide with each other before they jointly vanish, see Figures 4.20(b) and 4.21(b). We can therefore again confirm the benefits that communication between robots can bring about for the cooperative behaviour of robots in the formation. As mentioned earlier, due to the experimental setup limitations the phenomena of vanishing of the errors as well as of consensus of the errors can only be viewed approximately. However, the trend can still be clearly seen and as such the results still appear to validate our theoretical claims.

In order to compare the experimental results obtained in this section with simula-

tion results under similar settings, we give in Section 6.3 a simulation study based on the scenario of the experiments in this section to allow a fair comparison.

4.5 Discussion

In this chapter we have studied a coordination control problem for nonholonomic mobile robots with time-varying desired formation shapes. We have expressed position tracking error variables in a common coordinate frame and, therefore, we were able to show that the physical coordination of robots in the formation relates to the consensus phenomenon of tracking error variables given in a common coordinate system which in this work is the world frame. By combining terms in the control law concerning both tracking of the desired trajectories of individual robots and coordination with the robots' neighbours, we have proposed a control law that ensures both tracking and coordination simultaneously. Moreover, we have observed that formation behaviour of multiple robots in the group can be enhanced if robots can communicate with each other. If this is the case, robots in the formation not only aim to track their individual trajectories but they also explicitly act towards maintaining a desired formation shape.

Due to the separation of the two control objectives in the control law, i.e. individual trajectory tracking and maintaining formation, the control algorithm benefits from the ability to influence the two control objectives separately. In particular, by increasing the tracking gains with respect to the coupling gains, one can prioritise the trajectory tracking against the formation keeping, and vice versa.

Moreover, we have shown that both control objectives can be achieved irrespective of one another. As shown in the simulations and experiments, in the extreme cases, the robots either only track their individual desired trajectories with no interactions with other robots, or achieve pure coordination. In particular, this confirms that robots can form a desired formation geometry in spite of a nonzero position tracking error.

Another contribution of this chapter is the saturated formation controller. For this controller we can determine the maximum values of the resulting control inputs. The importance of studying the saturated version of the nominal formation control algorithms is specifically apparent in practical implementation. Since actual robots cannot realise infinite inputs, actuator limitations should be indeed considered and these are taken into account in the saturated formation controller.

An attractive feature of the results presented in this chapter is the fact that all formation control algorithms are distributed, i.e. they are executed at a local level. In other words, robots in the formation are only required to exchange information with their neighbours. Therefore, there is no need for a global communication network which is a highly beneficial property in practice.

Chapter 5

Formation control of car–like nonholonomic robots using the backstepping approach

5.1 Introduction

There has been considerable research done in the field of formation control of multiple mobile robots. However, to our knowledge, only little work regarding formations of car–like nonholonomic mobile robots has been performed. Nonetheless, this is an important subject to study because it covers a more general type of robots than the unicycle–type robots and therefore, further research is essential.

In the scope of tracking control of a single car–like mobile robot multiple re-

sults have been proposed in the literature, including the backstepping approach (Kumar and Sukavanam, 2008; Lefeber and Nijmeijer, 1999; Wang et al., 2006), dynamic feedback linearisation (Yang et al., 2004) or control algorithm designed for general nonholonomic systems in chained form, see eg. (De Luca et al., 1998; Lefeber et al., 2000; Morin and Samson, 2006, 2008). Similarly, existing algorithms to solve the formation control problem for a group of car–like mobile robots also utilise these techniques. For example, the control algorithms proposed in (Dong and Farrell, 2008; Dong et al., 2006) apply to formation control of general nonholonomic systems; hence they can also be used to control a formation consisting of car–like mobile robots. However, as mentioned in Section 1.5, the disadvantage of this approach is that only constant formation shapes are allowed which poses a considerable limitation. Therefore, in our work we allow for time–varying formation shapes.

In our contribution, we consider a formation consisting of N car–like mobile robots with indices $i \in \mathcal{I}$ where $\mathcal{I} = \{1, \ldots, N\}$. The kinematics of a car–like mobile robot with rear–wheel drive is assumed to be given by (cf. Section 2.1.2):

$$\begin{aligned} \dot{x}_i &= v_i \cos\theta_i, \\ \dot{y}_i &= v_i \sin\theta_i, \\ \dot{\theta}_i &= \frac{v_i}{l} \tan\varphi_i, \\ \dot{\varphi}_i &= \omega_i, \end{aligned} \tag{5.1}$$

where the state vector is $q_i(t) = (x_i(t), y_i(t), \theta_i(t), \varphi_i(t))^T$ denoting Cartesian position $p_i(t) = (x_i(t), y_i(t))^T$, the heading angle of the robot $\theta_i(t)$ and the steering angle of the front wheels $\varphi_i(t)$. The control inputs are the forward velocity of the

robot $v_i(t)$ and angular velocity of the front wheel $\omega_i(t)$ and l is the length of the robot. Having robot trajectories $q_i(t)$ at hand, the inputs $v_i(t)$ and $\omega_i(t)$ can be calculated as follows

$$\begin{aligned} v_i &= \sqrt{(\dot{x}_i)^2 + (\dot{y}_i)^2}, \\ \omega_i &= l\frac{(\dddot{y}_i\dot{x}_i - \dddot{x}_i\dot{y}_i)\left((\dot{x}_i)^2 + (\dot{y}_i)^2\right) - 3\left(\dot{x}_i\ddot{x}_i + \dot{y}_i\ddot{y}_i\right)\left(\ddot{y}_i\dot{x}_i - \ddot{x}_i\dot{y}_i\right)}{\left((\dot{x}_i)^2 + (\dot{y}_i)^2\right)^{-1/2}\left(\left((\dot{x}_i)^2 + (\dot{y}_i)^2\right)^3 + l^2\left(\ddot{y}_i\dot{x}_i - \ddot{x}_i\dot{y}_i\right)^2\right)}. \end{aligned} \tag{5.2}$$

The formation control problem, as explained in Section 2.2, relies on robots creating a desired, possibly time–varying, formation shape and tracking a given trajectory as a group. To this end, we again follow the virtual structure approach, see Section 2.2. Therefore, we define the so-called virtual centre and prescribe a desired trajectory for the virtual centre to track to be $q_{vc}^d(t) = \mathrm{col}(p_{vc}^d(t), \theta_{vc}^d(t), \varphi_{vc}^d(t)) = \mathrm{col}(x_{vc}^d(t), y_{vc}^d(t), \theta_{vc}^d(t), \varphi_{vc}^d(t))$ such that the corresponding forward velocity v_{vc}^d and angular velocity ω_{vc}^d are bounded. These may be calculated using expressions analogous to (5.2). We also define the desired time–varying formation shape with the aid of vectors $l_i^d(t) = \mathrm{col}\left(l_{ix}^d(t), l_{iy}^d(t)\right)$ such that $\frac{d}{dt}(l_i^d(t))$ are bounded, $\forall i \in \mathcal{I}$, that give desired Cartesian positions of each robot in reference to the virtual centre. Then, the desired orientations of robots are defined using the nonholonomic constraint $\dot{x}\sin\theta + \dot{y}\cos\theta = 0$. Consequently, we define desired trajectories for all individual robots in the formation as

$$p_i^d = p_{vc}^d + R(\theta_{vc}^d)l_i^d, \tag{5.3}$$

in which $p_i^d = (x_i^d, y_i^d)^T$, $\varphi_i^d = \mathrm{atan}\left(l\frac{\dot{\theta}_i^d}{v_i^d}\right)$ and $R(\theta_{vc}^d)$ is defined according to (2.32). Moreover, we can calculate the desired forward and angular velocities associated

with the desired trajectories (5.3) again using counterparts of (5.2). For the sake of completeness we include the resultant expressions for v_i^d and ω_i^d:

$$\begin{aligned} v_i^d &= \sqrt{\left(\dot{x}_i^d\right)^2 + \left(\dot{y}_i^d\right)^2}, \\ \omega_i^d &= l\frac{\left(\dddot{y}_i^d\dot{x}_i^d - \dddot{x}_i^d\dot{y}_i^d\right)\left(\left(\dot{x}_i^d\right)^2 + \left(\dot{y}_i^d\right)^2\right) - 3\left(\dot{x}_i^d\ddot{x}_i^d + \dot{y}_i^d\ddot{y}_i^d\right)\left(\ddot{y}_i^d\dot{x}_i^d - \ddot{x}_i^d\dot{y}_i^d\right)}{\left(\left(\dot{x}_i^d\right)^2 + \left(\dot{y}_i^d\right)^2\right)^{-1/2}\left(\left(\left(\dot{x}_i^d\right)^2 + \left(\dot{y}_i^d\right)^2\right)^3 + l^2\left(\ddot{y}_i^d\dot{x}_i^d - \ddot{x}_i^d\dot{y}_i^d\right)^2\right)}. \end{aligned} \tag{5.4}$$

To accommodate for the singularity of the car–like mobile robot when $\varphi_i = \pm\frac{\pi}{2}$, we state the following condition on desired trajectories of robots in the formation.

Assumption 1. All desired trajectories of robots satisfy $\varphi_i^d \in \left(-\frac{\pi}{2}, \frac{\pi}{2}\right)$.

We discuss in the sequel of this chapter how the condition $\varphi_i \neq \pm\frac{\pi}{2}$ can also be guaranteed for robot trajectories.

In view of the above description of the formation control problem, we now define error variables between actual robot states and the desired states as (Kanayama et al., 1990)

$$\begin{pmatrix} e_i^{xy} \\ \theta_i^e \end{pmatrix} = \begin{bmatrix} \cos\theta_i & \sin\theta_i & 0 \\ -\sin\theta_i & \cos\theta_i & 0 \\ 0 & 0 & 1 \end{bmatrix} \begin{pmatrix} e_i \\ \theta_i^d - \theta_i \end{pmatrix}, \qquad (i \in \mathcal{I}), \tag{5.5}$$

where $e_i = p_i^d - p_i$ is the tracking error in the global coordinate frame and e_i^{xy} is the tracking error variable in the robot-fixed coordinate frame. Using the notation from the previous chapter, we have $e_i^{xy} = R(-\theta_i)e_i$.

Differentiating (5.5) with respect to time leads to the following error dynamics

$$\begin{aligned}\dot{e}_i^{xy} &= \dot{R}(-\theta_i)e_i + R(-\theta_i)\dot{e}_i \\ &= \left(-\frac{v_i}{l}\tan\varphi_i\right) SR(-\theta_i)e_i + R(-\theta_i)\begin{pmatrix} v_i^d\cos\theta_i^d - v_i\cos\theta_i \\ v_i^d\sin\theta_i^d - v_i\sin\theta_i \end{pmatrix} \\ &= \left(-\frac{v_i}{l}\tan\varphi_i\right) Se_i^{xy} + \begin{pmatrix} v_i^d\cos\theta_i^e - v_i \\ v_i^d\sin\theta_i^e \end{pmatrix}, \qquad (5.6)\end{aligned}$$

$$\dot{\theta}_i^e = \frac{v_i^d}{l}\tan\varphi_i^d - \frac{v_i}{l}\tan\varphi_i, \qquad (5.7)$$

where S is the skew–symmetric matrix defined in (4.5). Note that we do not calculate the error dynamics of φ_i but instead we consider the dynamics of φ_i itself as in (5.1). In addition, in view of the earlier conditions on the feedforward velocities of the virtual centre $v_{vc}^d(t)$ and $\omega_{vc}^d(t)$ and the desired formation shape coordinate $l_i^d(t)$ we conclude that the desired forward speed $v_i^d(t)$, for all $i \in \mathcal{I}$ is bounded. Assume moreover that $v_i^d(t)$ is bounded away from zero, for all t, i.e. there exists $\underline{v}_i^d > 0$ such that

$$v_i^d(t) \geq \underline{v}_i^d, \qquad \forall t. \qquad (5.8)$$

As mentioned above, the control objective is twofold. First, we require the formation as a whole to track a given trajectory. Secondly, we want robots in the formation to create a desired formation shape. Both control objectives are satisfied when robots in the formation track their individual trajectories. We now explicitly define what the condition for the formation shape maintenance is re-

gardless of the trajectory tracking component in the spirit of the developments in Chapter 4. In particular, we consider the formation to be maintained if robots create the given formation geometry, i.e. when

$$p_i(t) - p_{vc}(t) = R(\theta_{vc}(t))l_i^d(t), \qquad \forall i \in \mathcal{I}, \tag{5.9}$$

for certain $p_{vc}(t)$ and $\theta_{vc}(t)$, or equivalently if

$$p_i^d(t) - p_i(t) = p_j^d(t) - p_j(t), \qquad \forall i, j \in \mathcal{I}. \tag{5.10}$$

Note that this allows for possible translations of the formation in the plane. However, in comparison with the formation geometry maintenance index defined in (3.54) the criterion above is more strict as no rotation or reflection of the whole formation is permitted.

Now, we define a coordination error between a pair of robots i, j similarly to the developments in the previous chapter and in (Kostić et al., 2010b; Sun et al., 2009) to be

$$\sigma_{ij}(t) = (p_i^d(t) - p_i(t)) - (p_j^d(t) - p_j(t)). \tag{5.11}$$

We then choose to redefine σ_{ij} so that the coordination error between robot i and its neighbours is expressed in the same coordinate system as the tracking error variables e_i^{xy} in (5.5). In the developments in Chapter 4, both the tracking error and the coordination error associated with a particular robot were expressed in the world frame. Hence, the coordinate frame was universal for all robots. However, in this chapter we show that it suffices to have the tracking error and

coordination errors of a robot $i \in \mathcal{I}$ in a common frame, as opposed to in the world coordinate frame for all robots in the formation. The reason why we have decided not to use errors given in the world frame is that it proved to simplify the stability analysis. Having said that, error variables expressed in the world frame still are partly used in the sequel of this chapter.

The coordination errors associated with robot $i \in \mathcal{I}$ expressed in the local coordinate frame of robot i is

$$\varepsilon_{ij}(t) = R^T(\theta_i)\sigma_{ij}(t) = e_i^{xy}(t) - R^T(\theta_i - \theta_j)e_j^{xy}(t). \tag{5.12}$$

Accordingly, taking into account (5.12) and (5.6) it can be demonstrated that ε_{ij} satisfies

$$\dot{\varepsilon}_{ij} = \left(-\frac{v_i}{l}\tan\varphi_i\right) S\varepsilon_{ij} + \begin{pmatrix} v_i^d\cos\theta_i^e - v_i \\ v_i^d\sin\theta_i^e \end{pmatrix} - R^T(\theta_{ij}) \begin{pmatrix} v_j^d\cos\theta_j^e - v_j \\ v_j^d\sin\theta_j^e \end{pmatrix}, \tag{5.13}$$

in which $\theta_{ij} = \theta_i - \theta_j = \left(\theta_i^d - \theta_i^e\right) - \left(\theta_j^d - \theta_j^e\right)$.

In the light of the introduced error variables, we may proceed with the problem statement in terms of the stability of the origins of the error dynamics (5.6), (5.7) and (5.13). Specifically, the formation control problem as defined above is solved when the dynamics of the tracking error variables (5.6, 5.7) are globally asymptotically stable for all robots in the formation. Of course, this implies that the coordination error variables $\varepsilon_{ij}(t)$ also converge to zero, for all $i, j \in \mathcal{I}$. Moreover, although we do not pose any explicit condition on the convergence of φ_i to φ_i^d, if all other error variables converge to zero, we can conclude that also

$\varphi_i \to \varphi_i^d$ as $t \to \infty$, $i \in \mathcal{I}$.

In the remainder of this chapter, we use the backstepping approach as presented for a single robot case by Lefeber and Nijmeijer (1999) to solve the formation control problem. This control algorithm is the starting point for our study with appropriate adjustments to accommodate for the formation control.

Similarly to the developments in the previous two chapters, the control algorithms for formations of car–like mobile robots in this chapter is based on local interaction between neighbouring robots. Therefore, they can be implemented locally and there is no need for a global communication network, which is a desirable feature in many practical applications. Our approach in this chapter mimics the technique presented in the previous two chapters. In particular, we add mutual coupling terms to facilitate the communication between robots so that each robot in the formation is influenced by the behaviour of its neighbours. This, as shown in the two previous chapters, enhances the ability of robots to explicitly act as a formation as opposed to tracking individual trajectories and hence implicitly fulfil the formation control problem specifications.

The outline of the rest of this chapter is as follows. First, in Section 5.2 we present our main results - the formation control algorithm. In Section 5.3 we include a simulation study and in Section 5.4 we discuss our results.

5.2 Control design

In this section we design the formation control algorithm to solve the formation control problem defined in the previous section by means of backstepping. For details on this technique, the reader is referred to Appendix B.4.

Note that the control design method is motivated by the developments in (Lefeber and Nijmeijer, 1999) in which a control strategy for a single robot is proposed. Our modifications are triggered by the benefits for robots in the formation that inter–robot communication provides. Consequently, the control law in (Lefeber and Nijmeijer, 1999) was altered to facilitate for communication of robots with their neighbours to enhance the formation behaviour.

In order to keep φ_i within $(-\frac{\pi}{2}, \frac{\pi}{2})$ as required given that $\varphi_i(0) \in (-\frac{\pi}{2}, \frac{\pi}{2})$, we introduce a new variable $\mu_i = \tan\varphi_i$, $i \in \mathcal{I}$ (cf. Yang et al., 2004). This implies that $\varphi_i = \operatorname{atan}\mu_i$ and therefore controlling μ_i results in $\varphi_i \in (-\frac{\pi}{2}, \frac{\pi}{2})$. Let

$$\dot{\mu}_i = \xi_i, \tag{5.14}$$

where ξ_i is an auxiliary control, $i \in \mathcal{I}$. Once the control input for ξ_i is derived, the original control input ω_i can be retrieved from

$$\dot{\varphi}_i = \frac{1}{1+\mu_i^2}\xi_i = \omega_i. \tag{5.15}$$

To use the backstepping control design method, assume in the first instance that

we can control θ_i^e directly through a virtual control $\bar{\mu}_i$, i.e. the dynamics of θ_i^e is given by

$$\dot{\theta}_i^e = \frac{v_i^d}{l}\tan\varphi_i^d - \bar{\mu}_i. \tag{5.16}$$

To find the control inputs v_i and $\bar{\mu}_i$ stabilising the origin of the error dynamics (5.6, 5.16), consider the Lyapunov function candidate

$$V(e_i^{xy}, \varepsilon_{ij}, \theta_i^e) = \sum_{i=1}^{N}\left[c_i^e (e_i^{xy})^T e_i^{xy} + \frac{1}{2}\sum_{j\in N_i} c_{ij}\varepsilon_{ij}^T\varepsilon_{ij} + (\theta_i^e)^2\right]. \tag{5.17}$$

Calculating its time derivative along the dynamics (5.6, 5.16) yields

$$\begin{aligned}\dot{V}(e_i^{xy}, \varepsilon_{ij}, \theta_i^e) \;&= \sum_{i=1}^{N}\left[\theta_i^e\left(v_i^d\left(c_i^e (e_i^{xy})^T + \sum_{j\in N_i} c_{ij}\varepsilon_{ij}^T\right)\begin{bmatrix}\dfrac{\cos\theta_i^e - 1}{\theta_i^e}\\ \dfrac{\sin\theta_i^e}{\theta_i^e}\end{bmatrix} + \frac{v_i^d}{l}\tan\varphi_i^d - \bar{\mu}_i\right)\right.\\ &\left. + (c_i^e x_i^e + \sum_{j\in N_i} c_{ij}\varepsilon_{ij}^x)(v_i^d - v_i)\right].\end{aligned} \tag{5.18}$$

Consider the temporary controller to be defined by

$$v_i = v_i^d + \chi_i(c_i^e x_i^e + \sum_{j\in N_i} c_{ij}\varepsilon_{ij}^x), \tag{5.19}$$

$$\bar{\mu}_i = \frac{v_i^d}{l}\tan\varphi_i^d + v_i^d\left(c_i^e (e_i^{xy})^T + \sum_{j\in N_i} c_{ij}\varepsilon_{ij}^T\right)\begin{bmatrix}\dfrac{\cos\theta_i^e - 1}{\theta_i^e}\\ \dfrac{\sin\theta_i^e}{\theta_i^e}\end{bmatrix} + c_i^\theta\theta_i^e, \tag{5.20}$$

where the function $\chi_i(\cdot)$ is continuously differentiable and satisfies $\chi_i(x)x > 0$ for $x \neq 0$ and $\chi_i(\cdot) < \underline{v}_i^d$, in which $\underline{v}_i^d$ is defined in (5.8). The reason for defining $\chi_i(\cdot)$ in this way is to ensure that $v_i \neq 0$ and its importance becomes apparent later

in this section. Clearly, with such a choice of $\chi_i(\cdot)$, the resultant control input v_i is bounded with a bound that can be specified off-line beforehand. Yet, this is a by-product of the control design as opposed to the control objective. Note that the resultant input $\bar{\mu}_i$ does not possess such a feature and can be arbitrarily large depending on the initial conditions.

The derivative of the Lyapunov function (5.18) when control inputs (5.19, 5.20) are applied becomes

$$\dot{V}(e_i^{xy}, \varepsilon_{ij}, \theta_i^e) = -\sum_{i=1}^{N} \left[c_i^\theta (\theta_i^e)^2 + (c_i^e x_i^e + \sum_{j \in N_i} c_{ij} \varepsilon_{ij}^x) \chi_i (c_i^e x_i^e + \sum_{j \in N_i} c_{ij} \varepsilon_{ij}^x) \right] \leq 0. \tag{5.21}$$

Hence, by Theorem B.11 we can show that $\lim_{t \to \infty} \dot{V} = 0$. Therefore, we conclude that as $t \to \infty$ we have

$$\theta_i^e \to 0, \tag{5.22}$$

and

$$\left(c_i^e e_i^{xy} + \sum_{j \in N_i} c_{ij} \varepsilon_{ij} \right) \begin{pmatrix} 1 \\ 0 \end{pmatrix} \to 0. \tag{5.23}$$

Using the dynamic equation (5.16) for θ_i^e

$$\dot{\theta}_i^e = -v_i^d \left(c_i^e (e_i^{xy})^T + \sum_{j \in N_i} c_{ij} \varepsilon_{ij}^T \right) \begin{bmatrix} \dfrac{\cos \theta_i^e - 1}{\theta_i^e} \\ \dfrac{\sin \theta_i^e}{\theta_i^e} \end{bmatrix} - c_i^\theta \theta_i^e, \tag{5.24}$$

and Lemma A.6, we infer that also

$$\left(c_i^e e_i^{xy} + \sum_{j \in N_i} c_{ij} \varepsilon_{ij} \right) \begin{pmatrix} 0 \\ 1 \end{pmatrix} \to 0, \tag{5.25}$$

which together with (5.23) implies

$$\begin{aligned} &\left(c_i^e e_i^{xy} + \sum_{j \in N_i} c_{ij} \varepsilon_{ij} \right) \\ &= \left(c_i^e e_i^{xy} + \sum_{j \in N_i} c_{ij} \left(e_i^{xy} - R^T(\theta_{ij}) e_j^{xy} \right) \right) \\ &= R^T(\theta_i) \left(c_i^e e_i + \sum_{j \in N_i} c_{ij} \left(e_i - R(\theta_j) e_j^{xy} \right) \right) \to 0, \end{aligned} \tag{5.26}$$

and consequently

$$\left(c_i^e e_i + \sum_{j \in N_i} c_{ij} \left(e_i - e_j \right) \right) \to 0, \tag{5.27}$$

when taking into account that the rotation matrix $R(\theta_i)$ is nonsingular for all θ_i. Note that the last condition is given with respect to the tracking error e_i in the global coordinate frame as opposed to previously considered e_i^{xy} which is with respect to a robot–attached moving frame. Now, we can write (5.27) in terms of the horizontal and vertical components of the tracking error $e_i = (e_i^x, e_i^y)^T$ for

$t \to \infty$

$$\begin{bmatrix} c_1^e + \sum_{j\in N_1} c_{1j} & -c_{12} & \cdots & -c_{1N} \\ \vdots & \ddots & \ddots & \vdots \\ -c_{N-1,1} & \ddots & c_{N-1}^e + \sum_{j\in N_{N-1}} c_{N-1,j} & -c_{N-1,N} \\ -c_{N1} & -c_{N2} & \cdots & c_N^e + \sum_{j\in N_N} c_{Nj} \end{bmatrix} e^x \to 0, \qquad (5.28)$$

$$\begin{bmatrix} c_1^e + \sum_{j\in N_1} c_{1j} & -c_{12} & \cdots & -c_{1N} \\ \vdots & \ddots & \ddots & \vdots \\ -c_{N-1,1} & \ddots & c_{N-1}^e + \sum_{j\in N_{N-1}} c_{N-1,j} & -c_{N-1,N} \\ -c_{N1} & -c_{N2} & \cdots & c_N^e + \sum_{j\in N_N} c_{Nj} \end{bmatrix} e^y \to 0, \qquad (5.29)$$

where $e^x = \mathrm{col}(e_1^x, \ldots, e_n^x)$ and $e^y = \mathrm{col}(e_1^y, \ldots, e_n^y)$. From Lemma A.5 it is evident that the matrices in (5.28) and (5.29) are nonsingular and hence $e_i \to 0$ as $t \to \infty$. Consequently $e_i^{xy} \to 0$ and $\varepsilon_{ij} \to 0$ as $t \to \infty$, for all $i, j \in \mathcal{I}$.

Note that because of the assumptions on v_i^d and the conditions that we pose on function χ_i, it can be assured that $v_i > 0$.

Clearly, in reality we cannot control θ_i^e directly with $\bar{\mu}_i$ as the dynamics of θ_i^e is given by (5.7). Therefore, using the backstepping technique as in (Lefeber and Nijmeijer, 1999) we define a new error variable for all $i \in \mathcal{I}$

$$z_i = v_i^d \tan\varphi_i^d - v_i\mu_i + v_i^d \left(c_i^e (e_i^{xy})^T + \sum_{j\in N_i} c_{ij}\varepsilon_{ij}^T \right) \begin{bmatrix} \dfrac{\cos\theta_i^e - 1}{\theta_i^e} \\ \dfrac{\sin\theta_i^e}{\theta_i^e} \end{bmatrix} + c_i^\theta \theta_i^e. \qquad (5.30)$$

Then, error dynamics of θ_i^e in (5.7) can be re–written to be

$$\begin{aligned}\dot{\theta}_i^e &= -v_i^d \left(c_i^e (e_i^{xy})^T + \sum_{j \in N_i} c_{ij} \varepsilon_{ij}^T \right) \begin{bmatrix} \dfrac{\cos\theta_i^e - 1}{\theta_i^e} \\ \dfrac{\sin\theta_i^e}{\theta_i^e} \end{bmatrix} - c_i^\theta \theta_i^e + \frac{1}{l} z_i \\ &= \frac{v_i^d}{l} \tan\varphi_i^d - \bar{\mu}_i + \frac{1}{l} z_i, \end{aligned} \tag{5.31}$$

and the dynamics of z_i is assumed to be given by

$$\dot{z}_i = l\dot{\bar{\mu}}_i - \dot{v}_i \mu_i - v_i \xi_i. \tag{5.32}$$

Let the Lyapunov function candidate be

$$\bar{V} = V + \frac{1}{2} \sum_{i=1}^{N} z_i^2. \tag{5.33}$$

Derivative of $\bar{V}$ along system dynamics is given by

$$\dot{\bar{V}} = \dot{V} + \sum_{i=1}^{N} z_i (\theta_i^e \frac{1}{l} + l\dot{\bar{\mu}}_i - \dot{v}_i \mu_i - v_i \xi_i). \tag{5.34}$$

Therefore, allowing

$$\xi_i = \frac{1}{v_i} \left(\theta_i^e \frac{1}{l} + l\dot{\bar{\mu}}_i - \dot{v}_i \mu_i + c_i^z z_i \right), \tag{5.35}$$

where from (5.19) it is clear that $v_i \neq 0$, gives that $\dot{\bar{V}} = \dot{V} - \sum_{i=1}^{N} c_i^z z_i^2$. Consequently, using the same lines of argument as above it can be shown that the origin of the error dynamics of $(e_i^{xy}, \theta_i^e, z_i)$ is globally asymptotically stable.

The actual control ω_i is given by

$$\omega_i = \frac{\cos^2 \varphi_i}{v_i} \left(\theta_i^e \frac{1}{l} + l\dot{\bar{\mu}}_i - \dot{v}_i \mu_i + c_i^z z_i \right). \tag{5.36}$$

It can be seen that $\varphi_i \in (-\frac{\pi}{2}, \frac{\pi}{2})$ is ensured by noticing that from (5.33) and (5.34) we have that $z_i = 0$ is stable and hence uniformly bounded. Therefore, since $v_i \neq 0$ from (5.30) it can be concluded that μ_i is also bounded. Therefore, $\varphi_i \in (-\frac{\pi}{2}, \frac{\pi}{2})$. Indeed, for φ_i approaching $\pm\frac{\pi}{2}$, the control input ω_i (5.36) tends to 0. Hence, $\varphi_i \in (-\frac{\pi}{2}, \frac{\pi}{2})$ is an invariant set as required.

We formally state the conditions under which the controller in (5.19, 5.36) solves the formation control problem in the following theorem.

Theorem 5.2.1. *Consider a group of N car–like mobile robots, each of which is described by the kinematic model* (5.1)*, a desired trajectory of the virtual centre $q_{vc}^d(t)$ such that the associated feedforward velocities v_{vc}^d and ω_{vc}^d are bounded. Let the desired formation shape be defined using bounded vectors $l_i^d(t)$, $i \in \mathcal{I}$, subject to $\frac{dl_i^d(t)}{dt}$ bounded. Moreover, denote by $q_i^d(t)$ the desired individual trajectories of robots with associated desired forward and angular velocities $v_i^d(t)$ and $\omega_i^d(t)$ satisfying Assumption 1 and $v_i^d > 0$ and ω_i^d is bounded. Let the formation control law be defined by (5.19, 5.36) with $c_i^e > 0$, $c_{ij} = c_{ji} > 0$, $c_i^\theta > 0$ and $c_i^z > 0$. Then, the origin of the closed–loop error dynamics (5.6, 5.19, 5.31, 5.32, 5.36) is globally asymptotically stable and for all pairs of robots $i, j \in \mathcal{I}$, $\varepsilon_{ij} \to 0$ as $t \to \infty$. Hence, the formation control problem is solved.*

Proof. Consider the Lyapunov function candidate

$$V(e_i^{xy}, \varepsilon_{ij}, \theta_i^e, z_i) = \sum_{i=1}^{N} \left[c_i^e (e_i^{xy})^T e_i^{xy} + \frac{1}{2} \sum_{j \in N_i} c_{ij} \varepsilon_{ij}^T \varepsilon_{ij} + (\theta_i^e)^2 + \frac{1}{l} z_i^2 \right]. \quad (5.37)$$

The time derivative of (5.37) along dynamics (5.6, 5.31, 5.32) with the controller given by (5.19, 5.36) is

$$\begin{aligned} \dot{V} &= \sum_{i=1}^{N} \left(-c_i^\theta (\theta_i^e)^2 + \frac{1}{l} \theta_i^e z_i + \frac{c_i^z}{l} z_i^2 - \frac{1}{l} \theta_i^e z_i - \eta_i \chi_i(\eta_i) \right) \\ &= -\sum_{i=1}^{N} \left(c_i^\theta (\theta_i^e)^2 + \frac{c_i^z}{l} z_i^2 + \eta_i \chi_i(\eta_i) \right), \end{aligned} \quad (5.38)$$

where $\eta_i = c_i^e x_i^e + \sum_{j \in N_i} c_{ij} \varepsilon_{ij}^x$. Therefore, we have $\dot{V} \leq 0$ and using Theorem B.11 leads to the conclusion that (5.22) and (5.23) are satisfied together with

$$z_i \to 0 \qquad \text{as} \qquad t \to \infty. \quad (5.39)$$

Therefore, applying Lemma A.6 leads again to (5.27) and, in terms of horizontal and vertical components of the tracking error, to (5.28) and (5.29). As according to Lemma A.5 the matrices in (5.28) and (5.29) are nonsingular, we have $e_i \to 0$ as $t \to \infty$ which implies that also $e_i^{xy} \to 0$ and $\varepsilon_{ij} \to 0$ as $t \to \infty$, for all $i, j \in \mathcal{I}$. Hence, the formation control problem is solved. □

Motivated by the results in the previous chapter, in the following corollary we give some additional conditions under which we can obtain the *coordination* of robots in the formation, see Section 4.2.2. The term *coordination* refers to relaxing the requirement of the formation control problem in that we only want robots in the

formation to create the desired formation shape but they are no longer required to track the desired trajectory as a group.

Corollary 5.2.2. *Consider a group of N car–like mobile robots, each of which is described by the kinematic model* (5.1). *Let the desired trajectory of the virtual centre be given by $q_{vc}^d(t)$ with bounded corresponding feedforward terms v_{vc}^d and ω_{vc}^d. Furthermore, let the desired formation shape be defined with bounded vectors $l_i^d(t)$, $i \in \mathcal{I}$ such that $\frac{dl_i^d(t)}{dt}$ is also bounded. From the desired trajectory of the virtual centre and the desired formation shape, the desired individual trajectories of robots $q_i^d(t)$ can be determined according to* (5.3). *Assume that for the resultant trajectory $q_i^d(t)$, the corresponding desired forward and angular velocities $v_i^d(t)$ and $\omega_i^d(t)$ satisfy Assumptions 1 and $v_i^d > 0$, and ω_i^d is bounded. Let the formation control law be defined by* (5.36) *and a modification of* (5.19) *with all position tracking gains set to zero $c_i^e = 0$. Moreover, assume $c_{ij} = c_{ji} > 0$, $c_i^\theta > 0$ and $c_i^z > 0$. Then, if the communication graph of the formation is connected, the set $\{e_i, \theta_i^e \,|\, i \in \mathcal{I}, j \in N_i, (\varepsilon_{ij}, \theta_i^e) = (0,0)\}$ is a globally attracting invariant set of (5.6, 5.31, 5.32) for all robots and the desired formation shape is created by all robots.*

Proof. (Sketch) The proof is similar to the one for Theorem 5.2.1 with the difference that we have $c_i^e = 0$, for all $i \in \mathcal{I}$. Therefore, $\theta_i^e \to 0$ as $t \to \infty$ and matrices in (5.28) in (5.29) are Laplacian matrices, see Definition C.3. Clearly, if the communication graph of the formation is connected, a Laplacian matrix of this graph has a single zero eigenvalue associated with the right eigenvector $\mathbf{1}_N = \mathrm{col}(1, \ldots, 1) \in \mathbb{R}^{N\times 1}$ (Olfati-Saber and Murray, 2004). Therefore, we conclude the consensus of the position tracking error variables given in the global

coordinate system, which implies that for all $i, j \in \mathcal{I}$, $\varepsilon_{ij} \to 0$ as $t \to \infty$. □

The attractive feature of the results presented in Theorem 5.2.1 is that we only give mild conditions regarding control parameters $c_i^e > 0$, $c_{ij} = c_{ji} > 0$, $c_i^\theta > 0$ and $c_i^z > 0$. Therefore, they can be chosen in a way that is suitable for a particular application. The meaning of these parameters is as follows. Tracking of individual robot trajectories can be influenced by c_i^e while to influence the formation shape keeping then mutual coupling terms c_{ij} should be adjusted. One can also decide if tracking of individual trajectories or formation shape keeping should be more important. In the first case, the position tracking gains c_i^e should dominate the mutual coupling gains c_{ij} and vice versa. The remaining parameters c_i^θ and c_i^z influence directly the convergence of θ_i^e and z_i to zero respectively.

5.3 Simulation results

In this section we present the simulation results of the formation control algorithm given in this chapter. As an illustrative example, we use a formation consisting of four car–like robots whose length is $l = 0.1$. The desired formation shape is a square, where the length of a side is equal to $0.15\sqrt{2}$. It is defined by $l_1^d = \mathrm{col}(0.15, 0)$, $l_2^d = \mathrm{col}(0, -0.15)$, $l_3^d = \mathrm{col}(-0.15, 0)$ and $l_4^d = \mathrm{col}(0, 0.15)$, as depicted in Figure 5.1. In all simulations, t denotes simulation time.

As in the previous two chapters in the case of a unicycle mobile robot, also in this work we study the influence of a disconnected and a connected communication

Robot number	**Control gains**		
Robot 1	$c_1^e = 30$ $c_{12} = 91$ $c_{14} = 85$	$c_1^\theta = 0.5$	$c_1^z = 44$
Robot 2	$c_2^e = 30$ $c_{21} = 91$ $c_{23} = 77$	$c_2^\theta = 0.5$	$c_2^z = 44$
Robot 3	$c_3^e = 30$ $c_{32} = 77$ $c_{34} = 81$	$c_3^\theta = 0.5$	$c_3^z = 44$
Robot 4	$c_4^e = 30$ $c_{41} = 85$ $c_{43} = 81$	$c_4^\theta = 0.5$	$c_4^z = 44$

Table 5.1: List of control parameters used in simulations in. In the case of a disconnected communication graph, all coupling gains are zero (completely decoupled robots).

graphs on the formation performance. The disconnected communication topology as shown in Figure 5.2(a) is in fact a completely decoupled case where there is no interaction between robots in the formation. On the other hand, in the connected communication topology all robots are assumed to have two neighbours, see Figure 5.2(b).

The initial conditions of the four robots in the formation are the following: $q_1(0) = \text{col}(0, 0.2, \frac{\pi}{18}, 0)$, $q_2(0) = \text{col}(2.3, -0.05, -\frac{\pi}{3}, 0)$, $q_3(0) = \text{col}(1.5, 0.6, -\frac{\pi}{4}, 0)$ and $q_4(0) = \text{col}(0.5, -1, \frac{\pi}{4}, 0)$. The control parameters are given in Table 5.1 and were selected as explained in Remark 3.3.1. Let us re–articulate that for the disconnected communication graph, all coupling gains c_{ij}, $i, j \in \{1, 2, 3, 4\}$, are equal zero. Moreover, for all robots the function $\chi_i(s)$ is assumed to be given by $\chi_i(s) = \frac{0.2}{\pi} \tan^{-1}(s)$.

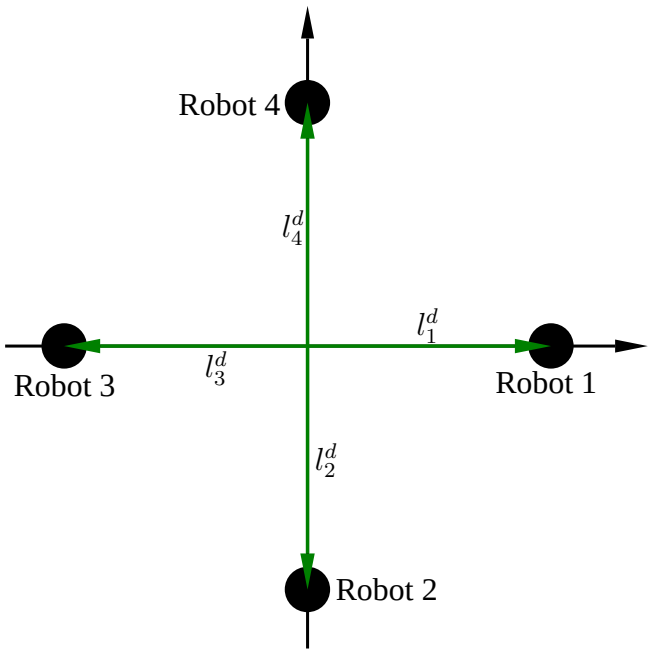

Figure 5.1: Desired formation shape used in the simulations.

All simulations in this section are done for $t \in [0, 30]$. During that time, at $t = 21$ we displace Robot 1 along $(\delta x, \delta y) = (0.2, 0.35)$ to observe how robots in the formation behave in face of a perturbation.

Simulation results are given in Figures 5.3–5.6. In Figures 5.3 and 5.4 we depict robot paths in the plane for a disconnected and a connected communication graph respectively. It can be seen that robots initially converge to the desired formation shape. Then, owing to the perturbation occurring to Robot 1, the formation shape temporarily ceases to be maintained. Here we need to consider two instances: when the communication graph is disconnected and when it is connected. In the first case, only the robots aware of the perturbation can react to the perturbation. In the case presented in simulations, all robots are completely decoupled so no robot, except for the very perturbed one Robot 1, is

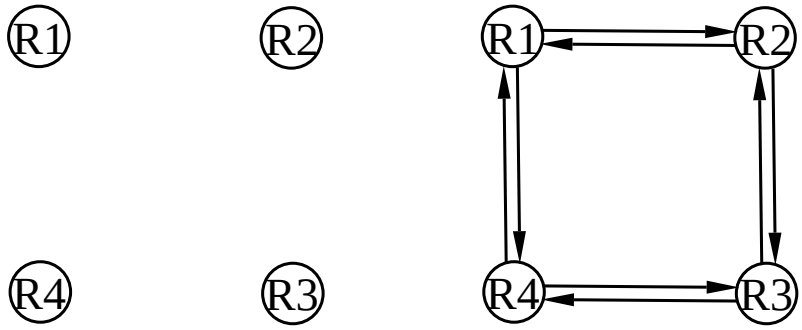

(a) (b)

Figure 5.2: Communication graph structures used in simulations: (a) disconnected graph (b) connected graph.

aware of the disturbance occurring to any other robot but themselves. Therefore, no unperturbed robots (Robots 2, 3 and 4) diverge from their desired trajectories in favour of formation shape preservation, see Figure 5.3. In contrast, when the communication graph is connected, after the perturbation all unperturbed robots diverge from their desired trajectories due to the connectivity of the communication graph of the formation. This means that because of the relatively strong coupling gains c_{ij} as compared to the tracking gains c_i^e, see Table 5.1, robots act primarily towards maintaining formation shape as opposed to purely tracking their individual desired trajectories (irrespective of the behaviour of other robots). For robots to be able to benefit from this mechanism, the communication graph of the formation needs to be connected as in such circumstances robots work explicitly towards coordination of the group. This is despite the lack of such a requirement in Theorem 5.2.1. Understandably, if robots face a perturbation, all members of the formation need to be aware of it through inter–agent communication to counteract the effect of the perturbation. This is shown in Figure 5.4.

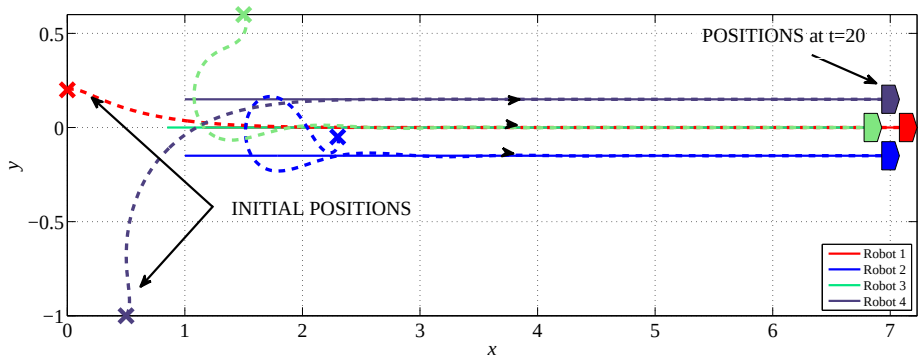

(a)

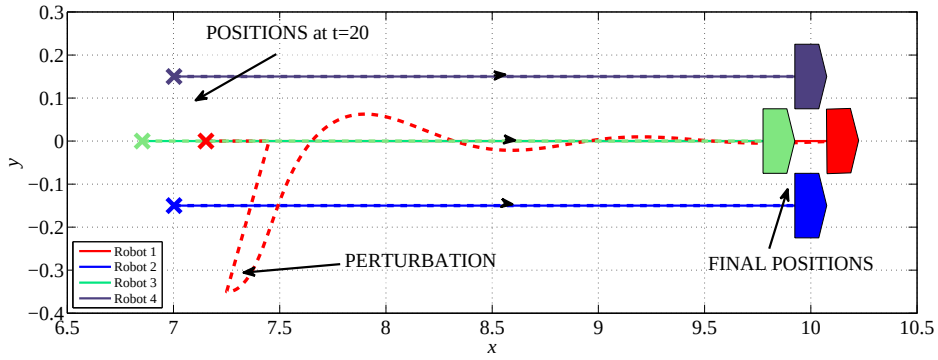

(b)

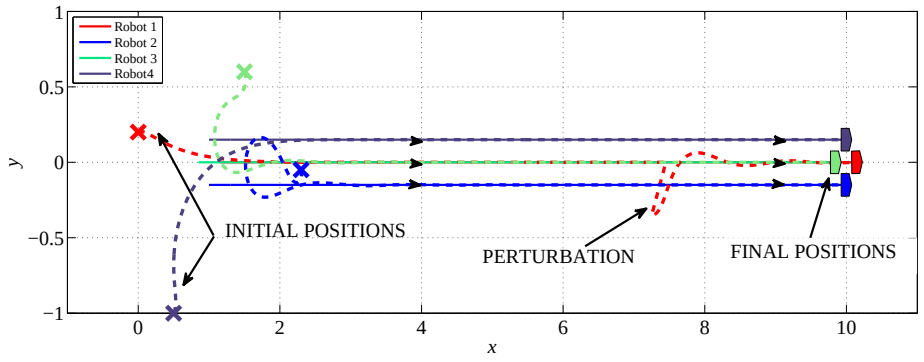

(c)

Figure 5.3: Desired robot paths (solid line) and actual robots paths (dashed line) in the plane in the case of a disconnected communication graph. (a) paths between $t = 0$ and $t = 20$ (b) paths between $t = 20$ and $t = 30$ (c) whole paths.

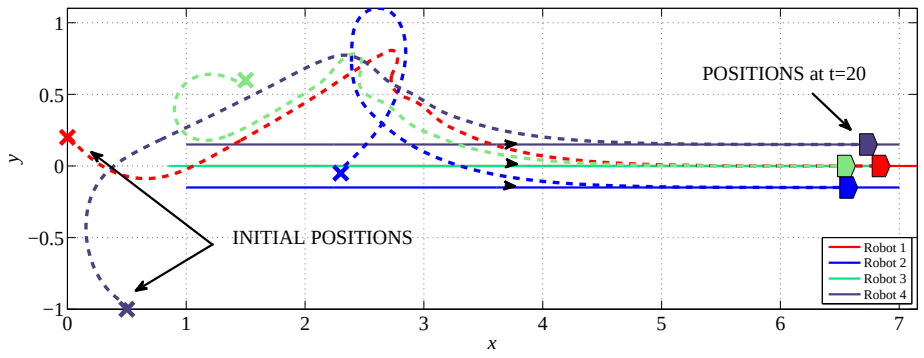

(a)

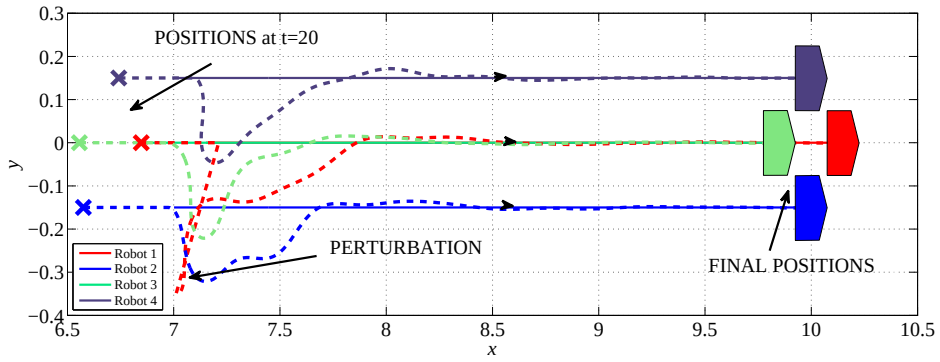

(b)

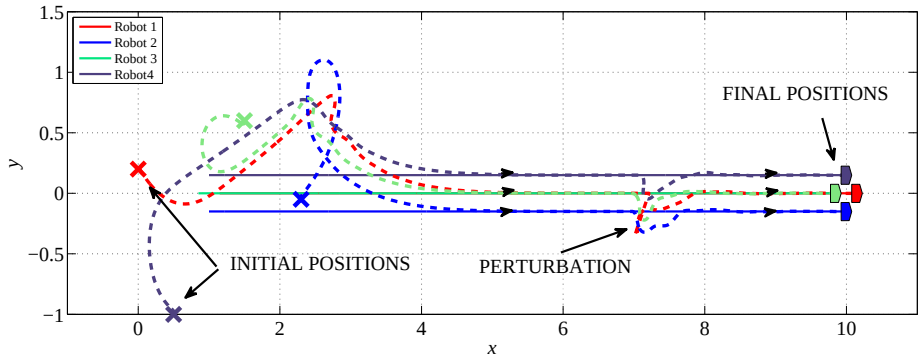

(c)

Figure 5.4: Desired robot paths (solid line) and actual robots paths (dashed line) in the plane in the case of a connected communication graph. (a) paths between $t = 0$ and $t = 20$ (b) paths between $t = 20$ and $t = 30$ (c) whole paths.

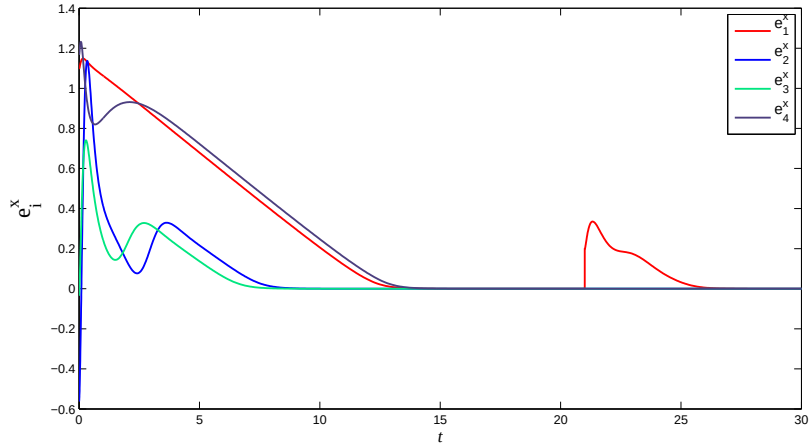

(a)

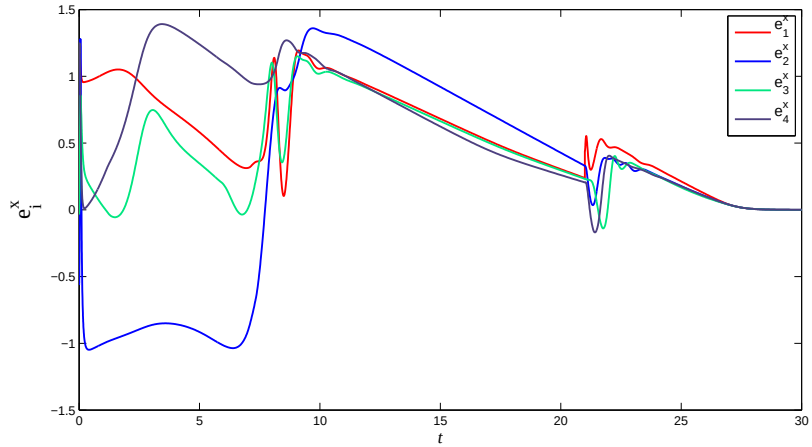

(b)

Figure 5.5: Tracking errors in the global coordinate frame (x – coordinate): (a) disconnected communication graph (b) connected communication graph.

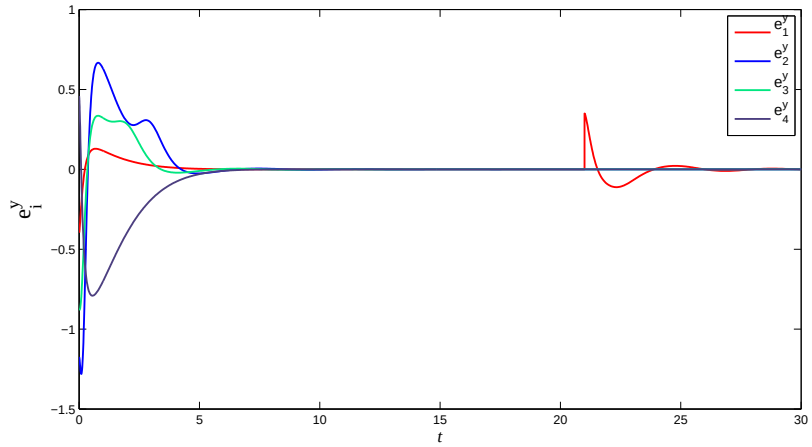

(a)

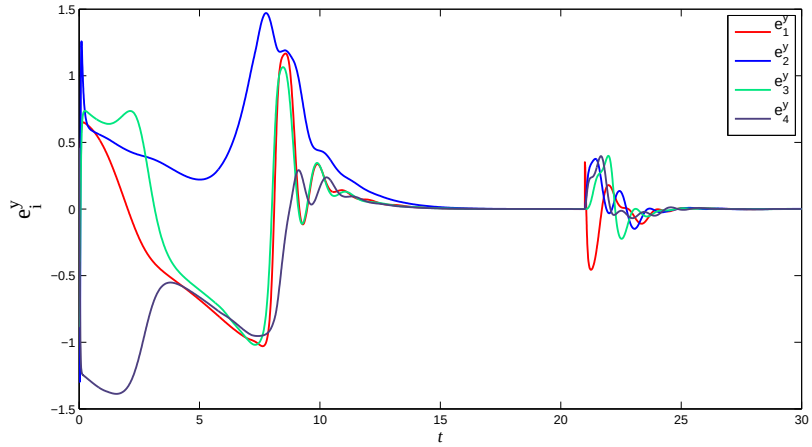

(b)

Figure 5.6: Tracking errors in the global coordinate frame (y – coordinate): (a) disconnected communication graph (b) connected communication graph.

In view of the developments from the previous chapter, where we established the connection between maintaining the formation shape and the consensus phenomena of the tracking error variables in the world frame, we can also study Figures 5.5–5.6. When robots are decoupled and hence unaware of each other, the tracking errors are inconsistent with respect to each other. In other words, there is no priority for robots to maintain the desired formation shape. Instead, robots purely track their individual trajectories, see Figures 5.5(a) and 5.6(a). Conversely, having in mind the relation between the tracking control gains c_i^e which are dominated by the coupling gains c_{ij}, $i, j \in \{1, 2, 3, 4\}$ when the communication graph is connected we expect to detect position error variables expressed in the world frame to coincide with each other. Indeed, both the vertical and horizontal coordinates of the position error variable are matching when the communication graph is connected, see Figures 5.5(b) and 5.6(b).

5.4 Discussion

In this chapter we have studied the formation control problem for a group of car–like mobile robots. We have proposed a formation control algorithm based on the backstepping approach. In addition, we have also examined the coordination problem in which the formation does not track the desired trajectory but it creates the desired formation shape and follows a trajectory that is ultimately translated relative to the desired one. For this strategy to work, all robots in the formation need to communicate with each other, possibly indirectly through other robots. In other words, the communication graph of the formation needs

to be connected. With respect to the results presented in the previous chapter, we can again confirm the beneficial influence of the connectivity of the communication graph of the formation. More specifically, allowing robots to communicate with each other assures that they implicitly act towards maintaining desired formation geometry as opposed to only tracking their individual desired trajectories. In particular, if the formation shape preservation is of importance, when some of the robots face perturbation, the others can only counteract it when aware of the perturbation through inter–robot communication.

Similarly to the formation control algorithms presented in the previous chapter, here we also have a rather wide freedom of choice of the control parameters. Therefore, the parameters can be selected in a way that would be most advantageous for a particular application, as discussed in previous chapters. More specifically, the relation between the values of the tracking gains and the coupling gains determines whether the formation shape maintenance or the individual trajectories tracking would be the prevailing behaviour.

Chapter 6

Comparison between the behaviour of robots in a formation under different control algorithms

6.1 Introduction

In this chapter we present a simulation study for formations of unicycle robots and for formations of car–like robots for various control algorithms introduced earlier in the thesis. The simulation results included in each of the three proceeding chapters serve well as the proof of concept to present various features of the

control algorithms. The purpose of the analysis in this chapter is to provide means of comparing the behaviour of robots in the formation when different control algorithms are applied. To this end, we present three distinctive kinds of simulations. The first set of simulations is similar to the experiments given in Section 3.4. This means that the formation consists of three robots where the desired formation shape is an equilateral triangle. We present simulation results for this case in Section 6.2. The second set of simulations, given in Section 6.3, is based on the experiment shown in Section 4.4. Therefore we consider a formation consisting of four robots. In the last set of simulations presented in this chapter we use a formation consisting of twelve robots. These simulation results are given in Section 6.4. In all simulations, t denotes simulation time.

The three sets of simulations presented in this chapter are all performed for different control algorithms for unicycle robots shown in Chapters 3 and 4, and for the control algorithm for a formation of car-like robots in Chapter 5. This is to allow objective comparison between the algorithms.

6.2 Simulations with three robots

In this section we give simulation results for simulations of a formation of three robots. The desired formation shape is an equilateral triangle as shown in Figure 3.3, where $l_1^d = \left(-0.15, -\frac{0.15}{\sqrt{3}}\right)^T$, $l_2^d = \left(0.15, -\frac{0.15}{\sqrt{3}}\right)^T$ and $l_3^d = \left(0, \frac{0.3}{\sqrt{3}}\right)^T$. The desired trajectory of the virtual centre is given by (3.56). To mimic the conditions in experiments in Section 3.4, we also use corresponding or indeed identical control

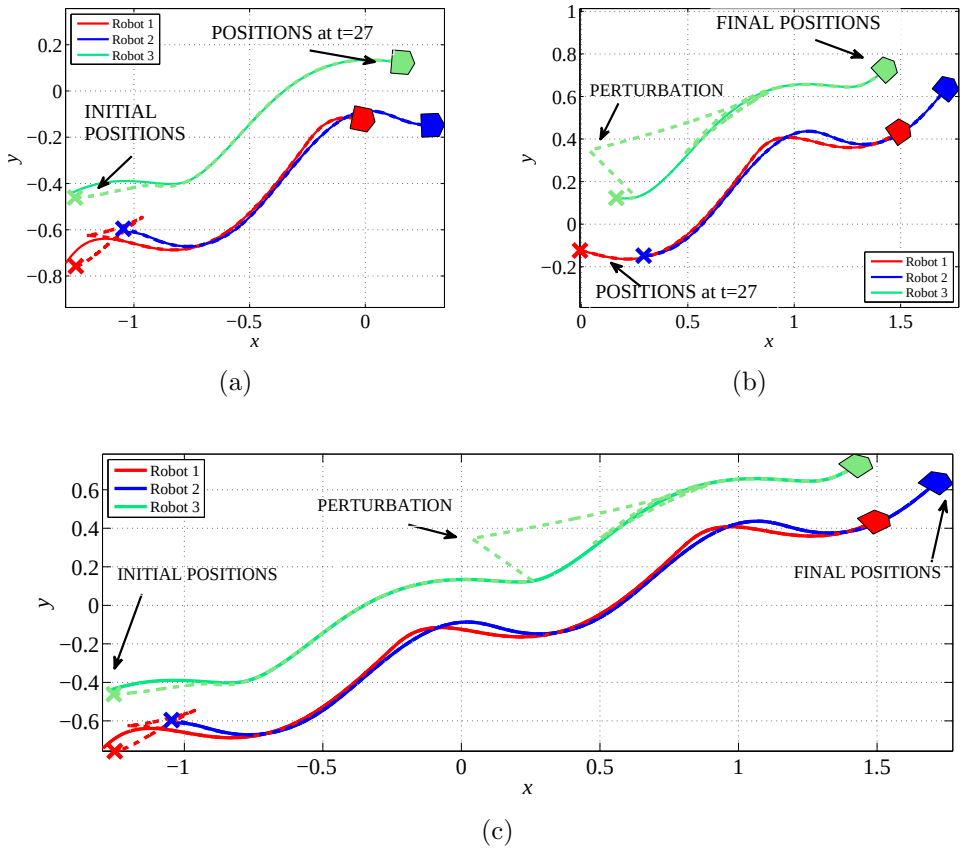

Figure 6.1: Desired robot paths (solid line) and actual robots paths (dashed line) in the plane in the case of a disconnected communication graph and controller (3.7). (a) paths between $t = 0$ and $t = 27$ (b) paths after $t = 27$ (c) whole paths.

parameters. Accordingly, we use $c_i^x = 1$, $c_i^y = 30$ and $c_i^\theta = 0.5$, $\widetilde{c}_{ij}^x = 2.5$, $\widetilde{c}_{ij}^y = 30$ and $\widetilde{c}_{ij}^\theta = 0.1$ for the simulations concerning the control algorithm in Chapter 3. For simulations with the use of the control algorithm defined in Chapter 4, we use $c_i^{xe} = 1$, $c_i^{ye} = 30$ and $c_i^\theta = 0.5$, $c_{ij}^{x\sigma} = 2.5$, $c_{ij}^{y\sigma} = 30$. For the controller defined in Chapter 5, we use $c_i^e = 30$, $c_i^\theta = 0.5$ and $\widetilde{c}_{ij} = 30$ and $\chi_i(s) = \frac{2}{\pi}\text{atan}(s)$. The saturation function for saturated controllers are $\alpha(s) = 0.05\tanh(s)$ and $\gamma(s) = 0.1\tanh(s)$ for the controller proposed in Chapter 3 and $\alpha(s) = 0.05\tanh(s)$ and

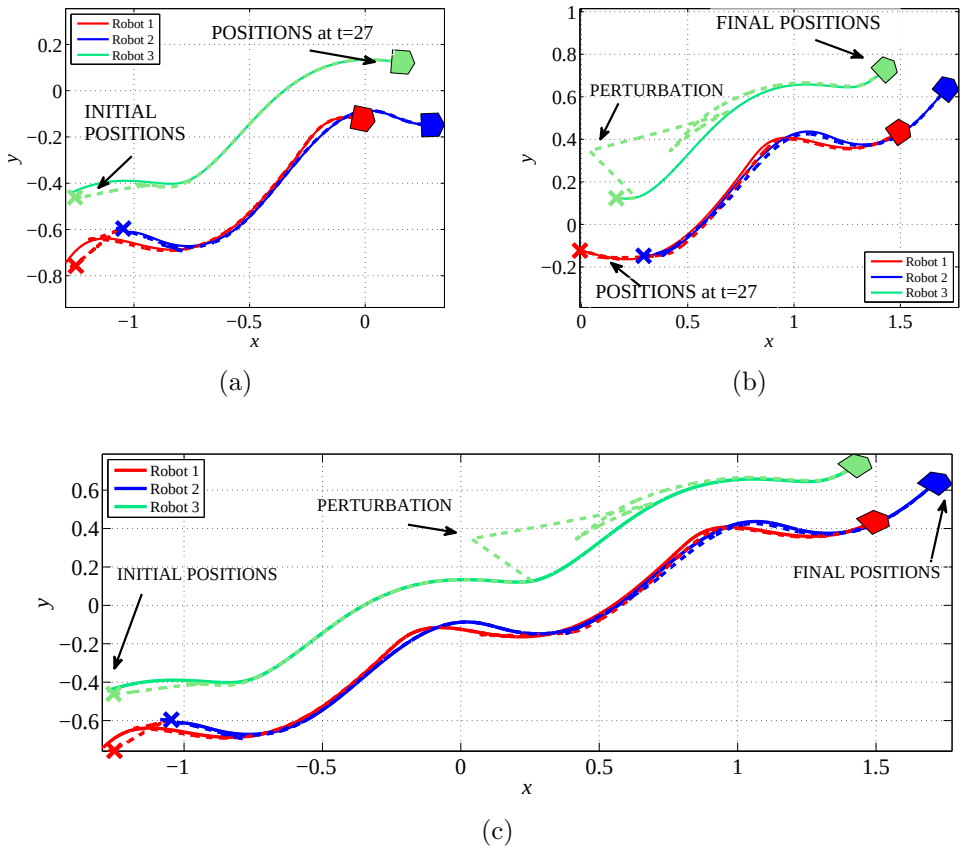

Figure 6.2: Desired robot paths (solid line) and actual robots paths (dashed line) in the plane in the case of a connected communication graph and controller (3.7). (a) paths between $t = 0$ and $t = 27$ (b) paths after $t = 27$ (c) whole paths.

$\beta(s) = 0.1\tanh(s)$ for the controller defined in Chapter 4. For the purpose of the pure coordination control scheme introduced in Chapter 4, we set all position tracking gains c_i^x and c_i^y to zero. As in the experiments in Section 3.4 upon which these simulations are based, we consider two communication structures: a disconnected one and a connected one. The disconnected one refers to all coupling gains set to zero, i.e. all robots are decoupled from each other. The connected communication structure is such that all robots can communicate with all other

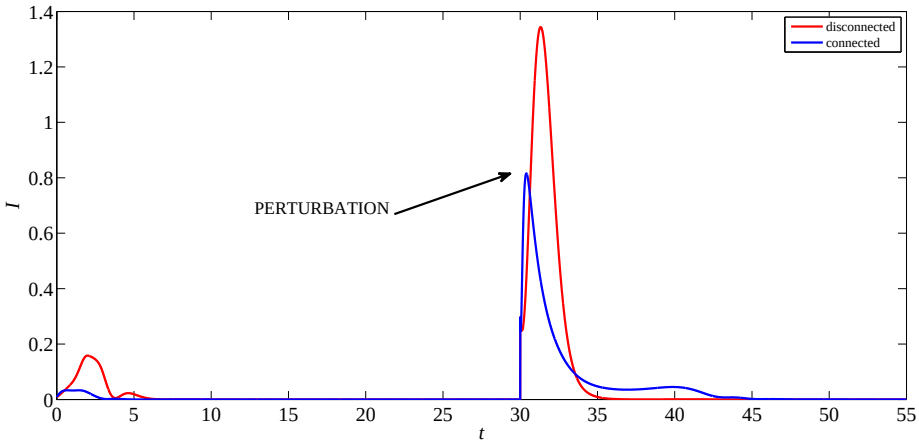

Figure 6.3: Comparison between formation geometry maintenance index I for a connected and a disconnected communication graph for triangular formation and controller (3.7).

robots. In other words, this is an all-to-all communication structure.

As a measure of formation maintenance we calculate the formation geometry maintenance index (3.54) to examine the influence of whether the communication graph is disconnected or connected on the formation behaviour. Moreover, as in previous simulation and experimental studies in this thesis, we use a perturbation to be able to observe more properties of the control algorithms. The perturbation is a displacement of Robot 3 at $t = 30$. The initial conditions are $x_1(0) = -1.25$, $y_1(0) = -0.76$, $\theta_1(0) = 0$, $x_2(0) = -1.05$, $y_2(0) = -0.60$, $\theta_2(0) = 0$, $x_3(0) = -1.25$, $y_3(0) = -0.46$, $\theta_3(0) = 0$ and in the case of the car-like robots, $\varphi_i(0) = 0$ for $i \in \mathcal{I}$.

In the first instance we present the results for the controllers given in Chapter 3, see Figures 6.1–6.6. The first three figures, Figures 6.1–6.3, were produced

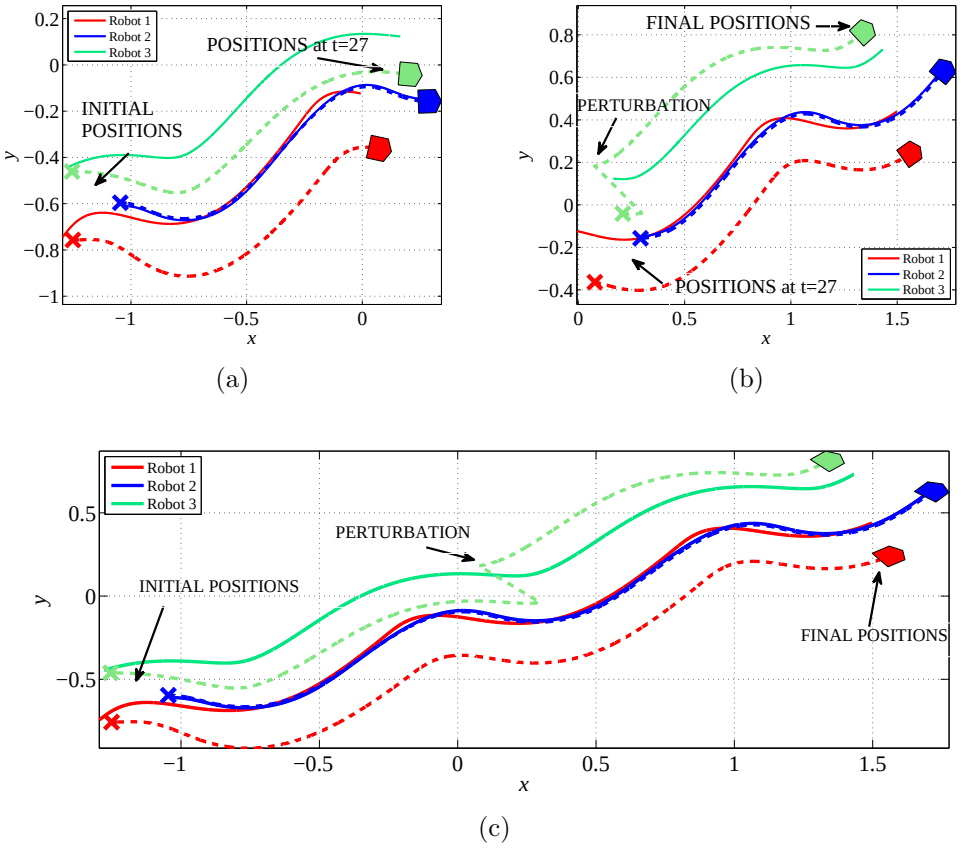

Figure 6.4: Desired robot paths (solid line) and actual robots paths (dashed line) in the plane in the case of a disconnected communication graph and controller (3.38). (a) paths between $t = 0$ and $t = 27$ (b) paths after $t = 27$ (c) whole paths.

using the controller in (3.7) while in simulations shown in Figures 6.4–6.6, the saturated version of that control algorithm (3.38) was employed. The obvious difference between the performance of the nominal controller (3.7) and the saturated controller (3.38) is that the saturated controller yields slower convergence of robots to their desired trajectories and to their desired positions within the formation. Indeed for the nominal case, we can observe the convergence to the desired trajectories while for the saturated controller this is not yet seen. However, both

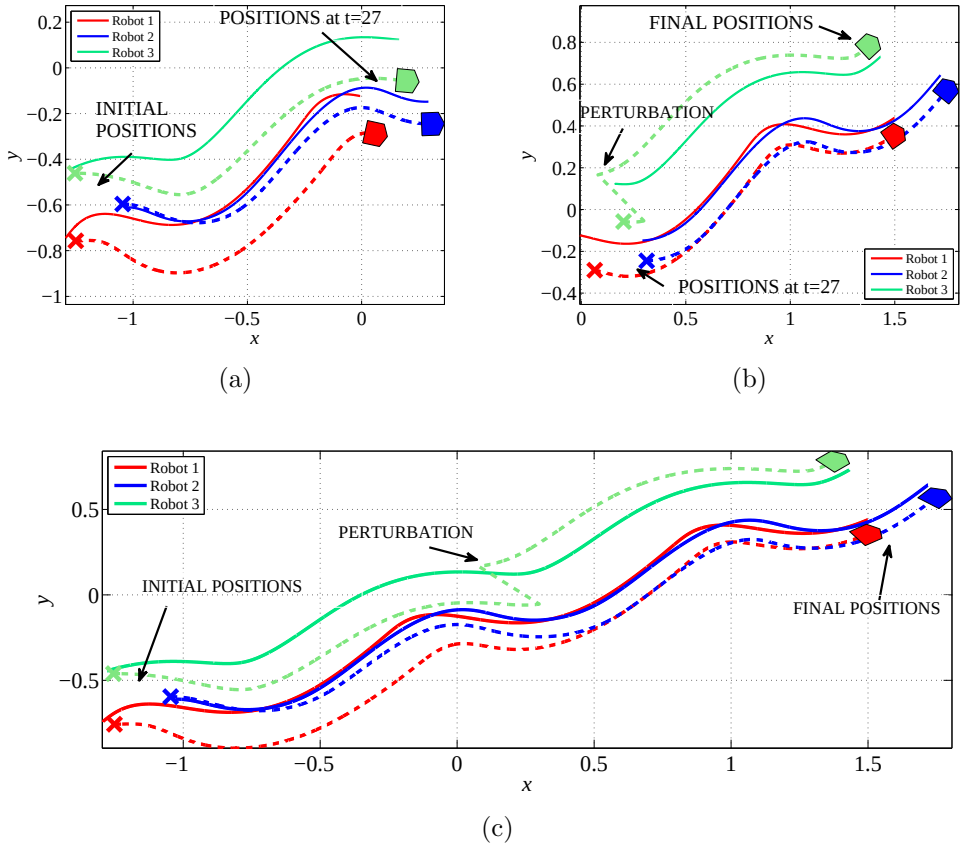

Figure 6.5: Desired robot paths (solid line) and actual robots paths (dashed line) in the plane in the case of a connected communication graph and controller (3.38). (a) paths between $t = 0$ and $t = 27$ (b) paths after $t = 27$ (c) whole paths.

for the nominal and saturated controllers the robots benefit from communication with other robots. When examining the formation geometry maintenance index, see Figures 6.3 and 6.6 it can be concluded that when robots communicate with other robots, the formation shape is better preserved than when no communication is allowed for both the nominal (3.7) and the saturated (3.38) controllers. However, for the nominal controller, the formation geometry maintenance index converges to zero much more rapidly, see Figures 6.3 and 6.6. On the other hand,

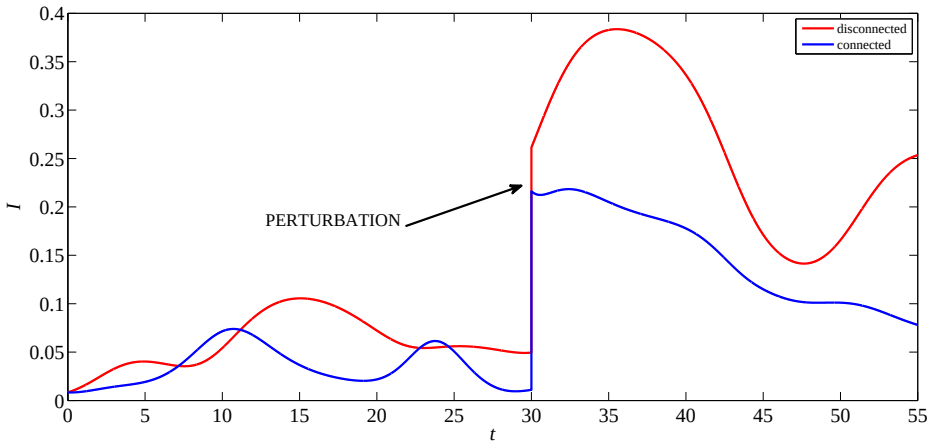

Figure 6.6: Comparison between formation geometry maintenance index I for a connected and a disconnected communication graph for triangular formation and controller (3.38).

for the saturated controller the index reaches smaller maximum value after the perturbation than when the nominal controller is used. This means that for the nominal controller the robots temporarily diverge further from the desired shape in order to counteract the perturbation and only after this brief transient, they converge to the desired formation shape. For the saturated controller, when the communication graph is connected, the robots slowly but consistently converge back to the desired formation shape with smaller maximum value of the index I after the perturbation but much longer transient.

As mentioned earlier, the experimental results in Section 3.4 were obtained in similar conditions to the simulation results shown in Figures 6.1–6.6 including the same control algorithm (3.7). This gives us an opportunity to evaluate the accuracy of the simulation results in comparison to the results obtained in experiments and hence judge upon practical applicability of the control algorithm.

In the case of the control algorithm (3.7), an exponential convergence rate of the error variables is shown theoretically in Chapter 3. The theoretical results are illustrated in Figures 6.1 and 6.2, in which we can observe the quick occurrence of robot paths coinciding with their desired paths, obtained in the simulations, which is equivalent with vanishing of the error variables. In experiments, see Figures 3.14 and 3.15, the convergence speed was not as rapid as in simulations, supposedly due to the fact that although it was the nominal controller (3.7) that was implemented, in real robots the actuators strength is limited. In comparison to the saturated controller (3.38), see Figures 6.4–6.6 and Figures 3.14–3.16, the results obtained in experiments exhibit faster convergence of robots trajectories to their desired trajectories. As far as the formation geometry maintenance index is concerned, the performance of the controller in experiments appears to lie again somewhere in between the one obtained in simulations for the nominal controller (3.7) and the saturated controller (3.38). Based on this discussion, in our view the performance of the robots in the formation obtained in experiments closely resembles the simulated one as seen in simulations, which supports the practical applicability of the control algorithm (3.7).

After simulations for the control algorithms introduced in Chapter 3, we move on to studying results obtained for the controllers given in Chapter 4. The simulation results are presented in Figures 6.7-6.18. We first examine the behaviour of a formation when controller (4.13, 4.14) is applied. We see that robots preserve the desired formation shape to a greater extent when communication is enabled, see Figure 6.9. Indeed when looking at robot paths, see Figures 6.7 and 6.8, it can be seen that for a connected communication graph, after the perturbation

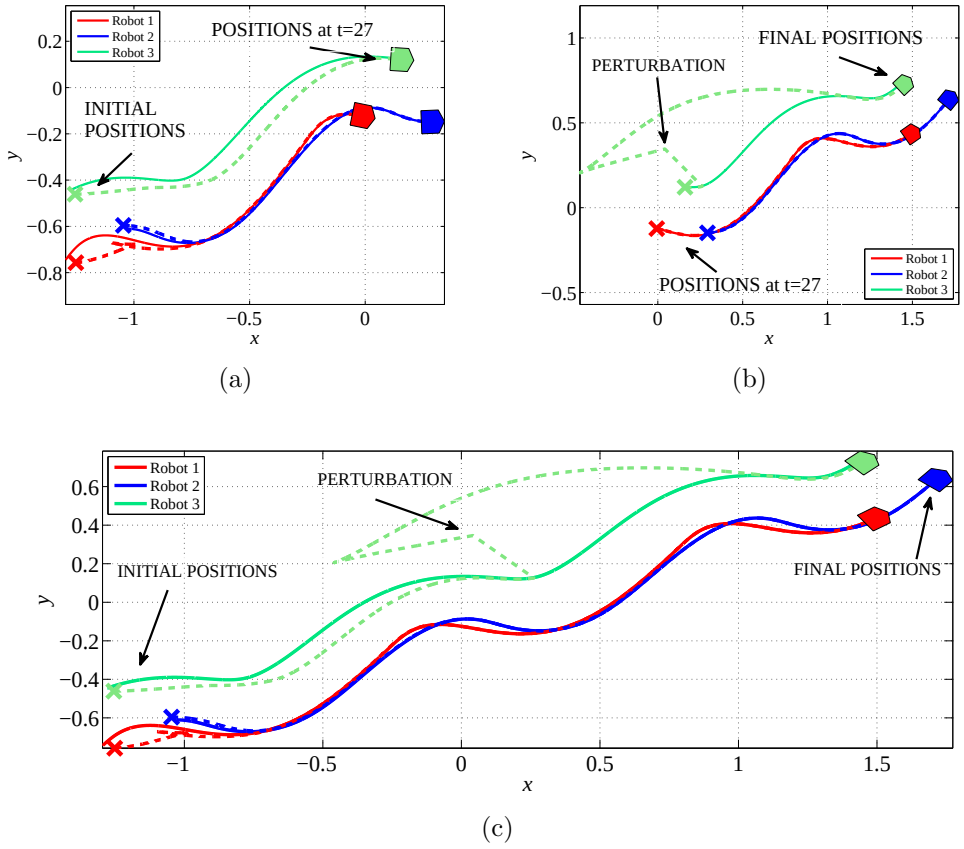

Figure 6.7: Desired robot paths (solid line) and actual robots paths (dashed line) in the plane in the case of a disconnected communication graph and controller (4.13, 4.14). (a) paths between $t = 0$ and $t = 27$ (b) paths after $t = 27$ (c) whole paths.

the unperturbed robots diverge from their desired paths in order to keep the formation shape. For the disconnected communication case, no such thing can be seen. A similar conclusion can be drawn for the saturated controller (4.42, 4.43), see Figures 6.10– 6.12. In fact, in the disconnected communication case robots have not managed to completely counteract the perturbation in the time of the simulation due to the limited magnitude of the control gains generated by the saturated controller. In the connected communication case, despite the limited

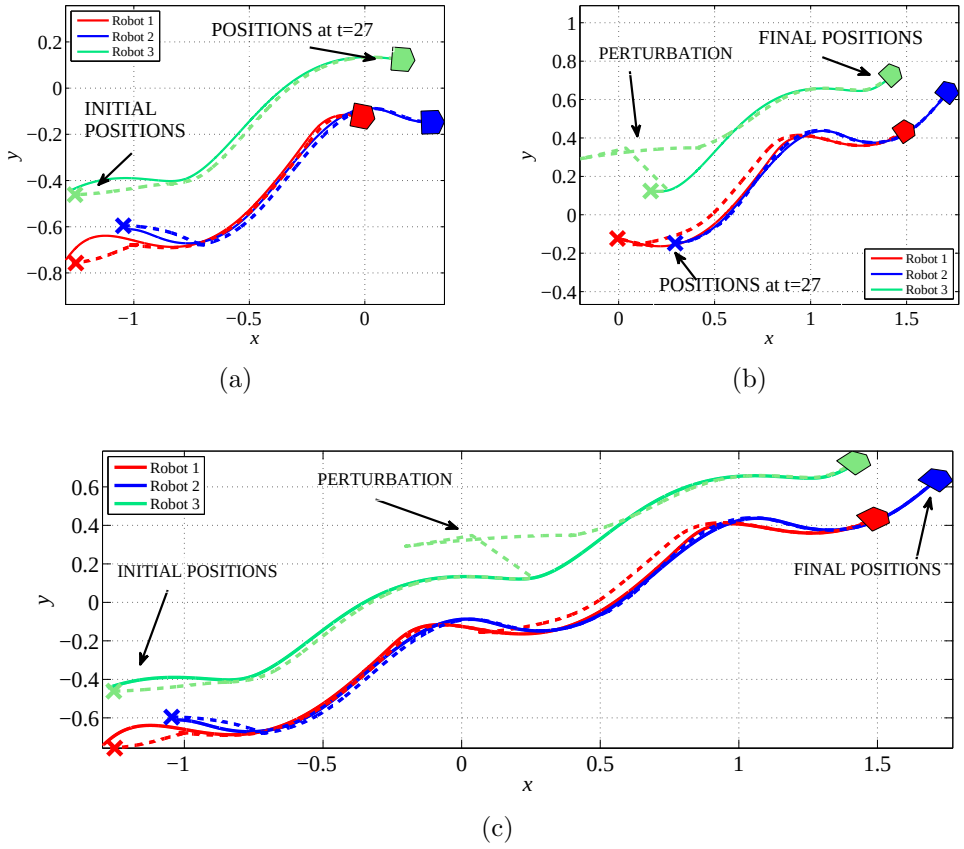

Figure 6.8: Desired robot paths (solid line) and actual robots paths (dashed line) in the plane in the case of a connected communication graph and controller (4.13, 4.14). (a) paths between $t = 0$ and $t = 27$ (b) paths after $t = 27$ (c) whole paths.

control inputs, the formation shape is restored after the perturbation within the simulation time.

As far as the pure coordination control scheme is concerned, we can again confirm the necessity for the communication graph to be connected for the pure coordination to be possible both for the nominal controller and the saturated controller, see Figures 6.13-6.15 and 6.16-6.18. It is seen in these figures, that when the robots do not communicate with other robots in the formation, the formation shape

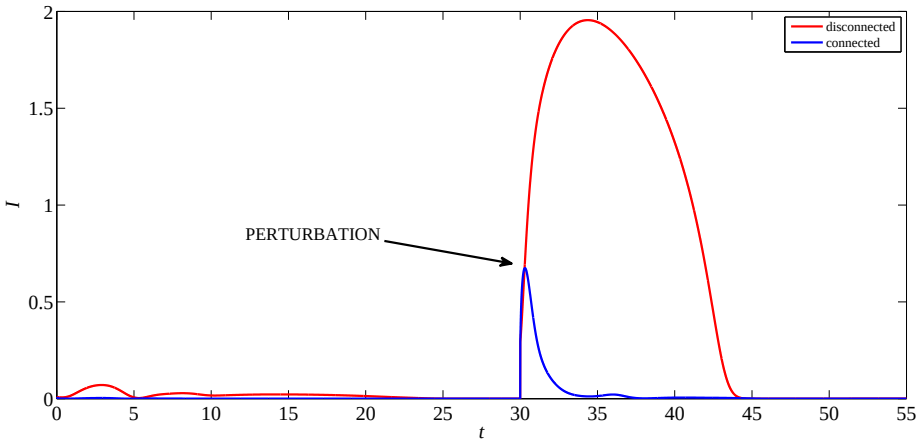

Figure 6.9: Comparison between formation geometry maintenance index I for a connected and a disconnected communication graph for triangular formation and controller (4.13, 4.14).

is not restored. Moreover, after the perturbation in the case of a disconnected communication graph, the formation shape is disturbed to such an extent that the formation geometry maintenance index I diverges. This illustrates the fact that the formation shape is different than the desired one and the robots carry on their motion in directions which further violate the formation shape. This is particularly seen for the saturated controller, see Figure 6.18. Note however that since it is the pure coordination controller, the robots do not aim to track their desired trajectories and in fact the desired trajectories are not tracked both for the nominal and saturated controller even when the communication graph is connected.

In terms of a different performance yielded by the nominal and saturated controllers, this can in truth be noticed. For example, we can see the difference by comparing the graphs presenting robots paths for the nominal and saturated

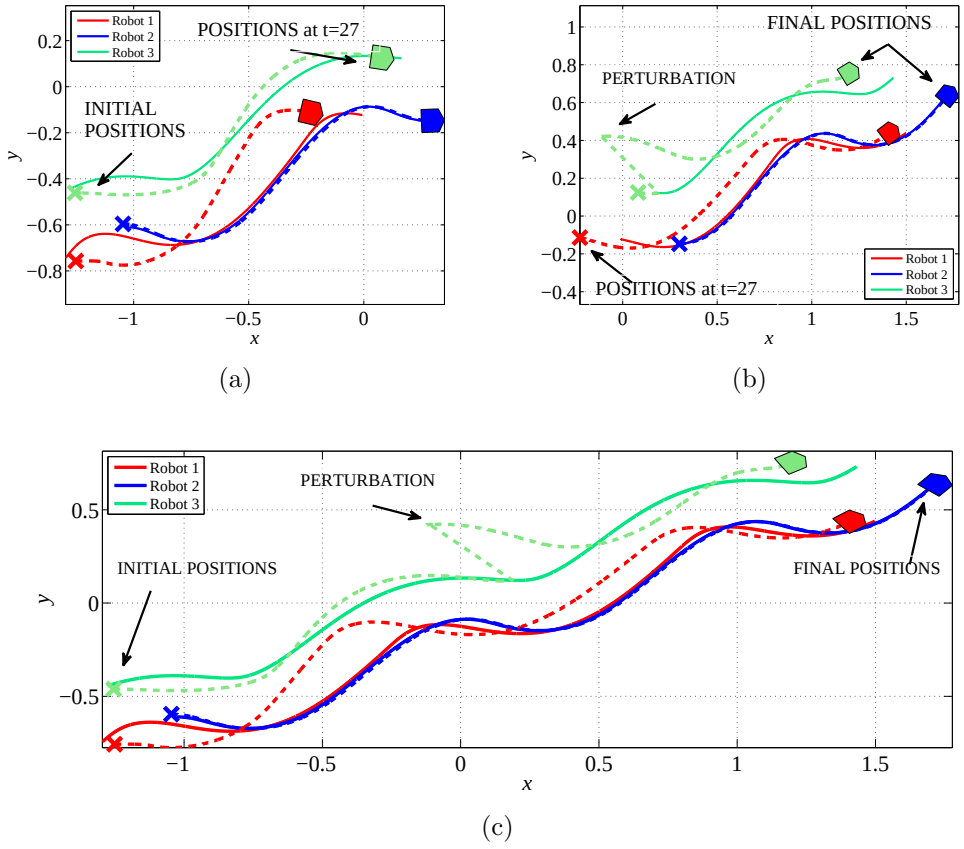

Figure 6.10: Desired robot paths (solid line) and actual robots paths (dashed line) in the plane in the case of a disconnected communication graph and controller (4.42, 4.43). (a) paths between $t = 0$ and $t = 27$ (b) paths after $t = 27$ (c) whole paths.

versions of the controller in (4.13, 4.14), see Figures 6.7 and 6.8 and Figures 6.10 and 6.11. It can be viewed that in the saturated case the robot paths do not coincide exactly with their desired paths, especially in the case of a disconnected communication graph. Interestingly, in terms of formation shape keeping, this task is solved well for both the nominal and saturated controllers as long as the communication between the robots is allowed, see Figures 6.9 and 6.12 and Figures 6.15 and 6.18.

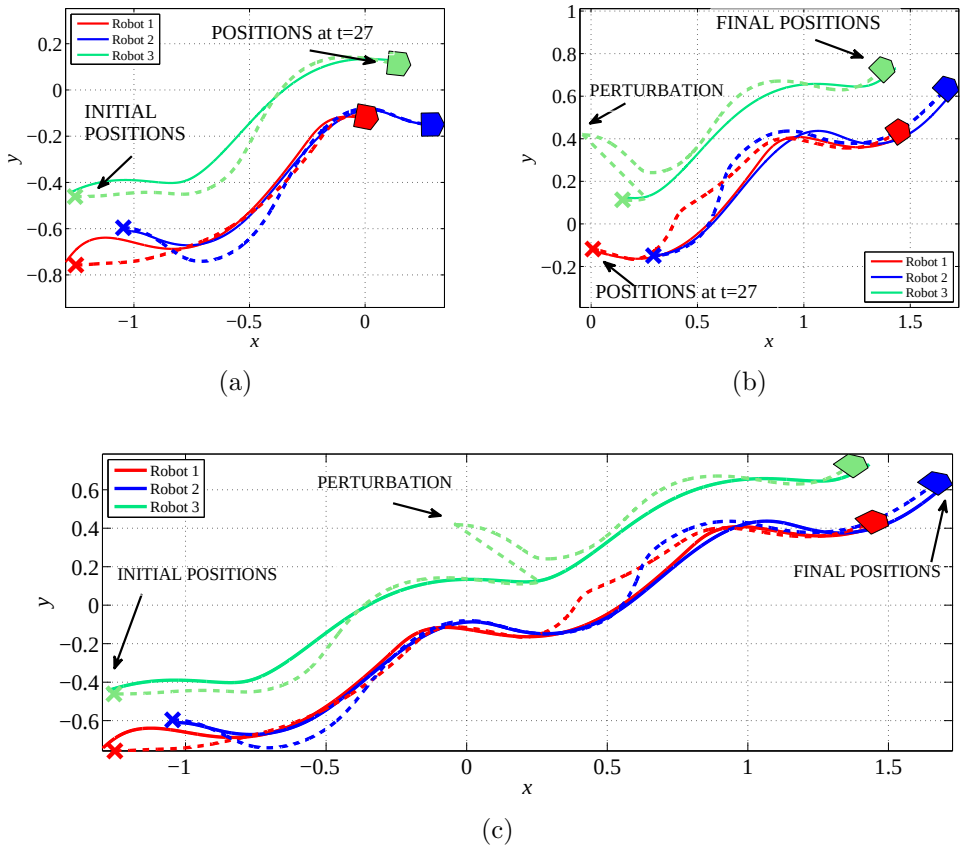

Figure 6.11: Desired robot paths (solid line) and actual robots paths (dashed line) in the plane in the case of a connected communication graph and controller (4.42, 4.43). (a) paths between $t = 0$ and $t = 27$ (b) paths after $t = 27$ (c) whole paths.

To be able to analyse the various control algorithms presented in the thesis to an even higher degree, we also performed simulations for a three robot formation and all settings as listed above for a formation of car-like mobile robots. The simulation results for this case are shown in Figures 6.19-6.21. Since the control parameters selected for the simulations satisfy all conditions mentioned in Theorem 5.2.1, it is shown theoretically in Chapter 5 that for these control parameters, the controller (5.19, 5.36) solves the formation control problem. Indeed,

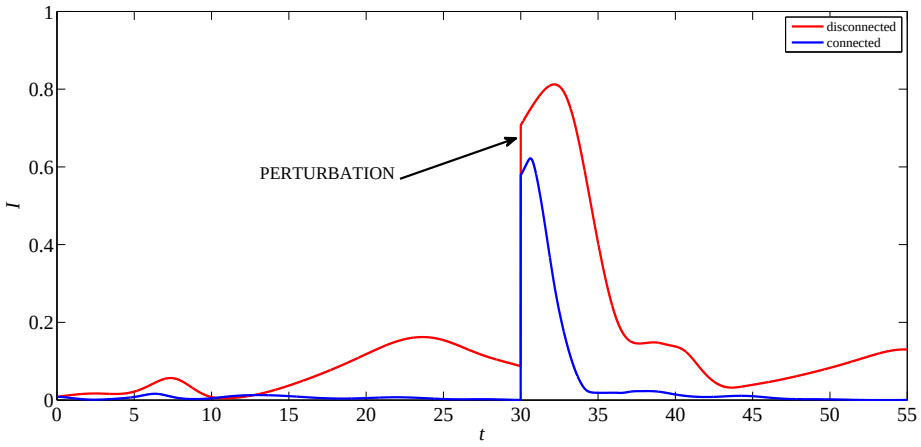

Figure 6.12: Comparison between formation geometry maintenance index I for a connected and a disconnected communication graph for triangular formation and controller (4.42, 4.43).

the simulation results illustrate the theoretical claim, albeit the actual paths of the robots obtained in simulations are still a bit off the desired trajectories, see Figures 6.19-6.20. The difference can be particularly seen for the case of the disconnected communication graph. A possible reason for the slower convergence of the error variables to zero is the fact that in the control law (5.19, 5.36), the forward speed of robots v_i, $i \in \mathcal{I}$ is limited. Therefore, the robots may require more time to correct their positions and achieve ideal tracking.

As far as the formation geometry maintenance index is concerned, it converges to zero swiftly. We can again observe the advantage of robots being able to communicate with each other, see Figure 6.21. The discrepancy between the convergence of the index for the connected and disconnected cases is especially visible after the perturbation, when the index for the disconnected communication case takes longer to vanish as opposed to the index for the connected communication case.

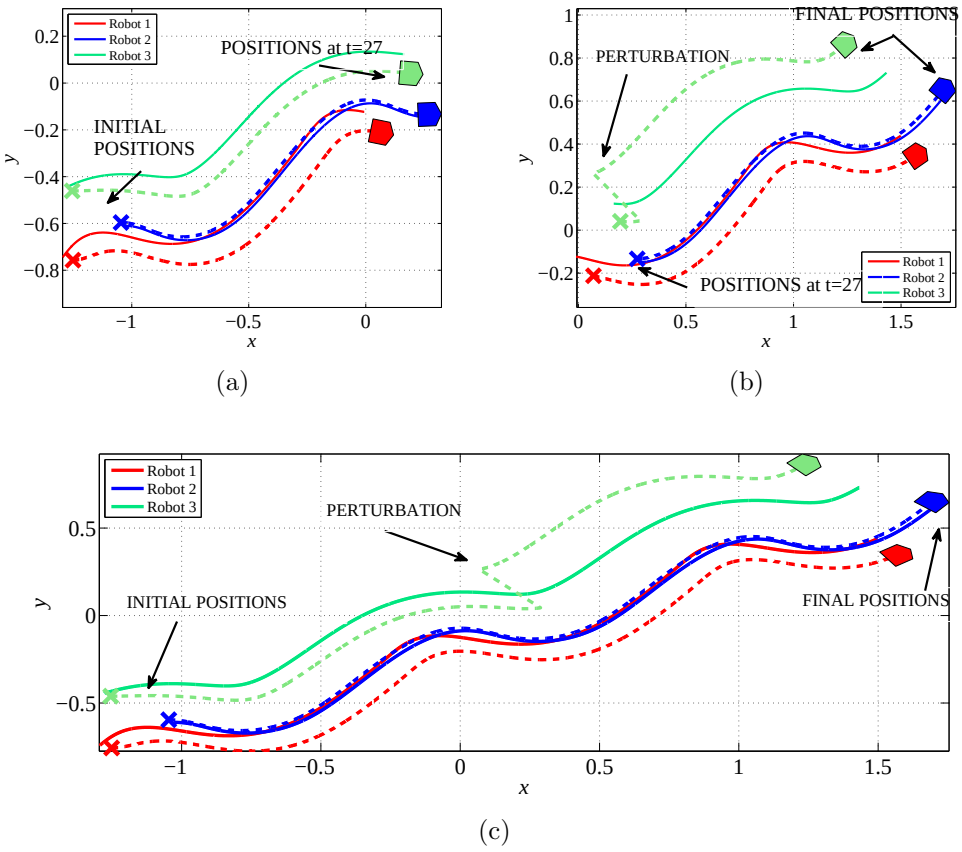

Figure 6.13: Desired robot paths (solid line) and actual robots paths (dashed line) in the plane in the case of a disconnected communication graph and controller (4.33, 4.34). (a) paths between $t = 0$ and $t = 27$ (b) paths after $t = 27$ (c) whole paths.

Overall, based on the simulation results given in this section, we conclude that out of the two saturated controllers (3.38) and (4.42, 4.43), the controller in (4.42, 4.43) generates faster convergence to the desired trajectories and better formation shape preservation, see Figures 6.4-6.6 and 6.10-6.12. On the contrary, the nominal controllers (3.7) and (4.13, 4.14), both generates comparable performance. This is with the exception for the disconnected case in which case the controller (3.7) outperforms (4.13, 4.14).

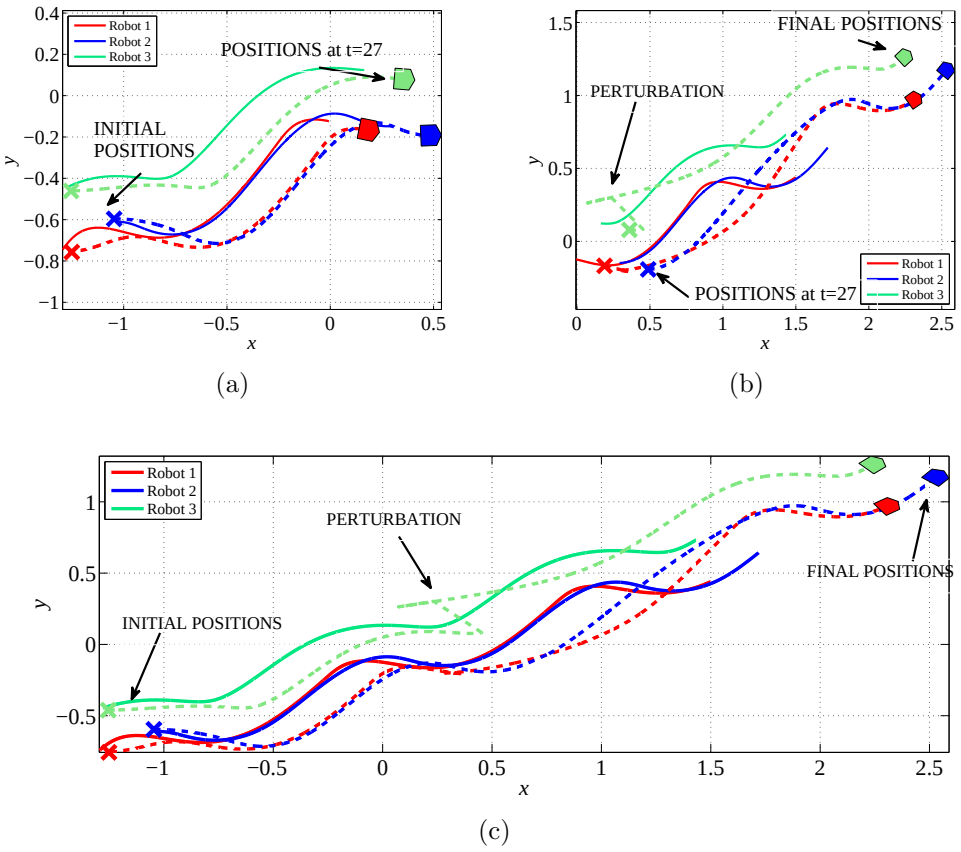

Figure 6.14: Desired robot paths (solid line) and actual robots paths (dashed line) in the plane in the case of a connected communication graph and controller (4.33, 4.34). (a) paths between $t = 0$ and $t = 27$ (b) paths after $t = 27$ (c) whole paths.

The behaviour obtained in simulations for car-like mobile robots shows slower convergence to desired trajectories than in the case of simulations for unicycle mobile robots. However, the desired formation shape is restored very well for the connected communication graph. In Figure 6.22 we depict formation geometry maintenance index for the connected communication graph and controllers (3.7), (3.38), (4.13, 4.14), (4.42, 4.43), (5.19, 5.36). From that figure, we conclude that the controller for car-like robot formations (5.19, 5.36) gives comparable

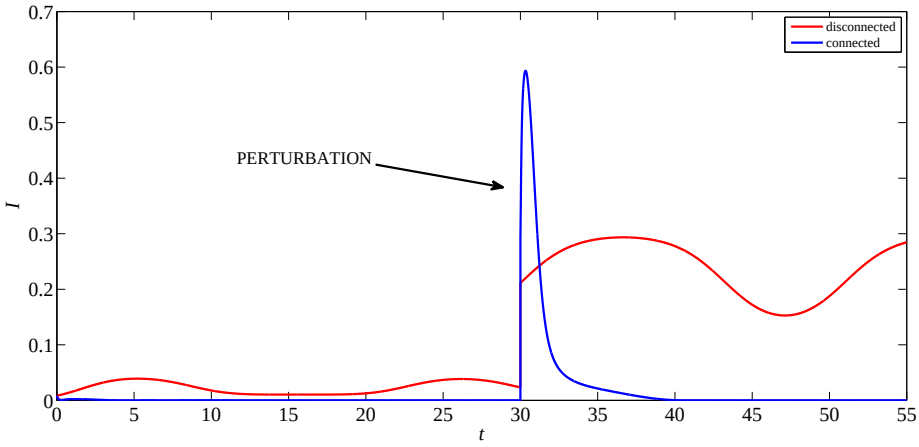

Figure 6.15: Comparison between formation geometry maintenance index I for a connected and a disconnected communication graph for triangular formation and controller (4.33, 4.34).

convergence speed to the desired formation shape as controllers (3.7) and (4.13, 4.14). The advantage of controller (5.19, 5.36) is that analogously to controller (3.38) it does not produces large overshoot after the perturbation. Conversely, for both (5.19, 5.36) and (3.38) the robots systematically converge back to the desired formation shape without diverging more from the desired formation shape. This is not the case for the remaining three controllers for which the robots first violate further the formation shape before they converge back to the required shape. It needs to be remarked though that this transient behaviour is only brief since for all controllers but (3.38) the convergence speed of the index I is fast.

Note that the control parameters used in this section were tuned for a controller for unicycle robot (3.7) and as such may not be quite suitable for other kinds of robots or even for different kinds of control algorithm for unicycle robots. From this analysis, it is apparent that different control algorithms require different

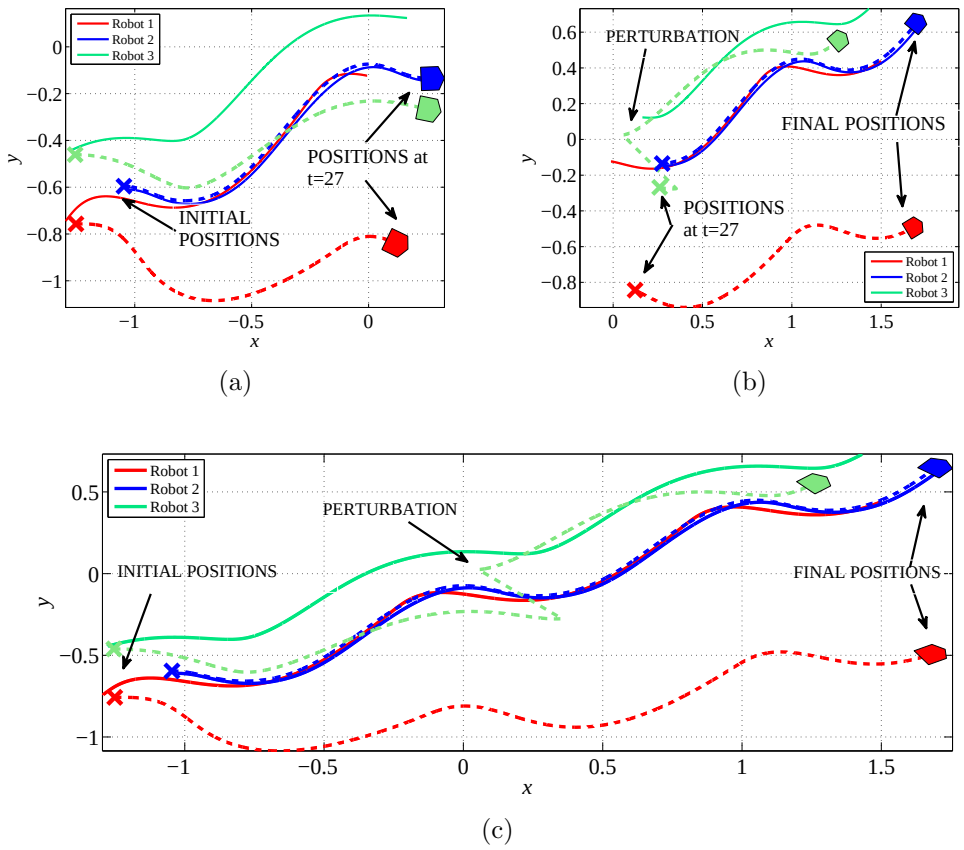

Figure 6.16: Desired robot paths (solid line) and actual robots paths (dashed line) in the plane in the case of a disconnected communication graph and controller (4.42, 4.43) with zero position tracking gains. (a) paths between $t = 0$ and $t = 27$ (b) paths after $t = 27$ (c) whole paths.

parameter tuning. The above simulations were performed for different control algorithms but with the use of the same or possibly corresponding values of control parameters. It is seen that the performance of the control algorithms varies and it is plausible that if parameter tuning process was done individually for each control algorithm, better performance might be obtained. Indeed, in earlier chapters of this thesis, parameters were tuned for each of the algorithms individually and in each case we were able to present satisfactory behaviour. In contrast, in this

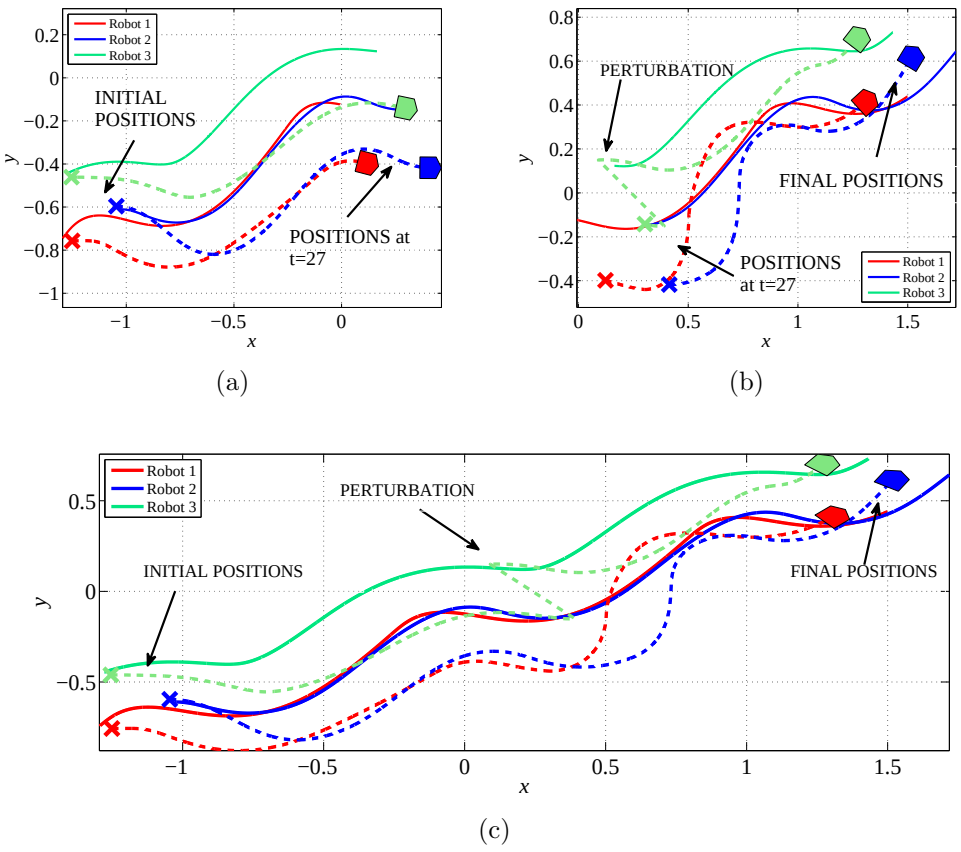

Figure 6.17: Desired robot paths (solid line) and actual robots paths (dashed line) in the plane in the case of a connected communication graph and controller (4.42, 4.43) with zero position tracking gains. (a) paths between $t = 0$ and $t = 27$ (b) paths after $t = 27$ (c) whole paths.

section no more parameter tuning was done and control parameters were copied from the ones used in experiments. Therefore, for some algorithms, one might expect better results if parameter tuning for each particular case was not omitted.

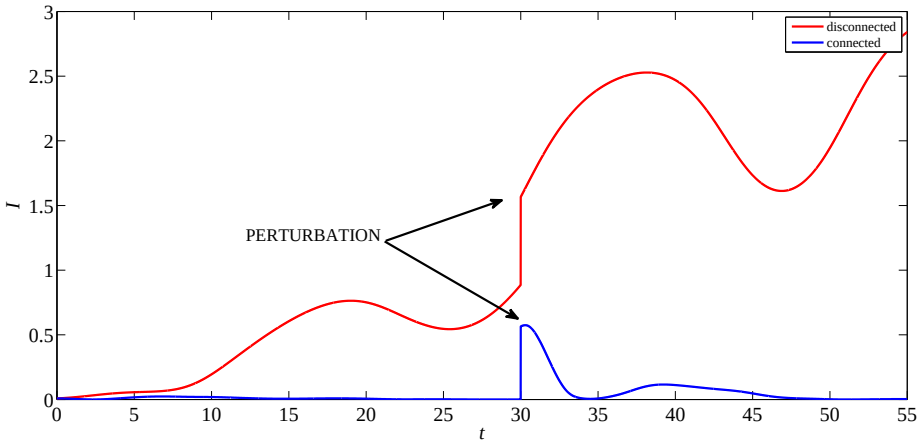

Figure 6.18: Comparison between formation geometry maintenance index I for a connected and a disconnected communication graph for triangular formation and controller (4.42, 4.43) with zero position tracking gains.

6.3 Simulations with four robots

In this section, we present simulation results based on the experiments given in Section 4.4. Consequently, the formation consists of four robots which are required to form the desired formation shape depicted in Figure 4.17 and the desired trajectory of the virtual centre is (4.68). Having equal simulation and experimental settings we compare in this section the experimental results with the simulation results for controllers (3.7), (4.13, 4.14) and (5.19, 5.36). We also compare simulation results for different controllers with each other.

The initial conditions used in the simulations are reproduced from the actual initial positions of robots in experiments given in Section 4.4 and are as follows: $p_1(0) = \text{col}(0.74, 0.00)$, $p_2(0) = \text{col}(0.56, 0.00)$, $p_3(0) = \text{col}(0.37, 0.00)$ and $p_4(0) = \text{col}(0.18, 0.01)$. In addition, $\theta_i(0) = 0$ and for car-like robots $\varphi_i(0) = \frac{\pi}{2}$ for

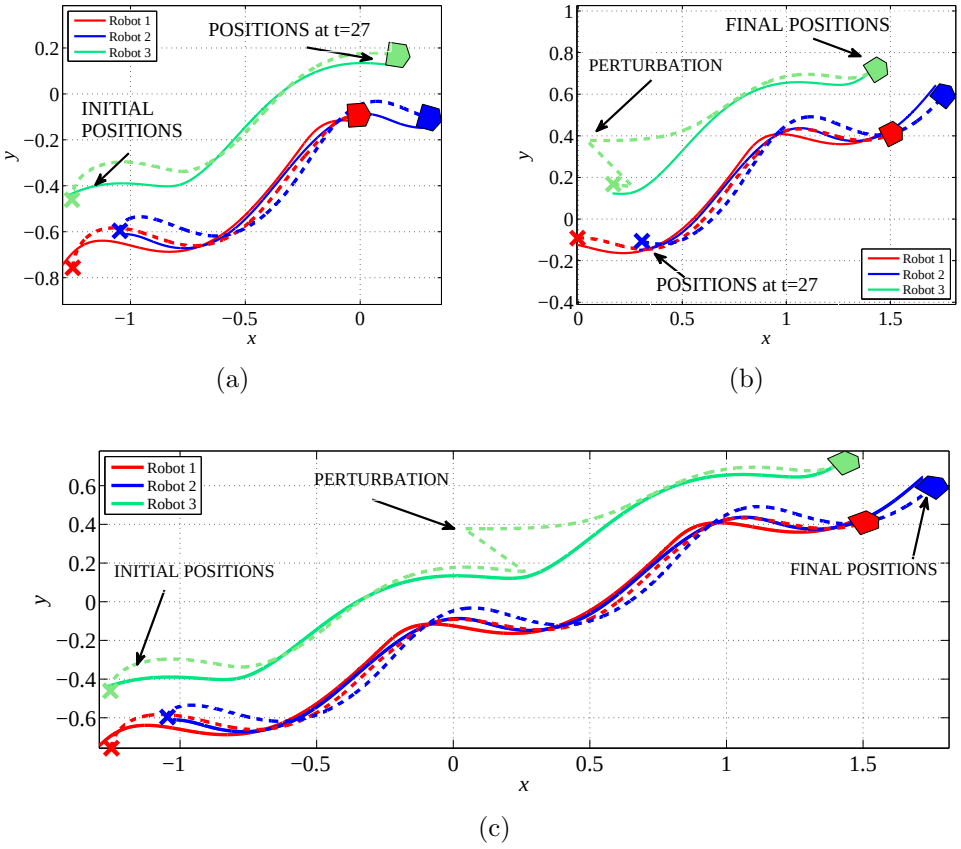

Figure 6.19: Desired robot paths (solid line) and actual robots paths (dashed line) in the plane in the case of a disconnected communication graph and controller (5.19, 5.36). (a) paths between $t = 0$ and $t = 27$ (b) paths after $t = 27$ (c) whole paths.

all robots $i \in \mathcal{I}$. Also following the run of the experiments in Section 4.4, a perturbation occurs to the formation. More specifically, Robot 3 is displaced from its current place at $t = 30$.

Together with the initial conditions, also the control parameters to be used in the simulations are copied as much as possible from the parameters used in the experiments. For controller (3.7), the parameters are $c_i^x = 5$, $c_i^y = 100$, $c_i^\theta = 1.5$,

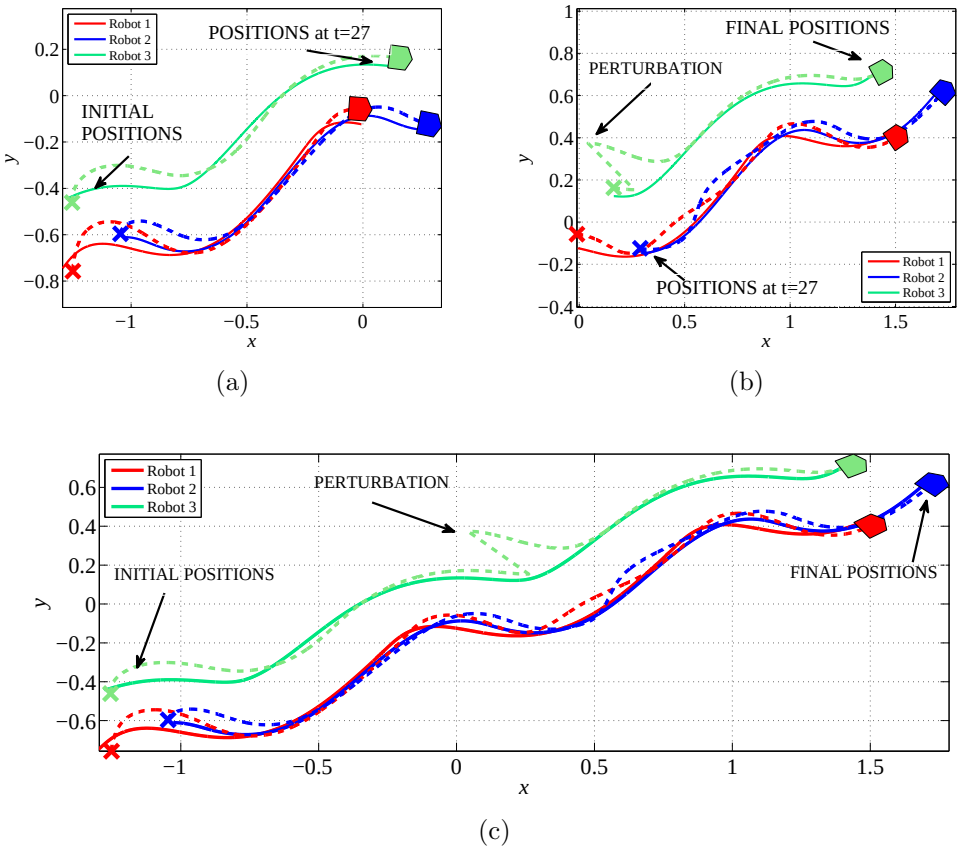

Figure 6.20: Desired robot paths (solid line) and actual robots paths (dashed line) in the plane in the case of a connected communication graph and controller (5.19, 5.36). (a) paths between $t = 0$ and $t = 27$ (b) paths after $t = 27$ (c) whole paths.

$\widetilde{c}^x_{ij} = 30$ and $\widetilde{c}^x_{ij} = 80$ and $\widetilde{c}^\theta_{ij} = 0.1$. For controller (4.13, 4.14), the parameters are: $c^{xe}_i = 5$, $c^{ye}_i = 100$, $c^\theta_i = 1.5$, $c^{x\sigma}_{ij} = 30$ and $c^{x\sigma}_{ij} = 80$. Furthermore, for controller (5.19, 5.36) we choose $c^e_i = 100$, $c^z_i = 50$, $c^\theta_i = 1.5$, $c_{ij} = 80$ and $\chi_i(s) = \chi^*_i \frac{2}{\pi}\text{atan}(s)$, where $\chi^*_i = 0.2i - 0.11$. As in the experiments, there are two communication structures examined: a disconnected one in which there is no communication links between any robots, and a connected one which corresponds to an all-to-all communication.

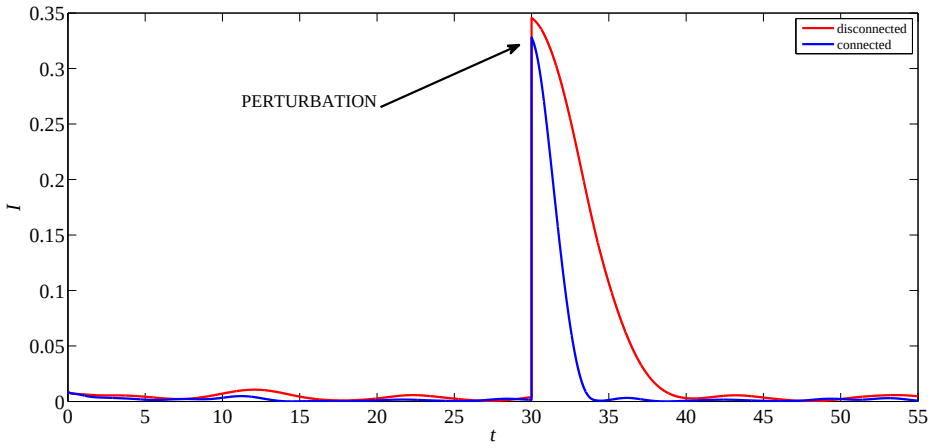

Figure 6.21: Comparison between formation geometry maintenance index I for a connected and a disconnected communication graph for triangular formation and controller (5.19, 5.36).

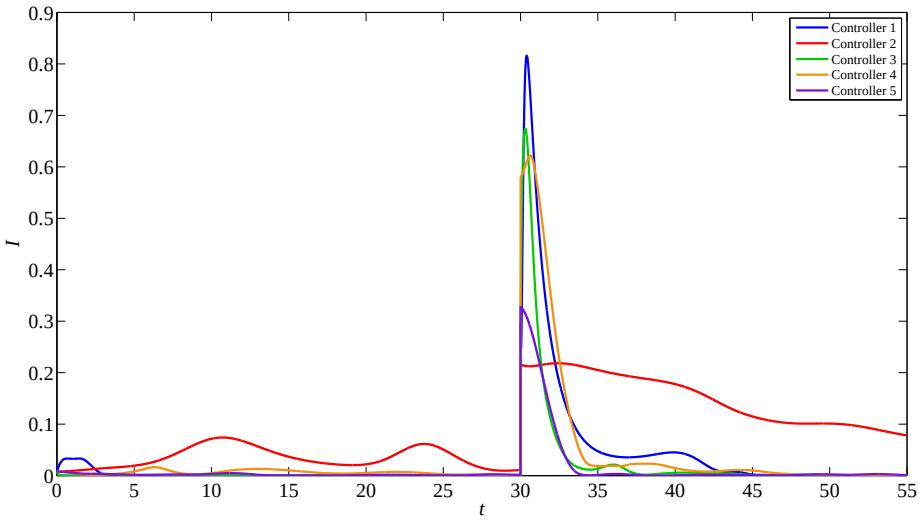

Figure 6.22: Comparison between formation geometry maintenance index I for a connected communication graph for triangular formation, and controller (3.7) (Controller 1), controller (3.38) (Controller 2), controller (4.13, 4.14) (Controller 3), controller (4.42, 4.43) (Controller 4) and controller (5.19, 5.36) (Controller 5).

In this section, conversely to the results in Section 6.2 where the formation geometry maintenance index (3.54) was used to verify formation shape keeping by the robots in the formation, we examine the coordination error $\sigma_i = e_i - e_j$ for all pairs of robots in the formation, $i, j \in \mathcal{I}$. Recall from Chapter 4 that when e_i is in consensus with e_j for all $i, j \in \mathcal{I}$, then the formation shape is attained. Consequently, if in the simulation results we observe consensus of the error variables, or in other words $\sigma_{ij} = 0$ for all pairs of robots in the formation, we conclude that the robots have reached the desired formation shape. Note that this does not say anything on whether robots track their desired trajectories or not.

Simulation results for controller (3.7) are shown in Figures 6.23-6.25. It can be seen that for the disconnected communication case, the tracking errors e_i go to zero rapidly, see Figures 6.24(a) and 6.25(a) and robots paths coincide with their desired paths promptly, see Figure 6.23(a). This originates from the exponential convergence rate of the controller. However, there is no priority for robots to keep the desired formation shape so when the perturbation happens, the unperturbed robots are unaware of it and cannot react. For the connected communication case, it can be viewed that in the instance of perturbation, all unperturbed robots try to adjust their positions to counteract the perturbation. When studying the paths of robots in the plane, see Figure 6.23(b), it is noticeable that robots diverge from their desired paths in order to keep the formation shape. However, in terms of consensus of the tracking error variables e_i, it is actually not immediately seen, see Figures 6.24(b) and 6.25(b). That is because in the control law (3.7) the coupling terms are of the form $x_i^e - x_j^e$ and $y_i^e - y_j^e$, where the error variables are given in local coordinate frames (3.5). It was discussed already in earlier

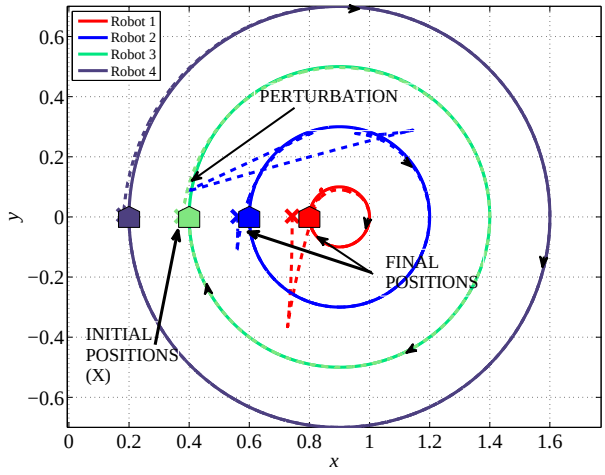

(a)

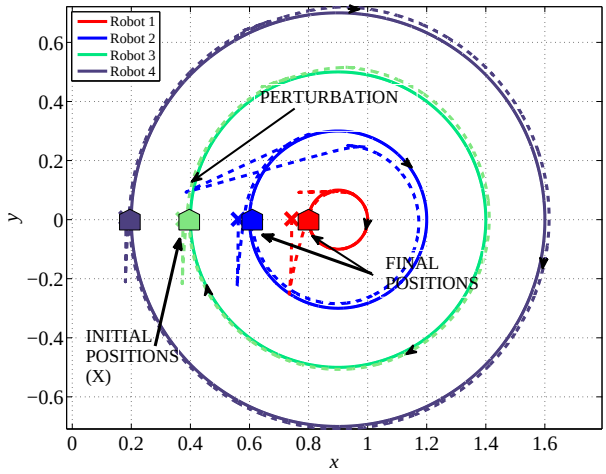

(b)

Figure 6.23: Desired robot paths (solid line) and actual robots paths (dashed line) in the plane obtained using the control algorithm (3.7) in the case of (a) a disconnected communication graph and (b) a connected communication graph.

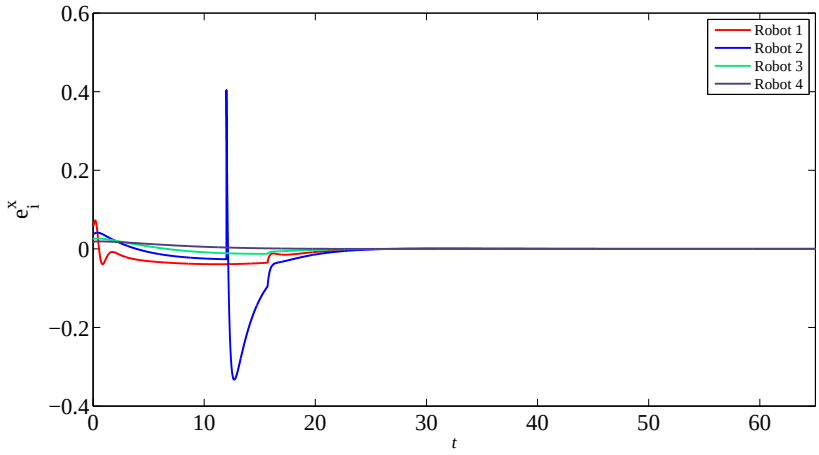

(a)

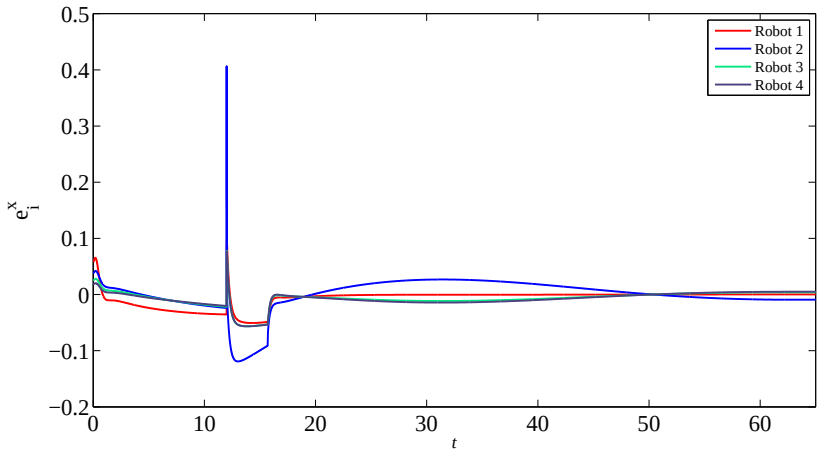

(b)

Figure 6.24: Horizontal components of tracking errors for (a) decoupled robots and (b) coupled robots in the case of the formation control algorithm (3.7).

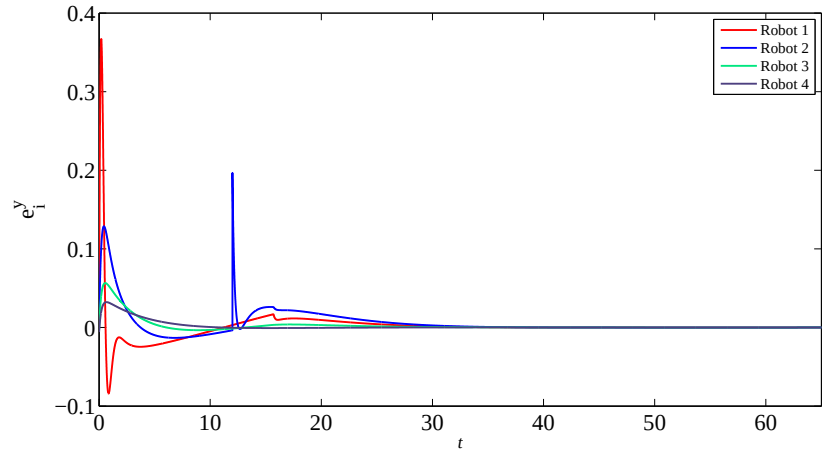

(a)

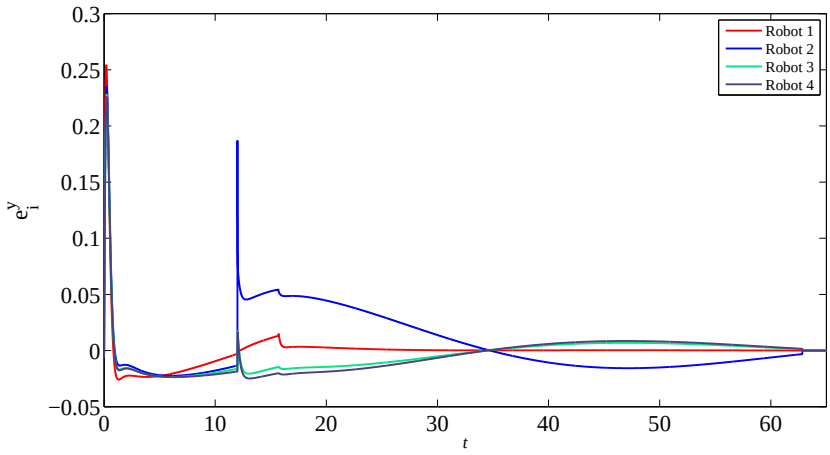

(b)

Figure 6.25: Vertical components of tracking errors for (a) decoupled robots and (b) coupled robots in the case of the formation control algorithm (3.7).

chapters of the thesis that for controller (3.7) it may actually hinder convergence when local coordinate frames of individual robots are adversely misaligned with respect to each other and when the communication graph is connected.

Conversely, in the formula for controller (4.13, 4.14), the coupling terms are expressed in the global coordinate frame. As such, the robots directly act towards formation shape keeping regardless of the orientation of local coordinate frames. Simulation results for this controller are presented in Figures 6.26-6.28. In this case, there is no doubt that consensus of the error variables is reached before the errors converge to zero, see Figures 6.27(b) and 6.28(b). One cannot see any such thing when the communication graph is disconnected, see Figures 6.27(a) and 6.28(a). On the other hand, the tracking of individual trajectories is improved when the communication graph is disconnected, see Figure 6.26. This is however at the cost of robots maintaining the desired formation shape: while the robots track the individual desired trajectories, the formation is not kept in face of a perturbation.

When comparing experimental results in Section 4.4 with the results in Figures 6.26-6.28, it is apparent that in simulations the controller yields faster convergence. However, it should be noted that in Section 4.4 the saturated version of controller (4.13, 4.14) was used. Moreover, actuators of actual robots are by nature limited. Therefore, while in simulations in theory an infinite control inputs can be generated, in experiments only limited control inputs are realisable which may slow down the convergence.

To summarise this section, simulation results for car-like mobile robots using

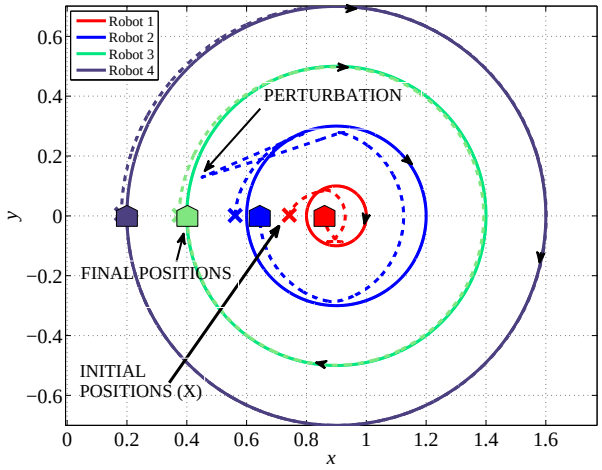

(a)

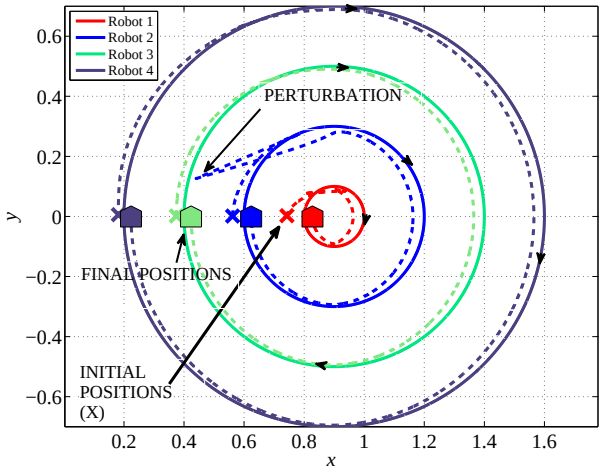

(b)

Figure 6.26: Desired robot paths (solid line) and actual robots paths (dashed line) in the plane obtained using the control algorithm (4.13, 4.14) in the case of (a) a disconnected communication graph and (b) a connected communication graph.

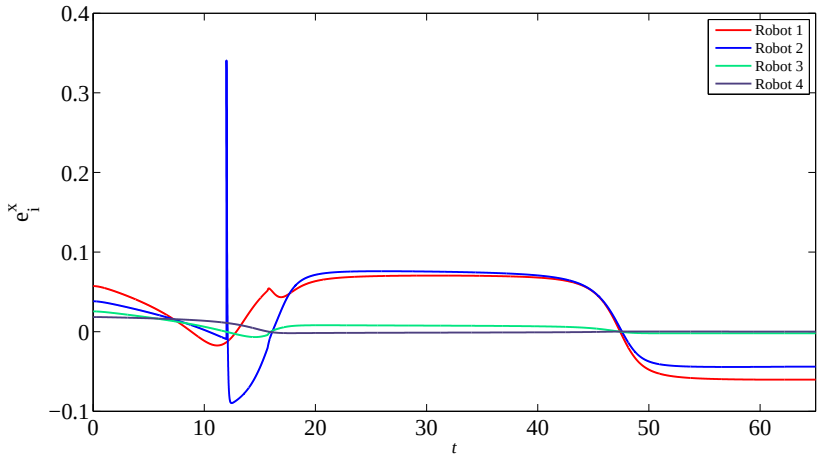

(a)

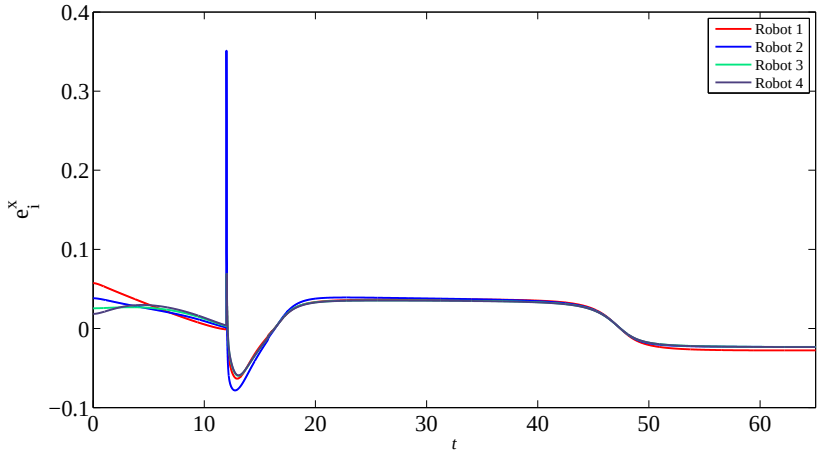

(b)

Figure 6.27: Horizontal components of tracking errors for (a) decoupled robots and (b) coupled robots in the case of the formation control algorithm (4.13, 4.14).

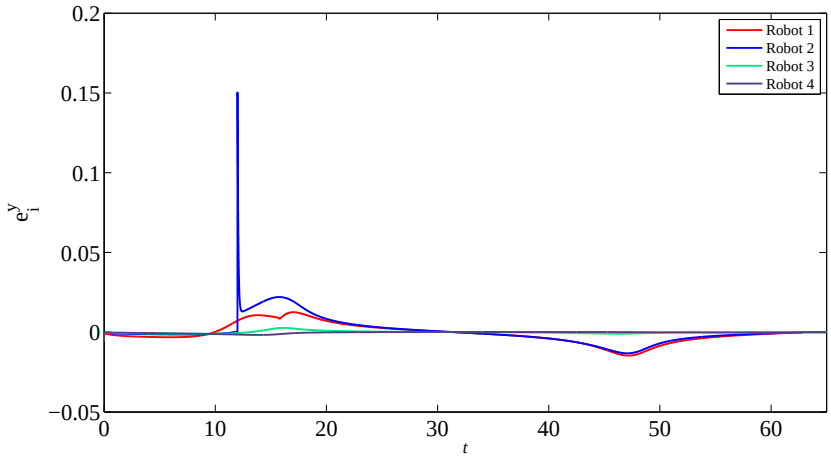

(a)

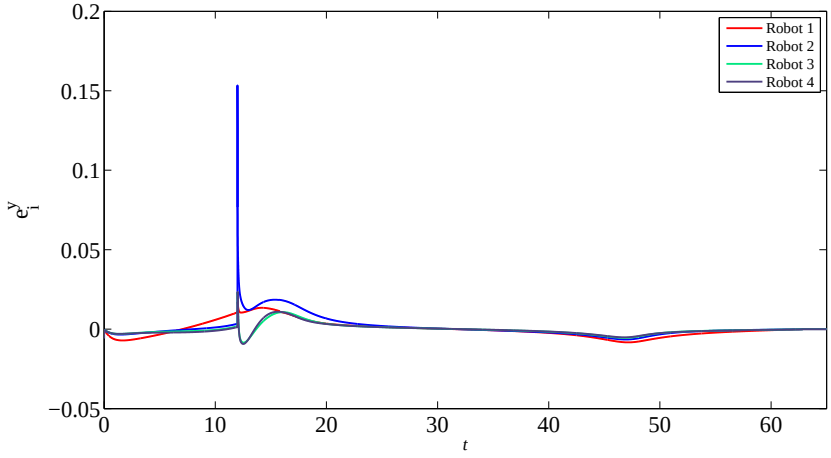

(b)

Figure 6.28: Vertical components of tracking errors for (a) decoupled robots and (b) coupled robots in the case of the formation control algorithm (4.13, 4.14) obtained in experiments.

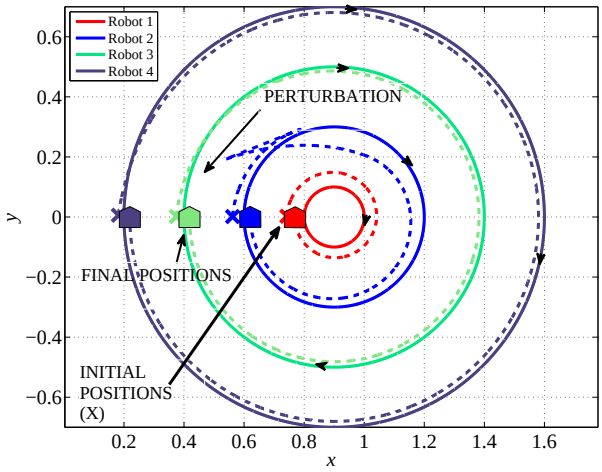

(a)

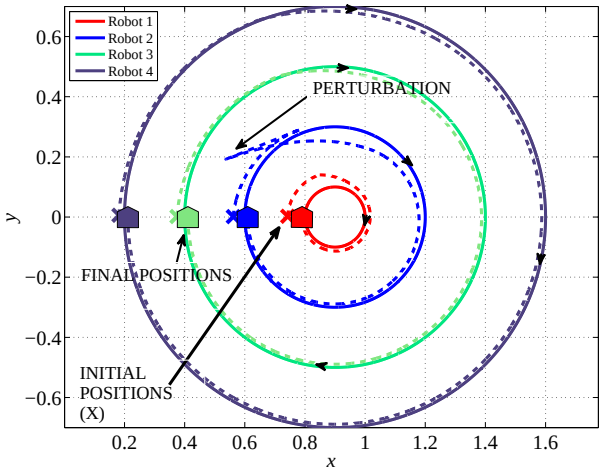

(b)

Figure 6.29: Desired robot paths (solid line) and actual robots paths (dashed line) in the plane obtained using the control algorithm (5.19, 5.36) in the case of (a) a disconnected communication graph and (b) a connected communication graph.

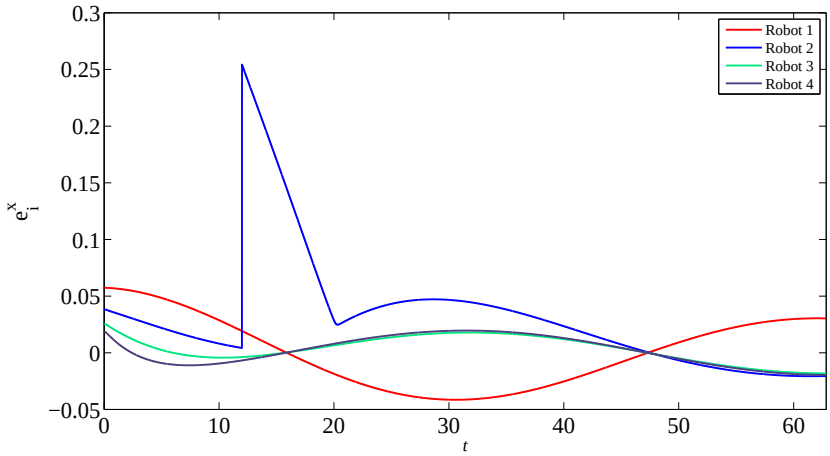

(a)

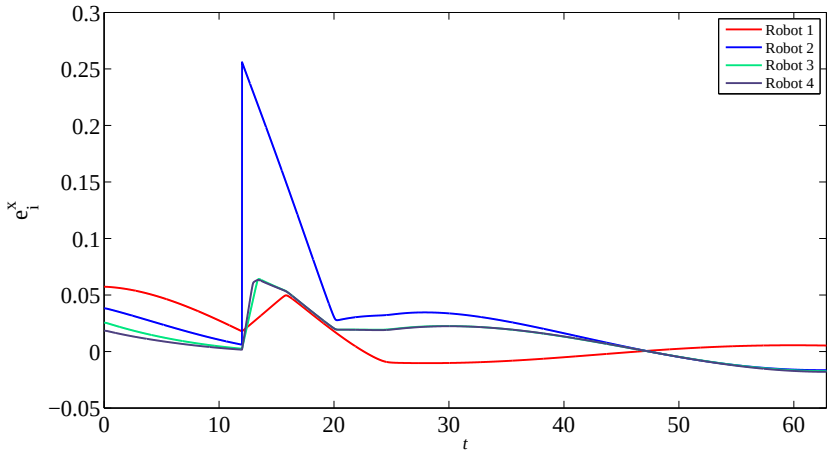

(b)

Figure 6.30: Horizontal components of tracking errors for (a) decoupled robots and (b) coupled robots in the case of the saturated formation control algorithm (5.19, 5.36).

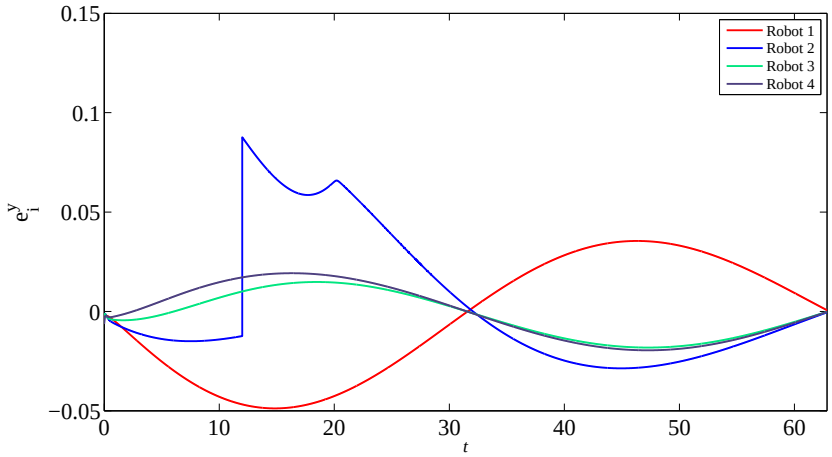

(a)

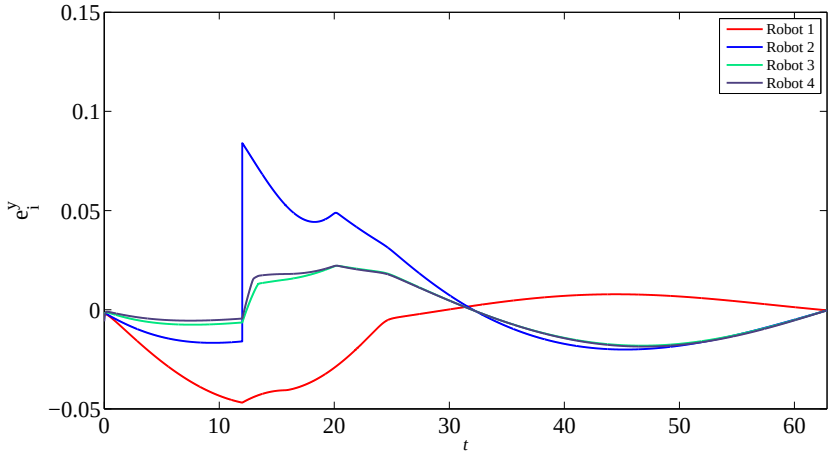

(b)

Figure 6.31: Vertical components of tracking errors for (a) decoupled robots and (b) coupled robots in the case of the saturated formation control algorithm (5.19, 5.36).

the controller in (5.19, 5.36) are given in Figures 6.29-6.31. In comparison to previous results presented in this section, the controller (5.19, 5.36) with such a choice of control parameters produces slower convergence. It is particularly visible in Figures 6.30 and 6.31 where one can see that the error variables have not vanished yet. Having said that, in the case of the connected communication graph one can observe the trend of error variables tending towards consensus which is tantamount to robots tending towards keeping the desired formation shape. Moreover, the magnitude of individual tracking errors is also smaller when robots can communicate with each other as opposed to the case when no communication between the robots is enabled. It can also be confirmed when looking at Figure 6.29: in the case of the connected communication case, robots paths better match the desired paths. Therefore, we can again confirm that the robots in the formation benefit from communicating with other robots, i.e. when the communication graph is connected.

6.4 Simulations with twelve robots

In this section we present simulation results for controllers (3.7), (4.13, 4.14) and (5.19, 5.36) with a formation of twelve robots. The motivation behind it is to show an example of how the controllers work for larger formations, as opposed to the other simulation results shown in the thesis where only three or four robots were used.

The desired formation shape used in the simulations in this section is shown

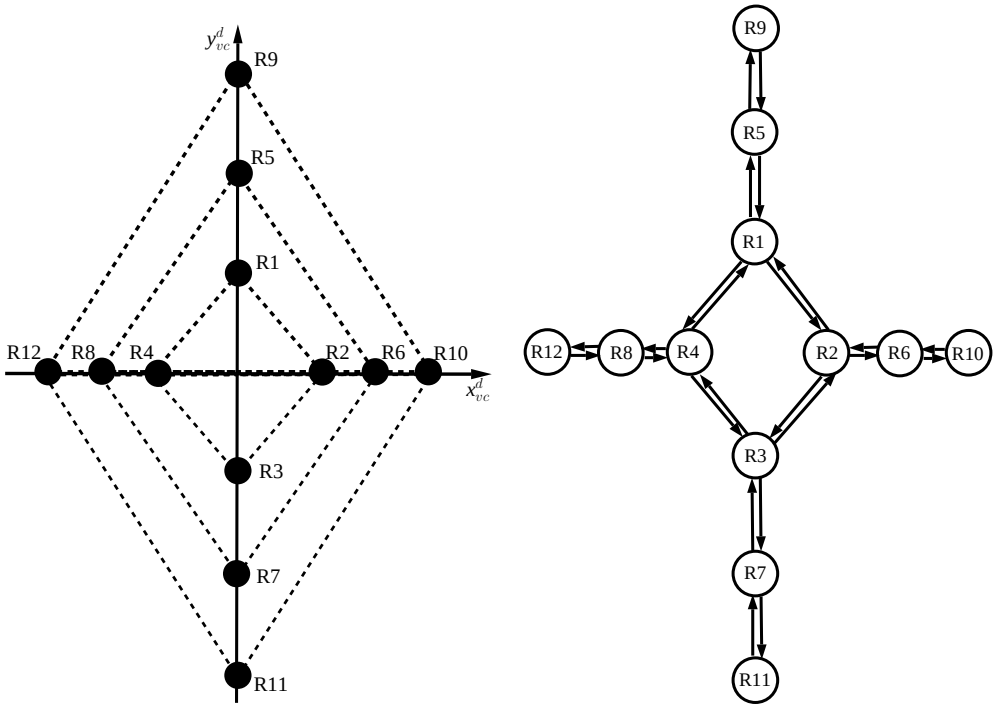

Figure 6.32: (a) desired formation geometry and (b) the communication structure used in the simulations for a twelve-robot formation.

in Figure 6.32(a), where the desired positions of individual robots with respect to the virtual centre are given by $l_1^d = \text{col}(0, 0.2)$, $l_2^d = \text{col}(0.15, 03)$, $l_3^d = \text{col}(0, -0.2)$, $l_4^d = \text{col}(-0.15, 0)$, $l_5^d = \text{col}(0, 0.4)$, $l_6^d = \text{col}(0.3, 0)$, $l_7^d = \text{col}(0, -0.4)$, $l_8^d = \text{col}(-0.3, 0)$, $l_9^d = \text{col}(0, 0.6)$, $l_{10}^d = \text{col}(0.45, 0)$, $l_{11}^d = \text{col}(0, -0.6)$ and $l_{12}^d = \text{col}(-0.45, 0)$. Furthermore, the desired trajectory of the virtual centre is given by

$$x^d_{vc}(t) = 0.025t,$$
$$y^d_{vc}(t) = 0.015 \sin(\tfrac{\pi}{6}t).$$

In contrast to the simulation results earlier in this chapter, in this section we

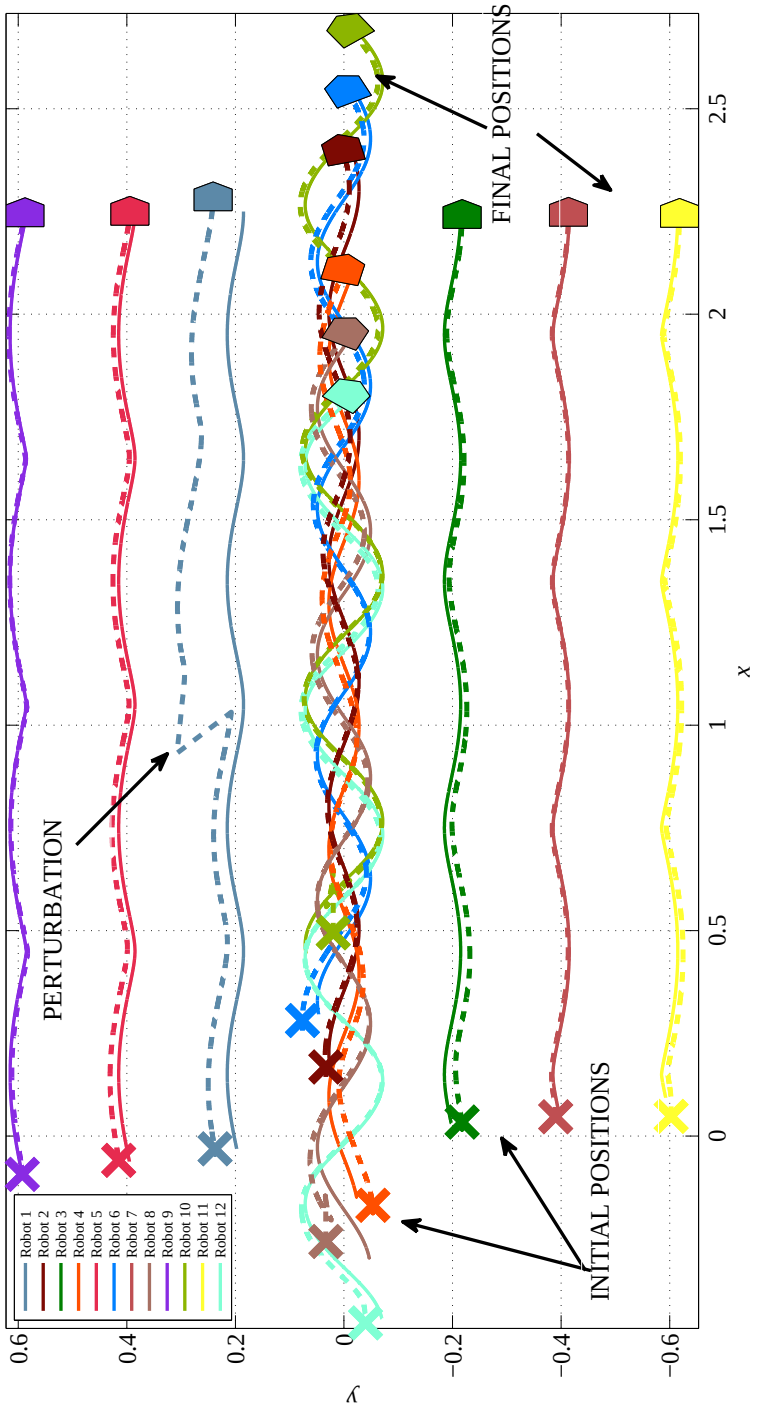

Figure 6.33: Desired robot paths (solid line) and actual robots paths (dashed line) in the plane obtained obtained using (3.7).

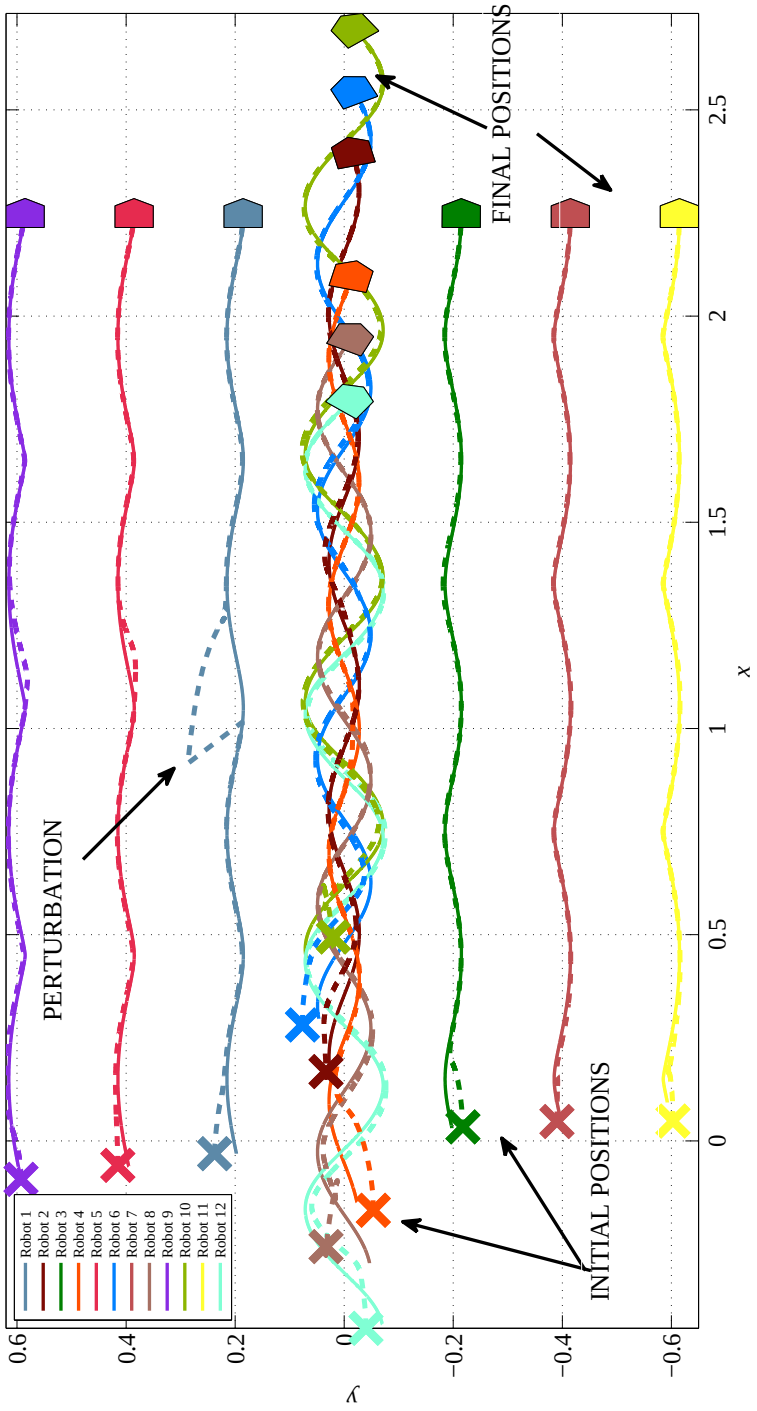

Figure 6.34: Desired robot paths (solid line) and actual robots paths (dashed line) in the plane obtained obtained using (4.13, 4.14).

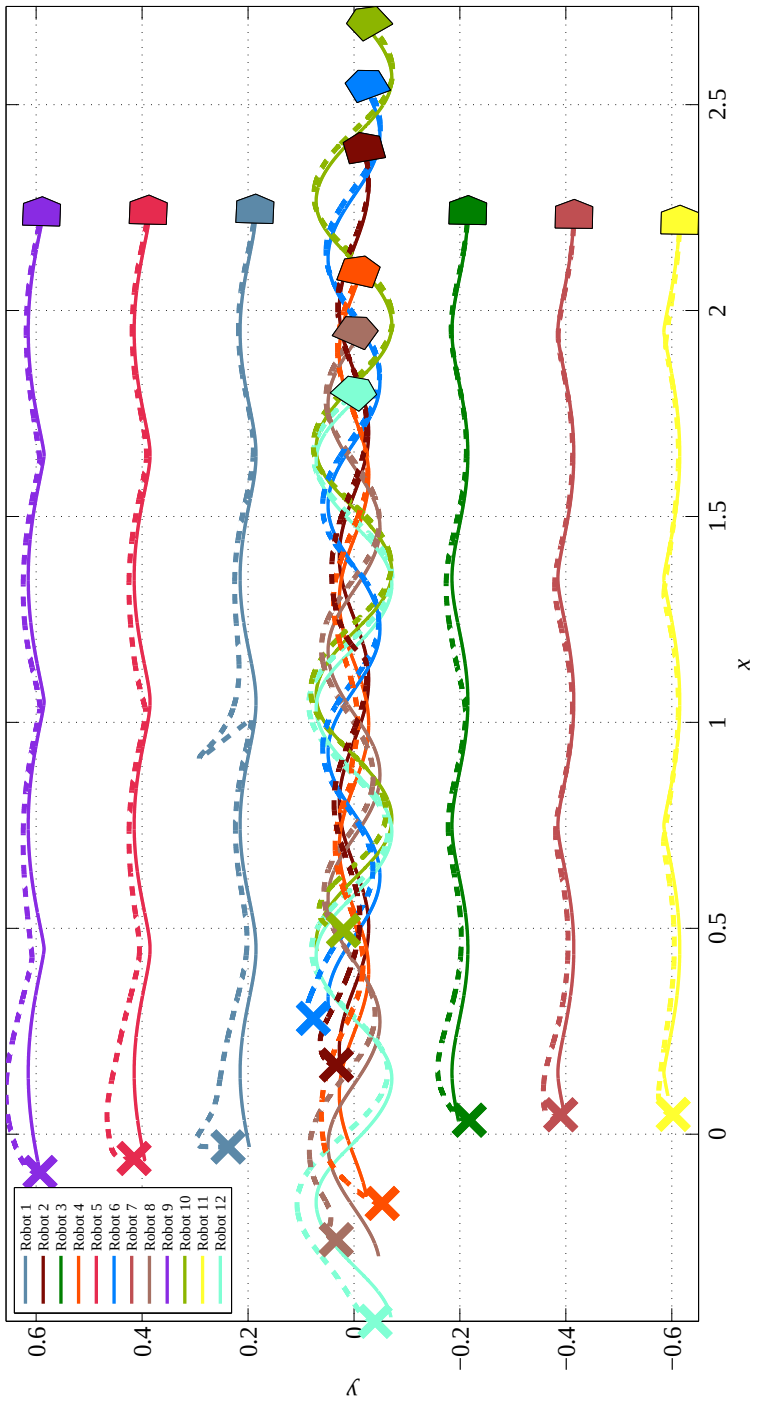

Figure 6.35: Desired robot paths (solid line) and actual robots paths (dashed line) in the plane obtained obtained using (5.19, 5.36).

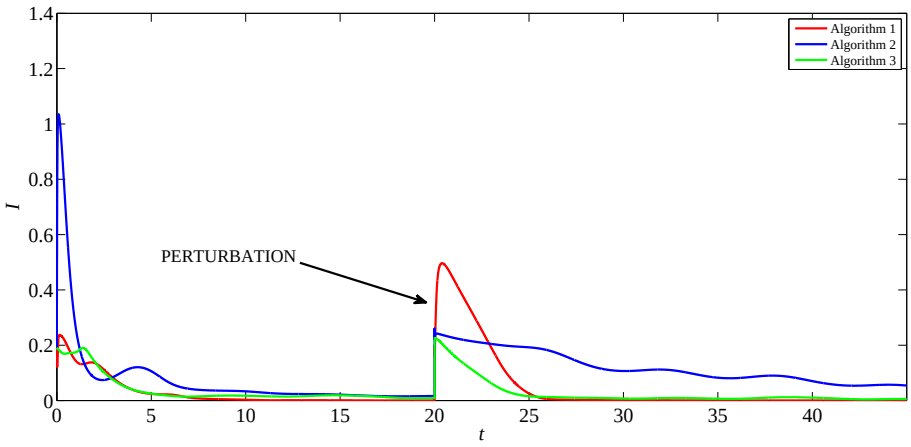

Figure 6.36: Comparison between formation geometry maintenance index I for a formation consisting of twelve robots using controller (4.13, 4.14) (Algorithm 1), (3.7) (Algorithm 2) and (5.19, 5.36) (Algorithm 3).

present simulation results for a connected communication case only. It is depicted in Figure 6.32(b). The initial conditions of the robots in the formation are: $p_1(0) = \text{col}(-0.03, 0.24)$, $p_2(0) = \text{col}(0.17, 0.03)$, $p_3(0) = \text{col}(0.03, -0.22)$, $p_4(0) = \text{col}(-0.17, -0.05)$, $p_5(0) = \text{col}(-0.06, 0.42)$, $p_6(0) = \text{col}(0.28, 0.08)$, $p_7(0) = \text{col}(0.05, -0.39)$, $p_8(0) = \text{col}(-0.26, 0.03)$, $p_9(0) = \text{col}(-0.09, 0.59)$, $p_{10}(0) = \text{col}(0.49, 0.02)$, $p_{11}(0) = \text{col}(0.05, -0.60)$ and $p_{12}(0) = \text{col}(-0.45, -0.04)$. In addition, $\theta_i(0) = 0$ and for car-like robots $\varphi_i(0) = \frac{\pi}{2}$ for all robots $i \in \mathcal{I}$. As with the previous simulations in this section, we perturb one of the robots in the formation to observe the reaction of other robots.

The control parameters chosen for the simulations in this sections are $c_i^x = 20$, $c_i^y = 100$, $c_i^\theta = 2.5$, $\widetilde{c}_{ij}^x = 30$, $\widetilde{c}_{ij}^y = 300$ and $\widetilde{c}_{ij}^\theta = 0.1$ for the controller defined in (3.7). For the controller in (4.13, 4.14), the parameters are: $c_i^{xe} = 20$, $c_i^{ye} = 100$, $c_i^\theta = 2.5$, $c_{ij}^{x\sigma} = 30$ and $c_{ij}^{x\sigma} = 300$. Moreover, for controller (5.19, 5.36) we

use $c_i^e = 100$, $c_i^z = 60$, $c_i^\theta = 2.5$, $c_{ij} = 300$ and $\chi_i(s) = \chi_i^* \frac{2}{\pi}\text{atan}(s)$ in which $\chi_i^* = 0.005$. These control parameters were chosen on the basis of trial and error, see Remark 3.3.1.

In Figures 6.33, 6.34 and 6.35 we plot the desired and actual paths in the case of controller (3.7), (4.13, 4.14) and (5.19, 5.36) respectively. The results show again that in face of perturbation, the unperturbed robots react to the perturbation and thus leave their desired trajectories in order to keep the formation shape. This is owing to the communication between the robots and is consistent with previous results given in the thesis.

It can be seen that for controller (3.7) the convergence speed is less rapid than for the other two controllers, particularly for Robots 1, 3, 5, 7, 9 and 11. It can be explained by the fact that the convergence speed for controller (3.7) depends on the value of the desired angular velocity of a robot. Therefore, since the desired angular velocities of Robots 1, 3, 5, 7, 9 and 11 are small, see Figure 6.33, the robots need more time to correct their tracking errors. In comparison, in Figure 6.34 it is seen that controller (4.13, 4.14) yields much faster convergence. In that figure, one notices that both at the beginning of the simulation as well as after the perturbation, robots quickly coincide with their desired trajectories. Somewhere in between the performance generated by controller (3.7) and controller (4.13, 4.14) is the performance obtained in simulations for controller (5.19, 5.36). For this controller, robots paths converge to their desired paths faster than for the first controller (3.7) but not as swiftly as for controller (4.13, 4.14). This statement is also confirmed by the results presented in Figure 6.36 which plots the formation

geometry maintenance index for the three controllers. Indeed, for controller (4.13, 4.14), the index has the smallest value, then for controller (5.19, 5.36) it is bigger except for just after the perturbation. For controller (3.7) the value of the index has the largest value throughout the simulation.

6.5 Discussion

In this chapter we have presented three series of simulations for various control algorithms given in the thesis. This was motivated by the need to more thoroughly analyse similarities and differences of the algorithms. It is noted that, in line with previous findings in the individual chapters earlier in the thesis, the communication between the robots enables the robots to concentrate on the common formation goal – the formation shape maintenance as opposed to tracking individual robot trajectories. Indeed, the simulation results in this section corroborate that claim and show that robots benefit from exchanging information with other robots in the formation. However, for the robots to be able to benefit from that mechanism to the greatest degree, an appropriate control algorithm should be selected to control the robots as different control algorithms have different strengths. Moreover, the simulation results show how important parameter tuning for each controller is. Indeed, control parameters suitable for one type of controller may prove unsatisfactory for other type of controller. What is more, parameter tuning is also reliant on the various settings of the simulation, e.g. on the desired trajectory of the formation and the desired formation shape. Accordingly, it is best if the parameters are adjusted for each particular case.

It is also worth mentioning that while no collision occurred in the simulations in this section, especially the simulation results in Section 6.4 advocate that it is desirable to develop a collision avoidance scheme to be incorporated with the existing formation control algorithms. Without a doubt, with a large number of robots in the formation, collisions between the robots can take place unless a proper collision avoidance scheme is introduced. Therefore, it is recommended that such a formation control algorithm with a collision avoidance scheme is worked on in the future.

In view of the simulation results in this chapter as well as in Chapters 3, 4 and 5, we can reiterate the interpretation of the tracking control gains and the mutual coupling gains. The simulation results confirm that by choosing stronger tracking gains in comparison to the mutual coupling gains, the robots in the formation focus on tracking of individual trajectories. Conversely, when the mutual coupling gains dominate the tracking gains, the robots' priority is to keep the desired formation shape with less attention paid to tracking robots' individual desired trajectories.

Chapter 7

Conclusions

In this chapter we summarise the developments of the thesis and state our recommendations for future work in the area of formation control. Our research covered various proposed solutions to the formation control problem in which multiple mobile robots in the formation are to create a desired formation shape and follow a desired trajectory as a whole. In what follows, we review the results, pointing out both the advantages as well as potential shortcomings of the introduced formation control algorithms. Based on that we present the open questions and research topics that we think are interesting to study in the future.

The first piece of work that is presented in this thesis is a formation control algorithm based on the cascaded approach. The cascaded approach is very useful in that it allows to split dynamic systems into separate systems in a cascaded way. The principles are that the resulting decomposed systems are easier to

analyse than the original system. In the settings studied in this thesis the obtained systems are both relatively simple linear systems while the original system was nonlinear. Hence, the application of the cascaded approach allowed the stability to be established in a more straightforward way. The control algorithm is then assembled by adding so–called mutual coupling terms into an existing trajectory tracking algorithm for a single robot. These mutual coupling terms represent communication or any other kind of information exchange protocol between robots to enable robots to be aware of the performance of other robots in the formation. The importance of providing robots with feedback information regarding other robots in the formation is particularly noticeable when there is a perturbation acting on one of the robots. Then through the communication mechanism, the information about the perturbed robot is sent to all other robots in the formation and the whole formation can counteract the perturbation to try to keep the formation shape. The implied condition for this mechanism to work is that the communication graph of the formation needs to be connected so that robots are aware of the behaviour of the rest of the group. The basic formation control algorithm is then extended in a twofold manner. First, we introduced a dynamic formation control algorithm in which both robot kinematics and dynamics are considered. Another extension is the saturated formation control algorithm which is particularly relevant in practical applications since it involves taking into consideration robot actuator limitations.

The applicability of the aforementioned control algorithms is broad and only mild conditions on the control parameters are imposed. However, a possible shortcoming of these controllers is the property that trajectories which are straight lines

are not feasible. This follows from the fact that the desired angular velocities of robots in the formation need to satisfy the persistence of excitation condition. A possible solution to this problem mentioned briefly by us after the introduction of the formation control algorithm consists of extending the definition of a persistently exciting signal to a δ – persistently exciting signal (Loria et al., 1999) and making some modifications to the formation control algorithm. In the literature such a modification is available for a stabilisation task of a single nonholonomic system. In the author's point of view though this additional work to allow robots to track trajectories like straight lines is not a major alteration in terms of working principles but it would be nonetheless an interesting technical extension. Note that such an issue does not exist in the other approach that we present for unicycle mobile robots in Chapter 4 as in in the settings in Chapter 4 the angular velocities can indeed be zero.

Our work regarding the cascaded approach to the formation control problem can also be continued by studying a saturated control law as in Chapter 3 in which also the feedback term for the vertical position error variable y_i^e is added in (3.37). Yet again, arguably this would not appear to be a groundbreaking discovery but rather an interesting technical extension. Of course, due to nonholonomic constraints, if there are terms in the control law for the horizontal position error variable x_i^e and the angular error variable θ_i^e then also the vertical position error variable y_i^e converges to zero. Nonetheless, from a theoretical point of view, it would be valuable to study the complete version of the saturated controller with a correction term in terms of y_i^e and then possibly compare the differences in performance for both controllers.

Another possible disadvantage of the cascaded formation control algorithm is the fact that all error variables are defined in local frames associated with each individual robot. This means that also the feedback information sent to a robot's neighbours in the form of the mutual coupling terms consists of information about the robot expressed in a local coordinate system of the sender robot, not the receiving robot. This means that each robot uses information about their neighbours expressed in a different coordinate system than its own error variables. Thus, those quantities may not be truly relevant for the considered robot and perhaps a different definition of coordination error would be more beneficial, especially if robot trajectories are such that the local coordinate systems of robots in the formation are misaligned considerably. In such circumstances, an error in a local coordinate system of one robot may be small but in another coordinate frame might be relatively large. To fix this issue, in the second approach studied in this thesis we have decided to express the tracking error of a particular robot and the coordination errors between this robot and its neighbours in the same coordinate frame. In particular, in this research it was the world frame in which all error variables – both tracking and coordination – are given. Hence all error variables are ultimately expressed in identical coordinate frames. The employment of the error variables in the world coordinate frame is unusual in the literature and plays an important role in the analysis of the closed–loop behaviour of the formation.

In the scenario considered in Chapter 4 we propose a number of control algorithms. The first control algorithm fulfils the formation control objectives mentioned earlier: robots create a desired formation geometry and such a geometrical structure follows a given desired trajectory as a whole. The second major forma-

tion control algorithm is designed to solve a restricted formation control problem. In particular, in the restricted formation control problem robots are still required to converge to a desired formation shape but trajectory tracking is not required. This is what we call the Pure Coordination scheme as robots achieve coordination but not necessarily trajectory tracking. We also proposed an extension of these formation control algorithms in which robot actuator limitations are taken into consideration. This resulted in saturated formation controllers. Moreover, we also discussed a leader–follower like strategy in which one selected robot – the leader – aims to track the desired trajectory while the other robots – the followers – only act towards coordination of the group. Then, if the formation communication graph is connected, the formation control problem is solved.

Based on the simulation and experimental results, we concluded that it is beneficial for robots in the formation if there is a sufficient level of information exchange or communication between the robots. The intuitive reason for this is that the formation behaviour is enhanced in the sense that robots could prioritise formation shape maintenance over individual trajectories tracking if robots are aware of the behaviour of other robots in the formation and with appropriate choice of the tracking and coordination control gains. In particular the balance between the tracking gains and the coordination gains determines the kind of prevailing behaviour of robots: tracking of individual trajectories or maintaining the desired formation shape. The importance of the connectivity of the communication graph is particularly visible when there are perturbations acting on robots in the formation. More specifically, when the connectivity of the formation is assured, should any disturbance occur to any member of the group, the rest of the robots

can be made aware of the disturbance and try to counteract its effect. In the case of the pure coordination controller as well as the leader–follower like controller, the condition of the connectivity of the communication graph is made explicit. However, also in other strategies when it is not directly required for the communication graph of the formation to be connected, we have illustrated in simulations and experiments that ensuring connectivity of the communication graph may improve the coordinated behaviour of robots. The explanation behind this phenomenon is that when the communication graph of the formation is connected then the coupling between robots is a means to ensure consensus of tracking error variables. This, as shown in the thesis, is tantamount to robots converging to their desired formation shape. It therefore shows the importance and benefits of including the mutual coupling in the formation control laws.

One possible extension of the results presented in Chapter 4 stems from Corollary 4.2.3 regarding the synchronisation of angular errors. In particular, in our current work, the coordination of robots in the formation holds only if the actual formation is translated with respect to the desired one as no rotation of the formation is permitted. However, in the future it might be interesting to further relax the definition of coordination of robots in the formation in such a way that only the geometric shape that the robots form is verified. This would allow for a possible translation as well as rotation of the whole formation on the plane. In light of the synchronisation of angular errors, note that when mutual distances between robots are identical to the desired distances and the formation is rotated with respect to the desired one, the angular errors are synchronised with each other. This further means that the heading angles are such that all robots in the

formation proceed in the same direction. The starting point for advances in relaxing the definition of coordination of the formation is to redefine the coordination error because in the way it is defined now, the angular errors need necessarily to converge to zero for coordination in the Pure Coordination scheme to be ensured.

In Chapter 5 of the thesis we introduced a similar approach as in Chapter 4 to solve the formation control problem for car–like mobile robots. The control law was developed using the backstepping method. In comparison to the results from Chapter 4, where all position error variables were expressed in the world frame, it was shown in this chapter that in fact it suffices if the tracking error of each particular robot is given in the same local coordinate frame as the coordination errors of that robot and indeed the coordinate frame does not have to be common for all robots in the formation. Therefore, in the work concerning car–like mobile robots, we decided to express tracking and coordination of each robot in a local coordinate system of that robot. In comparison to using the world frame to express all error variables as in Chapter 4, here the utilisation of the local frames lent itself to an arguably more straightforward stability analysis. However, the condition for coordination or in other words formation shape maintenance is still equivalent to consensus of the tracking error variables given in the world frame. To validate the applicability of the proposed formation control law, we performed a series of simulations. The conclusion that was drawn from the simulation results is again the advantageous influence of the connectivity of the communication graph of the formation on the cooperative behaviour of the robots.

One feature that could use some extra research in the area of formation control

of car–like robots is finding a saturated control law in which upper bounds for the magnitude of the control inputs v_i and ω_i can be pre-determined as needed, regardless of the initial conditions. One way of doing it is as it is shown in Chapter 3 and Chapter 4 in which the formation control algorithms are extended to accommodate for the actuator limitations. Another way that we foresee might possibly be helpful to solve the problem of accounting for actuator constraints is a strategy based on an anti-windup like scheme (Tarbouriech and Turner, 2009; Wu and Lin, 2010, 2011). However, a more extensive examination of this issue is unquestionably necessary.

Some of the remaining issues in the area of formation control that deserve further consideration are as follows.

1. The first, possibly most striking issue which is lacking in the formation control literature is a formation control algorithm for nonholonomic robots ensuring collision avoidance of robots in the formation. Indeed, there is quite an abundance of results for formation control with collision avoidance for single or double integrator agents, including (De Gennaro and Jadbabaie, 2006; De Gennaro et al., 2005; Dimarogonas and Kyriakopoulos, 2005, 2006; Tanner, 2004). Here, in principle, the collision avoidance is implemented by minimising a potential function in the sense that should a possible collision be detected, a repulsive behaviour is activated. For unicycle robots, the formation control problem with collision avoidance was studied by (Mastellone et al., 2007, 2008). The results in (Mastellone et al., 2007, 2008) also incorporated the error variables in the global coordinate frames but

the approach as such is completely different to what we study in this thesis. The proposed control algorithm was also based on potential functions and achieved trajectory tracking of the formation and convergence of robots to a desired location within the formation as well as collision avoidance between the robots. However, there was no communication between robots except for calculating the collision avoidance term while it was shown in our work that cooperative behaviour can be improved considerably when robots in the formation are allowed to exchange information with each other. Moreover, there are some technical issues with these papers. Namely, it is assumed that the desired trajectory of a robot is rendered constant when another robot is sensed in the detection region. This appears problematic as the desired trajectory of each robot should rather stem directly and solely from the desired trajectory of the whole formation and the desired formation shape. Arguably, such a desired trajectory of a robot is not to be tampered with despite a possible detection of a collision. It appears that it is rather the control inputs of the robots that robots might use when they detect a possible collision to act against it. Therefore, further research is still needed. Here, the results in (De Gennaro and Jadbabaie, 2006; De Gennaro et al., 2005; Dimarogonas and Kyriakopoulos, 2005, 2006; Mastellone et al., 2007, 2008; Tanner, 2004) can very well be considered as the first step in the development of a collision avoidance mechanism for formation control of nonholonomic robots.

2. It would also be interesting to design a control algorithm that would work for a more general type of robot, possibly utilising the chained form of a

mobile robot like in (Dong and Farrell, 2008; Dong et al., 2006). The appeal of such a research direction is in that this would be covering many types of robots including unicycle robots, car–like robots and robots with trailers. Having said that, although the results in (Dong and Farrell, 2008; Dong et al., 2006) would be possible to be applied to such systems, they only allow for constant formation shapes, which might be a serious limitation in some circumstances. Moreover, the chained form of many nonholonomic systems proposed in the literature to date are only defined locally, see Section 2.1.3. Therefore, the control algorithms would automatically also be burdened with singularities. Hence, research is not only needed on the design of a formation control algorithm for chained nonholonomic systems but also on investigation on whether global transformations of the kinematic models of robots into chained forms do exist.

3. Even though all the results in this thesis are distributed and hence require robots to communicate with their neighbours only, the set of neighbours of each robot is predetermined offline, before the start of an experiment. However, this is a bit unrealistic as in real life sets of neighbours of robots are likely to change as robots move. Therefore, an extension of the results presented in the thesis is necessary. However, this is a nontrivial task, because the stability analysis of the origin of a switched system relies on finding a common strict Lyapunov function if possible. For systems that do not admit a common strict Lyapunov function (or such a function cannot be easily found), the complexity of stability analysis rises considerably (Branicky, 1998; Hespanha, 2004; Hespanha et al., 2005; Lu and Brown,

2010). The problem is further complicated by the fact that the systems in the thesis are in general nonlinear and moreover time–varying.

Some interesting results on the influence of switching graph topologies on the formation behaviour in case of flocking were developed by Jadbabaie et al. (2003) which, nonetheless, was concerned with single integrator agents. Therefore, these results cannot be directly applied to systems with more complicated dynamic models such as nonholonomic systems are. The same issue arises for the results in (Tanner, 2004). However, the methodology presented in the aforementioned papers can perhaps help to elucidate the problem of switching graph topologies in formation control of nonholonomic robots when appropriate modifications are implemented. Nevertheless, this remains an open question for future research.

4. Another issue that might be interesting to investigate is to allow new robots to join an existing formation or leave a formation as well as for two groups to merge or for a formation to split into two groups. Such a feature was studied in (Chung and Slotine, 2009; Hsu and Liu, 2005). Nonetheless these papers did not consider the formation control problem as studied in this thesis but the synchronisation control problem (Chung and Slotine, 2009) or indeed the formation control problem but using the behavioural approach (Hsu and Liu, 2005).

   In the scenarios considered in the thesis, this additional feature would require redefining the formation control problem. This is because the problem we study now is highly reliant on the number of robots in the formation since the desired formation shape is given explicitly and depends on the

number of robots. To study a task in which group merging and splitting is allowed as well as allowing for individual robots to join or leave a formation, the formation control problem might still consist of following a desired trajectory as a whole and a more vague definition of the desired formation shape as compared to the current rather precise definition of the formation shape. Nonetheless, further research both in terms of technical realisation of such a feature as well as an adequate redefinition of the formation control problem is crucial.

5. It has been shown in the literature that the formation behaviour can be improved and in particular the convergence speed of the error variables can be increased if the formation control law is supplemented with a predictive mechanism, see (Chen et al., 2010; Huijberts et al., 2007; Voss, 2000; Zhang et al., 2008). The aim of the predictive mechanism is for agents to anticipate the future state of the other members of the group. Then, in the settings of the formation control problem studied in the thesis, robots may converge faster to their desired trajectories or create more rapidly the desired formation geometry in the transient or after a perturbation. However, for this mechanism to be enabled, more research is needed which remains for future investigation.

6. All our results apply to formations consisting of identical robots. However, it would be interesting to see how similar formation control algorithms work for formations of heterogenous robots. To that end, dynamics of such heterogenous formations need to be studied. It is believed that the general concepts of the results presented in the thesis may be suitable for

this extended case. Yet, further research to tackle all technical problems is required.

Appendix A

Mathematical preliminaries – basic definitions

This appendix is to present some mathematical preliminaries that are used throughout the thesis.

Definition A.1. (Khalil, 1996) Consider a vector $w \in \mathbb{R}^n$ and a scalar $p \in \mathbb{R}^+$. Then the p-norm $\|w\|_p$ of w is defined by

$$\|w\|_p = \big(\sum_{i=1}^{n} |w_i|^p\big)^{\frac{1}{p}}. \tag{A.1}$$

For $p = 2$, one obtains the so–called *Euclidean norm* denoted in this thesis as $\|w\|$.

Definition A.2. (cf. (Alvarez Aguirre, 2011; Ioannou and Sun, 1995; Khalil, 1996; Lefeber, 2000; Narendra and Annaswamy, 1989)) A vector signal $W(t)$ is

said to be persistently exciting if, for some constants $0 < \alpha_1 \leq \alpha_2$ and $\gamma > 0$, the following is true

$$\forall t \geq 0 \quad \alpha_1 I \leq \int_t^{t+\gamma} W(\tau) W^T(\tau) d\tau \leq \alpha_2 I. \tag{A.2}$$

The following definitions are taken *verbatim* from (Khalil, 1996).

Definition A.3. (Khalil, 1996) A continuous function $\beta(\cdot)\colon \mathbb{R}^+ \to \mathbb{R}^+$ is said to be of class $\mathcal{K}$ if it is strictly increasing and $\beta(0) = 0$. In addition, if $\beta(p) \to \infty$ as $p \to \infty$, it is said to belong to class $\mathcal{K}_\infty$.

Definition A.4. (Khalil, 1996) A continuous function $\beta : [0, a) \times [0, \infty) \to [0, \infty)$ is said to belong to to class $\mathcal{KL}$ if, for each fixed s, the mapping $\beta(r, s)$ belongs to class $\mathcal{K}$ with respect to r and, for each fixed r, the mapping $\beta(r, s)$ is decreasing with respect to s and $\beta(r, s) \to 0$ as $s \to \infty$.

The following lemma presents certain properties of a class of matrices that is exploited extensively in the thesis.

Lemma A.5. Consider a square matrix A of the following form

$$A = \begin{bmatrix} \alpha_1 + \sum\limits_{\substack{j \in \mathcal{J} \\ j \neq 1}} \alpha_{1j} & -\alpha_{12} & \dots & -\alpha_{1n} \\ \vdots & \ddots & \ddots & \vdots \\ -\alpha_{n-1,1} & \dots & \alpha_{n-1} + \sum\limits_{\substack{j \in \mathcal{J} \\ j \neq n-1}} \alpha_{n-1,j} & -\alpha_{n-1,n} \\ -\alpha_{n1} & -\alpha_{n2} & \dots & \alpha_n + \sum\limits_{\substack{j \in \mathcal{J} \\ j \neq n}} \alpha_{nj} \end{bmatrix} \tag{A.3}$$

in which $\mathcal{I} = \{1, \ldots, n\}$ and for all $i, j \in \mathcal{I}$ we have $\alpha_i > 0$ and $\alpha_{ij} \geq 0$. Then A is of full rank and all eigenvalues of A have positive real parts. Furthermore, if $\alpha_{ij} = \alpha_{ji}\ \forall i, j \in \mathcal{I}$, $i \neq j$, then A is a positive definite matrix.

Proof. Follows straightforwardly from the Geršgorin disc theorem (Horn and Johnson, 1990). □

The following lemmas are taken *verbatim* from (Jiang and Nijmeijer, 1997) and (Kostić et al., 2009, 2010b) respectively.

Lemma A.6. (Jiang and Nijmeijer (1997, Lemma 2), cf. Micaelli and Samson (1993, Lemma 1)) Consider a scalar system

$$\dot{x} = -\alpha x + \beta(t) \tag{A.4}$$

where $\alpha > 0$ and $\beta(t)$ is a bounded and uniformly continuous function. If, for any initial time $t_0 \geq 0$ and any initial condition $x(t_0)$, the solution $x(t)$ is bounded and converges to 0 as $t \to \infty$, then

$$\lim_{t \to \infty} \beta(t) = 0. \tag{A.5}$$

Lemma A.7. (Kostić et al., 2009, 2010b, Lemma 1) Consider a scalar system

$$\dot{x} = -\alpha(x) + \beta(t) \tag{A.6}$$

where α and β are bounded and uniformly continuous functions in x and t, respectively, such that $\alpha(0) = 0$ and $x\alpha(x) > 0$ if $x \neq 0$. If, for any $t_0 \geq 0$ and

any initial condition $x(t_0)$, the solution $x(t)$ is bounded and $\lim_{t\to\infty} x(t) = 0$, then

$$\lim_{t\to\infty} \beta(t) = 0. \tag{A.7}$$

Appendix B

Stability of dynamic systems

This appendix is based on the results provided in (Khalil, 1996; Sastry, 1999; Slotine and Li, 1991; Sørdalen and Egeland, 1995) and the reader is referred to these references for further details.

We consider a dynamic system given in the general form of a first order differential equation

$$\dot{x} = f(t, x), \tag{B.1}$$

in which $x \in \mathbb{R}^n$, $x(t_0) = x_0$ and $t \geq t_0$, t_0 and x_0 are initial conditions and $f(t, x)$ is continuous in t and smooth in x. Let us denote by $x(t, t_0, x_0)$ the unique solution of (B.1) at time $t \geq t_0$ starting at $x_0 = x(t_0)$. Further, let us assume that $f(t, x)$ is complete and hence solutions are defined for all t. If $f(t, x) = f(x)$, the system is called *autonomous* or *time-invariant*, otherwise it is named *non-autonomous* or *time varying*. Moreover, system (B.1) is called *linear*, if $f(t, x) = A(t)x + b(t)$,

where $A(t)\colon \mathbb{R} \to \mathbb{R}^{n\times n}$ and $b(t)\colon \mathbb{R} \to \mathbb{R}^n$ or *nonlinear*, whenever this statement does not hold.

Definition B.1. A state x_e is said to be an *equilibrium state* of (B.1) if

$$f(x_e) = 0 \quad \text{or} \quad f(t, x_e) = 0 \quad \forall t, \tag{B.2}$$

for an autonomous or a non-autonomous system respectively.

In the rest of this appendix, it is assumed that the equilibrium point of (B.1) is $x_e = 0$, i.e. $f(t, 0) = 0$.

Definition B.2. The equilibrium point $x_e = 0$ of (B.1) is

- stable if

$$(\forall\ t_0 \geq 0)(\forall\ \epsilon > 0)(\exists\ \delta > 0)\,(\|x_0\| < \delta \implies \|x(t, t_0, x_0)\| < \epsilon, \forall\ t \geq t_0), \tag{B.3}$$

- uniformly stable if

$$(\forall\ \epsilon > 0)(\exists\ \delta > 0)(\forall\ t_0 \geq 0)\,(\|x_0\| < \delta \implies \|x(t, t_0, x_0)\| < \epsilon, \forall\ t \geq t_0), \tag{B.4}$$

- globally asymptotically stable if it is stable and

$$(\forall\ t_0 \geq 0)(\forall x_0 \in \mathbb{R}^n)(\|x(t, t_0, x_0)\| \to 0 \text{ as } t \to \infty), \tag{B.5}$$

- globally uniformly asymptotically stable if it is globally asymptotically stable and there exists a class $\mathcal{KL}$ function β such that

$$(\forall\ t_0 \geq 0)(\forall x_0 \in \mathbb{R}^n)(\|x(t)\| \leq \beta(\|x_0\|, t - t_0), \forall\ t \geq t_0), \tag{B.6}$$

- globally exponentially stable if it is globally asymptotically stable and there exist $k > 0$, $\gamma > 0$ such that

$$(\forall\ t_0 \geq 0)(\forall x_0 \in \mathbb{R}^n)(\|x(t)\| \leq k\|x_0\|\mathrm{e}^{-\gamma(t-t_0)}, \forall\ t \geq t_0), \tag{B.7}$$

- globally $\mathcal{K}$–exponentially stable if it is globally asymptotically stable and there exist a class $\mathcal{K}$ function h and a positive constant γ such that

$$(\forall\ t_0 \geq 0)(\forall x_0 \in \mathbb{R}^n)(\|x(t)\| \leq h(\|x_0\|)\mathrm{e}^{-\gamma(t-t_0)}, \forall\ t \geq t_0). \tag{B.8}$$

B.1 Lyapunov's direct method and extensions

Hereinafter, we denote by $B(x, h)$ a ball centred at x with radius $h > 0$.

Definition B.3. A continuous function $V(t, x)\colon \mathbb{R} \times \mathbb{R}^n \to \mathbb{R}^+$ is called *locally positive definite* if

$$(\exists \beta \in \mathcal{K},\, h > 0)\left(V(t, 0) = 0 \quad \text{and} \quad V(t, x) \geq \beta(\|x\|) \quad \forall x \in B(0, h) \quad \forall t \geq 0\right) \tag{B.9}$$

Additionally, if the above statement holds for all $x \in \mathbb{R}^n$ and if $\beta \in \mathcal{K}_\infty$, then

$V(t,x)$ is called *positive definite*.

Definition B.4. A function $V(t,x)\colon \mathbb{R}\times\mathbb{R}^n \to \mathbb{R}^+$ is said to be *locally decrescent* if it is continuous and if there exists $\beta \in \mathcal{K}$ such that

$$(\exists h > 0)(\forall t > 0)(\forall x \in B(0,h)) \quad (V(t,x) \leq \beta(\|x\|)) \tag{B.10}$$

Furthermore if h may be chosen arbitrarily, $V(t,x)$ is called semiglobally decrescent. Moreover, if (B.10) holds for $h \to \infty$, hence $\forall x \in \mathbb{R}^n$ then $V(t,x)$ is said to be globally decrescent.

In the sequel, we define the derivative of $V(t,x)$ along solutions of (B.1) by $\dot{V}(t,x) = \frac{\partial V}{\partial t}(t,x(t)) + \frac{\partial V}{\partial x} f(t,x(t))$.

Theorem B.5. Consider (B.1) and a function $V(t,x)$ along with its derivative, $\dot{V}(t,x)$, calculated along trajectories of (B.1). Then, the following holds.

1. If $V(t,x)$ is locally positive definite and there exists $h > 0$ such that $\dot{V}(t,x) \leq 0$ for $x \in B(0,h)$, then $x_e = 0$ is stable.
2. If $V(t,x)$ is locally positive definite and decrescent and there exists $h > 0$ such that $\dot{V}(t,x) \leq 0$ for $x \in B(0,h)$, then the equilibrium point $x_e = 0$ is uniformly stable.
3. If $V(t,x)$ is locally positive definite and decrescent and $-\dot{V}(t,x)$ is locally positive definite, then the equilibrium point $x_e = 0$ of (B.1) is uniformly asymptotically stable.

4. If $V(t,x)$ is positive definite and decrescent and $-\dot{V}(t,x)$ is positive definite, then the equilibrium point $x_e = 0$ of (B.1) is globally uniformly asymptotically stable.

Theorem B.6. $x_e = 0$ is a locally exponentially stable equilibrium point of (B.1) if and only if there exist $h > 0$ and positive constants α_1, α_2, α_3, α_4 and a continuously differentiable function $V(t,x)$ such that for all $x \in B(0,h)$

$$\begin{aligned} \alpha_1\|x\|^2 \leq V(t,x) &\leq \alpha_2\|x\|^2 \\ \dot{V}(t,x) &\leq -\alpha_3\|x\|^2 \\ \left\| \frac{\partial V(t,x)}{\partial x} \right\| &\leq \alpha_4\|x\| \end{aligned} \tag{B.11}$$

in which time derivatives of $V(t,x)$ are calculated along solutions of (B.1). Furthermore, if the conditions in (B.11) hold for all $x \in \mathbb{R}^n$, $x_e = 0$ is a globally exponentially stable equilibrium point of (B.1).

The Lyapunov method for analysing asymptotic stability of dynamic systems requires $-\dot{V}(t,x)$ to be (locally) positive definite. However, it is not a trivial problem to find such a Lyapunov function. Therefore, an extension to this method that allows for this condition to be relaxed is provided by the LaSalle Invariance Principle, first introduced by LaSalle (1960), (see also Khalil, 1996; LaSalle and Lefschetz, 1961; Sastry, 1999; Slotine and Li, 1991).

Definition B.7. A subset $M \subset \mathbb{R}^n$ of (B.1) is called an (positively) invariant set if

$$(\forall t_0 \in \mathbb{R})(\forall x_0 \in \mathbb{R}^n)\left((x_0 \in M) \implies (\forall t \geq t_0)(x(t,x_0) \in M)\right). \tag{B.12}$$

Note that given a set S containing an equilibrium, there exists a non–empty largest invariant set M contained in S.

Theorem B.8. Consider (B.1) where $f(t,x) = f(x)$ (autonomous case), a smooth function $V(x)$, its derivative $\dot{V}(x)$ along the dynamics (B.1) and a set Ω_c defined by

$$\Omega_c = \left\{ x \in \mathbb{R}^n \;\middle|\; V(x) \leq c \right\}. \tag{B.13}$$

Suppose that Ω_c is bounded and that for all $x \in \Omega_c$, $\dot{V}(x)$ is nonpositive. Furthermore, define a subset $S \subset \Omega_c$ containing elements of Ω_c, for which $\dot{V}(x)$ vanishes, i.e. $S = \left\{ x \in \Omega_c \,\middle|\, \dot{V}(x) = 0 \right\}$. If M is the largest invariant set in S then

$$(\forall t_0 \in \mathbb{R})(\forall x_0 \in \mathbb{R}^n) \left((x_0 \in \Omega_c) \implies (\forall t \geq t_0)(x(t, t_0, x_0) \to M \quad \text{as} \quad t \to \infty) \right). \tag{B.14}$$

Corollary B.9. *If there exists $h > 0$ such that $M \cap B(0,h) = \{0\}$, then the origin of* (B.1) *is an asymptotically stable equilibrium point.*

The above proposition is useful in the case of autonomous systems. For time varying systems, we may employ Barbalat's lemma .

Lemma B.10. (*verbatim* (Khalil, 1996)) Let $\phi\colon \mathbb{R} \to \mathbb{R}$ be a uniformly continuous function on $[0, \infty)$. Suppose that $\lim_{t\to\infty} \int_0^t \phi(\tau)\, d\tau$ exists and is finite. Then

$$\phi(t) \to 0 \quad \text{as} \quad t \to \infty. \tag{B.15}$$

To illustrate the Barbalat's lemma, consider $\phi(t)$ such that $\int_0^\infty \phi(\tau)\mathrm{d}\tau = \frac{2t+5}{3t+2} - \frac{5}{2}$. The limit $\lim_{t\to\infty} \left(\frac{2t+5}{3t+2} - \frac{5}{2} \right)$ exists and is finite and can easily be calculated as

$\lim_{t\to\infty}\left(\frac{2t+5}{3t+2}-\frac{5}{2}\right)=\frac{2}{3}-\frac{5}{2}=\frac{-11}{6}$. Therefore, by Barbalat's lemma we conclude that $\phi(t)$ converges to 0 as $t\to\infty$. Indeed, by differentiation of $\int_0^\infty\phi(\tau)\mathrm{d}\tau$ we have $\phi(t)=\frac{\mathrm{d}}{\mathrm{d}t}\left(\frac{2t+5}{3t+2}-\frac{5}{2}\right)=\frac{-11}{(3t+2)^2}$ which clearly vanishes as t goes to ∞.

Barbalat's lemma itself is a useful result but it requires checking uniform continuity which may not be straightforward. The following theorem - the invariance principle equivalent for non-autonomous systems - is a consequence of Barbalat's lemma in which the uniform continuity is not explicitly required.

Theorem B.11. (Khalil, 1996) Consider system (B.1), where $f(t,x)$ is globally Lipschitz in x, uniformly in t and piecewise continuous in t. Denote by $V(t,x)$ a continuously differentiable function satisfying

$$\begin{aligned} W_1(x)\le V(t,x)\le W_2(x),\\ \dot{V}(t,x)\le -W(x), \end{aligned} \tag{B.16}$$

where $W_1(x)$ and $W_2(x)$ are continuous positive definite functions, $W_1(x)$ is radially unbounded and $W(x)$ is a continuous positive semidefinite function. Then all solutions $x(t)$ of (B.1) fulfil

$$W(x)\to 0 \quad \text{as} \quad t\to\infty. \tag{B.17}$$

In the following theorem we study stability of an equilibrium point of a linear time varying system

$$\dot{x}=A(t)x, \qquad y=Cx \tag{B.18}$$

in which $x\in\mathbb{R}^n$, $y\in\mathbb{R}^p$, $A(t)$ is continuous and $C\in\mathbb{R}^{p\times n}$. For this sys-

tem, we define the observability Gramian of the pair $(A(t), C)$ as $W(t, t+\delta) = \int_t^{t+\delta} \Phi^T(\tau, t) C^T(\tau) C(\tau) \Phi(\tau, t) d\tau$, in which $\Phi(\tau, t)$ is the state transition matrix of (B.18) (see (Rugh, 1993)).

Theorem B.12. (Khalil, 1996) Consider a linear time–varying system (B.18). Let $V(t, x)$ be a continuously differentiable Lyapunov function candidate and furthermore, let us denote its derivative calculated along solutions of (B.18) by $\dot{V}(t, x)$, i.e. $\dot{V}(t, x) = \dfrac{\partial V}{\partial t}(t, x(t)) + \dfrac{\partial V}{\partial x} A(t) x$. Assume that

$$k_1 \|x\|^2 \leq V(t, x) \leq k_2 \|x\|^2 \tag{B.19}$$

$$\dot{V}(t, x) = -x^T C^T C x \leq 0 \tag{B.20}$$

$$W(t, t+\delta) \geq k_3 I \tag{B.21}$$

where k_1, k_2 and k_3 are positive constants, I is the identity matrix of appropriate dimensions and $W(t, t+\delta)$ is the observability Gramian of the pair $(A(t), C)$. Then the origin of (B.18) is a globally exponentially stable equilibrium point.

Remark B.13. Condition (B.21) is satisfied if the pair $(A(t), C)$ is completely uniformly observable, see (Khalil, 1996).

B.2 Stability of invariant sets

In this section we are concerned with some additional properties of the dynamic system (B.1) in which $x = \mathrm{col}(z, y)$ and the dynamics can be written as

$$\begin{aligned} \dot{z} &= f_z(t, z, y), \\ \dot{y} &= f_y(t, z, y), \end{aligned} \tag{B.22}$$

where $f_y(t, z, 0) = 0$. In particular, we are interested in partial stability of (B.22) that is the stability of an invariant set $\{x = \mathrm{col}(z, y) \mid y = 0\}$. In other words, the stability property refers to a part of the variables only, see (Fradkov et al., 1999; Shiriaev and Fradkov, 2001).

Definition B.14. (Fradkov et al., 1999; Shiriaev and Fradkov, 2001) The origin of (B.22) is y-stable or in other words the set $\{x = \mathrm{col}(z, y) \mid y = 0\}$ is stable if

$$(\forall \epsilon > 0)\,(\forall t_0 \geq 0)\,(\exists \delta(\epsilon, t_0) > 0)\,(\|x(t_0)\| \leq \delta \implies (\forall t \geq t_0)(\|y(t, t_0, x(t_0))\| \leq \epsilon)). \tag{B.23}$$

Definition B.15. (Bernfeld et al., 2003) The set $\{x = \mathrm{col}(z, y) \mid y = 0\}$ is globally asymptotically stable if it is stable and for all $x(t_0)$

$$\lim_{t \to \infty} \|y(t, t_0, x(t_0))\| = 0. \tag{B.24}$$

A convenient method of investigating stability of invariant sets is the Lyapunov function approach. It is described in the following lemma.

Lemma B.16. (Fradkov et al., 1999; Shiriaev and Fradkov, 2001) Consider the

dynamic system (B.22), where $x = \text{col}(z, y)$. If there exists a Lyapunov function candidate $V(t, x)$ such that $V(t, x) \leq W_1(y)$, where $W_1(\cdot)$ is a positive definite function, and $\dot{V}(t, x) \leq 0$ then the set $\{x = \text{col}(z, y) \mid y = 0\}$ is stable. If in addition $\dot{V}(t, x) \leq W_2(y) < 0$, for $y \neq 0$ and where $W_2(\cdot)$ is positive definite, then the set $\{x = \text{col}(z, y) \mid y = 0\}$ is globally asymptotically stable.

As with the Lyapunov method for stability of an equilibrium point of a dynamic system, it is not trivial in many cases to find a strict Lyapunov function. However, asymptotic stability of an invariant set can be established with the aid of a weak Lyapunov function and then using Barbalat's lemma (Lemma B.10) or the results in Theorem B.11, to demonstrate attractivity (B.24).

B.3 Stability of cascaded systems

This section is concerned with stability analysis of a cascaded system of the following form

$$\begin{aligned} \dot{x}_1 &= f_1(t, x_1) + g(t, x_1, x_2)x_2, \\ \dot{x}_2 &= f_2(t, x_2), \end{aligned} \tag{B.25}$$

where $x_1 \in \mathbb{R}^p$, $x_2 \in \mathbb{R}^r$. The vector field $f_1(t, x_1)$ is smooth while both $f_2(t, x_2)$ and $g(t, x_1, x_2)$ are continuous in t and locally Lipschitz continuous in x_2 while $g(t, x_1, x_2)$ is in addition continuous in x_1. Moreover, assume that $f_1(t, 0) = 0$ and $f_2(t, 0) = 0$.

The following theorem is based on the results of Panteley and Loria (1998); Pan-

teley et al. (1998) and Aneke (2003).

Theorem B.17. Assume the following

1. the equilibrium point $x_e^1 = 0$ of the subsystem $\dot{x}_1 = f_1(t, x_1)$ is globally uniformly asymptotically stable,
2. the equilibrium point $x_e^2 = 0$ of the subsystem $\dot{x}_2 = f_2(t, x_2)$ is globally uniformly asymptotically stable,
3. the matrix function $g(t, x_1, x_2)$ satifies $\|g(t, x_1, x_2\| \leq k_1(\|x_2\|)+k_2(\|x_2\|)\|x_1\|$, where $k_1,\ \ k_2 \colon \mathbb{R}_0^+ \to \mathbb{R}_0^+$.

Then, the origin of the system (B.25) is globally uniformly asymptotically stable.

Corollary B.18. *If both $\dot{x}_1 = f_1(t, x_1)$ and $\dot{x}_2 = f_2(t, x_2)$ are globally exponentially stable and Assumption 3 in Theorem B.17 holds for $g(t, x_1, x_2)$, the origin of the cascaded system* (B.25) *is globally $\mathcal{K}$–exponentially stable.*

The following proposition considers a special case of a globally uniformly asymptotically stable nominal system that is perturbed with a signal vanishing at the origin. We use this result for stability analysis of the origin of a cascaded system. It is taken *verbatim* from (Panteley et al., 2001, Proposition 3). In this result, by $\|\phi(t)\|_1$ we denote an $\mathcal{L}_1$ norm of a time signal $\phi(t)$ defined by

$$\|\phi(t)\|_1 = \int_{t_0}^{\infty} \|\phi(\tau)\| \mathrm{d}\tau. \tag{B.26}$$

Proposition B.18.1. Consider the system

$$\dot{x} = F_0(t, x) + K(t, x), \tag{B.27}$$

and suppose the origin is uniformly globally stable. Suppose also that

1. F_0 is locally Lipschitz, $F_0(\cdot, t)$ is locally Lipschitz uniformly if t, and the origin of the system $\dot{x} = F_0(t, x)$ is globally uniformly asymptotically stable;

2. $K\colon \mathbb{R}_0^+ \times \mathbb{R}^n \to \mathbb{R}^n$ is continuous and there exist a continuous function $h\colon \mathbb{R}^n \to \mathbb{R}^m$, nondecreasing functions $\beta, k_1, k_2\colon \mathbb{R}_0^+ \to \mathbb{R}_0^+$, a class $\mathcal{K}_\infty$ function k, and a continuous positive definite function γ such that

$$\|K(t, x)\| \leq k_1(\|x\|)k(\|h(t, x)\|), \tag{B.28}$$

$$\|h(t, x)\| \leq k_2(\|x\|), \tag{B.29}$$

   and such that for all $(t_0, x_0) \in \mathbb{R}_0^+ \times \mathbb{R}^n$, and defining $\bar{h}(t) := h(t, x(t))$, all solutions of (B.27) satisfy

$$\|\gamma(\|\bar{h}\|)\|_1 \leq \beta(\|x_0\|). \tag{B.30}$$

Under these conditions, the origin of the system (B.27) is globally uniformly asymptotically stable.

B.4 Backstepping

The backstepping technique (Khalil, 1996) is a very useful tool in designing asymptotically stabilising controllers for certain types of systems. We discuss this technique for the simplest type of system to which it can be applied. We consider a system of the following form

$$\begin{aligned} \dot{x} &= f(x) + g(x)y, \\ \dot{y} &= u, \end{aligned} \tag{B.31}$$

where $x \in \mathbb{R}^n$, $y \in \mathbb{R}$, $f(x)$, $g(x)$ are smooth vector fields, $f(0) = 0$ and $u \in \mathbb{R}$. The main idea of backstepping is to consider each subsystem of (B.31) separately. Assume that there exists a function $\Phi(x)$ satisfying $\Phi(0) = 0$ such that the origin is asymptotically stable for the first part of (B.31) with $y = \Phi(x)$:

$$\dot{x} = f(x) + g(x)\Phi(x). \tag{B.32}$$

Hence, there exists a smooth positive definite function $V(x)$ such that $\dot{V}(x) = \frac{\partial V}{\partial x}\big[f(x) + g(x)\Phi(x)\big] < 0$ outside the origin. While y is unavailable to be set as $y = \Phi(x)$, the following is true

$$\dot{x} = \big[f(x) + g(x)\Phi(x)\big] + g(x)\big(y - \Phi(x)\big) := \big[f(x) + g(x)\Phi(x)\big] + g(x)z, \tag{B.33}$$

where the equilibrium point of $\dot{x} = \big[f(x) + g(x)\Phi(x)\big]$ is known to be asymptotically stable by definition of $\Phi(x)$. Using (B.33), system (B.31) may be trans-

formed into

$$\begin{aligned} \dot{x} &= \big[f(x) + g(x)\Phi(x)\big] + g(x)z, \\ \dot{z} &= v, \end{aligned} \tag{B.34}$$

where $v = u - \dot{\Phi}(x, z)$. Consequently, consider the Lyapunov function candidate $\overline{V}(x, z) = V(x) + \frac{1}{2}z^2$ with its time derivative along solutions of (B.34) with $v = -\frac{\partial V}{\partial x}g(x)z - kz$ given by

$$\dot{\overline{V}} = \frac{\partial V}{\partial x}\big[f(x) + g(x)\Phi(x)\big] + \Big(\frac{\partial V}{\partial x}g(x) + v\Big)z \leq \frac{\partial V}{\partial x}\big[f(x) + g(x)\Phi(x)\big] - kz^2 \leq 0, \tag{B.35}$$

where $k > 0$. By Lyapunov's direct method, the origin of (B.34) is asymptotically stable and since $\Phi(0) = 0$, we have that the origin of (B.31) is also asymptotically stable with

$$u = v + \dot{\Phi} = -\Big(\frac{\partial V}{\partial x}g(x) + k\Big)\Big(y - \Phi(x)\Big) + \frac{\partial \Phi}{\partial x}\Big(f(x) + g(x)y\Big). \tag{B.36}$$

Appendix C

Graph theory

We employ the following graph theory definitions from (Godsil and Royle, 2001) in the thesis.

Definition C.1. A graph $\mathcal{G}$ is a triple $\mathcal{G} = (\mathcal{V}, \mathcal{E}, \mathcal{A})$ where $\mathcal{V}$ is an index set representing *vertices*, $\mathcal{E} \subset \mathcal{V} \times \mathcal{V}$ denotes *edges* such that an ordered pair $(i, j) \in \mathcal{E}$ iff there is an edge between two vertices $i, j \in \mathcal{V}$, and $\mathcal{A}$ is the *adjacency matrix* which has entries a_{ij} such that

$$a_{ij} = \begin{cases} w_{ij} & \text{if } (i,j) \in \mathcal{E}, \\ 0 & \text{otherwise,} \end{cases} \tag{C.1}$$

in which $w_{ij} > 0$ is a weight. Hence, for all $i, j \in \mathcal{V}$ we have $(i, j) \in \mathcal{E}$ iff $a_{ij} \neq 0$.

Definition C.2. $N_i \subset \mathcal{V}$ is the set of neighbours of vertex $i \in \mathcal{V}$ defined by

$$N_i = \left\{ j \in \mathcal{V} \,\middle|\, j \neq i \text{ and } a_{ij} \neq 0 \right\}. \tag{C.2}$$

Definition C.3. The Laplacian matrix $\mathcal{L}$ associated with the graph $\mathcal{G}$ is an $n \times n$ matrix whose elements l_{ij} are defined as follows

$$l_{ij} = \begin{cases} \sum\limits_{\substack{k=1 \\ k \neq i}}^{n} a_{ik} & \text{if } j = i, \\ -a_{ij} & \text{otherwise.} \end{cases} \tag{C.3}$$

Definition C.4. A graph $\mathcal{G}$ is called *undirected* if $(i, j) \in \mathcal{E}$ whenever $(j, i) \in \mathcal{E}$. It is said to be *connected* if any two vertices may be connected by a path regardless of the sequence of the vertices involved en route. Otherwise the graph is said to be *disconnected*.

Appendix D

E-Puck mobile robot

The information in this appendix is based on (Mondada and Bonani, 2007; Mondada et al., 2009).

The E-Puck mobile robot, see Figure D.1, is an educational unicycle-type mobile robot developed at École Polytechnique Fédérale de Lausanne. It was built in response to the need for a desktop size, open source hardware and software robot which is reasonably priced and is user-friendly.

The E-Puck design consists of a Microchip dsPIC microcontroller which has a CPU running at 64 MHz and is fitted with a version of a GCC C compiler. The RAM available on E-Pucks is 8 kB and the flash memory is 144 kB. The E-Pucks are also equipped with eight IR proximity sensors for the robot to be able to sense other E-Pucks as well as any other obstacles. Moreover, a 3D accelerometer is mounted, which might be used to verify the angle of inclination as well as, for

Figure D.1: E-Puck robot. Photo from (Mondada and Bonani, 2007).

instance, to recognise a possible collision. The robot is differentially driven by means of two stepper motors which are such that a single revolution of a robot's wheel is made out of 1000 steps of the motor. Moreover, the robot is furnished with three microphones and a camera.

The user interface includes two LEDs to indicate the battery status of the robot and an RS232 input to connect the robot to a PC. As an alternative, a BlueTooth communication link is provided to be used for connection of the robots with a PC. This also allows for a robot to communicate with up to 7 other E-Pucks.

The diameter of an E-Puck robot is 75 mm and the height is about 50 mm with the addition of the size of the various extensions used (e.g. a camera, an IR distance scanner). The main body of the robot is made out of injected plastic parts which surround the battery. The maximum applicable forward speed is 0.13 $\frac{\mathrm{m}}{\mathrm{s}}$ and the maximum angular velocity is 1.7 $\frac{\mathrm{rad}}{\mathrm{s}}$.

References

S. Adinandra. private communication, 2012.

A. Alvarez Aguirre. *Remote Control and Motion Coordination of Mobile Robots*. PhD thesis, Eindhoven University of Technology, the Netherlands, 2011.

E. Aneke. *Control of Underactuated Mechanical Systems*. PhD thesis, Technische Universiteit Eindhoven, 2003.

T. Arai, E. Pagello, and L. E. Parker. Guest editorial: advances in multirobot systems. *IEEE Transactions on Robotics and Automation*, 18(5):655–661, 2002.

R. C. Arkin, A. K., W. A., and F. Cervantes-Pérez. Behavioral models of the praying mantis as a basis for robotic behavior. *Robotics and Autonomous Systems*, 32:39–60, 2000.

T. Balch and R. C. Arkin. Behavior-based formation control for multirobot teams. *IEEE Transactions on Robotics and Automation*, 14(6):926–939, 1998.

S. R. Bernfeld, C. Corduneanu, and A. O. Ignatyev. On the stability of invariant sets of functional differential equations. *Nonlinear Analysis: Theory, Methods & Applications*, 55(6):641–656, 2003.

I. I. Blekhman. *Synchronization in Science and Technology*. ASME Press, New York, 1988.

I. I. Blekhman, A. L. Fradkov, H. Nijmeijer, and A. Y. Pogromsky. On self-synchronization and controlled synchronization. *Systems & Control Letters*, 31 (5):299–305, 1997.

I. I. Blekhman, A. L. Fradkov, O. P. Tomchina, and D. E. Bogdanov. Self-synchronization and controlled synchronization: general definition and example design. *Mathematics and Computers in Simulation*, 58(4-6):367–384, 2002.

P.-A. Bliman and G. Ferrari-Trecate. Average consensus problems in networks of agents with delayed communications. *Automatica*, 44(8):1985–1995, 2008.

A. M. Bloch. *Nonholonomic Mechanics and Control*. Springer-Verlag, Berlin, 2003.

Y. Bouteraa, J. Ghommam, G. Poisson, and N. Derbel. Distributed synchronization control to trajectory tracking of multiple robot manipulators. *Journal of Robotics*, 2011.

M. S. Branicky. Multiple Lyapunov functions and other analysis tools for switched and hybrid systems. *IEEE Transactions on Automatic Control*, 43(4):475–482, 1998.

R. A. Brooks. A robust layered control system for a mobile robot. *IEEE Journal of Robotics and Automation*, 2(1):14–23, 1986.

J. B. Buck. Synchronous rhythmic flashing of fireflies. *The Quarterly Review of Biology*, 13(3):301–314, 1938.

J. B. Buck and E. Buck. Mechanism of Rhythmic Synchronous Flashing of Fireflies: Fireflies of Southeast Asia may use anticipatory time-measuring in synchronizing their flashing. *Science*, 159(3821):1319–1327, 1968.

W. Burgard, M. Moors, C. Stachniss, and F. E. Schneider. Coordinated multi-robot exploration. *IEEE Transactions on Robotics*, 21(3):376–386, 2005.

M. Burger. *Disturbance Rejection using Conditional Integrators: Applications to path manoeuvring under environmental disturbances for single vessels and vessel formations*. PhD thesis, Norwegian University of Science and Technology, 2011.

J. Caarls, P. P. Jonker, Y. Kolstee, J. Rotteveel, and W. van Eck. Augmented reality for art, design and cultural heritage – system design and evaluation. *EURASIP J. Image and Video Processing*, 2009.

G. Campion and W. Chung. Wheeled robots. In B. Siciliano and O. Khatib, editors, *Springer Handbook of Robotics*, pages 391–410. Springer, Berlin, Heidelberg, 2008.

G. Campion, B. d'Andrea Novel, and G. Bastin. Modelling and state feedback control of nonholonomic mechanical systems. In *Proceedings of the 30th IEEE Conference on Decision and Control*, pages 1184–1189, 1991.

Y. U. Cao, A. S. Fukunaga, and A. B. Kahng. Cooperative mobile robotics: Antecedents and directions. *Autonomous Robots*, 4:226–234, 1997.

C. C. Cheah, S. P. Hou, and J. J. E. Slotine. Region-based shape control for a swarm of robots. *Automatica*, 45(10):2406–2411, 2009.

J. Chen, D. Sun, J. Yang, and H. Chen. Leader-follower formation control of multiple non-holonomic mobile robots incorporating a receding-horizon scheme. *International Journal of Robotics Research*, 29(6):727–747, 2010.

J. Y. Chen, K. W. Wong, L. M. Cheng, and J. W. Shuai. A secure communication scheme based on the phase synchronization of chaotic systems. *Chaos*, 13:508–514, 2003.

Y. Q. Chen and Z. Wang. Formation control: a review and a new consideration. In *IEEE/RSJ International Conference on Intelligent Robots and Systems (IROS 2005)*, pages 3181–3186, 2005.

S.-J. Chung and J. J. E. Slotine. Cooperative robot control and concurrent synchronization of lagrangian systems. *IEEE Transactions on Robotics*, 25 (3):686–700, 2009.

L. Consolini, F. Morbidi, D. Prattichizzo, and M. Tosques. A geometric characterization of leader-follower formation control. In *Proceedings of the ICRA'07 IEEE International Conference on Robotics and Automation*, pages 2397–2402, 2007.

CRASAR, 2012. URL `http://crasar.org/`.

T. B. Curtin and J. G. Bellingham. Progress toward autonomous ocean sampling networks. *Deep Sea Research Part II: Topical Studies in Oceanography*, 56(3-5): 62–67, 2009.

T. B. Curtin, J. G. Bellingham, J. Catipovic, and D. Webb. Autonomous oceanographic sampling networks time. *Oceanography*, 6(3), 1993.

M. C. De Gennaro and A. Jadbabaie. Formation control for a cooperative multi-agent system using decentralized navigation functions. In *Proceedings of the American Control Conference*, pages 1346–1351, 2006.

M. C. De Gennaro, L. Iannelli, and F. Vasca. Formation control and collision avoidance in mobile agent systems. In *Proceedings of the IEEE International Symposium on Intelligent Control, Mediterranean Conference on Control and Automation*, pages 796–801, 2005.

A. De Luca, G. Oriolo, and C. Samson. Feedback control of a nonholonomic car-like robot. In J. Laumond, editor, *Robot Motion Planning and Control*, volume 229, pages 171–253. Springer Berlin / Heidelberg, 1998.

C. C. de Wit, G. Bastin, and B. Siciliano, editors. *Theory of Robot Control*. Springer-Verlag New York, Inc., Secaucus, NJ, USA, 1996.

P. DeLellis, M. diBernardo, F. Garofalo, and D. Liuzza. Analysis and stability of consensus in networked control systems. *Applied Mathematics and Computation*, 217(3):988–1000, 2010.

J. P. Desai, J. Ostrowski, and V. Kumar. Controlling formations of multiple mobile robots. In *Proceedings of the IEEE International Conference on Robotics and Automation*, volume 4, pages 2864–2869, 1998.

J. P. Desai, J. P. Ostrowski, and V. Kumar. Modeling and control of formations of nonholonomic mobile robots. *IEEE Transactions on Robotics and Automation*, 17(6):905–908, 2001.

D. V. Dimarogonas and K. J. Kyriakopoulos. Formation control and collision

avoidance for multi-agent systems and a connection between formation infeasibility and flocking behavior. In *Proceedings of the 44th IEEE Conference on Decision and Control and European Control Conference. CDC-ECC '05*, pages 84–89, 2005.

D. V. Dimarogonas and K. J. Kyriakopoulos. Distributed cooperative control and collision avoidance for multiple kinematic agents. In *Proceedings of the 45th IEEE Conference on Decision and Control*, pages 721–726, 2006.

D. V. Dimarogonas and K. J. Kyriakopoulos. On the rendezvous problem for multiple nonholonomic agents. *IEEE Transactions on Automatic Control*, 52 (5):916–922, 2007.

D. K. Do and J. Pan. Nonlinear formation control of unicycle-type mobile robots. *Robotics and Autonomous Systems*, 55(3):191–204, 2007.

W. Dong. Robust formation control of multiple wheeled mobile robots. *Journal of Intelligent & Robotic Systems*, 62:547–565, 2011.

W. Dong and J. A. Farrell. Cooperative control of multiple nonholonomic mobile agents. *IEEE Transactions on Automatic Control*, 53(6):1434–1448, 2008.

W. Dong, Y. Guo, and J. A. Farrell. Formation control of nonholonomic mobile robots. In *Proceedings of the American Control Conference*, pages 5602–5607, 2006.

R. Dougherty, V. Ochoa, Z. Randles, and C. Kitts. A behavioral control approach to formation-keeping through an obstacle field. In *Proceedings of the IEEE Aerospace Conference*, pages 168–175, 2004.

H. Endres, W. Feiten, and G. Lawitzky. Field test of a navigation system: autonomous cleaning in supermarkets. In *Proceedings of the ICRA '98. IEEE International Conference on Robotics and Automation*, volume 2, pages 1779–1781, 1998.

R. Fierro and F. L. Lewis. Control of a nonholonomic mobile robot: Backstepping kinematics into dynamics. *Journal of Robotic Systems*, 14(3):149–163, 1997.

R. S. Fisher, W. van Emde Boas, W. Blume, C. Elger, P. Genton, P. Lee, and J. Engel Jr. Epileptic seizures and epilepsy: Definitions proposed by the International League Against Epilepsy (ILAE) and the International Bureau for Epilepsy (IBE). *Epilepsia*, 46(4):470–472, 2005.

M. Fliess, J. Lévine, P. Martin, and P. Rouchon. Flatness and defect of non-linear systems: introductory theory and examples. *International Journal of Control*, 61(6):1327–1361, 1995.

F. A. C. C. Fontes. A general framework to design stabilizing nonlinear model predictive controllers. *Systems & Control Letters*, 42(2):127–143, 2001.

A. Forouzantabar, H. A. Talebi, and A. K. Sedigh. Bilateral control of master–slave manipulators with constant time delay. *Proceedings of the American Control Conference*, pages 1133–1138, 2011.

A. L. Fradkov, I. V. Miroshnik, and V. O. Nikiforov. *Nonlinear and adaptive control of complex systems*. Kluwer Academic Publishers, Dordrecht, the Netherlands, 1999.

C. Godsil and G. Royle. *Algebraic Graph Theory*, volume 207 of *Graduate Texts in Mathematics*. Springer, 2001.

E. Guizzo. Japan earthquake: Robots help search for survivors, 2011. URL `http://spectrum.ieee.org/automaton/robotics/industrial-robots/japan-earthquake-robots-help-search-for-survivors`. Accessed on 10/10/2011.

V. C. Gungor and G. P. Hancke. Industrial wireless sensor networks: Challenges, design principles, and technical approaches. *IEEE Transactions on Industrial Electronics*, 56(10):4258–4265, 2009.

K. Hatazaki, M. Konyo, K. Isaki, S. Tadokoro, and F. Takemura. Active scope camera for urban search and rescue. In *Proceedings of the IEEE/RSJ International Conference on Intelligent Robots and Systems*, pages 2596–2602, 2007.

J. P. Hespanha. Uniform stability of switched linear systems: extensions of lasalle's invariance principle. *IEEE Transactions on Automatic Control*, 49 (4):470–482, 2004.

J. P. Hespanha, D. Liberzon, D. Angeli, and E. D. Sontag. Nonlinear norm-observability notions and stability of switched systems. *IEEE Transactions on Automatic Control*, 50(2):154–168, 2005.

R. A. Horn and C. R. Johnson. *Matrix Analysis*. Cambridge University Press, 1990.

S. P. Hou, C. C. Cheah, and J. J. E. Slotine. Dynamic region following for-

mation control for a swarm of robots. In *Proceedings of the ICRA'09 IEEE International Conference on Robotics and Automation*, pages 1929–1934, 2009.

D. F. Hougen, S. Benjaafar, J. C. Bonney, J. R. Budenske, M. Dvorak, M. Gini, H. French, D. G. Krantz, P. Y. Li, F. Malver, B. Nelson, N. Papanikolopoulos, P. E. Rybski, S. A. Stoeter, R. Voyles, and K. B. Yesin. A miniature robotic system for reconnaissance and surveillance. In *Proceedings of the ICRA '00. IEEE International Conference on Robotics and Automation*, volume 1, pages 501–507, 2000.

T. Howsman, M. Craft, D. O'Neil, and J. T. Howell. A biologically inspired cooperative multi-robot control architecture. *NASA*, 2002.

M. A. Hsieh, Á. M. Halász, S. Berman, and V. Kumar. Biologically inspired redistribution of a swarm of robots among multiple sites. *Swarm Intelligence*, 2:121–141, 2008.

H. C.-H. Hsu and A. Liu. Multiagent-based multi-team formation control for mobile robots. *Journal of Intelligent & Robotic Systems*, 42:337–360, 2005.

Q. Hui and W. M. Haddad. Distributed nonlinear control algorithms for network consensus. *Automatica*, 44(9):2375–2381, 2008.

H. Huijberts, H. Nijmeijer, and T. Oguchi. Anticipating synchronization of chaotic Lur'e systems. *Chaos: An Interdisciplinary Journal of Nonlinear Science*, 17(1):013117, 2007.

I.-A. F. Ihle, J. Jouffroy, and T. I. Fossen. Formation control of marine surface

craft: A lagrangian approach. *IEEE Journal of Oceanic Engineering,*, 31(4): 922–934, 2006.

Y. Inada. Steering mechanism of fish schools. *Complexity International*, 8:1–9, 2001.

P. A. Ioannou and J. Sun. *Robust adaptive control*. Prentice-Hall, Inc., Upper Saddle River, NJ, USA, 1995.

A. Isidori. *Nonlinear Control Systems*. Springer-Verlag, London, UK, third edition, 2000.

A. Jadbabaie, J. Lin, and A. S. Morse. Coordination of groups of mobile autonomous agents using nearest neighbor rules. *IEEE Transactions on Automatic Control*, 48(6):988–1001, 2003.

M. Jager and B. Nebel. Dynamic decentralized area partitioning for cooperating cleaning robots. In *Proceedings of the ICRA '02. IEEE International Conference on Robotics and Automation*, volume 4, pages 3577–3582, 2002.

J. Jakubiak, E. Lefeber, K. Tchoń, and H. Nijmeijer. Two observer-based tracking algorithms for a unicycle mobile robot. *International Journal of Applied Mathematics and Computer Science*, 12(4):513–522, 2002.

J.-R. Jiang, Y.-L. Lai, and F.-C. Deng. Mobile robot coordination and navigation with directional antennas in positionless wireless sensor networks. In *Proceedings of the International Conference on Mobile Technology, Applications, and Systems*, pages 80:1–80:7, 2008.

Z.-P. Jiang and H. Nijmeijer. Tracking control of mobile robots: A case study in backstepping. *Automatica*, 33(7):1393–1399, 1997.

B. Jung and G. S. Sukhatme. Tracking targets using multiple robots: The effect of environment occlusion. *Autonomous Robots*, 13(3):191–205, 2002.

T. Kamegawa, K. Saikai, S. Suzuki, A. Gofuku, S. Oomura, T. Horikiri, and F. Matsuno. Development of grouped rescue robot platforms for information collection in damaged buildings. In *Proceedings of the SICE Annual Conference*, pages 1642–1647, 2008.

T. Kamegawa, N. Sato, M. Hatayama, Y. Uo, and F. Matsuno. System integration for grouped rescue robots systemn using robohoc network. In *Proceedings of the IROS'10 Workshop on Robots and Sensors integration in future rescue INformation system ROSIN'10*, 2010.

T. Kamegawa, N. Sato, M. Hatayama, Y. Uo, and F. Matsuno. Design and implementation of grouped rescue robot system using self-deploy networks. *Journal of Field Robotics*, 2011.

Y. Kanayama, Y. Kimura, F. Miyazaki, and T. Noguchi. A stable tracking control method for an autonomous mobile robot. In *Proceedings of the ICRA'90. IEEE International Conference on Robotics and Automation*, pages 384–389, 1990.

G. A. Kantor, S. Singh, R. Peterson, D. Rus, A. Das, V. Kumar, G. Pereira, and J. Spletzer. Distributed search and rescue with robot and sensor teams. In *Proceedings of the 4th International Conference on Field and Service Robotics*, 2003.

H. K. Khalil. *Nonlinear Systems*. Macmillan, New York, 1996.

E. Klarreich. Discovery of coupled oscillation put 17th-century scientist ahead of his time. *Society for Industrial and Applied Mathematics News*, 35(8), 2002.

A. Kolling and S. Carpin. Multirobot cooperation for surveillance of multiple moving targets - a new behavioral approach. In *Proceedings of the ICRA'06 IEEE International Conference on Robotics and Automation*, pages 1311–1316, 2006.

D. Kostić, S. Adinandra, J. Caarls, N. van de Wouw, and H. Nijmeijer. Collision-free tracking control of unicycle mobile robots. In *Proceedings of the 48th IEEE Conference on Decision and Control*, pages 5667–5672, 2009.

D. Kostić, S. Adinandra, J. Caarls, and H. Nijmeijer. Collision-free motion coordination of unicycle multi-agent systems. In *Proceedings of the American Control Conference*, pages 3186–3191, 2010a.

D. Kostić, S. Adinandra, J. Caarls, N. van de Wouw, and H. Nijmeijer. Saturated control of time-varying formations and trajectory tracking for unicycle multi-agent systems. In *Proceedings of the 49th IEEE Conference on Decision and Control*, pages 4054–4059, 2010b.

U. Kumar and N. Sukavanam. Backstepping based trajectory tracking control of a four wheeled mobile robot. *International Journal of Advanced Robotic Systems*, 5:403–410, 2008.

V. Kumar, D. Rus, and G. S. Sukhatme. Networked robots. In B. Siciliano and

O. Khatib, editors, *Springer Handbook of Robotics*, pages 943–958. Springer, 2008.

G. Lafferriere, A. Williams, J. Caughman, and J. J. P. Veerman. Decentralized control of vehicle formations. *Systems & Control Letters*, 54(9):899–910, 2005.

E. Lalish, K. A. Morgansen, and T. Tsukamaki. Formation tracking control using virtual structures and deconfliction. In *Proceedings of the 45th IEEE Conference on Decision and Control*, pages 5699–5705, 2006.

J. LaSalle. Some extensions of Liapunov's second method. *IRE Transactions on Circuit Theory*, 7(4):520–527, 1960.

J. P. LaSalle and S. Lefschetz. *Stability by Liapunovs's Direct Method*. Academic Press, New York, 1961.

J.-P. Laumond, editor. *Robot Motion Planning and Control*, volume 229. Springer Berlin / Heidelberg, 1998.

J. R. T. Lawton and R. W. Beard. Synchronized multiple spacecraft rotations. *Automatica*, 38:1359–1364, 2002.

J. R. T. Lawton, R. W. Beard, and B. J. Young. A decentralized approach to formation maneuvers. *IEEE Transactions on Robotics and Automation*, 19(6): 933–941, 2003.

E. Lefeber. *Tracking Control of Nonlinear Mechanical Systems*. PhD thesis, Universiteit Twente, 2000.

E. Lefeber and H. Nijmeijer. Adaptive tracking control of nonholonomic systems: an example. In *Proceedings of the 38th IEEE Conference on Decision and Control*, volume 3, pages 2094–2099, 1999.

E. Lefeber, A. Robertsson, and H. Nijmeijer. Linear controllers for exponential tracking of systems in chained-form. *International Journal of Robust and Nonlinear Control*, 10:243–263, 2000.

W. Leroquais and B. d'Andrea Novel. Transformation of the kinematic models of restricted mobility wheeled mobile robots with a single platform into chain forms. In *Proceedings of the 34th IEEE Conference on Decision and Control*, volume 4, pages 3811–3816, 1995.

M. A. Lewis and K.-H. Tan. High precision formation control of mobile robots using virtual structures. *Autonomous Robots*, 4:387–403, 1997.

X. Li, J. Xiao, and Z. Cai. Backstepping based multiple mobile robots formation control. In *Proceedings of the IEEE/RSJ International Conference on Intelligent Robots and Systems, (IROS 2005)*, pages 887–892, 2005.

Y. Li, M. T. Thai, and W. Wu, editors. *Wireless Sensor Networks and Applications*. Springer US, 2008.

J. Lin, A. S. Morse, and B. D. O. Anderson. The multi-agent rendezvous problem. In *Proceedings of the 42nd IEEE Conference on Decision and Control*, volume 2, pages 1508–1513, 2003.

A. Loria, E. Panteley, and A. Teel. A new persistency–of–excitation condition for

UGAS of NLTV systems: Application to stabilization of nonholonomic systems. In *Proceedings of 5th European Control Conference*, 1999. paper no. 500.

J. Lu and L. J. Brown. A multiple Lyapunov functions approach for stability of switched systems. In *Proceedings of the American Control Conference*, pages 3253–3256, 2010.

S. Luke, K. Sullivan, L. Panait, and G. Balan. Tunably decentralized algorithms for cooperative target observation. In *AAMAS '05: Proceedings of the fourth international joint conference on Autonomous agents and multiagent systems*, pages 911–917. ACM, 2005.

S. Mastellone, D. M. Stipanović, and M. W. Spong. Remote formation control and collision avoidance for multi-agent nonholonomic systems. In *Proceedings of the ICRA'07 IEEE International Conference on Robotics and Automation*, pages 1062–1067, 2007.

S. Mastellone, D. M. Stipanović, C. R. Graunke, K. A. Intlekofer, and M. W. Spong. Formation control and collision avoidance for multi-agent nonholonomic systems: Theory and experiments. *The International Journal of Robotics Research*, 27(1):107–126, 2008.

D. Mayne and H. Michalska. Receding horizon control of nonlinear systems. *IEEE Transactions on Automatic Control*, 35(7):814–824, 1990.

D. Mayne, J. Rawlings, C. Rao, and P. Scokaert. Constrained model predictive control: Stability and optimality. *Automatica*, 36(6):789–814, 2000.

A. Micaelli and C. Samson. Trajectory tracking for unicycle-type and two-steering-wheels mobile robots. Technical report, INRIA, 1993.

H. Michalska and D. Mayne. Receding horizon control of nonlinear systems. In *Proceedings of the 28th IEEE Conference on Decision and Control, 1989.*,, pages 107–108, 1989.

P. Miller. The genius of swarms. *National Geographic Magazine*, 2007.

F. Mondada and M. Bonani. E-puck education robot, 2007. URL `http://www.e-puck.org/`.

F. Mondada, M. Bonani, X. Raemy, J. Pugh, C. Cianci, A. Klaptocz, S. Magnenat, J.-C. Zufferey, D. Floreano, and A. Martinoli. The e-puck, a robot designed for education in engineering. In *Proceedings of the 9th Conference on Autonomous Robot Systems and Competitions*, pages 59–65, 2009.

P. Morin and C. Samson. Trajectory tracking for nonholonomic vehicles. In K. Kozlowski, editor, *Robot Motion and Control*, volume 335 of *Lecture Notes in Control and Information Sciences*, pages 3–23. 2006.

P. Morin and C. Samson. Motion control of wheeled mobile robots. In B. Siciliano and O. Khatib, editors, *Springer Handbook of Robotics*, pages 799–826. Springer, 2008.

E. Mosekilde, Y. Maistrenko, and D. Postnov. *Chaotic Synchronization: Applications to Living Systems*. World Scientific, Singapore, 2002.

N. Moshtagh and A. Jadbabaie. Distributed geodesic control laws for flocking

of nonholonomic agents. *IEEE Transactions on Automatic Control*, 52(4):681–686, 2007.

R. R. Murphy. Human-robot interaction in rescue robotics. *IEEE Transactions on Systems, Man, and Cybernetics, Part C: Applications and Reviews*, 34(2): 138–153, 2004.

R. M. Murray and S. S. Sastry. Nonholonomic motion planning: steering using sinusoids. *IEEE Transactions on Automatic Control*, 38(5):700–716, 1993.

R. M. Murray, S. S. Sastry, and L. Zexiang. *A Mathematical Introduction to Robotic Manipulation*. CRC Press, Inc., Boca Raton, FL, USA, 1st edition, 1994.

K. S. Narendra and A. M. Annaswamy. *Stable Adaptive Systems*. Prentice Hall, Englewood Cliffs, NJ, 1989.

National Geographic, 2011. URL `http://nationalgeographic.com/`.

H. Nijmeijer. A dynamical control view on synchronization. *Physica D: Nonlinear Phenomena*, 154(3-4):219–228, 2001.

H. Nijmeijer and T. Oguchi. Anticipating synchronization of of nonlinear systems with uncertainties. volume 6, 2006.

E. Nuño, R. Ortega, N. Barabanov, and L. Basañez. A globally stable PD controller for bilateral teleoperators. *IEEE Transactions on Robotics*, 24(3):753–758, 2008.

E. Nuño, L. Basañez, and R. Ortega. Adaptive control for the synchronization of multiple robot manipulators with coupling time-delays. In *Proceedings of the*

IEEE/RSJ International Conference on Intelligent Robots and Systems, (IROS 2010), pages 3308–3313, 2010.

R. Olfati-Saber. Flocking for multi-agent dynamic systems: algorithms and theory. *IEEE Transactions on Automatic Control*, 51(3):401–420, 2006.

R. Olfati-Saber and R. M. Murray. Consensus protocols for networks of dynamic agents. *Proceedings of the American Control Conference*, 2:951–956, 2003a.

R. Olfati-Saber and R. M. Murray. Flocking with obstacle avoidance: cooperation with limited communication in mobile networks. In *Proceedings of the 42nd IEEE Conference on Decision and Control*, volume 2, pages 2022–2028, 2003b.

R. Olfati-Saber and R. M. Murray. Consensus problems in networks of agents with switching topology and time-delays. *IEEE Transactions on Automatic Control*, 49(9):1520–1533, 2004.

R. Olfati-Saber, J. A. Fax, and R. M. Murray. Consensus and cooperation in networked multi-agent systems. *Proceedings of the IEEE*, 95(1):215–233, 2007.

E. Panteley and A. Loria. On global uniform asymptotic stability of nonlinear time-varying systems in cascade. *Systems & Control Letters*, 33(2):131–138, 1998.

E. Panteley, E. Lefeber, A. Loria, and H. Nijmeijer. Exponential tracking control of a mobile car using a cascaded approach. In *Proceedings of the IFAC Workshop on Motion Control*, pages 221–226, 1998.

E. Panteley, A. Loria, and A. Teel. Relaxed persistency of excitation for uniform

asymptotic stability. *IEEE Transactions on Automatic Control*, 46(12):1874–1886, 2001.

L. E. Parker. Multiple mobile robot systems. In B. Siciliano and O. Khatib, editors, *Springer Handbook of Robotics*, pages 921–941. Springer, 2008.

A. S. Pikovsky, M. G. Rosenblum, M. A. Zaks, and J. Kurths. Phase synchronization of regular and chaotic oscillators. In H. Schuster, editor, *Handbook of Chaos Control*, pages 305–328. Wiley-VCH, 1999.

A. S. Pikovsky, M. G. Rosenblum, and J. Kurths. Phase synchronization in regular and chaotic systems. *International Journal of Bifurcaation and Chaos*, 10(10):2291–2305, 2000.

S. A. P. Ramaswamy and S. N. Balakrishnan. Formation control of car-like mobile robots: A Lyapunov function based approach. In *Proceedings of the American Control Conference*, pages 657–662, 2008.

W. Ren. Consensus strategies for cooperative control of vehicle formations. *Control Theory & Applications, IET*, 1(2):505–512, 2007a.

W. Ren. Multi-vehicle consensus with a time-varying reference state. *Systems & Control Letters*, 56(7-8):474–483, 2007b.

W. Ren and R. W. Beard. Virtual structure based spacecraft formation control with formation feedback. In *AIAA Guidance, Navigation, and Control Conference*, 2002. AIAA 2002–4963.

W. Ren and R. W. Beard. A decentralized scheme for spacecraft formation flying

via the virtual structure approach. In *Proceedings of the American Control Conference*, volume 2, pages 1746–1751, 2003.

W. Ren and R. W. Beard. Formation feedback control for multiple spacecraft via virtual structures. *IEE Proceedings - Control, Theory and Applications*, 151 (3):357–368, 2004.

W. Ren and N. Sorensen. Distributed coordination architecture for multi-robot formation control. *Robotics and Autonomous Systems*, 56(4):324–333, 2008.

W. Ren, R. W. Beard, and E. M. Atkins. A survey of consensus problems in multi-agent coordination. *Proceedings of the American Control Conference*, pages 1859–1864, 2005.

C. W. Reynolds. Flocks, herds, and schools: A distributed behavioral model. *Computer Graphics*, 21(4):25–34, 1987.

A. Rodriguez-Angeles. *Synchronization of Mechanical Systems*. PhD thesis, Eindhoven University of Technology, 2002.

A. Rodriguez-Angeles and H. Nijmeijer. Co-ordination of two robot manipulators via nonlinear estimated state feedback. In *Proceedings of the 5th IFAC Symposium Nonlinear Control Systems*, pages 255–260, 2001a.

A. Rodriguez-Angeles and H. Nijmeijer. Coordination of two robot manipulators based on position measurements only. *International Journal of Control*, 74: 1311–1323, 2001b.

A. Rodriguez-Angeles and H. Nijmeijer. *Synchronization of Mechanical Systems*. World Scientific Publishing Co., Singapore, 2003.

A. Rodriguez-Angeles and H. Nijmeijer. Mutual synchronization of robots via estimated state feedback: A cooperative approach. *IEEE Transactions on Control Systems Technology*, 12(4):542–554, 2004.

M. G. Rosenblum, A. S. Pikovsky, and J. Kurths. Phase synchronization of chaotic oscillators. *Physical Review Letters*, 76(11):1804–1807, 1996.

W. J. Rugh. *Linear System Theory*. Prentice Hall, Englewood Cliffs, New Jersey, 1993.

D. Rus, B. Donald, and J. Jennings. Moving furniture with teams of autonomous robots. In *Proceedings of the EEE/RSJ International Conference on Intelligent Robots and Systems (IROS 1995)*, volume 1, pages 235–242, 1995.

A. Sadowska, H. Huijberts, D. Kostić, N. van den Wouw, and H. Nijmeijer. Formation control of unicycle robots using the virtual structure approach. In *Proceedings of the 15th International Conference on Advanced Robotics, (ICAR 2011)*, pages 365–370, 2011a.

A. Sadowska, T. H. A. van den Broek, H. Huijberts, D. Kostić, N. van den Wouw, and H. Nijmeijer. A virtual structure approach to formation control of unicycle mobile robots using mutual coupling. *International Journal of Control*, 84(11): 1886–1902, 2011b.

A. Sadowska, D. Kostić, N. van de Wouw, H. Nijmeijer, , and H. Huijberts. Design and implementation of distributed formation controllers for unicycle mobile agents. *in preparation*, 2012a.

A. Sadowska, D. Kostić, N. van den Wouw, H. Huijberts, and H. Nijmeijer. Distributed formation control of unicycle robots. In *Proceedings of the ICRA'12 International Conference on Robotics and Automation*, pages 1564–1569, 2012b.

S. Sastry. *Nonlinear Systems; Analysis, Stability and Control*. Springer Verlag, New York, 1999.

A. V. Savkin. Coordinated collective motion of groups of autonomous mobile robots: Analysis of vicsek's model. *IEEE Transactions on Automatic Control*, 49(6):981–983, 2004.

R. Sepulchre. Consensus on nonlinear spaces. *Annual Reviews in Control*, 35(1): 56–64, 2011.

A. S. Shiriaev and A. L. Fradkov. Stabilization of invariant sets for nonlinear systems with applications to control of oscillations. *International Journal of Robust and Nonlinear Control*, 11(3):215–240, 2001.

B. Siciliano, L. Sciavicco, L. Villani, and G. Oriolo, editors. *Robotics - Modelling, Planning and Control*. Springer-Verlag New York, Inc., Secaucus, NJ, USA, 2009.

S. Singh, G. Kantor, and D. Strelow. Recent results in extensions to simultaneous localization and mapping. In *Proceedings of the International Symposium of Experimental Robotics*, pages 210–221, 2002.

J. J. E. Slotine and W. Li. *Applied Nonlinear Control*. Prentice-Hall International, 1991.

O. J. Sørdalen and O. Egeland. Exponential stabilization of nonholonomic chained systems. *IEEE Transactions on Automatic Control*, 40(1):35–49, 1995.

M. W. Spong, S. Hutchinson, and M. Vidyasagar. *Robot Modeling and Control*. John Wiley & Sons, Inc., 2006.

I. Stewart. Mathematical recreations: The synchronicity of firely flashing. *Scientific American*, 1999.

S. H. Strogatz. Spontaneous synchronization in nature. In *Proceedings of the IEEE International Frequency Control Symposium*, pages 2–4, 1997.

D. Sun, C. Wang, W. Shang, and G. Feng. A synchronization approach to trajectory tracking of multiple mobile robots while maintaining time-varying formations. *IEEE Transactions on Robotics*, 25(5):1074–1086, 2009.

K.-H. Tan and M. A. Lewis. Virtual structures for high-precision cooperative mobile robotic control. In *Proceedings of the IEEE/RSJ International Conference on Intelligent Robots and Systems, (IROS 1996)*, volume 1, pages 132–139, 1996.

H. G. Tanner. Flocking with obstacle avoidance in switching networks of interconnected vehicles. In *Proceedings of the ICRA'04 IEEE International Conference on Robotics and Automation*, pages 3006–3011, 2004.

S. Tarbouriech and M. C. Turner. Anti-windup design: an overview of some recent advances and open problems. *IET Control Theory Applications*, 3(1): 1–19, 2009.

S. Thrun. Simultaneous localization and mapping. In M. Jefferies and W.-K. Yeap, editors, *Robotics and Cognitive Approaches to Spatial Mapping*, volume 38, pages 13–41. Springer Berlin / Heidelberg, 2008.

S. Thrun, D. Hahnel, D. Ferguson, M. Montemerlo, R. Triebel, W. Burgard, C. Baker, Z. Omohundro, S. Thayer, and W. Whittaker. A system for volumetric robotic mapping of abandoned mines. In *Proceedings of the ICRA '03. IEEE International Conference on Robotics and Automation*, volume 3, pages 4270–4275, 2003.

T. H. A. van den Broek, N. van de Wouw, and H. Nijmeijer. Formation control of unicycle mobile robots: a virtual structure approach. In *Proceedings of the 48th IEEE Conference on Decision and Control, held jointly with the 28th Chinese Control Conference. CDC/CCC 2009.*, pages 8328–8333, 2009.

S. V. Viscido, J. K. Parrish, and D. Grunbaum. Individual behavior and emergent properties of fish schools: a comparison of observation and theory. *Marine Ecology Progress Series*, 273:239–249, 2004.

H. U. Voss. Anticipating chaotic synchronization. *Physical Review E*, 61(5): 5115–5119, 2000.

L.-S. Wang, F.-R. Chang, and P.-S. Tsai. Continuation method of backstepping tracking control for car-like mobile robots. In *Proceedings of the IEEE International Conference on Systems, Man and Cybernetics, SMC '06.*, volume 3, pages 2018–2023, 2006.

L. G. Weiss. Autonomous Robots in the fog of War. *IEEE Spectrum*, August 2011.

A. Weitzenfeld, A. Vallesa, and H. Flores. A biologically-inspired wolf pack multiple robot hunting model. In *Proceedings of the IEEE 3rd Latin American Robotics Symposium, LARS '06*, pages 120–127, 2006.

Welcome to Malaysia, 2010. URL `http://www.malaysiasite.nl`.

X. Wu and Z. Lin. Anti-windup in anticipation of actuator saturation. In *Proceedings of the 49th IEEE Conference on Decision and Control*, pages 5245–5250, 2010.

X. Wu and Z. Lin. On immediate, delayed and anticipatory activation of anti-windup mechanism: Static anti-windup case. *IEEE Transactions on Automatic Control*, PP(99):1–6, 2011.

Z. Wu, Z. Guan, X. Wu, and T. Li. Consensus based formation control and trajectory tracing of multi-agent robot systems. *Journal of Intelligent and Robotic Systems*, 48(3):397–410, 2007.

E. Yang, D. Gu, T. Mita, and H. Hu. Nonlinear tracking control of a car-like mobile robot via dynamic feedback linearisation. In *Proceedings of Control 2004, University of Bath*, 2004.

H. Yu, J. Jian, and Y. Wang. Flocking motion of mobile agents with a leader based on distance-dependent adjacency matrix. In C. Xiong, H. Liu, Y. Huang, and Y. Xiong, editors, *Intelligent Robotics and Applications*, volume 5314, pages 1165–1174. Springer Berlin / Heidelberg, 2008.

H.-T. Zhang, M. Z. Chen, S. Guy-Bart, T. Zhou, and J. M. Maciejowski. Col-

lective behavior coordination with predictive mechanisms. *IEEE Circuits and Systems Magazine*, 8(3):67–85, 2008.

Y. Zou. *Distributed control of multiple vehicle system using constraint forces.* PhD thesis, Oklahoma State University, 2008.